Surface Spectroscopic and Electrochemical Investigations of Aromatic and Heteroaromatic Thiols on Gold Single Crystal Surfaces

by

Caroline Whelan

A thesis submitted for the Degree of

Doctor of Philosophy

Research Supervisors: Dr. C.J. Barnes and Prof. M.R. Smyth

School of Chemical Sciences

Dublin City University

July 1998

Declaration

I hereby certify that this material, which I now submit for assessment on the programme of study leading to the award of Doctor of Philosophy (PhD) is entirely my own work and has not been taken from the work of others save and to the extent that such work has been cited and acknowledged within the text of my work.

Signed July 1998

Caroline Whelan

Caroline Whelan

ID No.: 94970441

For my parents

Acknowledgements

My sincerest thanks to the following people without whom I may have followed a very different path.

My supervisors, Dr. Colin Barnes and Prof. Malcolm Smyth, for the opportunities and encouragement they've given me over the past four years. The character building experience will not be forgotten!

Prof. Norman Brown at the University of Ulster for stimulating discussions and introducing me to the delights of Belgian beer. Norman and his research group, in particular Dr. Chris Walker and Dr. Colin Anderson, have been instrumental in facilitating and assisting much of the research at Coleraine, Daresbury and Namur.

Dr. Gary Attard and his students, Rob, Bev, Ahmad and Ali, at the University of Wales for introducing me to the joys of electrochemistry and Dr. Xiaofan Yang for her patience while teaching me the basics of ECSTM.

Prof. Jean-Jacques Pireaux, Dr. Chantal Gregoire and Dr. Li Yu for their contribution to HREELS measurements at Namur, Belgium.

Prof. M. Pessa and Mr. P. Pussa for the use of their XPS facilities at Tampere University of Technology, Finland.

Dr. Danny Law and Dr. Graham Beamson for their technical support and insightful discussions during XPS measurements at the RUSTI unit, Daresbury.

The Physics department for allowing me to scavenge for materials and equipment, in particular Catherine and Charles (the power supply has been much appreciated).

Stephen and Brendan, the 'odd couple,' for entertainment and walks around the park.

Joey, Jim, David, Damien, Olga, Siobhan, Gemma, Mick, Enda, Emmanuel and all those who have passed through J204/J208 over the past four years for many laughs and lively discussions (scientific and other).

My family, Seamus, Joan, Keith, Josephine, Shawna, Michelle and 'little' Seamus, for supporting (emotionally and financially) the eternal student lifestyle and for their belief in me.

My adoptive family, the Ryans, Fiona and Bill for many a counselling 'session' over pints in the Tavern.

Hilary for showing me the other side of life and the value of a credit card.

Mick for the career advise and sharing a strange taste in movies.

Oonagh, Maria and Deirdre for your enduring friendship. What more can I say ?

TABLE OF CONTENTS

ABSTRACT

This thesis is devoted to the study of aromatic and heteroaromatic thiol self-assembly on Au single crystal surfaces. A range of surface spectroscopic and electrochemical techniques have been used to investigate the formation of complex assemblies in terms of the types of surface intermediates formed, adsorbate orientation and the mechanism of adsorption from the gas and liquid phases.

The self-assembly process is reviewed, with particular emphasis on aromatic self-assembled monolayers (SAMs). The applicability of a range of surface sensitive probes to the characterisation of such assemblies, differences between adsorption from the gas phase and the liquid phase and limitations with respect to *ex situ* techniques are discussed.

Initial work focused on an electrochemical and X-ray photoelectron spectroscopy (XPS) investigation of the self-assembly of heteroaromatic thiols, 2-mercaptobenzothiazole and 2-mercaptobenzimidazole, in terms of their surface bonding and molecular orientation following adsorption from the liquid and vapour phases, with additional information on substrate contamination effects.

The structural and behavioural complexities of the heteroaromatic thiols motivated us to revert to the simplest aromatic thiol, benzenethiol. The coverage dependent surface bonding, molecular orientation and growth mechanism of benzenethiol on Au(111) are discussed, highlighting differences in SAM composition and bonding configurations between adlayers prepared by gas phase and liquid phase adsorption.

The influence of atomic steps on SAM formation compared to benzenethiol adsorption on an atomically flat surface is addressed. This study represents the first report of manipulation of the thiolate adlayer structure and molecular orientation by controlled addition of surface defects using Au(322), a stepped surface, as a substrate for self-assembly.

PUBLICATIONS

This thesis is based on the following publications:

1. The Influence of Heterocyclic Thiols on the Electrodeposition of Cu on Au(111).
   C.M. Whelan, M.R. Smyth and C.J. Barnes, J. Electroanal. Chem., **441** (1998) 109.

2. A XPS Study of Heterocyclic Thiol Self-Assembly on Au(111).
   C.M. Whelan, M.R. Smyth, C.J. Barnes, N.M.D. Brown and C.A. Anderson, Appl. Surf. Sci., in print.

3. A HREELS, XPS and Electrochemical Study of Benzenethiol Adsorption on Au(111).
   C.M. Whelan, M.R. Smyth and C.J. Barnes, Langmuir, in press.

4. Benzenethiol Adsorption on Au(111) Studied by Synchrotron ARUPS, HREELS and XPS.
   C.M. Whelan, M.R. Smyth, C.J. Barnes, N.M.D. Brown and C.G.H. Walker, submitted to Surf. Sci.

5. A HREELS Study of Benzenethiol Adsorption on Au(111) and Au(322).
   C.M. Whelan, M.R. Smyth, C.J. Barnes, C. Gregoire and J.-J. Pireaux, in preparation.

6. Surface Structural Transitions Induced by Repetitive Underpotential Deposition of Ag on Au(111).
   C.M. Whelan, M.R. Smyth, C.J. Barnes, G.A. Attard and X. Yang, submitted to J. Electroanal. Chem.

Chapter 1

Surface Characterisation of Aromatic Thiol Adsorption on Single Crystal Surfaces

1. Introduction

Chemical derivatisation of solid surfaces has long featured as a means of manipulating interfacial properties in relation to processes such as wetting, adhesion, lubrication, corrosion and electrocatalysis [1-5]. Understanding the factors that govern the formation of stable derivatising layers is therefore of both fundamental and technological importance. The recent theme of film formation based upon coherently organised self-assembled monolayers (SAMs) on solid surfaces, is beginning to address the need for interfacial structures exhibiting dense functionalisation, with simple procedures for fabrication, characterisation and manipulation [5-8].

A major challenge in contemporary surface science is the investigation of these ordered arrays in terms of elucidation of substrate-overlayer structure, adsorbate-substrate bonding configuration, intermolecular interactions between neighbouring adsorbate molecules and the energetics of adsorption from the gas and liquid phase. To this end chemisorption of alkyl derivatives on a variety of substrates, in particular *n*-alkanethiols on Au surfaces, have received much attention in recent years and a comprehensive understanding of such systems has emerged [4-8]. In contrast, characterisation of SAMs consisting of unsaturated systems is in its infancy.

Aromatic thiols are ideal candidates for self-assembly due to their structure and chemical reactivity which provide the essential features to allow derivatisation with multiple chemically specific side groups, potentially offering SAMs with differing properties to *n*-alkanethiols, and is of interest with respect to basic aspects of the surface bonding. This is important for the development of aromatic SAM-substrate couples with technological applications and indeed many novel systems have been reported [9-13]. Hence, the purpose of this review is to highlight the applicability of a selection of surface sensitive techniques to the characterisation of model adsorption studies on single crystal metal surfaces for aromatic thiol self-assembly.

2. SAM Formation

2.1 The self-assembly process

As mentioned in the introduction, much of our understanding of SAMs at a fundamental level (substrate-head group bonding, molecular orientation, intermolecular interactions) is based on the study of *n*-alkanethiols on Au(111) which has been extensively reviewed [4-8]. Hence, this system will be discussed briefly in an effort to develop an understanding of more complex assemblies.

Self-assembly describes the spontaneous chemisorption, from the liquid or gas phase, of molecules possessing a polar head group designed to specifically interact with and chemically bind to substrate surface sites. Fig. 1 illustrates a schematic view of a self-assembled *n*-alkanethiol molecule on a solid substrate. In the case of thiol adsorption from the liquid phase on Au(111), the traditional approach to SAM preparation, self-assembly appears to involve two steps consisting of an initial adsorption process which occurs rapidly, described by simple diffusion controlled Langmuir kinetics, followed by a slower ordering (recrystallisation) step, as the system approaches equilibrium [14-20].

The first step is dominated by molecule-substrate interactions which anchor the thiol (R-SH) chemical functionality to specific substrate surface sites via a strong directional Au-thiolate chemisorption bond [21-24]. In considering the bond energies for RS-H, H_2 and RS-Au (87, 104 and 40 kcal mol^{-1}, respectively), the net energy for adsorption can be estimated at -5 kcal mol^{-1} (exothermic) [23,25-28]. The reaction probably occurs by the following mechanism:

$$RS\text{-}H + Au_{(n)}^{0} \rightarrow RS^{\delta-}Au^{\delta+}.Au_{(n-1)}^{0} + \tfrac{1}{2} H_2$$

resulting in the formation of a surface bound thiolate intermediate occupying every third hollow site and hence adopting a $(\sqrt{3}\times\sqrt{3})R30°$ overlayer structure [29-32]. This represents the highest coordination site for the adsorbate. The hydrogen atoms recombine and readily desorb from Au(111) at 115 K [33].

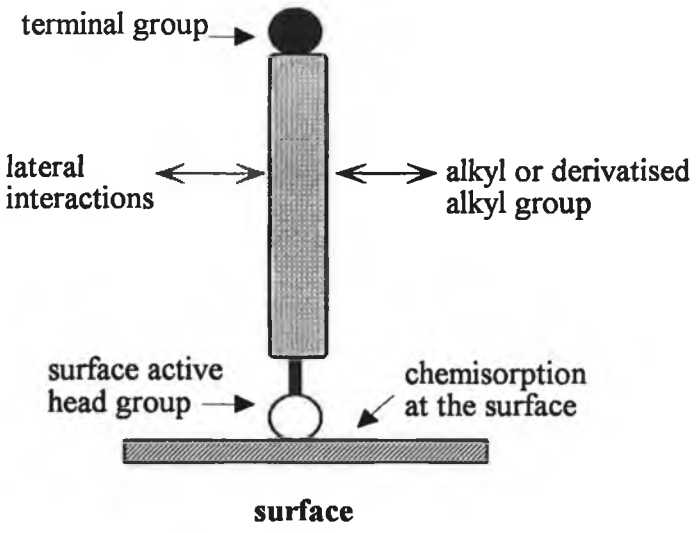

Figure 1 A schematic view of the forces in a self-assembled monolayer.

The adsorption energy for a dialkyl disulphide is more favourable than the corresponding thiol (-12 kcal mol^{-1} for each RS^{-} group). However, there is no strong evidence for dimerisation of thiols to form disulphides following adsorption, presumably due to steric constraints, and in fact several studies have shown that dialkyl disulphide adsorption results in sulphur-sulphur bond cleavage producing a surface thiolate intermediate [23,28,34,35].

The second self-assembly step maximises lateral intermolecular van der Waals (VDW) attractions (which are long-range in comparison with the chemisorption bond) between low polarity alkyl chain segments of the molecule. A strong chemisorption interaction with the substrate is maintained, resulting in a Au-S-C bond angle of ~120° [6,36]. The energy associated with this process depends on the chain length and studies have shown that the adsorption kinetics increase with alkyl chain length due to an increase in VDW interactions (>0.8 kcal mol^{-1} of CH_2 groups) [15,26]. Given that the sulphur-sulphur atom spacing (4.99 Å) is greater than the distance of closest approach of the alkyl chains (4.24 Å), the fully extended chains tilt ~30° with respect to the surface normal towards the next nearest neighbour to maximise their VDW interactions [6,7,23,36-38].

During this surface recrystallisation process, the alkyl chains emerge from a disordered state to form a two-dimensional crystal. The packing density of

approximately 5×10^{14} chains cm^{-2} is similar to that found in bulk, crystalline *n*-alkanes [6,21]. Hence, microstructural reorganisation of the monolayer yields a well-defined two-dimensional overlayer with highly ordered chain-terminating groups (semi-crystalline at room temperature) exhibiting a specific chemical functionality which dictates the interactions between the SAM and the contacting phase [39,40].

Under certain conditions, aromatic groups may be introduced into these assemblies without adversely affecting the packing and order of the monolayer [41-43]. Fully conjugated linear molecules with unsubstituted aromatic structures have been self-assembled successfully from the liquid phase on Au [44,45]. In the case of alkyl chains containing bulky aromatic groups (chromophores), it has been reported that both self-assembly steps are coupled. Chain disorder, caused by an increase in the chain-chain spacing due to electrostatic interaction between the 'bulky' structures, impedes thiol group chemisorption by blocking access to adsorption sites [41]. In addition, the quality of the monolayer produced has been found to be dependent on both the size of the chromophore, its dipole moment and its position in the alkyl chain which disrupts the cylindrical symmetry and effects the orientation and the packing arrangement adopted by the two-dimensional assembly [42]. This is presumably due to π-π interactions and because the alkyl units below the aromatic group and anchored to the substrate experience a restriction in their rotational motions, while those above can easily rotate. The rate of adsorption is a function of the total number of alkyl carbons in the molecule and, in particular, depends on the alkyl chain length above the bulky group, with an increase in disorder as the π-system approaches the monolayer-air interface due to electrostatic repulsions. Hence, the length of the upper chain provides the main driving force for crystalline-like monolayer formation by maximising VDW interactions. Coadsorption experiments between *n*-alkanethiols and molecules which incorporate aromatic groups show that the latter compete quite effectively for coordination to adsorption sites [43].

2.2 Adsorption of 'simple' aromatic thiols

In general, self-assembly of thiols consisting of alkyl chains with/without aromatic groups tends to be dominated by the energetics of the Au-S bonding while

adsorbate-adsorbate interaction are lesser contributors. 'Simple' aromatic thiols such as benzenethiol (C_6H_5SH) are particularly interesting, since bond formation could, in principle, involve two chemisorption bonds; a polar covalent metal-sulphur bond and a secondary interaction between the π-system and the substrate. In an effort to understand possible bonding characteristics of aromatic thiols on metal surfaces, it is worth discussing benzene adsorption on transition metal surfaces which has been studied extensively.

Similar to *n*-alkanes, lateral interactions in solid benzene are mainly determined by weak van der Waals interactions, but with the added complication that the molecule possesses a permanent electrostatic quadrupole moment, and carbon atoms in the molecule are strongly coupled via ionicovalent interactions. The shape of the molecule remains almost planar when it is incorporated into a crystal lattice. Different crystalline packing configurations between two benzene molecules can be envisaged [46]. The rings may be co-planar such that the C-H bond on one molecule is directed toward the centre of a C-C bond on the other or a C-H bond on one molecule may be co-linear with a C-H bond on the second molecule. Alternatively, the molecules may pack directly above one another with the planes of the rings parallel or with the plane of one molecule perpendicular with respect to another in so-called 'stacked' and 'edge-to-face' configurations, respectively. It has been found that the crystal structure of solidified benzene, determined by X-ray and neutron diffraction, assumes the edge-to-face configuration [46,47].

Three possible bonding mechanisms have been postulated for adsorption of unsaturated hydrocarbons, e.g., acetylene, propylene, benzene and pyridine, on metal surfaces depending on the reactivity of the metal [48-50]. The first involves rehybridisation of the carbon sp electrons from sp^2 to sp^3 concurrent with the formation of σ bonds between the carbon atoms and metal atoms (so-called di-σ-adsorbed). For benzene, rehybridisation can cause ring expansion, ring 'puckering' and C-H bond bending out of the ring plane and requires a significant increase in molecular energy, which is only possible if such rehybridisation results in stronger chemisorption bonding [50].

The second mechanism involves the formation of a π donor bond between the carbon-carbon π-orbitals and the surface, similar to organometallic transition metal

complexes, and leads to a π-adsorbed species. In this donor-acceptor type bond, charge is transferred from the highest filled occupied π-orbitals of benzene to the metal, while much less charge is transferred in the opposite direction to the unoccupied π*-orbitals. Depopulation of the π-orbitals results in the bond between the molecule and the surface while population of the π*-orbitals leads to a weakening of the intramolecular carbon-carbon bonds. Hence, while the molecule is largely unperturbed in comparison with di-σ-adsorbed species, a weakening of internal bonds is expected (e.g., 0.4 Å increase in bond length for benzene on Pd(111) compared with gas phase benzene) as the delocalised π-system maximises overlap with the low-lying unoccupied metal valence orbitals [51,52]. It should be noted that the degree of rehybridisation can vary depending on the adsorbate-substrate couple and cases of intermediate to π-adsorbed or di-σ-adsorbed species can exist, e.g., acetylene adsorbed on Ni(110) [53].

Finally, for benzene and related aromatic adsorbates, a σ-type dissociative bonding can occur (which involves removal of hydrogen from the molecule) through one of the ring carbons, with the plane of the ring inclined at an angle with respect to the surface plane. In this case, the energetics of the system must be considered in terms of C-H bond cleavage, resultant metal-carbon bonding and possibly metal-hydrogen bond formation, e.g., 100, 43 and 57 kcal mol^{-1}, respectively, for conversion of pyridine to pyridyl species on Pt(111) [54]. In addition, the six carbon atoms are no longer equivalent, and hence the loss in delocalisation or resonance energy (36 kcal mol^{-1} for gas phase benzene) must be counteracted by a gain in the metal-carbon bond energy [54].

A discussion of benzene adsorption on all transition metal surfaces is beyond the scope of this review. Instead, benzene chemisorption on Rh(111) will be taken as an example. Adsorption is associative at 300 K with the molecular plane parallel to the surface forming a $c(2\sqrt{3}\times4)rect\text{-}C_6H_6$ structure at a surface coverage of 0.125 monolayers [55-58]. Hence, unlike the edge-to-face packing arrangement found in crystalline benzene, the molecule assumes a lower packing density and parallel bonding geometry. This is explained by the preferred bonding to the surface which occurs predominantly through the delocalised π-electrons of the aromatic ring system (π-adsorbed), without significant rehybridisation, in agreement with benzene adsorption on other metal surfaces [55,56]. Two molecular adsorption sites are populated (hollow

and on-top sites) and several ordered phases can be formed between 300 and 400 K, depending on the benzene coverage, without significant changes in the bonding geometry [55,57]. However, there is evidence for a change in bonding mode due to ring distortion concurrent with coordination site switching (from on-top to three-fold hollow) as the surface becomes crowded at high coverage [58].

In considering benzenethiol adsorption on Rh(111), self-assembly may be determined by competition between the desired Rh-thiolate bond formation and bonding between the substrate and the π-orbitals of the phenyl ring system, as is the case for benzene adsorption on Rh(111). The packing arrangement assumed by this system may differ considerably from *n*-alkanethiolates or molecular benzene. Repulsive lateral adsorbate-adsorbate interactions tend to stabilise their total energy by forming two-dimensional dispersed phase overlayers, with adsorbates distributed homogeneously over the surface, while mutually attractive interactions tend to promote two-dimensional islanding (with a high local coverage). Similar to *n*-alkanethiolates, a surface bound phenylthiolate species may adopt a largely vertical molecular orientation. Alternatively, in addition to sulphur-Rh bonding, a flat-lying benzene-like bonding geometry, displaying surface specificity imparted by the delocalised character of the π-system and the delocalised free electrons in the metal, is also possible. This situation may be further complicated by temperature and coverage dependent bonding configurations. In particular, at high adsorbate coverages surface crowding effects (reducing the adsorption energy) become more important and hence the conformation adopted, in terms of the molecular tilt or rotation about the molecular axis, may be influenced by steric interactions between the aromatic rings. Such interactions are generally minimised by tilted bonding geometries, which would leave the phenyl ring essentially unperturbed by sulphur atom chemisorption to the substrate and make the carbon-sulphur and carbon-hydrogen bonds less accessible for activation by the surface. This is important, given that the S-C and S-H bond dissociation energies for a phenylthiolate are comparable (89 and 82 kcal mol^{-1}, respectively) [25].

The estimated heats of desorption (ΔH_D) for benzene on Rh(111) chemisorbed to a saturation coverage of 0.125 monolayers of molecular π-bonded benzene and 0.21 monolayers of sulphur-bonded benzenethiolate are 23.3 and 16.6 kcal mol^{-1},

respectively [55,59]. The thiolate adopts an upright configuration, maximising the packing density and, hence, the number of sulphur-Rh bonds formed. However, at a low coverage of 0.07 monolayers, the ring plane adsorbs parallel with respect to the surface plane (ΔH_D = 26.7 kcal mol^{-1}) indicating that, in addition to sulphur-Rh bonding, the π system coordinates strongly with the metal surface. As the coverage increases (50-100% saturation), two desorption states coexist (26.7 and 16.6 kcal mol^{-1}) as ring-ring repulsive interactions become important and steric effects force a reorientation to an upright geometry, thus inhibiting ring-substrate bonding.

The example of benzenethiol adsorption on Rh(111) highlights two features which may be characteristic of aromatic thiol adsorption. First, at low coverages when the adsorbate two-dimensional density is low, a flat-lying molecular orientation allows additional chemisorption energy (~10 kcal mol^{-1}) to be liberated via the bonding of the ring π-orbitals with the metal. Second, a phase transition to an upright geometry at higher coverage is favoured, even in the presence of adsorbate-adsorbate repulsive interactions, in order to maximise the sulphur-metal interactions.

It is this additional complexity at a fundamental level, in terms of possible competitive bond formation (metal-sulphur and metal-conjugated ring) combined with lateral adsorbate-adsorbate interactions which may lead to coverage dependent molecular orientations, drives current research on aromatic self-assembly. The interplay and final balance of these system dependent forces, that controls the equilibrium structure of a SAM, is very difficult to predict.

2.3 Substrate preparation

Self-organisation of organic molecules on surfaces is a complex process and a possible starting point involves the study of model systems. This work requires a substrate of known structure. Polycrystalline material leads to a range crystallographic planes being presented for the self-assembly process. The use of single crystals with well-defined adsorption sites and few surface defects yield a substantial gain in detailed information about the adsorbate-substrate complex.

The classic technique for preparing clean and well defined single crystals involves argon ion sputtering and thermal annealing in a ultra-high-vacuum (UHV) chamber until subsequent checks using low energy electron diffraction (LEED) and Auger electron spectroscopy or X-ray photoelectron spectroscopy (AES/XPS) reveal a surface of the desired crystallography free from detectable contamination. Alternatively, clean surfaces can be generated by thermal annealing outside a UHV environment using the 'flame-annealing' procedure, developed by Clavilier for single crystal electrodes [60]. This involves annealing the crystal in a gas-oxygen flame followed by cooling in air, hydrogen or an inert gas and immediately quenching in ultra-pure water. Surfaces are then transferred to the experimental set-up with a protective water film that inhibits environmental contamination. Interfacial characterisation of crystals prepared under such conditions relies primarily on the comparison of cyclic voltammetry curves with literature reports of workers capable of performing *in situ* electrochemistry combined with UHV techniques (EC-UHV). Epitaxial growth by vapour deposition in high vacuum onto mica also yields atomically smooth and well-ordered single crystal films [61]. This method is limited to the preparation of Au(111) and Ag(111) surfaces, the latter suffering oxidation upon exposure to air [36]. Finally, disordered interfacial atoms can either be activated to diffuse to stable ordered sites or be dissolved to expose ordered layers by electrochemical annealing (based on the application of appropriate potential cycling conditions). However, this technique is the least favoured method of substrate preparation as studies have shown that electrochemical annealing may give rise to a defect rich, imperfect surface [62].

2.4 SAM preparation

Self-assembly from the gas phase is achieved by exposing a clean single crystal in UHV to a volatile adsorbate, purified by repeated freeze-pump-thaw cycles, using a controllable gas doser. Low molecular weight residual gases of a vacuum chamber (carbon monoxide, oxygen, water and hydrogen) will not chemisorb on Au at 300 K such that moderate vacuum levels are sufficient to prevent surface contamination and

substrate cleanliness prior to SAM formation should not be an issue (unless low vapour pressure contaminants which may physisorb are present) [63,64]. However, reactive metals such as Mo, Cu and Ni are more susceptible to adventitious pick-up. In addition, desulphurisation of some thiols may occur upon expansion into the gas manifold via reaction with the stainless steel walls of the vacuum chamber [65]. Hence, passivation of the dosing lines by repeated exposure to sample gas is recommended and the dosing vapour composition should be periodically checked *in situ*, by means of mass spectrometry, to detect possible contamination and/or degradation.

Liquid phase SAM formation involves immersion of the substrate in a dilute solution of the molecule of interest in an organic solvent (concentration, choice of solvent, and immersion times vary between studies). Samples are then washed with copious amounts of solvent and dried with a flow of inert gas. It is generally reported that there are no considerable solvent effects and, practically, the solubility properties of the thiol dictate the choice of solvent [5,15,28].

2.5 Gas phase versus liquid phase self-assembly

In comparison with liquid phase self-assembly, adsorption of thiols from the gas phase has received much less attention. Nevertheless, differences between the two methods of film preparation are apparent, in particular, in terms of substrate cleanliness prior to self-assembly, the thiol arrival rate (flux) at the surface and the adsorbate growth mechanism.

Deposition of adventitious material, such as hydrocarbons and other organic compounds that exist in the air, on the substrate upon exposure to atmospheric pressure is of concern prior to liquid phase self-assembly. It is quite likely that even in the case of Au, a relatively inert metal towards chemisorption, the surface will be covered with a physisorbed layer of organic material prior to derivatisation [15]. This situation is further complicated by the possibility of adsorption of solvent molecules or solvent decomposition products upon contact with the surface. Substrate contamination affects the kinetics of adsorption but is reported to be displaced by the *n*-alkanethiol in the process of monolayer formation, although it is not clear whether

this process is driven to completion [15,36]. However, the behaviour of aromatic thiols in such a displacement mechanism remains undetermined and, hence, contamination effects must be considered. The extent of substrate contamination can be estimated by XPS analysis. Static secondary ion mass spectrometry (SSIMS) provides a method of determining the chemical nature of the contaminating species present on the surface and, hence, identification of the exact source of contamination.

The substantially higher thiol arrival rate at the surface achieved in solution, compared with dosing in vacuum, may lead to considerable differences in the self-assembly process. Film consolidation (discussed earlier) in terms of maximum packing density may require high thiol fluxes to reach completion. For example, the reactive sticking probabilities in UHV of ethane- and methane-thiol on Au(111) surfaces are lower than the corresponding disulphides [23,66]. In contrast, in solution, thiols more rapidly approach saturation coverage reflecting the steric constraints encountered by the larger disulphides. The low reactivity of gas phase ethane- and methane-thiol has been explained in terms of the initial molecular precursor and transition state for dissociation of the S-H bond, which are stabilised by incremental heats of adsorption (1.9 kcal mol^{-1} per methylene group). Apparently this activation barrier is not exhibited by disulphides which readily undergo S-S bond cleavage regardless of chain length.

While increasing the thiol chain length significantly enhances the sticking probability in UHV, this is counteracted by an increase in steric effects due to strong chain-chain interactions. As the surface coverage approaches saturation coverage, the densely packed polymethylene chains inhibit impinging gas phase molecules from adsorbing at unoccupied substrate sites. In contrast, in solution a dynamic and reversible adsorption process is part of the mechanism for attaining equilibrium coverage by maximising the packing density. Adsorption-desorption processes (in the presence of a continuous thiol flux) and surface diffusion may occur in UHV. However, the significantly higher flux in solution mean that exchange and transport of surface species allowing a facile annealing mechanism are much more important [8,28].

A two-dimensional island growth mechanism, accompanied by lifting of the Au(111)-($\sqrt{3}\times22$) herrringbone reconstruction to the (1×1) bulk truncated phase, has been reported for adsorption of mercaptohexanol in vacuum [66,67]. At low exposures, island growth has been observed by STM with sulphur atoms bonding to

three-fold hollow sites and alignment of the molecular axis with the surface plane [67]. The surface then undergoes a orientational phase transition with the development of thiolate islands in which the molecular axis is aligned along the surface normal. These islands grow laterally, at the expense of the surface-aligned phase, and finally coalesce to form a compact monolayer. Similarly, LEED has been used to study the ordering of a range of *n*-alkanethiols (1-10 CH_2 units in length with CH_3 terminal groups) adsorbed from the gas phase on Au(111) between 300 and 350 K [66]. The diffraction patterns revealed the lifting of the substrate reconstruction prior to completion of the monolayer, a self-assembly mechanism involving island formation and overlayer structures of the form $(n\sqrt{3}\times\sqrt{3})R30°$ (where n = 1-6). However, too few gas phase adsorption studies have been reported to determine whether this uptake behaviour is a general phenomenon. Nevertheless, it is fair to say that the description of self-assembly in terms of a two step mechanism involving diffusion controlled Langmuir kinetics (discussed in section 2.1) is oversimplified in the case of gas phase adsorption.

Differences in self-assembly process between the gas and liquid phase raise an interesting question. Is it indeed possible to adopt a 'fundamental' approach, i.e., UHV thiol dosing on an atomically clean surface, to studying SAMs which are predominately prepared in solution for the majority of applications ? An analogous case is the study of UHV adsorption of gases on single crystal metal surfaces in an effort to understand 'real' catalysts comprising metal particles adsorbed on or imbedded in support materials. A great deal of information regarding catalysis has been derived from such model UHV studies. Hence, it can be argued that gas phase studies are relevant to solution studies. In order to elucidate the interplay of different forces that control the liquid phase self-assembly process, it is necessary to explore the fundamental chemistry of model monolayer-substrate systems, allowing broader conclusions on the properties of 'real' SAMs to be drawn.

3. Surface Characterisation

3.1 Surface characterisation of SAMs

In investigating SAMs we are generally interested in the substrate and adlayer structure, film composition and surface bonding information. A single technique is incapable of providing such comprehensive characterisation and, hence, the majority of studies outlined in the preceding discussion rely on a combination of probes for detailed analysis. Fig. 2 illustrates a typical UHV chamber designed for a multitechnique approach. In addition to the need for UHV ($< 10^{-9}$ Torr), essential instrumental requirements include a sample manipulator, ion sputtering and annealing facilities and a fast insertion lock/transfer system in the case of EC-UHV experiments. Analysis facilities often include an XPS source and electron energy analyser (XPS/AES), diffraction optics for LEED and a mass spectrometer.

A selection of surface sensitive techniques will be outlined with a brief introduction to the basis of each technique, the types of information provided and suitable examples of their application to the study of benzenethiol adsorption (from the gas phase unless otherwise indicated) on single crystal metal surfaces. This is the simplest aromatic thiol and has received much attention in terms of surface characterisation. In addition, *ex situ* studies of this system will be covered briefly, in an effort to highlight the difficulties encountered in characterising complex assemblies in the absence of UHV based techniques.

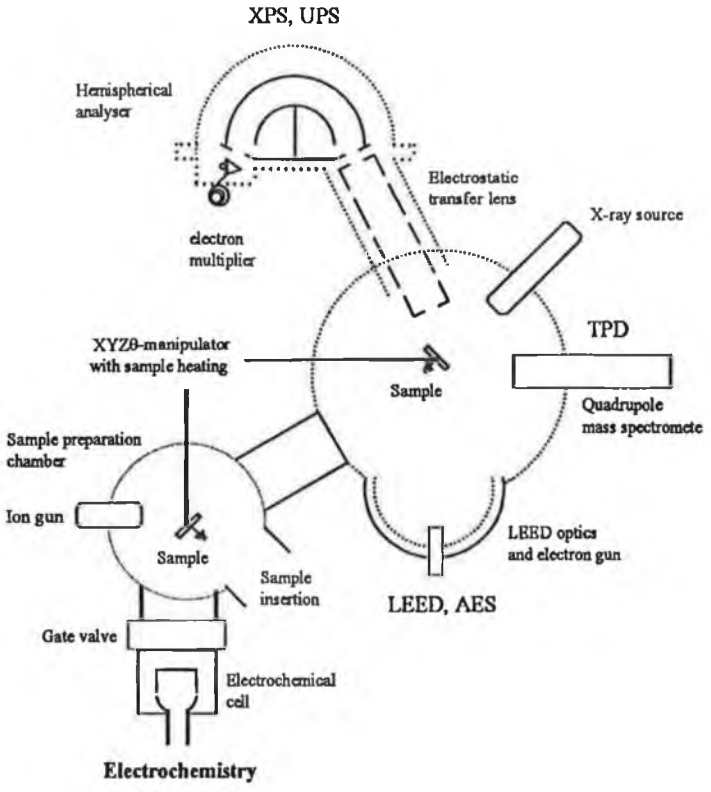

Figure 2 A schematic diagram of a typical UHV system designed for a multitechnique approach to SAM characterisation.

3.2 Surface compositional techniques

X-ray photoelectron spectroscopy

Surface analysis by X-ray photoelectron spectroscopy (XPS) involves irradiating a sample in vacuum with monoenergetic soft X-rays and energy analysing emitted core level electrons resulting from photoionisation [68,69]. Since the inelastic scattering length or 'mean free path' of low-energy electrons in solids is very small, the detected electrons originate from the top few atomic layers, making XPS a surface sensitive technique. The spectrum obtained, which is unique for each element, is as a plot of number of detected photoelectrons versus their kinetic energy (or binding energy).

Identification of chemical states comes from measurement of peak positions (based on Einstein's photoelectric equation), and changes in binding energies of core electrons as a function of the chemical environment are observed in terms of a 'chemical shift' in binding energy [70]. Therefore, in addition to providing identification of atoms, XPS provides information on the charges associated with the bonding between atoms through subtle shifts in the exact binding energy values from 0.1 up to 10 eV or more [71].

Quantitative surface elemental composition can be extracted from peak areas or intensities directly related to the quantity of that particular element at the sample surface, and most elements can be detected at 0.1% atomic abundance. In addition, sampling depth in XPS is a function of the angle of emission of the photoelectrons. By varying the angle of emission or 'take-off angle' towards grazing, the surface sensitivity is enhanced as more surface atoms are probed with respect to bulk [72]. Angular resolved XPS provides a non-destructive depth profile to determine overlayer thicknesses, distinguishes between surface phenomena and substrate properties, and allows conclusions to be reached about the orientation or depth distribution of different components on the surface.

A second technique for compositional analysis is Auger electron spectroscopy (AES). However, the relatively high incident flux densities makes AES prone to radiation damage when analysing organic species which are highly susceptible to beam induced modification [73].

3.3 Electronic structural techniques

Ultraviolet photoelectron spectroscopy

Ultraviolet photoelectron spectroscopy (UPS) is a particularly useful tool for the study of adsorbed species on surfaces [68,74-76]. Photons, of lower energy than those used in XPS (typically 10-100 eV), are used to excite electrons from valence levels of surface localised atoms which are subsequently energy analysed and

presented in the form of a plot of number of electrons photoemitted, appearing as a series of bands as a function of their kinetic energy.

At a basic level, data analysis often involves obtaining 'difference spectra' by subtracting the clean surface spectrum from the adsorbate-covered counterpart and, hence, identifying valence electron emission features from the molecular orbitals of the adsorbed species which are then compared with a corresponding gas phase spectrum [77]. The molecular orbitals generally suffer an adsorption-induced shift following chemisorption and alignment with the gas phase spectrum can often be achieved using a molecular orbital which does not participate in bonding to the surface [78]. Since the electronic valence structure is a unique fingerprint of a particular species, this allows identification of the adsorbed species, and provides information on the valence states that participate in bond formation between a surface and an adsorbate. Modification of substrate band emission from states spatially localised within the topmost atomic layers (surface states) are sensitive to the local environment of the surface and can provide additional information about the adsorbate-substrate complex [79].

Molecules adsorbed on a single crystal surface usually have a well-defined orientation with respect to the substrate. From polarisation dependent selection rules, based on the surface-molecule bond symmetry, it can be predicted whether emission from a specific orbital at a given polarisation is allowed or forbidden. Variation of the direction of the electric vector of the incident light (such that the parallel or perpendicular components are increased or decreased) with respect to the intermolecular axis, achieved by variation of the angle of incidence of the light, provides information on the molecular orientation [74-76]. Hence, in angle-resolved UPS (ARUPS), the application of polarisation-dependent selection rules allows assignment of peaks within the spectrum to specific orbitals to obtain the orientation and local adsorption symmetry of adsorbed species. In addition, for molecules adsorbed in an ordered overlayer, two-dimensional band structures can be mapped and interpreted in terms of adsorbate-adsorbate interactions [78].

Isosbestic points, which describe a common crossing point of superimposed spectra corresponding to successively greater adsorbate coverages, have been observed in UPS spectra [80]. Single or multiple isosbestic point occurrence up to saturation coverage verifies the formation of a single or multiple (of constant ratio)

adsorbate species on the surface, respectively. The absence or continuous shifting of an isosbestic point indicates the existence of more than one adsorbed species with a continuously varying ratio. Finally, in the case of a system involving multiple adsorbates and an isosbestic point shifting position as a function of coverage, one of the adsorbed species predominates in the exposure range of each isosbestic point. Hence, the absence or presence of isosbestic points provides information on the nature of the adsorption process.

Work function measurement

The work function (ϕ) is the minimum energy required to remove an electron from the highest occupied energy level, the Fermi level (E_F), of a solid such that it no longer experiences a long range Coulomb interaction with the positive hole created by its removal. Measurement of ϕ provides valuable information, as it is critically dependent on the local surface geometry and electronic structure due to electron 'overspill' at the surface which creates a dipole layer, the structure of which is dependent on the local geometric structure of the interface. Work function changes ($\Delta\phi$) are induced by atomic and molecular adsorption due to charge redistribution effects and hence can be used to study adsorption processes on surfaces and, in particular, distinguish between adsorption of electropositive and electronegative species. Although a number of techniques are available, we will restrict our discussion to the measurement of $\Delta\phi$ using UPS [81]. Here the full width of a UPS spectrum, between the E_F and the point of inflection of the secondary electron tail, is measured and subtracted from the fixed photon energy used to excite photoemission to give a direct estimate of the $\Delta\phi$.

3.4 Surface bonding techniques

Electron energy loss spectroscopy

A monoenergetic beam of low energy electrons (1-10 eV) inelastically scattered by a solid loses energy through promotion of a transition from a lower to a higher vibrational level of adsorbed species. In high resolution electron energy loss spectroscopy (HREELS), the number of scattered electrons in one direction is recorded as a function of their kinetic energy. This technique facilitates complete spectral analysis of adsorbates in the vibrational loss region from 4000 to *ca.* 100 cm^{-1} and has been widely applied to the study of adsorption on metal surfaces even at coverages corresponding to a fraction of a monolayer [82].

Although in the adsorbed state new modes may be encountered, comparison of the vibrational frequencies with infrared spectroscopic assignments for unadsorbed compounds generally reveal the nature and bonding of the adsorbate. More elaborate studies can provide structural information, allowing adsorption site determination, qualitative predictions of bond strength and a semi-quantitative estimate of bond length [82]. In addition, by applying the so-called metal-surface selection rule (MSSR), relative peak intensities are valuable indicators of molecular orientation.

Operating in specular geometry (i.e., angle of incidence equals the angle of reflection), the dipolar mechanism for electron scattering results in the principle energy losses. The symmetry-based selection rules associated with this process are the same as those involved in the excitation of dipole-active vibrations in infrared spectroscopy. According to the MSSR, metal conduction electrons distort the incoming electronic charge such that its lines of force are terminated perpendicular to the surface and, hence, only those vibrations can be excited which have components of oscillating dipole moment perpendicular to the surface and give rise to energy loss features. When electrons are collected off-specular directions, short-range interactions between the incident electron and the oscillator at the surface give rise to additional energy losses due to an 'impact scattering' mechanism. Several selection rules associated with the impact mechanism have been evaluated and allow the assignment of vibrations with a

net atomic displacement and, where appropriate, net dipole changes parallel to the metal surface.

Most analyses of HREELS spectra are made in terms of the symmetry properties of an isolated adsorption complex. However, under certain circumstances, symmetry based selection rules cannot be applied strictly and caution is needed in interpreting weak spectral features. Overall, the capability to detect both parallel and perpendicular vibrational components is an important property of HREELS.

Thermal desorption spectroscopy

An adsorbate species is bound on a surface with a specific amount of energy termed the adsorption energy. Adsorbates can be excited thermally to the extent that the surface-adsorbate bond is broken resulting in desorption. In thermal desorption spectroscopy (TDS), a temperature ramp (1-100 Ks^{-1}) is applied to an adsorbate-covered surface, usually via resistive heating by passing an electrical current through the sample or electron beam bombardment of the back of the sample, and the rate of gas evolution corresponding to the desorption of atoms or molecules is monitored by mass spectroscopy. Most spectrometers allow compositional analysis of desorbing species by simultaneous detection of multiple masses. TDS is particularly useful for determining decomposition reaction mechanisms of surface intermediates and is often enhanced by the use of isotopically substituted molecules.

The heat of adsorption can be estimated from the desorption profile displayed as a pressure-temperature curve using the desorption peak maximum temperature [81,83]. Relative adsorbate surface coverages are determined from the peak integrated intensity, and to obtain absolute coverages the TDS signal must be calibrated by measuring the peak area produced from a adsorbate system of known coverage. In addition, coverage dependent shifts in the desorption peak temperature, as well as multiple desorption peaks, are often observed due to variation of lateral adsorbate-adsorbate interactions as a function of coverage and/or the existence of more than one binding site with different activation energies for desorption [84]. However, it is difficult to assign coverage dependent changes in the desorption profile without

additional information, from for example vibrational spectroscopy which reveals more directly coverage dependent site switching.

3.5 Surface structural techniques

Low energy electron diffraction

The de Broglie equation forms the basis of the interference of electrons at surfaces and the observation of a diffraction pattern representing two-dimensional surface structure. Low energy electron diffraction (LEED) is concerned with the fraction of elastically backscattered electrons produced when a collimated beam of low energy electrons (20-1000 eV) is incident on an ordered surface [85]. The angular distribution of backscattered electrons can be observed as a diffraction pattern on a fluorescent screen. A major limitation in LEED studies of adsorption complexes is the susceptibility of many organic species to electron beam induced degradation, alleviated to some extent recently by the development of sophisticated experimental equipment to allow rapid measurement of low diffraction intensities [86]. Nevertheless, assuming the adsorbate is unaffected upon exposure to the primary electron beam, determination of the direction of the interference maxima by inspection of the diffraction pattern, which is simply the reciprocal lattice of the substrate, provides the size and orientation of the unit cell of the surface structure relative to that of the substrate.

A LEED diffraction pattern merely reveals the two-dimensional periodicity of the surface structure while the positions of atoms within the unit cell, including adsorbed species relative to the substrate atoms, can only be evaluated from analysis of the intensities of the diffracted beams. Such measurements (generally taken using a computer-interfaced video camera) involve following intensity variation from beam to beam or as a function of primary electron beam energy. Quantitative analysis of the intensity of diffraction and its dependence on electron energy, collected as intensity/voltage (I/V) spectra, facilitates complete structural analysis, including bond lengths and angles [86,87]. However, structural determination is indirect, and consists of postulating a structural model, including the possibility of multiple electron

scattering, calculation of LEED I/V spectra and comparison of theoretical calculations with experimental data via reliability factor analysis. Spot profiles are collected at a fixed electron energy to yield information on partially disordered structures (deviations from ideal two-dimensional periodicity) reflected by the occurrence of extra spots or a broadening of the intensity distribution around a diffraction spot, e.g., elongation into streaks due to one-dimensional disorder.

In conclusion, although observation of a diffraction pattern enables conclusions to be drawn about the substrate geometry, its response to chemical bond formation with adsorbates (e.g., lifting of a surface reconstruction), the degree of surface order within the overlayer and the adsorption process, in terms of two-dimensional adsorbate islanding or dispersed phase growth, a full structural determination is non-trivial and requires extensive computational analysis.

Scanning tunneling microscopy

Scanning tunneling microscopy (STM) is an excellent technique for probing structural and electronic properties at surfaces with atomic resolution [88,89]. The essence of STM lies in the quantum-mechanical tunneling of electrons through a potential barrier when the electronic wavefunctions of two conductors overlap. A piezoelectric translator moves an atomically sharp metallic tip to within a few nanometers of a conducting surface and a small potential difference is applied between them causing a 'tunneling' current (exponentially dependent on the surface-tip separation distance) to flow. For positive or negative bias voltage, tunneling of electrons occurs between tip states and empty conduction band or filled valence band states, respectively, in the sample producing a small measurable current.

Direct visualisation of features corresponding to individual atoms or molecules on a surface are obtained by monitoring the tip-sample distance (at constant tunnel current) or the magnitude of the sample current (at fixed tip-sample distance) as the tip is scanned across the sample surface. Such images are not true topography but rather the surface tunneling probability which depends on both the topography and the variation in the abundance and energies of electrons, revealing electronic properties

atom-by-atom. The advantages of STM over diffraction techniques are that it provides a direct view of the surface atomic arrangement, including disordered systems, it can be operated in air, liquid or vacuum and can often probe organic adsorbate species non-destructively.

3.6 Synchrotron techniques

X-ray absorption fine structure spectroscopy

X-ray absorption fine structure (XAFS) spectroscopy provides insight into the unoccupied (mainly) electronic energy levels and geometric structure of substrate-adsorbate systems [90,91]. The technique involves irradiation of a sample with X-ray photons of sufficient energy to cause photoemission from a core level. The photon absorption cross-section is monitored as a function of photon energy (and hence requires a synchrotron radiation source) and presented as a plot of absorption coefficient versus photon energy. The X-ray absorption spectrum is characterised by a sharp increase in absorption (termed an 'absorption edge') when the exciting radiation equals the binding energy of a core level electron within the sample.

Near the absorption threshold, the absorption cross-section (measured by monitoring the rate of core hole production using Auger emission or X-ray fluorescence) oscillates due to localised excitation of a core electron into regions of high final densities of state (antibonding orbitals located between the Fermi level and the vacuum level and unbound 'scattering resonances'). Near-edge X-ray absorption fine structure (NEXAFS) deals with the energy region immediately above the absorption edge (to 50 eV beyond the edge) where atomic transitions and multiple scattering of the photoelectron by atoms surrounding the absorbing atom are important. Generally, this provides qualitative information about the chemical environment of the absorbing atom and adsorbate molecular orientation may be determined from spectral intensity changes observed in polarisation-dependence studies. Quantitative information including bond angles, molecular orientation and intermolecular distances can also be estimated by NEXAFS measurements.

Weaker oscillations in the absorption cross-section occur further out from the absorption edge. This is due to the influence of the wave-field of the backscattered electron at the ion core which modulates the cross-section. Oscillation frequency depends on the distance between the absorbing atom and its nearest neighbours whereas the amplitude depends on the number and type of neighbours as well as their distance from the adsorbing atom and the light polarisation relative to the internuclear bond axis. Hence, at high kinetic energies (>50 eV) single scattering theory is utilised in surface extended X-ray absorption fine structure (SEXAFS). Polarisation dependent SEXAFS is used to characterise the structure surrounding an emitter.

4. Benzenethiol Adsorption on Metal Surfaces

4.1 Surface intermediates

In order to interpret UPS results for benzenethiol (BT) adsorption, it is necessary to discuss the electronic structure of the molecule in the gas phase and the corresponding interaction diagram shown in Fig. 3 [92,93]. In the low ionisation potential region (IP < 11 eV), the three bands labelled X_1, X_2 and X_3 correspond to molecular orbitals of π symmetry and their composition is based on the outermost doubly degenerate benzene orbital and the non-bonding sulphur orbital. The sulphur 3p orbital perpendicular to the benzene ring interacts with only one of the $1e_{1g}$ orbital components resulting in a pair of mixed sulphur π orbitals split almost symmetrically about the $1e_{1g}$ orbital energy. Hence, bands X_1 and X_3 have a large contribution from sulphur while X_2 has purely aromatic ring character. In region A, between 11.0 and 13.5 eV, three bands originating from the aromatic ring are assigned to $3e_{2g}$ (which splits in the interaction diagram and arises from the degenerate $3e_{2g}$ benzene orbital with a significant amount of sulphur mixing), $1a_{2u}$ and sulphur orbitals. Four ionisation bands occur between 13.5 and 16.0 eV, two arising from the splitting of the benzene $3e_{1u}$ degenerate orbital and one from each of the virtually unaffected $1b_{2u}$ and $2b_{1u}$ orbitals of benzene, assigned as peaks B and C, respectively. Finally, peak D at 16.7 eV corresponds to the benzene $3a_{1g}$ orbital. Overall, X_1, X_3 and A contain major sulphur character while the remaining bands closely resemble those found for unsubstituted benzene [92,78].

Agron and Carlson have studied BT adsorption on Cu(111) using ARUPS [94]. UPS difference spectra collected as a function of emission angle showed a correlation (within 0.2 eV) of peaks A, B, C and D with the gas phase spectrum suggesting that these orbitals were not directly involved in bonding to the substrate. In contrast, X_1, X_2 and X_3 appeared as a single broad band indicating that BT bonds to Cu through its sulphur orbitals. This is fully consistent with the gas phase assignments describing molecular π orbitals X_1 and X_3 with substantial sulphur contributions causing them to split and broaden following adsorption while X_2 remains essentially unaffected.

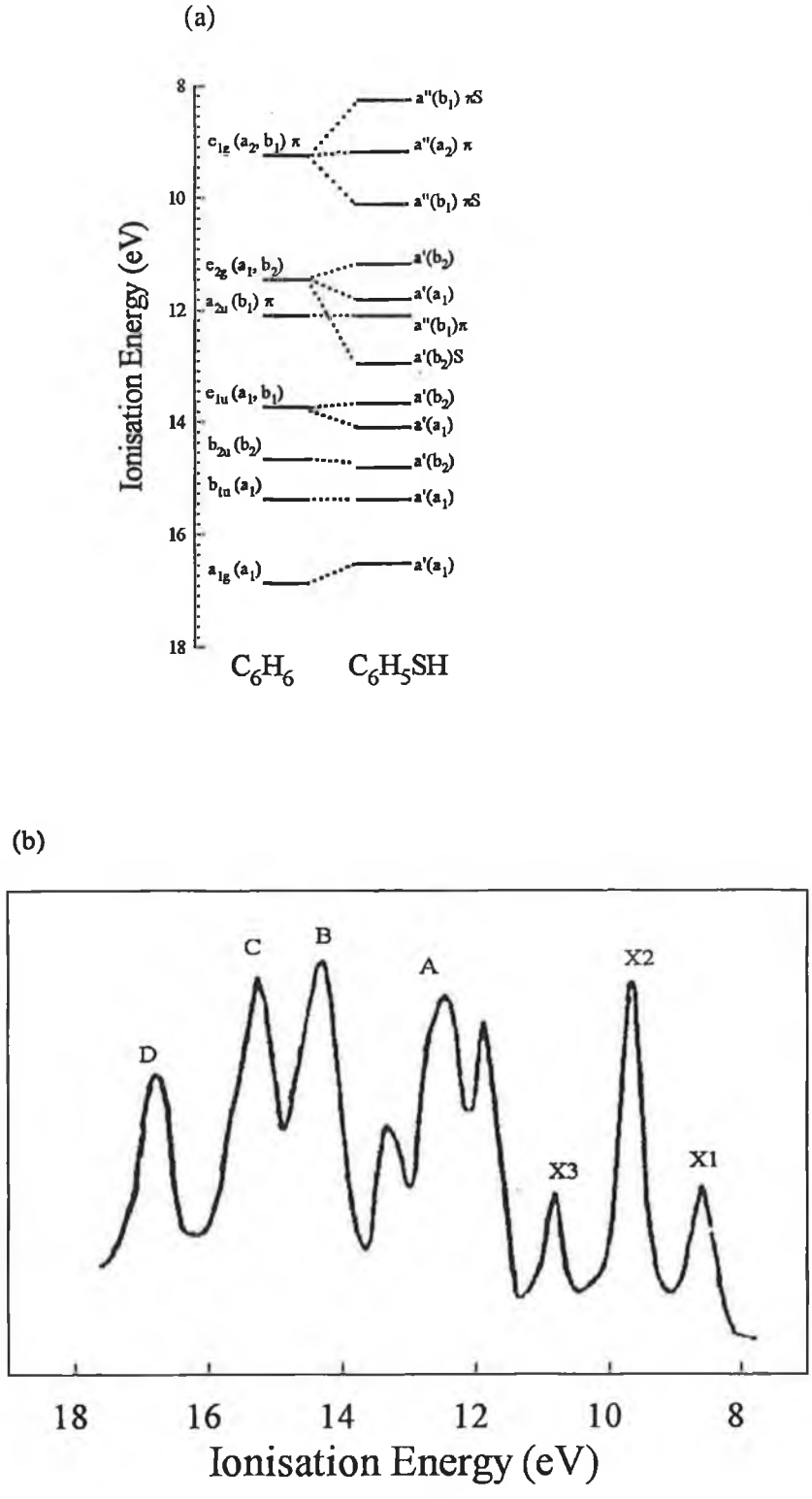

Figure 3 (a) Benzenethiol interaction diagram and band assignments. C_s and pseudo-C_{2v} (bracketed) symmetries are shown. (b) He II photoelectron benzenethiol gas phase spectrum adapted from the work of Agron *et al.* [93].

Similarly, Agron *et al.* have reported UPS spectra of BT adsorbed on Cu(110) as a function of coverage which revealed the gradual attenuation of the Cu-*d* band with the emergence of addition bands attributed to the molecular orbitals of the adsorbate [93]. Excellent correlation with the gas phase spectrum for BT was observed with the exception of those bands corresponding to orbitals with substantial sulphur character, which were shifted ~0.8 eV to higher binding energies upon adsorption, suggesting that surface bonding occurred via the sulphur atom rather than the π-orbitals of the phenyl ring. Further, the loss of the sulfhydryl hydrogen during adsorption, consistent with the formation of a benzenethiolate intermediate, was inferred by the absence of the S-H σ band.

A more comprehensive study of BT, and the related 1,2-benzenedithiol (BDT), on Cu(110) has been studied as a function of coverage and temperature by Shen *et al.* using a range of electron spectroscopic techniques [65]. Fig. 4 shows the UPS thermo-evolution from physisorbed BT multilayers adsorbed at 100 K to a chemisorbed layer, observed at 184 K for BT. The presence and behaviour of isosbestic points identified in the UPS spectra collected as a function of BT exposure at 300 K, suggested the coadsorption of atomic sulphur due to C-S bond cleavage and benzenethiolate at low exposures (2 L) [80]. This was confirmed by XPS analysis, indicating a sulphur (2p) to carbon (1s) ratio of 2.6:6.0. Similarly, BDT loses its sulfhydryl hydrogens upon adsorption and limited desulphurisation was suspected. The resulting atomic sulphur acted as an inhibitor to reduce the reactivity of the surface towards further C-S bond scission but allowed S-H bond dissociation. While the absence of a S-H stretching vibration and negative $\Delta\phi$ values confirmed the formation of molecular surface intermediates at high coverages, HREELS and work function changes (-0.74 and -0.6 eV for BT and BDT, respectively) did not support desulphurisation of either molecule at low coverage. It must be stressed, however, that at low adsorbate coverage, work function measurements do not unequivocally distinguish between molecular and atomic adsorption [95].

BT adsorption on Rh(111) has been investigated by Bol *et al.* using TDS, HREELS and XPS [59]. At sub-monolayer and saturation coverages, the molecule adsorbed dissociatively to form benzenethiolate and hydrogen at 100 K and C-S bond scission commenced at 250 K producing surface atomic sulphur and benzene. At 0.07

ML thiolate coverage, benzene remained bonded on the surface up to 450 K, at which point vibrational spectra indicated that a phenyl or benzyne surface intermediate was formed, while near saturation coverage (0.21 ML) a significant fraction of benzene was evolved into the gas phase due to molecular crowding effects discussed in section 4.4.

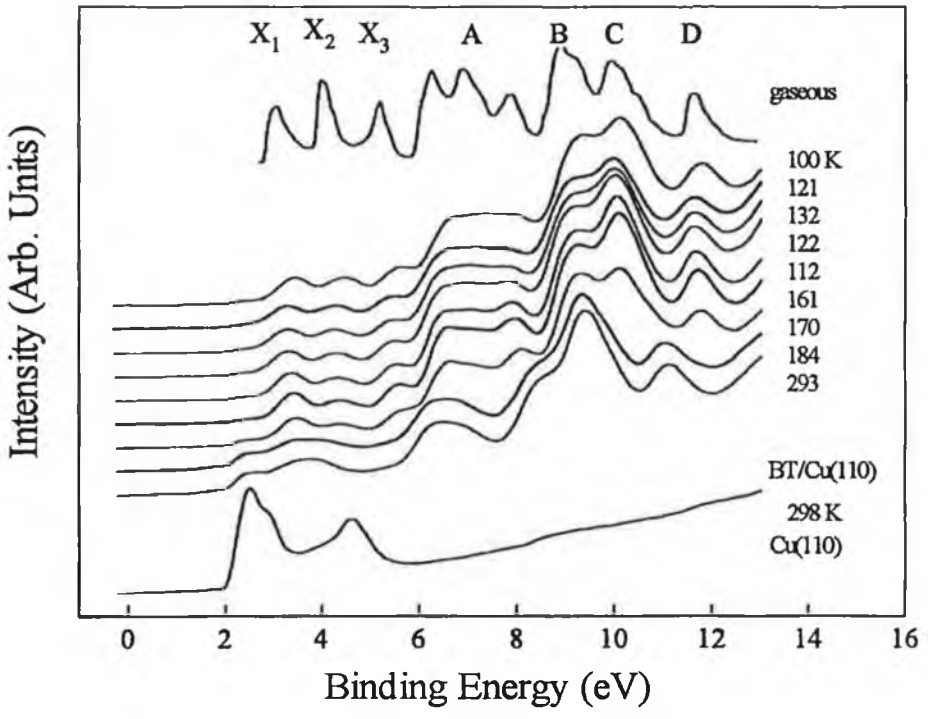

Figure 4 UPS monitored thermo-evolution of benzenethiol adsorbed on the Cu(110) surface adapted from the work of Shen *et al.* [65]. The benzenethiol gas phase spectrum is aligned with the lowest temperature adsorbate spectra.

A HREELS, XPS and TPD investigation of BT adsorption on Mo(110) has been carried out by Roberts and Friend [96]. At 120 K, dissociation of the S-H bond occurred and the C-S bond remained intact, consistent with thiolate formation. Low coverage benzenethiolate reacted (<600 K) to form carbon, sulphur and molecular hydrogen. In contrast, at high exposures, decomposition resulted in the formation of gaseous benzene and surface benzyne (both with atomic sulphur) at 350 and 370 K, respectively.

More recently, Chen *et al.* have studied BT adsorbed as condensed multilayers at 180 K followed by heating to 225 K to form a chemisorbed monolayer on Co-Mo(110) phases [97]. For all Co coverages (0.25 to 1.3 ML), both atomic sulphur and a thiolate were identified by XPS and HREELS. The primary surface intermediate formed was benzenethiolate and vibrational spectra are virtually identical to those reported for BT/Mo(110) [96]. While the products and reaction pathways for BT adsorption and decomposition are qualitatively similar to those on Mo(110), Co overlayers were found to have a marked effect on the temperature and selectivity for benzene evolution. The coverage dependent reaction kinetics exhibited by BT on clean Mo(110) and Co-Mo(110) phases are discussed in more detail in section 4.5.

Takata *et al.* have studied BT adsorption on Ni(100) by S K-edge NEXAFS [98]. Comparison of a BT multilayer (adsorbed at 130 K) K-edge spectra with that of the solid state revealed similar resonance features at both normal and grazing X-ray incidence angles implying random orientation within the physisorbed multilayers. Temperature-dependent NEXAFS (138 to 473 K) indicated desorption of BT multilayers at 180 K, resulting in a chemisorbed monolayer, and S-C bond scission at >200 K leaving atomic sulphur. Indirect evidence for dissociative chemisorption with loss of sulfhydryl hydrogen was provided upon consideration of the molecular orientation and the Ni-S bonding distance (see section 4.3).

Adsorption of BT on a Ni(110) surface has been examined by Huntley [99]. The sulphur (2p) core level emission indicated that at low temperatures and low coverages BT adsorption on Ni(110) reacted to form atomic sulphur as the primary surface sulphur species with a small amount of molecular species. HREELS indicated the presence of phenyl or benzyne species due to C-S bond scission even at low temperatures (100 K) resulting in passivation of the surface and stabilisation of the thiolate species. While the carbon (1s) spectrum was identical to that obtained from benzene on Ni(110), the HREELS spectra were inconsistent with π-bonded benzene. As the coverage increased, the contribution from molecular species became more dominant but decomposition to atomic sulphur (accounting for 1/3 of surface bound sulphur) and aryl fragments did occur. This was supported by HREELS spectra which showed the attenuation of the S-H stretching vibration relative to BT in the condensed phase and hence the primary adsorbate species was benzenethiolate. Annealing to 200

K initiated C-S bond scission resulting in surface atomic sulphur accompanied by benzene evolution and only atomic sulphur and carbon were observed above 400 K.

BT adsorption on Ni(111) results in the formation of a thiolate intermediate involving S-H bond scission at 100-110 K as evidenced by HREELS [100-102]. Kane *et al.* found that hydrogen remained on the surface following dissociative BT adsorption and played an important role in the subsequent decomposition of the thiolate species to benzene at higher temperatures [100,101]. Rufael *et al.* reported substantial C-S bond cleavage above 190 K evidenced by sulphur (2p) photoemission at a lower binding energy with complete decomposition of the thiolate by 300 K to atomic sulphur and a phenyl or benzyne group [102]. The presence of surface carbon from aryl decomposition and subsurface adsorption of carbon occurred above 500 and 600-800 K, respectively.

Adsorption of BT on Au(110) has been investigated by Jaffey and Madix [103]. Following multilayer desorption at 190 K, cleavage of the S-H bond <300 K was activated by the Au(110) surface or preadsorbed atomic sulphur. In Fig. 5, the evolution of H_2 and a mixture of H_2 and H_2S from clean and sulphided surface, respectively, during TDS of chemisorbed species was ascribed to thiolate formation from only half of the thiol adsorbed. Above 400 K, a number of different decomposition species identified mass spectroscopically were evolved as a function of BT dosing (and hence as a result of a surface reaction-limited processes). These included BT, biphenyl, dibenzothiophene, diphenyl disulphide (only on a surface with 0.2 ML of atomic sulphur) and possibly thianthrene.

Stern *et al.* have studied BT and related compounds adsorbed on Pt(111) electrodes [104]. This is the first of two examples where the overlayers were prepared by adsorption from aqueous solutions and characterised by EC-UHV techniques. HREELS spectra correlated closely with the IR spectrum from a solid sample with the exception of the S-H stretching vibration. The absence of this band suggested that BT formed a thiolate following adsorption. Similarly, liquid phase self-assembly of BT on Pt(111) and Ag(111) has been investigated by Gui *et al.* using AES, HREELS and LEED in combination with electrochemistry [105]. On both metal surfaces, BT lost its sulfhydryl hydrogen during adsorption to form benzenethiolate.

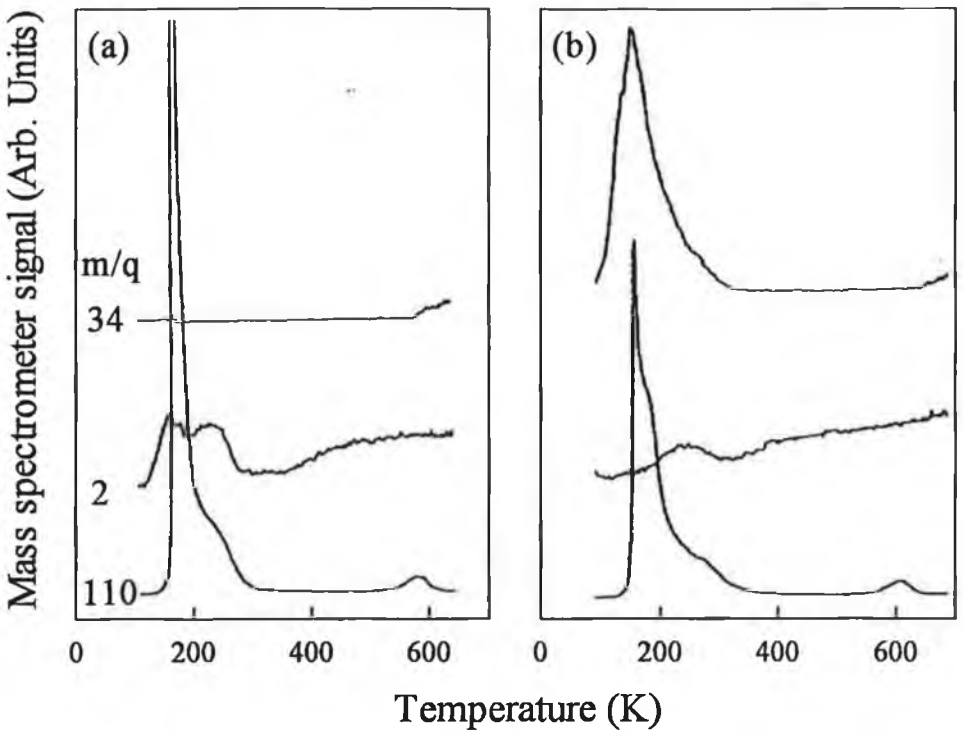

Figure 5 TDS spectra showing the evolution of benzenethiol, H_2 and H_2S following adsorption of benzenethiol on (a) clean Au(110) and (b) previously exposed Au(110) with a coverage of 0.24 and 0.19 monolayers of sulphur and carbon, respectively (adapted from the work of Jaffey and Madix) [103].

4.2 Molecular orientation of surface intermediates

Agron and Carlson examined the relative intensity of bands C and X which increased and decreased, respectively, as a function of decreasing emission angle in ARUPS, indicating that the molecule orients on the Cu(111) surface [94]. Studies of benzene adsorbed in a flat-lying orientation on metal surfaces when interaction between the π-electrons and the surface occurs shows the opposite behaviour in terms of angular dependence. Hence, the authors speculated that benzenethiolate assumes a largely perpendicular bonding configuration on Cu(111), supported by a saturation coverage of 0.63 ML of sulphur determined by XPS.

Experimentally derived orbital energies and intensities can be compared with a molecular-orbital correlation diagram to determine molecular orientation and bonding. Considering the effect of BT adsorbing (with/without S-H bond scission) either parallel via π-bonding or perpendicular via the sulphur atom bonding to the surface, Agron *et al.* concluded that the adsorbate was aligned perpendicular with respect to Cu(110) [93]. In addition, polarisation-dependence of the UPS band intensities and comparison with symmetry allowed/forbidden transitions confirmed that the plane of the phenyl ring was perpendicular to the surface.

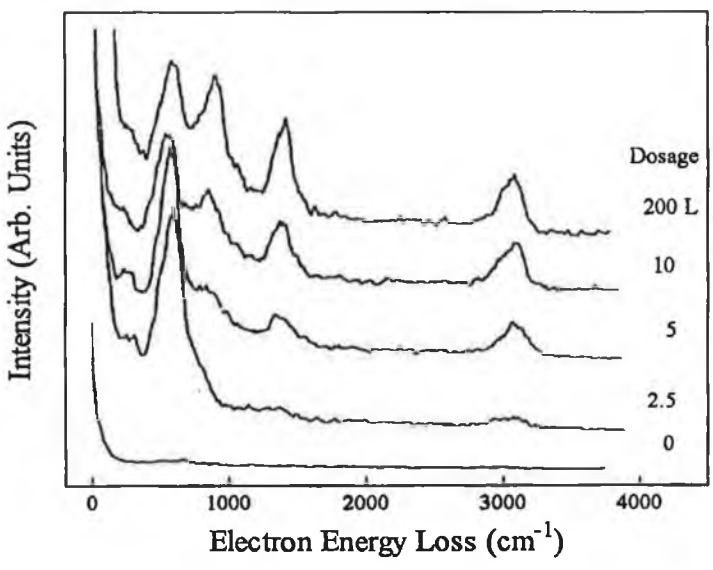

Figure 6 HREELS spectra of benzenethiol adsorption on Cu(110) at 300 K as a function of exposure, adapted from the work of Shen *et al.* [65].

Benzenethiolate and 1,2-benzenedithiolate orientational changes on Cu(110) as a function of adsorbate coverage have been reported Shen *et al.* [65]. In Fig. 6, a strong HREELS vibrational band at 750 cm^{-1} assigned to C-C and C-H out-of-plane bending ($\gamma_{C\text{-}C}$ and $\gamma_{C\text{-}H}$) is seen to decrease in intensity, relative to the C-H stretching at 3000 cm^{-1} ($\nu_{C\text{-}H}$), as the adsorbate coverage increases. In specular scattering geometry, this intensity variation provides information on the orientation of the phenyl ring relative to the Cu(110) surface plane by applying the MSSR discussed earlier [82]. As the out-of-plane C-H deformation mode is the dominant band at low exposures, this

indicates that the benzenethiolate intermediate adopts an adsorption geometry with its phenyl ring parallel to the substrate surface. However, the subsequent decrease in the 750 cm^{-1} band and concomitant increase in the in-plane C-H stretching, implies that reorientation occurs. The out-of-plane C-H stretching vibration is not completely dipole inactive indicating that the phenyl ring assumes an upright but slightly tilted orientation at higher surface coverages. Similar behaviour was observed for 1,2-benzenedithiolate adsorption as a function of exposure.

Bol *et al.* have also reported coverage-dependent reorientation of BT on Rh(111) based on variation in the intensity of the γ_{C-H} and ν_{C-H} vibrational bands [59]. With increasing BT exposure, there was clear evidence of ring reorientation from a parallel to a largely perpendicular bonding geometry with respect to the surface plane. In addition, comparison with a previous study of molecular benzene adsorbed in a flat-lying bonding configuration on Rh(111), allowed the authors to assign an energy loss feature observed at 315 cm^{-1} to Rh-phenyl ring stretching, providing evidence of coordination of the π-system with the substrate at low coverages.

The capability of NEXAFS to determine orientation of complex molecules has been demonstrated by Stohr and Outka in the case of a BT monolayer on Mo(110) [106]. The molecule contains a variety of intramolecular bonds which give rise to pronounced carbon K-edge resonances corresponding to transitions to π^* and σ^* antibonding molecular orbitals, those characteristic of benzene and a C-S σ^* resonance. NEXAFS spectra and proposed assignments are given in Fig. 7. By comparing spectra collected at normal and grazing X-ray incidence, the bonding geometry can be deduced. Analysis of the angle-dependent resonance intensity ratios derived from the C=C π^*, C=C σ^* and C-S σ^* resonances in the carbon K-shell spectra revealed that the plane of the aromatic ring and the C-S bond were tilted by 23 and 27° from the surface normal, respectively. Similarly, Roberts and Friend reported a tilted geometry (20° with respect to the surface normal) for benzenethiolate adsorbed at high coverage on Mo(110) from NEXAFS data [96]. In addition, the authors suggested that coverage dependent decomposition kinetics (outlined in section 4.5) may be related to molecular reorientation to the formation of a benzyne surface intermediate with the aromatic ring almost perpendicular with respect to the surface plane.

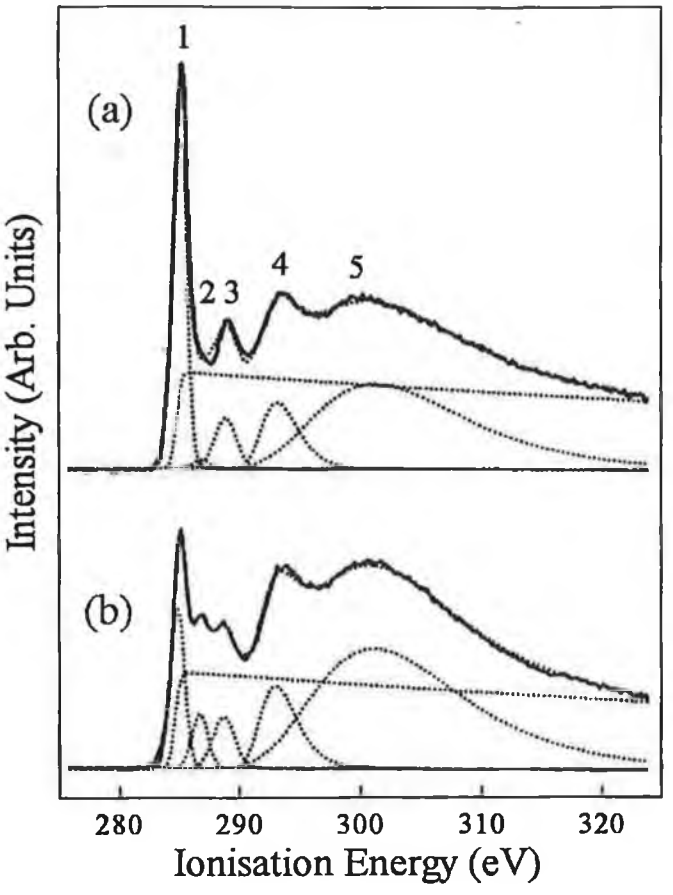

Figure 7 Carbon K-shell NEXAFS spectra of benzenethiol chemisorbed on Mo(110) collected at (a) normal and (b) at 20° grazing incidence, adapted from the work of Stohr and Outka [106]. Raw data (—) and a fit (·····) to: peak 1, C=C π^*; peak 2, C-S σ^*; peak 3, C=C π^* and C-H; and peak 4 and 5, C=C σ^*.

Interestingly, Rufael *et al.* observed a difference in HREELS spectra between low and high coverage benzenethiol adsorption on Ni(111) [102]. At low coverage, the C-H stretching region consisted of two contributions at 2915 and 3011 cm^{-1} while saturation coverage yielded a single vibrational band at 3060 cm^{-1}. The authors suggested that this shift may be related to partial rehybridisation of the aromatic ring with the surface at low coverage. At saturation coverage, the intensity of both in-plane stretching and out-of-plane bending mode suggest the adsorbate is not parallel to the surface but adopts a tilted geometry. In addition, above 240 K a phenyl fragment

resulting from C-S bond cleavage was found to tilt more strongly towards the surface normal than the thiolate intermediate. However, reorientation occurred above 300 K resulting in a spectrum which closely resembled π-bonded benzene in a parallel bonding arrangement with respect to Ni(111). The authors speculated that this orientational transition may be related to substrate structural changes.

Benzenethiolate adsorption on Pt(111) and Ag(111) has been studied by Stern *et al.* and Gui *et al.* [104,105]. While not discussed in any detail by the authors, examination of the HREELS spectra reveals a weak HREELS vibrational band at 750 cm^{-1} ($\gamma_{C\text{-}C}$ and $\gamma_{C\text{-}H}$) relative to the C-H stretching at 3000 cm^{-1} ($\nu_{C\text{-}H}$). This indicates that the benzenethiolate intermediate adopts a largely upright adsorption geometry on both surfaces.

The surface coverage of reaction intermediates resulting from desulphurisation of BT following adsorption on Ni(110) at 100 K has been examined using TDS, isotopic labeling, XPS, AES and LEED [99]. Given that the benzene adsorbs parallel to the Ni(110) surface with a saturation coverage of 0.25 ML, a maximum coverage of 0.45 ML for the BT derived intermediate suggests a bonding geometry in which the phenyl ring is strongly inclined toward the surface normal (confirmed by the high intensity of the C-H stretching vibration in the HREELS spectra). Similarly, the desorption of H_2 and H_2S was used by Jaffey and Madix to estimate the amount of benzenethiolate formed on Au(110) [103]. Comparison of the experimentally derived thiolate coverage of 0.12-0.16 ML with the VDW estimates of coverages based on flat-lying and upright bonding geometries (0.2 and 0.47 ML, respectively), clearly indicates that a layer of flat-lying molecules can be accommodated by this value.

4.3 Overlayer structure

The surface structure of BT on Ni(100) has been elucidated by Takata *et al.* using S K-edge SEXAFS and NEXAFS to determine the adsorption geometry, the adsorption site, molecular orientation and bond distances [98]. NEXAFS showed strong polarisation dependent behaviour for those peaks ascribed to σ^*(S-C) and S-Ni resonances. The σ^*(S-C) resonance intensity increase at grazing incidence indicates

that the S-C bond axis assumes a largely perpendicular orientation with respect to the Ni surface.

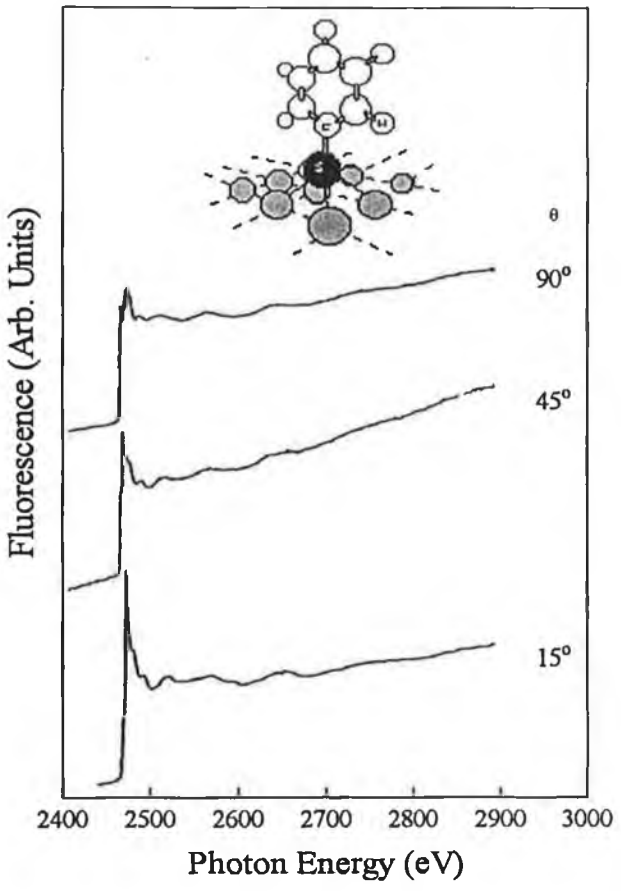

Figure 8 Raw S K-edge SEXAFS spectra of benzenethiol adsorbed on Ni(100) at 120 K followed by heating to 200 K, measured at X-ray incidence angles of 90, 45 and 15° (with respect to the surface plane). Adapted from the work of Takata *et al.* [98]. Inset: a schematic diagram of benzenethiol adsorbed at the 4-fold hollow site of the Ni(100) surface with S-Ni and S-C distances of 2.25 and 1.84 Å, respectively.

In Fig. 8, SEXAFS S K-edge spectra collected at different X-ray incident angles exhibit strong oscillations in a region associated with the presence of S-Ni bonds. Manipulation of the data using Fourier transforms and empirical curve fitting allowed extraction of the S-Ni and C-S coordinations and interatomic distances. The authors concluded that the thiolate adsorbed at the 4-fold hollow site (Fig. 8 inset) with S-Ni and S-C distances of 2.25 and 1.84 Å, respectively. Similarity between NEXAFS spectra from a c(2×2)S/Ni(100) overlayer and following benzenethiolate C-

S bond cleavage (>200 K) leaving surface atomic sulphur provided further proof for occupancy of the 4-fold hollow site.

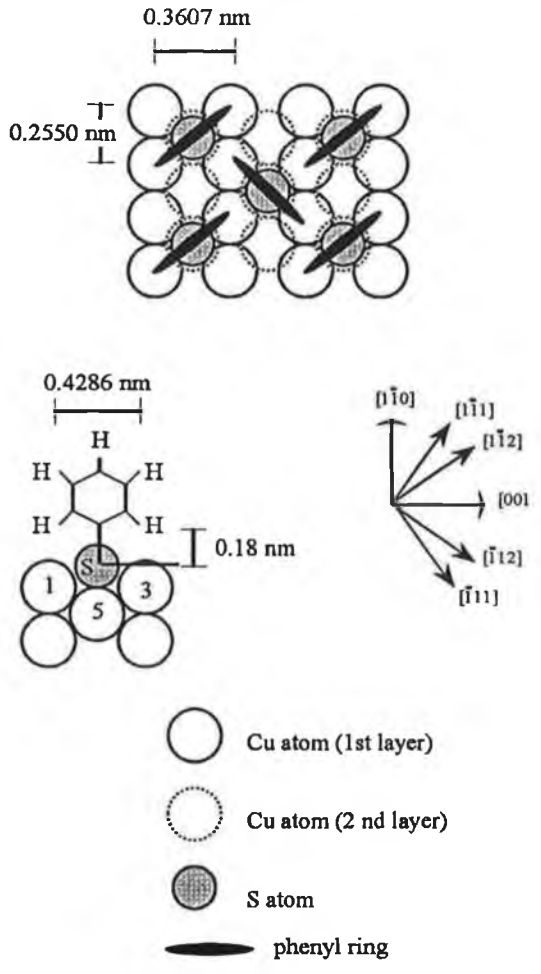

Figure 9 Schematic diagram of benzenethiol adsorbed on Cu(110) in a c(2×2) geometry showing substrate atoms, bonding sites and phenyl ring orientation in which alternate rows are parallel to the [111] azimuthal direction [93].

Having assigned an upright bonding configuration for benzenethiolate on Cu(110) using ARUPS, Agron *et al.* attempted to solve the question of the adsorption geometry and phenyl ring azimuthal orientation [93]. Since the VDW radius of the adsorbate (3.7 Å) is similar to the lattice spacing in the [001] direction but exceeds that in the [110] direction, the molecule must occupy alternate sites in the [110] direction to give the closest packing in registry with the substrate and adopt a c(2×2) geometry.

Various azimuthal orientations were considered by packing the rings, based on molecular cross-sections, parallel to the [110], [001], [111] and [112] azimuthal directions. The c(2×2) coverage of 0.5 ML will not permit free rotation of the phenyl rings and substantial overlap of the ring hydrogens must be avoided, thus eliminating several molecular packing arrangements. Nevertheless, a choice of conformations exists and the final selection of the [111] configuration shown in Fig. 9 is based minimising adsorbate overlap with maximum substrate coverage. This is consistent with bulk packing of rings in aromatic crystals (see section 2.2).

The HREELS study of BT and BDT adsorption on Cu(110) revealed differences in surface order between the monolayers systems [65]. Low exposures resulted in an increase in the elastic peak intensity for both adsorbates, which is strongly dependent on surface order. This intensity increase was further enhanced following continued BT exposure suggesting formation of a highly ordered monolayer. The opposite was found for higher coverages of 1,2-benzenedithiolate which forms a disordered adlayer due to the restriction imposed by the presence of two sulphur-metal bonds preventing free rotation.

Stern *et al.* and Gui *et al.* reported the absence of long range order following BT adsorption on Pt(111) as evidenced by a diffuse LEED pattern [104,105]. In contrast, a sharp $(\sqrt{7}\times\sqrt{31},88°)R40.9°$ LEED pattern was observed for BT on Ag(111). Since the area of the $(\sqrt{7}\times\sqrt{31})$ unit mesh is 122.1 $Å^2$ and the area of a BT molecule in a vertical orientation (suggested by vibrational data) is 24.79 $Å^2$ based on covalent and VDW radii, the maximum number of adsorbate species per unit cell (consisting of 17 Ag atoms) is four with the benzene rings closely packed face-to-face.

4.4 Adsorbate-adsorbate interactions

The uptake of chemisorbed BT on Ni(110) as determined by AES and TDS was found by Huntley to increase linearly with exposure up to saturation coverage of 0.45 ML [99]. This suggests a coverage independent sticking probability perhaps due to a precursor-mediated adsorption mechanism. The 0.45 ML surface coverage is less than that found for sulphur (0.55-0.6 ML) resulting from H_2S adsorption on this

surface, probably due to steric effects within the overlayer induced by the bulky aromatic pendent group. In addition, benzene desorption at 470 K was accompanied by a lower temperature state at 235 K as benzenethiol exposures increase (>0.36 ML). This was tentatively explained by the author as a sign of adsorbate-adsorbate 'crowding' of the aromatic groups at high coverages. The molecules may respond by adopting a more upright configuration with respect to the surface, inducing considerable strain on the C-S bond. This may indeed manifest as a reduction in thiolate stability resulting in the low temperature desorption peak. Initial thiolate reaction resulting in benzene evolution would thus alleviate the strain within the system, allowing a more favourable bonding geometry to be adapted, observed as a higher temperature desorption state.

Evidence of steric crowding effects have been presented in the work of Bol *et al.* for BT adsorption to high coverages on Rh(111) [59]. The orientation of the phenyl ring and the commencement of C-S bond cleavage and, hence, benzene production depends strongly on the thiolate coverage. At low coverage (0.07 ML), HREELS revealed that the π-system bonds to the surface and TDS showed a single benzene desorption state at 450 K which is close to that reported for molecular benzene desorbing from Rh(111) [55,57]. As the thiolate coverage increased (>0.1 ML), the phenyl ring reoriented to a largely upright configuration and a second desorption state was observed at 280 K. There are two factors which may contribute to the high coverage, low temperature desorption process. Firstly, steric effects due to repulsive ring-ring interactions may destabilise the thiolate intermediate by lowering the heat of adsorption and, secondly, bonding to the surface is inhibited by a high surface concentration of atomic sulphur remaining after C-S bond cleavage, such that the majority (85%) of benzene is evolved directly into the gas phase.

4.5 Thermal stability of overlayers

The practical application of isosbestic points in UPS spectra have been detailed by Anderson and Nyberg in the study of BT adsorption Cu(410) [80]. In Fig. 10, the photoemission difference spectra reveal the presence of an isosbestic point in the low

exposure limits (1 to 5 L), the absence of molecular bands at high binding energies and, characteristic of atomic adsorbates, an increase in intensity at low binding energies (4 to 6 eV). Molecular bands develop at higher exposures. The initial adsorbate species appears to saturate between 5 and 10 L with no further evidence of an isosbestic point suggesting that molecular adsorption occurs on a completely 'preadsorbed' surface.

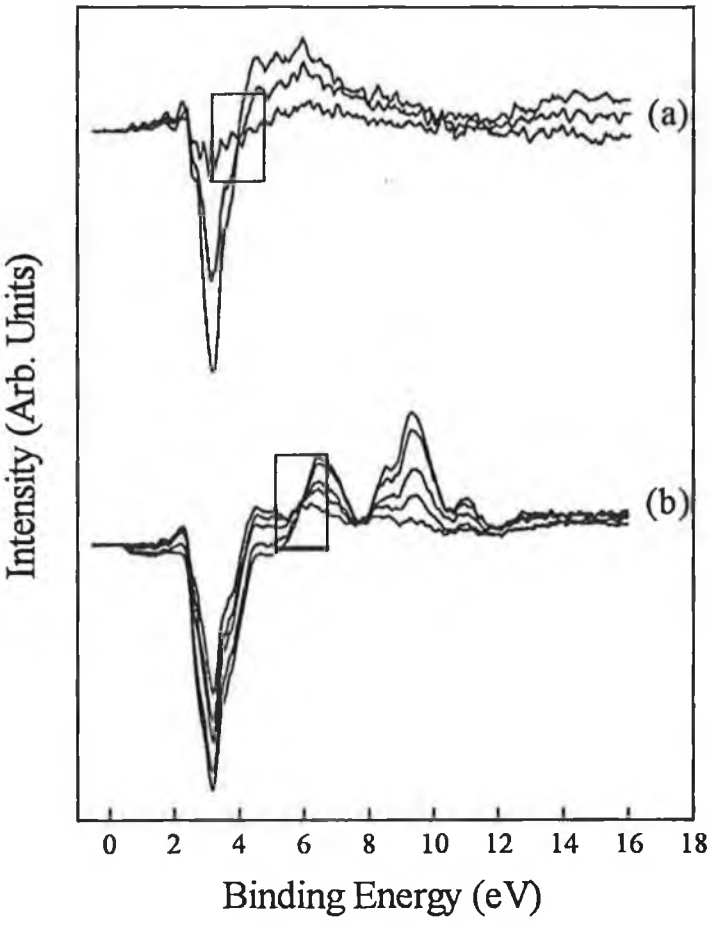

Figure 10 UPD difference spectra of benzenethiol adsorbed on Cu(410) following exposures of (a) 1, 3 and 5 and (b) 10, 15, 20, 40 and 250 L. Isosbestic points are inset. Adapted from the work of Anderson and Nyberg [80].

The authors postulated that BT decomposition resulting in surface atomic sulphur occurs prior to molecular adsorption. This is not surprising given that low coverage desulphurisation has also been observed on Cu(110) and in comparison the stepped Cu surface would be predicted to be more reactive [94].

Integration of the carbon (1s) and sulphur (2p) photoemission intensities have been used by Roberts and Friend to measure the surface stoichiometry following adsorption and decomposition of BT on Mo(110) [96]. In particular, the data indicated that at high exposures, 40% of benzenethiolate reacted to form gaseous benzene and atomic sulphur while 60% decomposed to surface benzyne and atomic sulphur. In addition, the thiolate reaction kinetics were coverage dependent with the activation energy for decomposition increasing with increasing exposure. This was attributed to inhibition of C-S bond cleavage at higher thiolate coverages due to a reduction in surface reactivity or thiolate reorientation. The authors proposed two competing phenyl thiolate reaction pathways dependent on the surface hydrogen atom concentration on Mo(110). At high hydrogen coverage, gas phase benzene and atomic sulphur are formed from hydrogenolysis of the C-S bond. Atom recombination and thiolate hydrogenolysis decreases the hydrogen atom coverage, resulting in chemisorbed benzyne (C_6H_4) and atomic sulphur formation from thiolate dehydrogenation. The benzyne formed is stabilised against C-H bond scission, resisting decomposition to gaseous dihydrogen and atomic carbon until 680 K, by the presence of sulphur and an upright bonding geometry due to a weakened metal-benzene interaction.

More recently, Chen *et al.* reported that desulphurisation of BT on Co-Mo(110) phases to benzene and atomic sulphur (>250 K) competes with decomposition to molecular hydrogen and adsorbed carbon [97]. In particular, the onset temperature decreased from 250 to 180 K and the selectivity increased from 40 to 65% for benzene production, as the coverage of Co increased from 0 to 1.3 ML. This indicates that C-S bond scission occurs at lower temperatures on Co overlayers than on clean Mo(110). Similarly, molecular hydrogen evolution shifts to lower temperature with increasing Co coverage, reflecting a greater tendency for C-H bond scission on Co.

Rufael *et al.* have identified two coverage dependent pathways for benzene desorption from benzenethiol layers on Ni(111) [102]. At coverages < 0.1 ML, desorption of benzene occurs at 400 K assigned to a desorption-limited process. Increasing the coverage results in the emergence of additional desorption features at

much lower temperatures attributed to a reaction-limited process caused by the presence of surface sulphur which inhibits benzene chemisorption.

Kane *et al.* demonstrated competition between hydrogen addition and alkylation in the formation of toluene (accompanied by methane and benzene) from the reaction of coadsorbed methanethiol and BT on Ni(111) [101]. At 100 K, both thiols react stoichiometrically to form thiolates and surface hydrogen. While toluene evolution is limited by C-S bond scission and hence increases with thiolate coverage, increasing the source of hydrogen decreases this yield by up to 25%. Substrate oxidation counteracts this effect by reacting with hydrogen to form water, facilitating a 20 fold increase in toluene production. Hence, carbon-carbon bond formation from coadsorption of an aryl- and alkane-thiol is enhanced by suppression of hydrogen addition.

In a later publication, Kane *et al.* reported on the role of hydrogen in the formation of benzene from benzenethiolate on Ni(111) [100]. In agreement with Rufael *et al.*, at saturation coverage of BT (0.21 ML) surface hydrogen recombination (from thiolate decomposition) was accompanied by partial aromatic ring and surface hydrocarbon dehydrogenation. In the presence of preadsorbed hydrogen, AES showed a decrease in thiol adsorption and, while the temperature at which C-S bond cleavage occurred was unchanged, a decrease in the amount of carbon remaining on the surface following decomposition was observed. At low BT coverage (0.1 ML), the benzene yield decreased substantially and high temperature desorption dominated. Increasing the availability of surface hydrogen, enhanced benzene formation.

Huntley characterised the mechanism of adsorption and desulphurisation of BT on a Ni(110) surface [99]. Using a combination of techniques including TDS, deuterium labelling, XPS and HREELS, a hydrogenolysis mechanism was proposed. Saturation of the surface with deuterium/hydrogen prior to BT adsorption, resulted in an increase in the rate of benzene formation indicating that addition of hydrogen is the rate-limiting step. This was supported by XPS data which suggested benzene desorption accompanied C-S bond scission. Similar to the experiment described by Kane *et al.*, substrate oxidation prior to BT adsorption reduced the availability of hydrogen leading to attenuation of low temperature benzene desorption and shifted the onset to higher temperature [100,101].

Benzenethiolate decomposes on Au(110) at >400 K via three mechanisms to give a range of high molecular weight products [103]. At >600 K, cleavage of C-S bonds results in competitive thiolate-phenyl combination and phenyl groups recombination to form biphenyl and diphenyl sulphide, respectively. Desorption of mass 110 at 630 K is surprising and the authors proposed a precursor structure, which bonds to the surface via a sulphur atom and a benzene ring carbon atom, formed by hydrogen transfer between thiolate intermediates. Formation of this precursor would provide a source of hydrogen necessary for benzenethiol formation and reaction between two such species (accompanied by sulphur removal) provides an explanation the simultaneous detection of dibenzothiophene. Again, this study highlights the importance of hydrogen availability which is a common feature of benzenethiolate decomposition processes [99-102].

4.6 Ex situ characterisation of SAMs

While a few studies deal with self-assembly of benzenethiol from the liquid phase on (111) textured Au films, polycrystalline surfaces have been more widely used as substrates. Hence, the following discussion is not restricted to well defined single crystal substrates due to the limited number of *ex situ* studies available for review.

Surface order within a monolayer of BT adsorbed from the liquid phase on Au (111) textured films on mica has been studied by Dhirani *et al.* using scanning tunneling microscopy (STM) which revealed the absence of molecular periodicity [107]. Similarly, contact angle measurements and ellipsometry reported by Sabatani *et al.* indicated that the molecule forms poorly defined layers on Au (evaporated on glass) [108]. This behaviour was attributed to a non-perpendicular orientation of the phenyl ring with respect to the surface plane resulting in poor packing within the monolayer.

Tao *et al.* have investigated liquid phase self-assembly of BT on Au(111) films on mica using cyclic voltammetry, reflection absorption infrared spectroscopy (RAIRS), STM, ellipsometry and contact angle measurements [109]. In electrochemical experiments, the desorption peak observed in the current-potential curve was measured as an estimate of surface coverage which would appear to be

difficult in the case of BT as the desorption features are broad and ill-defined. Nevertheless, relating the integrated area under the voltammetric peak to the number of molecules desorbed from the surface as a thiolate, a saturation coverage of 0.2 ML of sulphur was determined. Estimation of a layer thickness of 1.3 Å does not accommodate the molecular dimensions of the adsorbates which was attributed to uncertainty associated with ellipsometry measurements, i.e., the possibility of substrate contamination. RAIRS showed a negative shift in the ring stretch mode region (from 1472 to 1515 cm^{-1}), attributed to a molecular orientation in which the BT phenyl ring is inclined towards the Au surface in agreement with Sabatani *et al.* and in fact the surface coverage of 0.2 ML is close to that predicted for a largely flat-lying orientation on the basis of the VDW dimensions of the molecule [108]. In conflict with the previous studies of a strongly tilted intermediate, Carron and Hurley have used surface enhanced Raman spectroscopy (SERS) to determine the molecular orientation of benzenethiol adsorbed on Au, Ag and Cu films and reported tilt angles of between 5 and 14 ° with respect to the surface normal [110]. However, it must be emphasised that in this case the substrates were polycrystalline.

Recently, the electronic structure and orientation of BT self-assembled from aqueous solutions on polycrystalline Au has been studied by Abduaini *et al.* using UPS and Penning ionisation electron spectroscopy (PIES) with excitation energies of 21.22 and 19.82 eV, respectively [111]. The authors reported close correspondence between PIES spectra from BT in the gas phase and chemisorbed as a monolayer with the exception of orbitals with substantial sulphur character involved in bonding with the substrate. The observed binding energy shift of 0.8 eV for the sulphur-π orbitals compares well with ARUPS studies of BT on Cu(110) by Agron *et al.* (section 4.1) [93]. Relative band intensities were used to extract information regarding the molecular orientation of BT on Au, which was found to be upright at 300 K. Interestingly, heating the monolayer to 500 K induced disorder within the layer and the molecule became more strongly tilted away from the surface normal. The authors considered the change in orientation to be caused by desorption of a small number of physisorbed molecules which remained weakly bound to the chemisorbed monolayer following its removal from solution. At 600 K, desorption of chemisorbed species occurred and the UPS spectrum showed the emergence of the Au 5d bands which were

not observed prior to self-assembly due to contamination in air, suggesting that the substrate was 'cleaned' by adsorption and desorption of BT.

A SERS study by Sandroff and Herschbach of BT and BDT adsorption from the liquid phase on Ag films (evaporated onto silica) revealed the formation of a thiolate intermediate [112]. Hence, in agreement with previous studies of *n*-dialkyl disulphide self-assembly, diphenyl dithiol undergoes S-S bond scission to form the corresponding thiolate species as evidenced by the absence of a S-S stretch (523 cm^{-1}). This is in contrast with gas phase adsorption of BT and BDT on Cu(110) which resulted in the formation of thiolate and dithiolate species, respectively [65]. In addition, the ring stretching frequencies indicated that the phenyl ring was flat-lying on Ag in disagreement with the largely upright bonding geometry reported by Carron and Hurley [110].

BDT adsorption on Ag and Au films (evaporated onto glass) has also been investigated by Lee *et al.* using RAIRS, quartz crystal microbalance and ellipsometry [113]. The molecule was found to chemisorb as a dithiolate intermediate with tilt angles of 51 and 38° (with respect to the surface normal) on Au and Ag, respectively. In disagreement with the work of Sandroff and Herschbach, which reported monomolecular self-assembly of thiolate species on Ag from 10^{-3} M solution, Lee *et al.* observed multilayered film formation on Ag upon adsorption from concentrated solutions, 10^{-3} to 10^{-5} M, and monolayers could be only be formed by immersion in very dilute solutions (10^{-6} M) [112].

5. Discussion

In agreement with *n*-alkanethiol self-assembly on metal surfaces, BT gas phase adsorption to saturation coverage on Cu(110), Cu(111), Cu(410), Au(110), Ni(100), Ni(110), Ni(111), Mo(110) and Rh(111) single crystals and Co-Mo(110) phases, involves S-H bond cleavage below 300 K producing benzenethiolate as the primary surface intermediate [59,65,80,93,94,96-103]. Similarly, liquid phase self-assembly of BT, on Pt(111) and Ag(111) single crystal electrodes results in dissociative chemisorption and the formation of a thiolate species [104,105].

With the exception of Au(110), for which arguments based on surface coverage estimation imply a flat-lying bonding geometry, the molecular orientation adopted by the thiolate adsorbed from the gas phase to saturation coverage has been reported to be largely upright but tilted away from the surface normal [103,59,65,93,94,96-105]. In the case of Ni(100), the adsorption geometry, adsorption site, molecular orientation and bond distances for have been determined from SEXAFS and NEXAFS data [98]. The thiolate adsorbs in an upright configuration at the 4-fold hollow site with S-Ni and S-C distances of 2.25 and 1.84 Å, respectively. NEXAFS data has also been used to assign a 23° tilt from the surface normal for the plane of the benzenethiolate ring on Mo(110) [106]. These two systems are the only studies in which the molecular orientation or structure of the overlayer have been determined with a high degree of accuracy. In general, little is known about the surface structure adopted by benzenethiolate and the phenyl ring orientation has been indirectly deduced from the polarisation- or angle-dependence of ARUPS band intensities, application of the MSSR in HREELS measurements and comparison of surface coverage with theoretical packing densities.

Few studies have investigated the coverage dependence of BT bonding. There is, however, sufficient evidence from the characterisation of BT adsorption on Rh(111), Cu(110) and Ni(111) to suggest that self-assembly is indeed determined by competition between metal-thiolate bond formation and bonding between the substrate and the π-orbitals of the phenyl ring system [59,65,102]. On Cu(110), a coverage-dependent reorientation of benzenethiolate from a flat-lying to upright bonding configuration has been reported [65]. Evidence of benzene ring rehybridisation was

observed for BT adsorbed on Ni(111) at low coverage, indicative of a parallel bonding geometry, while at saturation coverage the molecule adopted a tilted geometry [102]. Parallel π-bonding of BT on Rh(111) is suggested by the higher heat of desorption for benzene (~10 kcal mol^{-1}) and the presence of a Rh-phenyl ring vibrational loss at low exposures [59]. At higher coverages, the number of Rh-sulphur bonds are maximised by reorientation of the thiolate to a more upright geometry which is influenced by ring-ring lateral interactions. The uptake behaviour of chemisorbed BT on Ni(110) also suggests molecular crowding effects within the overlayer induced by the bulky phenyl group [99]. However, it is fair to say that in-depth investigation of molecular orientation and, in particular, adsorbate-adsorbate interactions as a function of coverage is sadly lacking in studies of BT adsorption behaviour.

The adoption of a largely flat-lying benzenethiolate monolayer on Au(110) is rather surprising [103]. While this may serve to maximise the interaction of the benzene ring π-system with the surface, due to the weak nature of the interaction of molecular benzene on Au surfaces, the energy gain for flat-lying intermediate would be predicted to be small. A phase transition to an upright geometry at higher coverage would increase packing density and, hence, maximise the number of sulphur-metal bonds formed. It is possible that the loss of chemisorption interaction of the phenyl ring with the Au(110) surface, inherent in a phase transformation from a flat-lying to an upright orientation, is counteracted by an increase in energy due to an increased lateral repulsion between neighbouring sulphur atoms as the two-dimensional density is increased making the transition unfavourable.

The products and reaction pathways for BT adsorption and decomposition are quite complex. At low coverages, C-S bond scission has been observed following BT adsorption on Cu(110), Cu(410), Ni(110) and Co-Mo(110) phases [65,80,99,97]. This often results in passivation of the surface against further desulphurisation and stabilisation of a thiolate species at higher exposures due to a reduction in surface reactivity [65,99]. In many cases, a phenyl or benzyne intermediate remains bonded to the substrate following decomposition of low coverages of thiolate [59,96,99,102]. At higher exposures, benzene is evolved directly into the gas phase as atomic sulphur inhibits coordination of the aromatic ring with the surface [102]. In addition, in studies where hydrogen remains bonded to the surface following dissociative BT adsorption,

or transfers from one thiolate species to another in the case of formation of a precursor structure on Au(110), the thiolate decomposition mechanism frequently depends on hydrogen availability [59,99-103]. This has been demonstrated by following the decomposition process in the presence of coadsorbed and preadsorbed hydrogen or by reducing the surface hydrogen atom concentration (through substrate oxidation) [100,101].

Ex situ characterisation of BT SAMs is plagued by problems associated with using 'non-ideal' substrates, i.e., polycrystalline materials and evaporated films, which present multiple adsorption sites and a high surface defect density for the adsorption process and adventitious contamination of the substrate upon exposure to the ambient prior to self-assembly. While serious discrepancies exist between different studies of benzenethiol on Au, Ag and Cu, it is fair to conclude that the molecule adsorbs as a thiolate intermediate and the phenyl ring assumes a tilted, as opposed to perfectly upright or flat-lying, orientation with respect to the surface plane [107-113].

Table 1 Summary of gas phase adsorption of BT on metal surfaces.

Substrate	Technique(s)	Points of Interest	Reference
Cu(111)	ARUPS, XPS	thiolate, upright orientation	94
Cu(410)	UPS	atomic sulphur + thiolate, isosbestic points	80
Cu(110)	ARUPS, $\Delta\phi$ HREELS, XPS,	thiolate + atomic sulphur, coverage-dependent reorientation	65,93
Rh(111)	TDS, XPS, HREELS	thiolate, coverage-dependent reorientation, steric crowding	59
Mo(110)	NEXAFS, TDS, XPS, HREELS	thiolate, 23° tilt, coverage-dependent decomposition	96,106
Co-Mo(110)	TDS, XPS, HREELS	atomic sulphur + thiolate, selectivity for benzene evolution	97
Ni(100)	NEXAFS, AES SEXAFS, LEED	thiolate, upright orientation, S-Ni = 2.25 Å, C-S = 1.84 Å	98
Ni(110)	HREELS, TDS, XPS, AES, LEED	atomic sulphur + thiolate, adsorbate-adsorbate interactions	99
Ni(111)	TDS, HREELS, XPS, AES, LEED	thiolate + hydrogen, rehybridisation	100-102
Au(110)	TDS, AES	thiolate, flat-lying orientation	103
Ag(111)	HREELS, AES	thiolate, upright orientation	105
Pt(111)	HREELS, AES	thiolate, upright orientation	104,105

6. Conclusions

Adsorption of aromatic thiols, for which benzenethiol acts as a prototype system, is of interest with respect to the basic aspects of adsorbate-substrate interactions which potentially involves two chemisorption bonds; a metal-sulphur bond and a secondary interaction between the π-system and the substrate. Benzenethiol adsorption on metal surfaces has been extensively studied using a wide range of characterisation tools. The *ex situ* approach has yielded very little detailed information. While there is general agreement that benzenethiol monolayers self-assembled from the liquid phase are disordered and comprise of a thiolate surface intermediate, a discrepancy exists as to whether the molecular orientation adopted is strongly tilted or largely upright with respect to the surface normal. In contrast, identification of surface intermediates, determination of molecular orientation and adsorbate surface coverage, insight into adsorbate-adsorbate interactions and complex decomposition mechanisms have been provided by surface sensitive UHV techniques (Table 1). Common to all these studies, benzenethiolate is identified as the primary surface bound intermediate at high exposures and, with the exception of Au(110), a largely upright bonding configuration has been determined with a slight inclination of the phenyl ring (~20°). However, coverage dependent molecular orientations and reaction kinetics, evidence of phenyl ring-substrate bonding and steric crowding effects suggest that, even in the case of such a simple aromatic thiol, elucidation of the mechanism of self-assembly is non-trivial. Hence, in order to develop a comprehensive understanding of aromatic SAMs it is necessary to adopt a 'fundamental' approach, involving model adsorption studies on single crystal metal surfaces.

7. References

[1] A.J. Bard, H.D. Abruna, C.E.D. Chidsey, L.R. Faulkner, S.W. Feldberg, K. Itaya, M. Majada, O. Melroy, R.W. Murray, M.D. Porter, M.P. Soriaga and H.S. White, J. Phys. Chem., **97** (1993) 7147 and selected references cited therein.

[2] D. Mandler and I. Turyan, Electroanalysis, **8** (1996) 207.

[3] D.R. Jung and A.W. Czanderna, Crit. Rev. Solid State Mater. Sci, 19 (1994) 1.

[4] D.L. Allara, Biosens. Bioelectron., **10** (1995) 771.

[5] A. Ulman, An Introduction to Ultrathin Organic Films: from Langmuir-Blodgett to Self-Assembly, Academic, New York, 1991.

[6] L.H. Dubois and R.G. Nuzzo, Annu. Rev. Phys. Chem., **43** (1992) 437.

[7] A. Ulman, Chem. Rev., **96** (1996) 1533.

[8] G.E. Poirier, Chem. Rev., **97** (1997) 1117.

[9] L. Sun, B. Johnson, T. Wade and R.M. Crooks, J. Phys. Chem., **94** (1990) 8869.

[10] J.J. Hickman, D. Ofer, P.E. Laibinis, G.M. Whitesides and M.S. Wrighton, Science, **252** (1991) 688.

[11] D.M. Collard and C.N. Sayre, J. Electroanal. Chem., **375** (1994) 367.

[12] R.J. Willicut and R.L. McCarley, J. Am. Chem. Soc., **116** (1994) 10823.

[13] T. Ito, P. Buhlmann and Y. Umezawa, Anal. Chem., **70** (1997) 255.

[14] S.R. Cohen, R. Naamam and J. Sagiv, J. Phys. Chem., **90** (1986) 3054.

[15] C.D. Bain, E.B. Troughton, Y.T. Tao, J. Evall, G.M. Whitesides and R.G. Nuzzo, J. Am. Chem. Soc., **111** (1989) 321.

[16] S.R. Wasserman, G.M. Whiteides, I.M. Tidswell, B.M. Ocko, P.S. Pershan and J.D. Axe, J. Am. Chem. Soc., **111** (1989) 5852.

[17] R.C. Thomas, L. Sun and R.M. Crooks, Langmuir, 7 (1991) 620.

[18] L. Sun and R.M. Crooks, J. Electrochem. Soc., **138** (1991) L23.

[19] M. Buck, M. Grunze, F. Eisert, J. Fischer and F. Trager, J. Vac. Sci. Technol. A, **10** (1992) 926.

[20] G. Hahner, Ch. Woll, M. Buck and M. Grunze, Langmuir, **9** (1993) 1955.

[21] M.D. Porter, T.B. Bright, D.L. Allara and C.E.D. Chidsey, J. Am. Chem. Soc., **109** (1987) 3559.

[22] R.G. Nuzzo, F.A. Fusco and DL. Allara, J. Am. Chem. Soc., **109** (1987) 2358.

[23] R.G. Nuzzo, B.R. Zegarski and L.H. Dubois, J. Am. Chem. Soc., **109** (1987) 733.

[24] Y. Li, J. Huang, R.T. McIver and Hemminger, J. Am. Chem. Soc., **114** (1992) 2428.

[25] S.W. Benson, Chem. Rev., **78** (1978) 23.

[26] Nuzzo, L.H. Dubois and DL. Allara, J. Am. Chem. Soc., **112** (1990) 558.

[27] Whitesides and P.E. Laibinis, Langmuir, **6** (1990) 87.

[28] J.B. Schlenoff, M. Li and H. Ly, J. Am. Chem. Soc., **117** (1995) 12528.

[29] C.E.D. Chidsey, G.-Y. Liu, Y.P. Rowntree and G. Scoles, J. Chem. Phys., **91** (1989) 4421.

[30] C.A. Widrig, C.A. Alves and M.D. Porter, J. Am. Chem. Soc., **113** (1991) 2805.

[31] C.A. Alves, E.L. Smith and M.D. Porter, J. Am. Chem. Soc., **114** (1992) 1222.

[32] P. Fenter, P. Eisenberger and K.S. Liang, Phys. Rev. Lett., **70** (1993) 2447.

[33] A.J. Leavitt and T.P. Beebe, Jr., Surf. Sci., **314** (1994) 23.

[34] H.A. Biebuyck, C.D. Bain and G.M. Whitesides, Langmuir, **10** (1994) 1825.

[35] C.D. Bain, H.A. Biebuyck and G.M. Whitesides, Langmuir, **5** (1989) 723.

[36] P.E. Laibinis, G.M. Whitesides, D.L. Allara, Y.-T. Tao, A.N. Parikh and R.G. Nuzzo, J. Am. Chem. Soc., **113** (1991) 7152.

[37] L. Strong and G.M. Whitesides, Langmuir, **4** (1988) 546.

[38] C.E.D. Chidsey and D.N. Loiacono, Langmuir, **6** (1990) 709.

[39] N. Camillone, C.E.D. Chidsey, G.-Y. Liu, T.M. Putvinski and G. Scoles, J. Chem. Phys., **94** (1991) 8493.

[40] L.H. Dubois, B.R. Zegarski and R.G. Nuzzo, J. Electron Spectrosc. Relat. Phenom., **54/55** (1990) 1143.

[41] S.D. Evans, E. Uranker, A. Ulman and N. Ferris, J. Am. Chem. Soc., **113** (1991) 4121.

[42] S.-C. Chang, I. Chao and Y.-T. Tao, J. Am. Chem. Soc., **116** (1994) 6792.

[43] L. Zhang, T. Lu, G.W. Gokel and A.E. Kaifer, Langmuir, **9** (1993) 786.

[44] R.W. Zehner and L.R. Sita, Langmuir, **13** (1997) 2973.

[45] J.M. Tour, L. Jones, D.L. Pearson, J.J.S. Lamba, T.P. Burgin, G.M. Whitesides, D.L. Allara, A.N. Parikh and S.V. Atre, J. Am. Chem. Soc., **117** (1995) 9529.

[46] D.J. Evans, R.O. Watts, Mol. Phys., **31** (1976) 83.

[47] R.W.G. Wyckoff, Crystal Structures, Vol. 6, Pt. 1, Interscience Pulications, USA, 1969.

[48] J.C. Bertolini and J. Massardier in: The Chemical Physics of Solid Surfaces and Heterogeneous Catalysis, Vol. 4, D.A. King and D.P. Woodruff, Eds., Elsevier, New York, 1982.

[49] S. Lehwald, H. Ibach and J.E. Demuth, Surf. Sci., **78** (1978) 577.

[50] J.E. Demuth and D.E. Eastman, Phys. Rev. B, **13** (1976) 1523.

[51] H. Hoffmann, F. Zaera, R.M. Ormerod, R.M. Lambert, L.P. Wang and W.T. Tysoe, Surf. Sci., **232** (1990) 259.

[52] F. Cermic, O. Dippel and E. Hasselbrink, Surf. Sci., **342** (1995) 101.

[53] V.H. Grassian and E.L. Muetterties, J. Phys. Chem., **91** (1987) 389.

[54] B.J. Bandy, M.A. Chesters, M.E. Pemble, G.S. McDougall and N. sheppard, Surf. Sci., **139** (1984) 87.

[55] B.E. Koel, J.E. Crowell, C.M. Mate and G.A. Somorjai, J. Phys. Chem., **88** (1984) 1988.

[56] M. Neumann, J.U. Mack, E. Bertel and F.P. Netzer, Surf. Sci., **155** (1995) 9160.

[57] M. Neuber, F. Schneider, C. Zubragel and M. Neumann, J. Phys. Chem., **99** (1995) 9160.

[58] T. McCabe and D.R. Lloyd, Surf. Sci., **331-333** (1995) 88.

[59] C.W.J. Bol, C.M. Friend and X. Xu, Langmuir, **12** (1996) 6083.

[60] Clavilier, J.; Faure, R.; Guinet, G.; Durand, R. *J. Electroanal. Chem.* **1980**, 106, 205.

[61] J.A. DeRoss, T. Thundat, L.A. Nagahara and S.M. Lindsay, Surf. Sci., **256** (1991) 102.

[62] P.N. Ross in: Structure of Electrified Interfaces, J. Lipowski and P.N. Ross, Eds., VCH Publishers, Inc., New York, 1993.

[63] M.A. Chesters and G.A. Somorjai, Surf. Sci., **52** (1975) 21.

[64] J. Krim, Thin Solid Films, **137** (1986) 297.

[65] W. Shen, G.L. Nyberg and J. Liesgang, Surf. Sci., **298** (1993) 143.

[66] L.H. Dubois, B.R. Zegarski and R.G. Nuzzo, J. Chem. Phys., **98** (1993) 678.

[67] G.E. Poirier and E.D. Pylant, Science, **272** (1996) 1145.

[68] Handbook of X-ray and Ultraviolet Photoelectron Spectroscopy, D. Briggs, Ed., Heydon & Son, London, 1978.

[69] D. Briggs and M.P. Seah, Practical Surface Analysis by Auger and X-ray Photoelectron Spectroscopy, John Wiley & Sons, New York, 1991.

[70] K. Siegbahn, C. Nordling, G. Johansson, J. Hedman, P.F. Heden, K. Hamrin, U. Gelius, T. Bergmark, L.O. Werme, R. Manne and Y. Baer, ESCA Applied to Free Molecules, North-Holland, Amsterdam, 1969.

[71] Moulder, J.F., Stickle, W.F., Sobol, P.E., Bomben, K.D. Handbook of Photoelectron Spectroscopy; Perkin-Elmer Corporation, Physical Electronics Division: Eden Prairie, MN 55344, 1992.

[72] C.S. Fadley, Prog. Surf. Sci., **16** (1984) 275.

[73] G.C. Smith, Updates in Applied Physics and Electrical Technology, Surface Analysis by Electron Spectroscopy, Plenum Press, New York, 1994.

[74] N.V. Richardson and A.M. Bradshaw in: Electron Spectroscopy, Vol. 5, Eds., C.R. Brundle and A.D. Baker, Academic Press, New York, 1981.

[75] B. Feuerbacher and B. Fitton, Electron Spectroscopy for Surface Analysis, Ed., H. Ibach, Springer-Verlag, New York, 1977.

[76] H.-P. Steinruck in: Surface Science Techniques, Eds., J.M. Walls and R. Smith, Elsevier Science, Great Britain, 1994.

[77] G.L. Nyberg and W. Shen in: Surface Science, Principles and Current Applications, Ed. R.J. MacDonald, E.C. Taglauer and K.R. Wandelt, Springer, New York, 1996.

[78] H.-P. Steinruck, J. Phys.: Condens. Matter, **8** (1996) 6465.

[79] A. Goldmann and R. Matzdorf in: Surface Science, Principles and Current Applications, Ed. R.J. MacDonald, E.C. Taglauer and K.R. Wandelt, Springer, New York, 1996.

[80] S.E. Anderson and G.L. Nyberg, Appl. Surf. Sci., **22/23** (1985) 325.

[81] D.P. Woodruff and T. Delchar, Modern Techniques of Surface Science, Cambridge University Press, Cambridge, 1986.

[82] H. Ibach and D.L. Mills, Electron Energy Loss Spectroscopy and Surface Vibrations, Academic, London, 1982.

[83] P.A. Redhead, Vacuum, **12** (1962) 203.

[84] G. Attard and C. Barnes, Surfaces, Oxford University Press, New York, 1998.

[85] G. Ertl and J. Kuppers, Low Energy Electrons and Surface Chemistry, VCH, Weinheim, 1985.

[86] K. Heinz, Rep. Prog. Phys., **58** (1995) 637.

[87] K. Heinz, Rep. Prog. Sci., **27** (1988) 239.

[88] D.A. Bonnel, Scanning Tunneling Microscopy, VCH, New York, 1993.

[89] M.D. Ward and H.S. White in: Modern Techniques in Electroanalysis, Eds., P. Vanysek, John Wiley & Sons, New York, 1996.

[90] D.C. Koningsberger and P. Prins, X-ray Absorption: Principles, Applications, Techniques of EXAFS, SEXAFS and XANES, John Wiley & Sons, New York, 1988.

[91] A. Caballero and A. Munoz-Paez in: Encyclopedia of Analytical Science, Vol. 8., Ed., A. Townshend, Academic Press, 1995.

[92] F. Carnovale, M.H. Kibel, G.L. Nyberg and J.B. Peel, J. Electron Spectrosc. Relat. Phenom., **25** (1982) 171.

[93] P.A. Agron, T.A. Carlson, W.B. Dress and G.L. Nyberg, J. Electron Spectrosc. Relat. Phenom., **42** (1987) 313.

[94] P.A. Agron and T.A. Carlson, J. Vac. Sci. Technol., **20** (1982) 815.

[95] M.P. Kiskinova, Surf. Sci. Rep., **8** (1988) 359.

[96] J.T. Roberts and C.M. Friend, J. Chem. Phys., **88** (1988) 7172.

[97] D.A. Chen, C.M. Friend and H. Xu, Surf. Sci., **395** (1998) L221.

[98] Y. Takata, T. Yokoyama, S. Yagi, N. Happo, H. Sato, K. Seki, T. Ohta, Y. Kitajima and H. Kuroda, Surf. Sci., **259** (1991) 266.

[99] D.R. Huntley, J. Phys. Chem., **96** (1992) 4550.

[100] S.M. Kane, T.S. Rufael, J.L. Gland, D.R. Huntley and D.A. Fischer, J. Phys. Chem. B, **101** (1997) 8486.

[101] S.M. Kane, D.R. Huntley and J.L. Gland, J. Am. Chem. Soc., **118** (1996) 3781.

[102] T.S. Rufael, D.R. Huntley, D.R. Mullins and J.L. Gland, J. Phys. Chem., **98** (1994) 13022.

[103] D.M. Jaffey and R.J. Madix, J. Am. Chem. Soc., **116** (1994) 3020.

[104] D.A. Stern, E. Wellner, G.N. Salaita, L. Laguren-Davidson, F. Lu, N. Batina, D.G. Frank, D.C. Zapien, N. Walton and A.T. Hubbard, J. Am. Chem. Soc., **110** (1988) 4885.

[105] J.Y. Gui, D.A. Stern, D.G. Frank, F. Lu, D.C. Zapien and A.T. Hubbard, Langmuir, **7** (1991) 955.

[106] J. Stohr and D.A. Outka, Phys. Rev. B, **36** (1987) 7891.

[107] A.-A. Dhirani, R.W. Zehner, R.P. Hsung, P. Guyot-Sionnest and L.R. Sita, J. Am. Chem. Soc., **118** (1996) 3319.

[108] E. Sabatani, J. Cohen-Boulakia, M. Breuning and I. Rubenstein, Langmuir, **9** (1993) 2974.

[109] Y.-T. Tao, C.-C. Wu, J.-Y. Eu, W.-L. Lin, K.-C. Wu and C.-h. Chen, Langmuir, **13** (1997) 4018.

[110] K.T. Carron and L.G. Hurley, J. Phys. Chem., **95** (1991) 9979.

[111] A. Abduaini, S. Kera, M. Aoki, K.K. Okudaira, N. Ueno and Y. Harada, J. Electron Spectrosc. Relat. Phenom., **88-91** (1998) 849.

[112] C.J. Sandroff and D.R. Herschbach, J. Phys. Chem., **86** (1982) 3277.

[113] Y.J. Lee, I.C. Jeon, W.-k. Paik and K. Kim, Langmuir, **12** (1996) 5830.

Chapter 2

The Influence of Heterocyclic Thiols on the Electrodeposition of Cu on Au(111)

Abstract

We report the influence of two structurally related heterocyclic thiols, 2-mercaptobenzothiazole and 2-mercaptobenzimidazole, on the underpotential (UPD) and bulk deposition of Cu on Au(111). X-ray photoelectron spectroscopy analysis of the organic adlayers reveal that after self-assembly from the liquid phase, the primary adsorbate species is consistent with a thiolate. The Au(111)-($\sqrt{3}\times22$) reconstruction is lifted to the (1×1) phase upon thiol self-assembly. At sub-monolayer thiol coverages, a new UPD feature is observed, whose intensity goes through a maximum at intermediate thiol coverages. This feature is consistent with Cu adsorption in the vicinity of chemisorbed thiol. A thiol coverage dependent study of Cu UPD suggests formation of small two-dimensional thiol islands. At saturation coverage, the adsorbates passivate the surface towards Cu UPD and significantly hinder bulk processes.

Investigation of a previously reported potential-dependent reorientation of 2-mercaptobenzothiazole disputes a structural mechanism of ring 'opening' and 'closing' of the thiol layer. Instead, we suggest that instability of the thiol during cycles of Au oxide formation and reduction results in irreversible desorption of the thiol and complete restoration of Cu UPD.

1. Introduction

The structure of the metal|electrolyte interface, and that of atoms and molecules adsorbed at this interface, are of tremendous interest to electrochemists, reflecting the fundamental importance of such systems in basic research, technology and industry. Underpotential deposition (UPD) describes the formation of monolayer metal deposits on a foreign metal substrate at potentials positive from the reversible Nernst potential for formation of bulk phase [1,2]. Due to the particular properties of the electrified interface, the chemical potential of adatoms deposited at underpotentials under thermodynamic equilibrium can be varied over a wide range by simply changing the electrode potential. Hence, the adatom coverage is changed with applied potential. The existence of stronger attractive forces between atoms of the deposited metal, and atoms of the substrate than between like atoms of the bulk, can induce marked changes in the adatom properties and growth behaviour depending on the substrate [3].

Cyclic voltammetry, sensitive to the mechanism of deposition and therefore providing information on structural transitions, as well as interactions between the surface and the UPD layer, provides a means of probing the energetics of the system and allows for indirect characterisation of the processes taking place. Attributing the often complex features in the voltammogram to specific processes occurring on the surface requires correlation of the voltammetric peaks with different adlayer structures determined by *in situ* and *ex situ* surface spectroscopic techniques [4].

As a consequence of atomic imaging studies, largely by scanning tunneling microscopy (STM), electrodeposition of metallic deposits has been demonstrated to be a much more complex phenomenon than was first postulated. In addition to the predominant influence exerted by the substrate in the form of the substrate structure, composition and crystallographic orientation, many other parameters affect the structural phases formed including adsorbate-substrate interactions, electrode potential, electrolyte composition and, in particular, anion coadsorption. The presence of anions at the interface can play a decisive role in the formation of an ordered UPD adlayer structure as specifically adsorbing anions do not merely compete for available substrate sites, but actually change the surface properties as a whole; thus, influencing the adatom-substrate bond [3]. Such an influence can be observed in the prototypical

UPD of Cu on Au(111) in sulphuric acid, arguably the most extensively studied UPD system, with specifically adsorbing anions causing multiple peaks to appear in the cyclic voltammogram assigned to different Cu adlayer phases [5,6,7].

A major challenge in contemporary electrochemistry is the elucidation of the surface structure of electrodes in solution with and without adsorbates [8]. In the following study, we have focused on the influence of heteroaromatic thiols chemisorbed on Au(111) on metal UPD on that surface. Similar to the importance of specifically adsorbing anions, derivatisation of the electrode surface by organic molecules can be predicted to play a structure-determining role in the metal adatom growth process.

Interest in the properties of thin-film organic materials, especially coherently organised monolayer assemblies, has grown enormously in recent years. This is primarily due to the ease of fabrication, characterisation and manipulation of self-assembled monolayers (SAMs) [9]. These model interfacial structures are based upon the spontaneous adsorption of molecules with polar head groups designed to specifically interact with and chemically bind to a substrate from the gas, or more traditionally, the liquid phase. A comprehensive range of data has been accumulated and interpreted for self-assembly of *n*-alkanethiols on various substrates [10]. It has been reported that under certain conditions, aromatic groups may be introduced into these assemblies without adversely affecting the packing and order of the monolayer [11]. To date, such studies have focused on simple aromatic systems such as benzenethiol or the inclusion of such 'bulky' structures within the alkyl chains [11-15]. In contrast, information regarding self-assembled heteroaromatic thiols is sparse [16-18].

Our research has been directed towards two structurally related heterocyclic thiols, 2-mercaptobenzothiazole (2MBT) and 2-mercaptobenzimidazole (2MBI), chemisorbed from the liquid phase on Au(111). These molecules have been selected as suitable candidates for the formation of self-assembled monolayers (SAMs) due to their structure and chemical reactivity, which are essential properties in allowing direct complexation and derivatisation, important for development of SAM based chemical and biological sensors [19].

Clearly, a prerequisite for understanding the thiol-induced changes must involve a precise description of the metal-adatom behaviour during UPD prior to substrate modification. To this end, we have chosen the model UPD couple involving Cu growth on Au(111) in sulphuric acid. The characteristic current-potential response from this system shows two distinct adsorption peaks [20, 21], assigned unambiguously from a variety of surface sensitive techniques, to the formation of two ordered Cu adlayers [22-25]. By systematically following Cu UPD in the presence of self-assembled adsorbates, from sub-monolayer to full 'physical monolayer' thiol coverages, it should be possible to correlate changes in UPD features to a possible growth mechanism for these complex organic moieties. Likewise, electrodeposition of bulk Cu on thiol modified Au(111) in sulphuric acid has been investigated.

Interestingly, a previous study of 2MBT self-assembled on a polycrystalline Au surface has reported a potential-dependent 'opening' and 'closing' of the monolayer to Cu UPD involving a molecular reorientation of 2MBT [26]. We have reinvestigated this structural transition and provide new evidence that electrochemical stripping of the thiol rather than a molecular reorientation is responsible for the electrochemical response observed.

2. Experimental

All work reported here was performed on a Au(111) single-crystal (6 mm × 8 mm × 1.5 mm) oriented to within 0.5° of the (111) plane (Metal Crystals and Oxides). The crystal had 0.2-0.3 mm deep grooves spark eroded into the edges to allow secure electrical connection to a potentiostat by means of a Pt wire (99.99% purity, Goodfellow Cambridge). Three 0.25 mm slots passing through the bulk of the crystal allowed connection of a thermocouple and spot-welding to sample manipulators/mounts for XPS analysis. These grooves and slots were positioned as close to the unpolished, back face of the crystal as possible.

In electrochemical studies, the Au(111) working electrode was cleaned prior to electrochemical measurements by the flame-annealing technique [27]. This involved heating the crystal to just below its melting temperature in a micro-Bunsen flame, and then cooling slowly in a flow of inert gas (high purity nitrogen) prior to quenching and formation of a meniscus contact with the electrolyte solution. This ensures minimal contribution from the crystallographically poorly defined edges of the sample, such that the electrochemical response obtained is characteristic of the Au(111) face. As a check that the flame-anneal-cooling procedure gave rise to an atomically clean surface, cyclic voltammograms for Au(111) in 0.1 M sulphuric acid were collected and found to be in excellent agreement with literature reports [28-31]. For XPS analysis, a clean Au(111) surface was prepared prior to self-assembly by argon ion bombardment with thermal annealing to 700 K in vacuum followed by rapid transfer, minimising exposure of the substrate to the laboratory atmosphere by means of an inert glove-box system, to the thiol solution.

The heterocyclic thiols shown in Fig. 1, 2-mercaptobenzothiazole and 2-mercaptobenzimidazole, were supplied by Aldrich (98% purity) and used as received. Liquid phase self-assembly of sub-monolayer and monolayer films was performed by immersion of a clean Au(111) surface (flame-annealed, inert gas-cooled or argon ion-bombarded and thermally annealed) in 10^{-6}M thiol solution at ambient temperature (20 ± 1°C), and under continuous mild agitation. This concentration has been determined to allow sub-monolayer and saturation ('physical monolayer') coverages to be studied as a function of immersion time. 'Physical monolayer' films formed under these

conditions were found to block Cu UPD, inhibit bulk Cu processes and reduce substrate oxidation as effectively as films prepared by immersion in 1 mM thiol solutions. HPLC grade methanol was used as solvent (99.9% assay, LAB SCAN, Analytical Sciences). Following film formation, the sample was rinsed with copious amounts of methanol and quickly transferred to the electrochemical cell/X-ray photoelectron spectrometer.

High resolution XPS investigations were performed on a Scienta ESCA 300 photoelectron spectrometer at the RUSTI facilities in Daresbury Laboratory, U.K. The spectrometer was operated at a base pressure of 10^{-9} Torr using a monochromated Al Kα rotating anode operated at 14 KV and 20 mA. Photoelectrons were detected by a hemispherical analyser and a two-dimensional position-sensitive detector (micro-channel plates with CCD camera). Different combinations of pass energy (20-1000 eV) and slit-aperture width allowed variation of energy resolution depending on the nature of the analysis. For the data displayed here, collected at normal emission, an energy resolution of 0.55 eV was employed. Further details of the XPS experiments have been described elsewhere [32].

All electrochemical experiments were performed in two-compartment electrochemical Pyrex glass cells, with provisions for crystal cooling and solution degassing, constructed according to the design of Evans and Attard [33]. The first compartment was equipped with the Au single-crystal working electrode and a Pt mesh counter electrode of large geometrical area located in a luggin capillary with the second compartment containing a reference electrode. The electrochemical cell, its accessories and all glassware required for the preparation of electrolytes and thiol solutions were cleaned by soaking for >12 h in a dilute solution of $KMnO_4$ (99.8% purity, Aldrich) in concentrated sulphuric acid (97-99% GPR, BDH). These items were then steamed and rinsed thoroughly with deionised water (18.2 $M\Omega cm^{-1}$). Two such electrochemical cells were used in tandem during experiments in which the unmodified/modified Au electrode was subjected to cycling treatment in 0.1 M sulphuric acid (as discussed in section 3.6) and then quickly transferred, protected by a drop of electrolyte, to a second cell containing 0.1 M sulphuric acid and 1 mM Cu^{2+}.

Deaerated aqueous 0.1 M sulphuric acid (doubly distilled, ultrapure grade, Aldrich) prepared with deionised water was used as the supporting electrolyte and 1

mM Cu^{2+} solutions were prepared by dissolution of $CuSO_4.5H_2O$ (99.999% purity, Merck) in base electrolyte. All working solutions were purged and blanketed with research grade nitrogen (99.9995%, B.O.C. Special Gases) purified by an oxygen trap (Supelco Chromatography) which decreases oxygen impurities to less than 0.005 p.p.m. Electrode potentials are given with respect to the reversible $Cu|Cu^{2+}$ electrode (Cu wire, 99.999% purity, Goodfellow Cambridge) which served as a reference electrode in the Cu^{2+} containing solutions. A Au wire (99.999% purity, Goodfellow Cambridge) was used as a quasi-reference electrode in solutions not containing metal ions. Reference electrodes were cleaned by immersion in concentrated nitric acid (69% GPR, BDH) and rinsed with copious amounts of deionised water. Cyclic voltammetry was performed using a BAS CV-50W potentiostat (Bioanalytical Systems). The working electrode was immersed in the electrolyte prior to connection to the potentiostat. Under these conditions, we did not observe Cu adsorption on the Au(111) surface prior to the application of potential control. The voltammograms shown are the result of the first potential sweep (unless otherwise indicated in the figure captions).

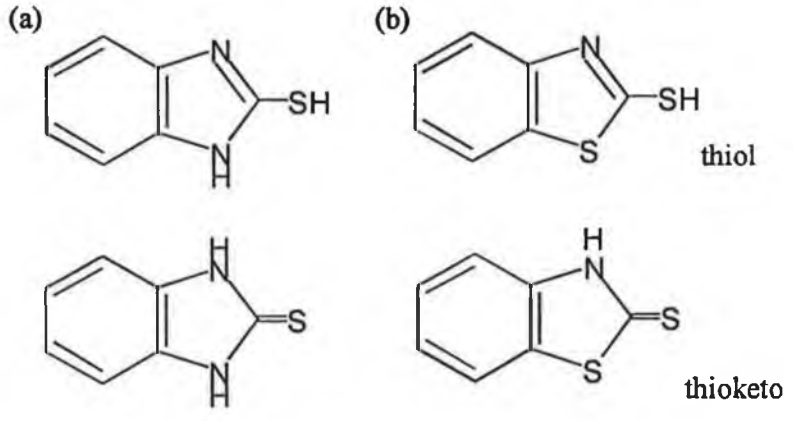

2-Mercaptobenimidazole 2MBI

2-Mercaptobenothiazole 2MBT

Figure 1 Heterocyclic molecules self-assembled on Au(111) in their (a) thiol and (b) thioketo forms.

3. Results and Discussion

3.1 X-ray photoelectron spectroscopy of thiols on Au(111)

Examination of the structural formula of 2MBI in Fig. 1a reveals that there is a single sulphur atom and two chemically distinct nitrogen environments, in the protonated and unprotonated forms. In contrast, 2MBT contains two sulphur and a single nitrogen environment. However, both molecules may exist in two conformations, the thiol and thioketo tautomers shown in Fig. 1a and b, respectively. In the case of 2MBI, the chemical environment of the nitrogens in the thioketo form are similar, leading to the expectation of a rather small chemical shift. On the basis of high resolution core level spectra of the crystalline samples used in this work, we found that the thioketo form dominates, in agreement with IR, NMR and X-ray analysis and previous XPS studies [34-37]. In Fig. 2a, the nitrogen (1s) core level spectrum from a liquid phase self-assembled 2MBI monolayer film on Au(111) reveals two nitrogen peaks at 398.5 and 399.7 eV with the relative area under the two peaks approximately equal. Hence, unlike the solid state, two nitrogen environments are distinguishable. It is possible that the orientation of the molecule is such that one of the nitrogen heteroatoms interacts with the surface causing the nitrogens to be inequivalent regardless of the tautomeric form (although it is highly probable that such an interaction would result in nitrogen deprotonation). However, the chemical shift between the nitrogen (1s) peaks is large (1.2 eV) and agrees with that expected for unprotonated and protonated nitrogen in molecules of this type, suggesting that the molecule is bonded in its thiol form [37]. Further evidence for the presence of the thiol tautomer is provided upon analysis of a self-assembled 2MBT monolayer film prepared from the liquid phase. A single nitrogen (1s) peak was observed at 398.6 eV, as shown in Fig. 2a, which corresponds closely to the 398.5 eV peak ascribed to the 2MBI unprotonated nitrogen atom. The sulphur (2p) region from a 2MBI monolayer appears as a poorly resolved two component peak in Fig. 2b attributed to the spin orbit split 2p levels with binding energies of 162.0 and 163.2 eV. The primary adsorbate species is thus consistent with a chemisorbed thiolate self-assembled on the Au(111) surface [38-40]. The sulphur (2p) core level spectrum from a 2MBT monolayer indicates multiple

contributions to the observed lineshape. The three peaks displayed in Fig. 2b are assigned to a minimum of two chemically inequivalent sulphur atoms. The thiolate sulphur atom results in a $2p_{3/2}$ peak at 162.1 eV with the $2p_{1/2}$ peak (163.3 eV) overlapping the sulphur heteroatom $2p_{3/2}$ peak at 163.6 eV followed by its corresponding $2p_{1/2}$ peak at 164.8 eV. This series of core level binding energies and lineshapes corresponds to the intrinsic photoemission expected for 2MBT as the thiol tautomer, and is again assigned to the formation of a thiolate on Au(111) [38-40].

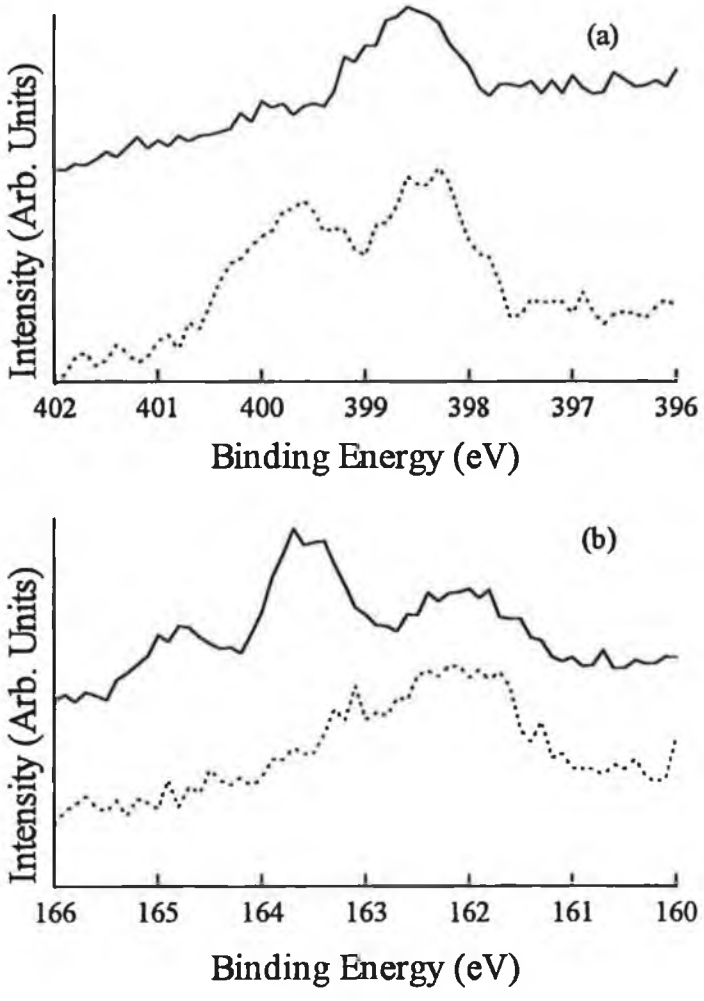

Figure 2 High resolution XPS spectra of the (a) nitrogen (1s) and (b) sulphur (2p) core levels from monolayers of 2MBI (·····) and 2MBT (——) self-assembled on Au(111) from 1×10^{-6} M thiol solutions.

The thickness of the 2MBI overlayer was estimated from the attenuation of the Au($4f_{7/2}$) signal upon self-assembly. The relationship describing the decrease in substrate XPS intensity upon deposition of a film of thickness *d* is:

$$I_d = I_o \exp(-d/\lambda \sin\theta)$$

where (I_o) and (I_d) are the Au($4f_{7/2}$) signal before and after adsorption of 2MBI, λ is the inelastic mean free path (IMFP) and θ is the take-off angle = 90° (the angle between the sample surface and the photoelectrons accepted by the analyser). Over the energy range 500-1500 eV, Laibinis *et al.* have found that the IMFP in hydrocarbon films is proportional to the kinetic energy of the photoelectrons [41]:

$$\lambda\,(\text{Å}) = 9.0 + 0.022\ \text{KE (eV)}$$

where KE is the kinetic energy of the Au($4f_{7/2}$) photoelectron (1402.6 eV). This gives an estimate of the IMFP in the 2MBI layer as 40 Å yielding a layer thickness of 4.5 Å. However, as this equation applies only to *n*-alkanethiols, an error may be expected when using it for cyclic systems such as 2MBI, as the two-dimensional density will be different. The IMFP for photoelectrons in hydrocarbon layers may also be determined using the Bethe equation which takes the material density into consideration [41,42]:

$$\lambda \cong (\text{KE}) / [E_p^2 \beta \ln(\gamma \text{KE})]$$

where KE is the kinetic energy of the Au($4f_{7/2}$) photoelectron (1402.6 eV), E_p is the free-electron plasmon energy (19.7 eV), β and γ are empirical parameters. We estimated E_p from

$$E_p = 28.8\,(N_v\,\rho/A)^{1/2}$$

where N_v is the total number of valence electrons per molecule (46), ρ is the density of the material (1.52 gcm^{-3}), and *A* is the molecular weight (150.20). While γ (0.123 eV^{-1}) can be related to the density of the material by

$$\gamma = 0.151\rho^{-0.49}$$

the value of β (0.034 $eV^{-1}Å^{-1}$) is taken from the work of Laibinis *et al.* [41]. Using these expressions, a value of 21 Å was calculated for the IMFP, yielding a thickness of 2.3 Å for the 2MBI layer on Au(111). It is clear that large errors are involved in the determination of layer thickness by this method dependent on the value of the IMFP adopted. Nevertheless, such a small layer thickness (2.3-4.5Å) is consistent with a

single monolayer adopting a flat-lying geometry with the plane of the ring parallel or close to parallel with the Au(111) surface.

A second method was used to cross-check the film thickness/surface coverage. Based upon a known coverage of 0.33 monolayers of sulphur upon gas phase adsorption of ethanethiol on Au(111) which forms a $(\sqrt{3}\times\sqrt{3})R30°$ overlayer structure [43], we have calculated the corresponding surface coverage for 2MBI to be 0.16 monolayers using the ratio of the integrated intensity of the S(2p) to Au($4f_{7/2}$) (ignoring differential attenuation of the sulphur and Au signals by the different monolayers which should be small at the high outgoing kinetic energies utilised). This method of coverage estimation was validated upon comparison with published data for butanethiol self-assembled from the liquid phase on Au(111), which yielded a similar value (0.14 monolayers of 2MBI) [44]. A coverage of 0.16 monolayers corresponds to a surface density of 2.2×10^{14} molecules cm^{-2}, which compares with packing densities for upright (2.9×10^{14} molecules cm^{-2}) and flat (1.7×10^{14} molecules cm^{-2}) molecular orientations estimated using van der Waals' radii. Clearly, the experimentally derived surface density agrees best with a flat-lying geometry, and is strongly suggestive of a single molecular monolayer being formed, and significant double layer formation may be ruled out.

In conclusion, the film thicknesses, sulphur coverages and packing density data suggest monomolecular self-assembly of 2MBI on Au(111) and support a bonding arrangement in which the molecular orientation is such that the ring lies flat, i.e., is aligned parallel to the substrate surface, although geometries involving a small inclination of the plane of the ring are possible. Similar results were obtained for the 2MBT monolayer on Au(111). A more detailed discussion of qualitative and quantitative XPS data from these films will be presented elsewhere [32].

3.2 The influence of thiols on specific anion adsorption on Au(111)

An excellent 'fingerprint' for clean, well-defined Au(111) involves collecting the characteristic current-potential curve in sulphuric acid aqueous electrolyte. The resulting voltammogram, shown in Fig. 3, comprises of three distinct features and is in good agreement with that previously reported in the literature [28-31]. A pronounced current response at -420 mV was exhibited on the anodic scan (the counterpart of which is missing on the cathodic scan). This sharp peak is unique to a single-crystal plane of (111) orientation and is associated with reversible removal of the reconstruction via a structural transition induced by sulphate-specific anion adsorption [45,46]. The surface is reconstructed negative of this peak requiring a critical anion concentration to lift the ($\sqrt{3}\times22$) structure to the (1×1) phase. An adjacent broad feature seen at approximately -240 mV corresponds to a medium coverage of the (1×1) electrode surface by anions. Small reversible peaks observed at more positive potentials (95 mV anodic and 35 mV cathodic), reflects an abrupt order-disorder transition resulting in the formation of a two-dimensional overlayer of anions consisting of well-ordered domains [29,30].

Collection of a characteristic cyclic voltammogram for Au(111) in sulphuric acid is not only an excellent check for substrate preparation, but may also be used to investigate the behaviour of the reconstructed substrate structure upon adsorption of thiols.

Immersion of an originally reconstructed Au(111) surface in 10^{-6} M methanol solution of either 2MBI or 2MBT results in the removal of ($\sqrt{3}\times22$) phase with the thiol adsorption inducing the lifting the reconstruction to the (1×1) bulk truncated structure. The lowest self-assembly time of 10 s is shown in curve (a) in Figs. 4 and 5. Comparison with the corresponding voltammogram for unmodified Au(111) shown in Fig. 3, indicates that the sharp peak at -420 mV, signalling the removal of the reconstruction has disappeared, being replaced by a single broad reversible peak (-417 mV) and a two-component feature (-405 and -340 mV) after 2MBI and 2MBT adsorption, respectively. The -405 mV peak (which subsequently disappears after 20 s immersion in 2MBT) may reflect partial removal of the reconstruction by 2MBT chemisorption, leaving small domains of reconstructed substrate. On the negative scan,

a broad peak is observed at -431 mV after immersion in 2MBI, while the corresponding feature for 2MBT is seen at -434 mV. While the remainder of the voltammogram is unchanged in its general appearance, the reversible peaks are shifted to more positive potentials by approximately 50 mV in comparison with unmodified Au(111). Such a peak potential shift suggests stabilisation of the surface by the organic adsorbate; hence, more positive potentials must be reached before specific anion adsorption can occur [47].

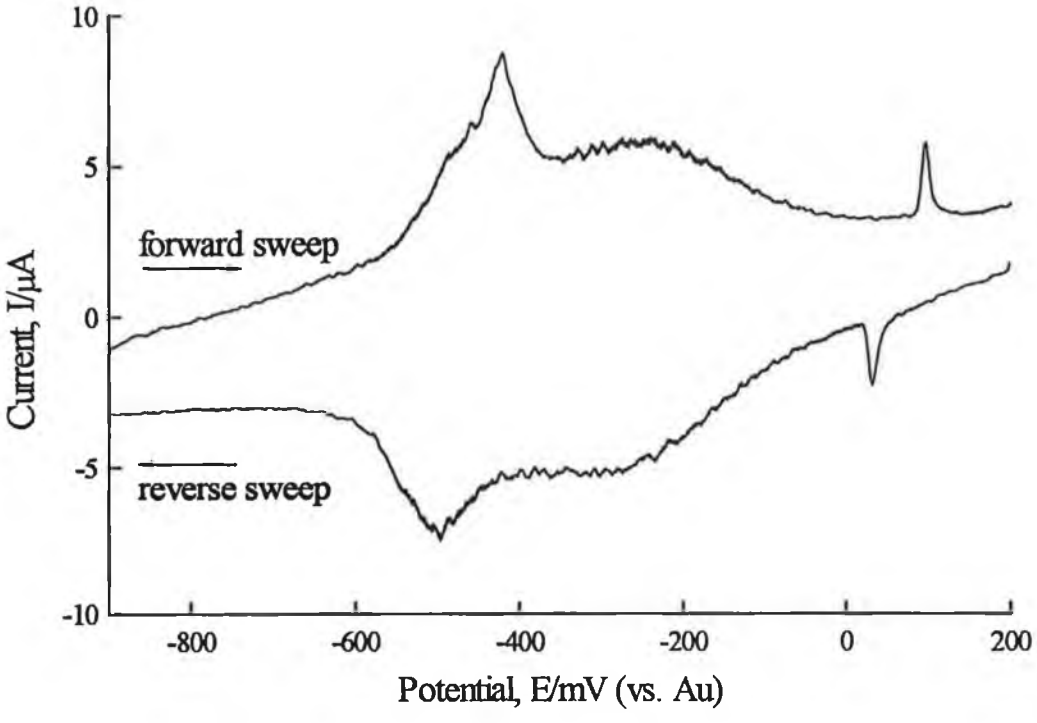

Figure 3 Cyclic voltammogram of Au(111) in 0.1 M H_2SO_4 at a scan rate of 100 mVs^{-1}.

With increasing immersion times, the small reversible peaks at 95 mV (cathodic) and 145 mV (anodic) gradually diminish. Following 50 and 60 s in 2MBT and 2MBI, respectively, this feature is no longer visible as seen in Figs. 4b and 5b. This indicates that the order-disorder transition resulting in the formation of well-ordered domains of anions is not possible due to the presence of chemisorbed thiol on the

surface. Finally, in Figs. 4c and 5c, the thiol self-assembly at full 'physical monolayer' coverage results in a broad capacitive double-layer with all characteristic features of unmodified Au(111) in sulphuric acid quenched.

These results, the lifting of the Au(111)-($\sqrt{3}\times22$) reconstruction, and the inhibition of two-dimensional island growth of specifically adsorbed anions, contribute considerably to our understanding of heterocyclic thiol self-assembly. These adsorbates are clearly able to deconstruct the surface structure to the (1×1) bulk truncated phase well in advance of the formation of a complete 'physical monolayer'. Inhibition of two-dimensional anion island growth suggests that, at sub-monolayer coverages, both thiols self-assemble through a mechanism which does not involve large two-dimensional islands. Such a growth mechanism would naturally leave large areas of clean Au(111) at low/intermediate thiol coverages upon which two-dimensional anion island growth may still occur. However, in contrast if the adsorbate were to chemisorb in a completely dispersed mode, we would expect inhibition of two-dimensional island growth of specifically adsorbing anions at lower immersion times (hence, surface coverages) than those observed. Hence, we tentatively postulate a self-assembly mechanism involving growth of small two-dimensional thiol islands.

Background experiments for the immersion of the Au(111)-($\sqrt{3}\times22$) surface in pure solvent were performed under conditions identical to self-assembly. It was found that the reconstruction is lifted to the (1×1) phase following 150 s exposure to methanol, but two-dimensional island growth of anions remains unaffected at least up to 600 s immersion as indicated by the presence of the anion order-disorder peaks (longer times were not examined). Hence, the contribution of solvent effects to the observed electrochemistry are not substantial for the immersion times of interest during the study of self-assembled thiols.

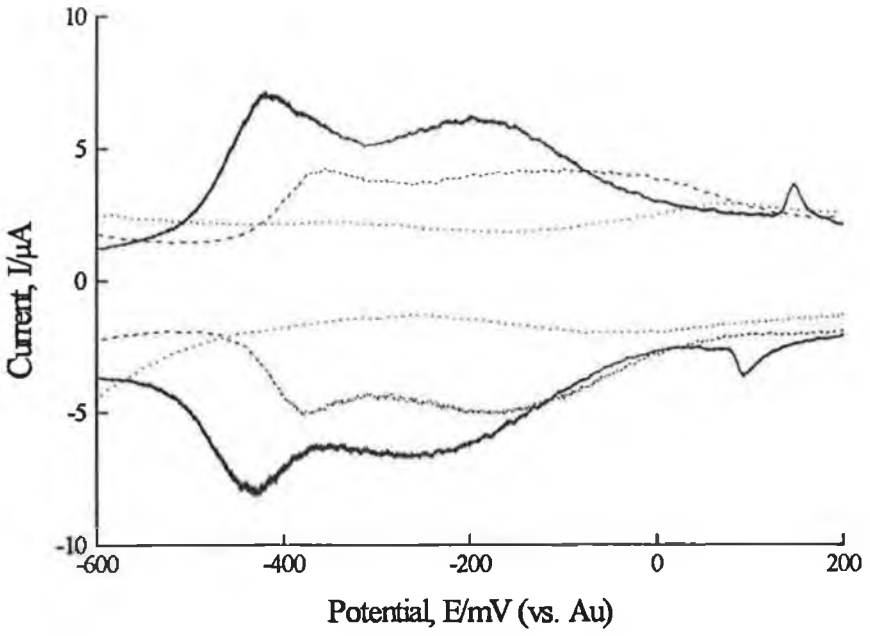

Figure 4 Cyclic voltammograms of 2MBI modified Au(111) in 0.1 M H_2SO_4 at a scan rate of 100 mVs^{-1}. Immersion times shown are (a) 10 (——), (b) 50 (– – –) and (c) 360 (·····) s in 1×10^{-6} M thiol solution.

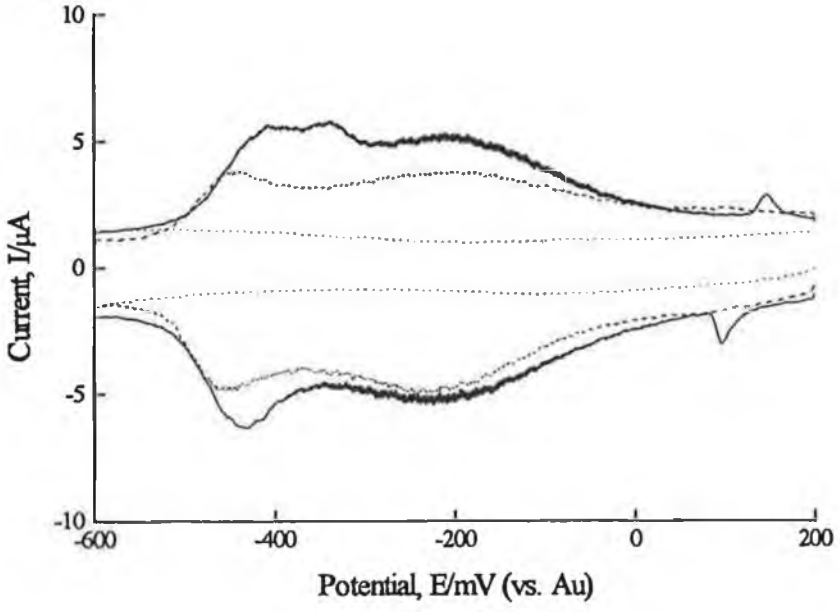

Figure 5 Cyclic voltammograms of 2MBT modified Au(111) in 0.1 M H_2SO_4 at a scan rate of 100 mVs^{-1}. Immersion times shown are (a) 10 (——), (b) 60 (– – –) and (c) 420 (·····) s in 1×10^{-6} M thiol solution.

3.3 Thiol induced modification of Cu UPD on Au(111)

UPD of Cu on Au(111) in the presence of sulphuric acid has been extensively studied both experimentally and theoretically [48-50]. Based on *in situ* SPM (scanning probe microscopy) [5,21,51-54], *in situ* spectroscopies [22-25,55] and *ex situ* [56,57] measurements, it is well known that the electrodeposition of Cu proceeds in three distinct growth stages: random, $(\sqrt{3}\times\sqrt{3})R30°$ and (1×1). A typical voltammogram for the UPD of Cu on Au(111) in 0.1 M sulphuric acid (vs. $Cu|Cu^{2+}$) shown in Fig. 6 agrees well with published data [20,21]. The sulphate anions adsorb at positive potentials forming a $(\sqrt{3}\times\sqrt{3})$ phase on Au. This lattice becomes disordered, and mobile anions are desorbed as the potential decreases undergoing a phase transition as Cu ions randomly adsorb on free substrate sites, resulting in a broad foot at the positive side of the first peak. This step is accompanied by readsorption of anions creating a $(\sqrt{3}\times\sqrt{3})$ template leaving a honeycomb lattice for adsorption of Cu. The first peak of the voltammogram, observed at 213 mV, corresponds to a coverage of 2/3 monolayers of Cu. As the (1×1) phase is formed, anions are displaced by Cu from their $(\sqrt{3}\times\sqrt{3})$ positions, filling the remaining 1/3 of available Au adsorption sites, corresponding to the completion of a pseudomorphic full monolayer coverage of Cu. This is observed as the second peak in the voltammogram at 44 mV. The anions then move above the plane of Cu adatoms forming a highly ordered overlayer [25]. The corresponding $(\sqrt{3}\times\sqrt{3})$ and (1×1) dissolution peaks are found at 234 and 105 mV, respectively.

Since Cu UPD on Au(111) is well understood, it was chosen as a useful probe in advancing our knowledge concerning the self-assembly of heterocyclic thiols on Au(111). Each feature in the voltammogram on unmodified Au(111) can be assigned to a particular Cu adatom structure. Hence, if the substrate is modified by adsorption of thiols, it is reasonable to assume that this modification will be reflected in the current-potential response. The resultant changes may suggest a growth mechanism for this class of thiol self-assembled on Au(111). The effect of thiol chemisorption on Cu UPD features on Au(111) have been investigated as a function of self-assembly time in 1×10^{-6} M thiol solution in methanol.

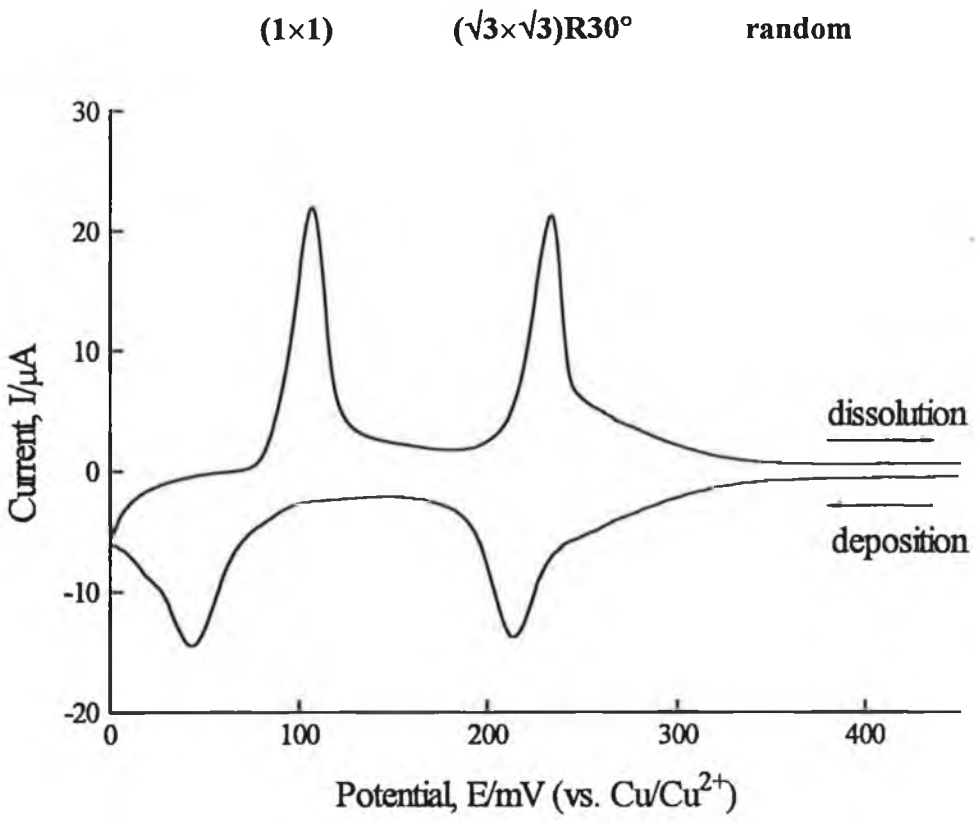

Figure 6 A cyclic voltammogram of Cu UPD on Au(111) showing the random, $(\sqrt{3}\times\sqrt{3})R30°$ and (1×1) Cu adatom growth phases in 0.1 M H_2SO_4 + 1 mM Cu^{2+} at a scan rate of 10 mVs^{-1}.

A background check on the effect of the organic solvent on Cu UPD was undertaken. The Au(111) surface was immersed in methanol, and the resulting voltammograms for Cu UPD collected as a function of immersion time. A decrease in the integrated response was observed, e.g., 15% decrease following 300 s immersion possibly due to decomposition of methanol on the substrate, reducing the total surface area available for Cu deposition. Hence, the solvent does not significantly alter the UPD features of Cu on Au(111) during the immersion times of interest. Exposure to methanol for extended periods (in excess of 300 s) results in minor changes in the UPD peaks which may be attributed to the accumulation of adsorbed impurity species present in the solvent, or to decomposition of methanol at substrate active sites (step

edges and other defects). The nature and identity of impurity or decomposition species responsible for these effects are unknown at this point.

A small sample of the series of voltammograms resulting from immersion of Au(111) in 2MBT are shown in Fig. 7. It can be seen in Fig. 7a that at low immersion times, the Cu adsorption continues to occur in discrete domains producing well-defined peaks characteristic of Cu UPD on Au(111). In addition, a new feature emerges at 123 mV as a minor constituent of the voltammogram on the deposition sweep. The corresponding stripping peak appears to overlap the $(\sqrt{3}\times\sqrt{3})R30°$ peak at 233 mV giving rise to a shoulder at 246 mV on the positive side of the main peak. As the new feature becomes increasingly prominent, the $(\sqrt{3}\times\sqrt{3})R30°$ phase is slowly attenuated, while the full Cu monolayer (1×1) peak remains essentially unaffected following 40 s immersion as shown in Fig. 7b. In Fig. 7c, the $(\sqrt{3}\times\sqrt{3})R30°$ phase has been completely quenched following 90 s immersion. The new adsorption peak gradually shifts towards bulk potentials and continues to grow as self-assembly times increase, reaching a maximum between 100 and 150 s immersion before decreasing as blocking coverages are approached. The corresponding stripping feature moves to more positive potentials showing the irreversible nature of this new Cu growth phase. The broad nature of these peaks suggest that the presence of thiolate species may induce a disordered Cu growth phase by offering a wide spectrum of local environments, such that UPD occurs at a number of energetically distinct sites. In general, as thiol coverages increase, all characteristic responses to Cu deposition and dissolution on Au(111) broaden, shift in potential and decrease in intensity. It was observed that UPD peaks become almost indistinguishable as the monolayer presence dominates. In particular, for immersion times greater than 180 s, the absence of any clearly discernible Cu adsorption features is characteristic as shown in Fig. 7d. However, despite the apparent suppression of all deposition peaks, the appearance of stripping features up until complete blocking of UPD indicates that although deposition is ill-defined, the formation of a Cu adlayer does occur. In Fig. 7e, Cu UPD is completely inhibited after 360 s of 2MBT self-assembly.

In Fig. 8, the relevant voltammograms at selected immersion times for Cu UPD on 2MBI modified Au(111) are shown. Its behaviour is similar to that of 2MBT with the same trend in shifting peak potentials, peak shape changes and the emergence of

new features. It can be seen in Fig. 8a that in addition to the peaks characteristic to Cu UPD on Au(111), on the deposition sweep, a new feature arises at 150 mV with its

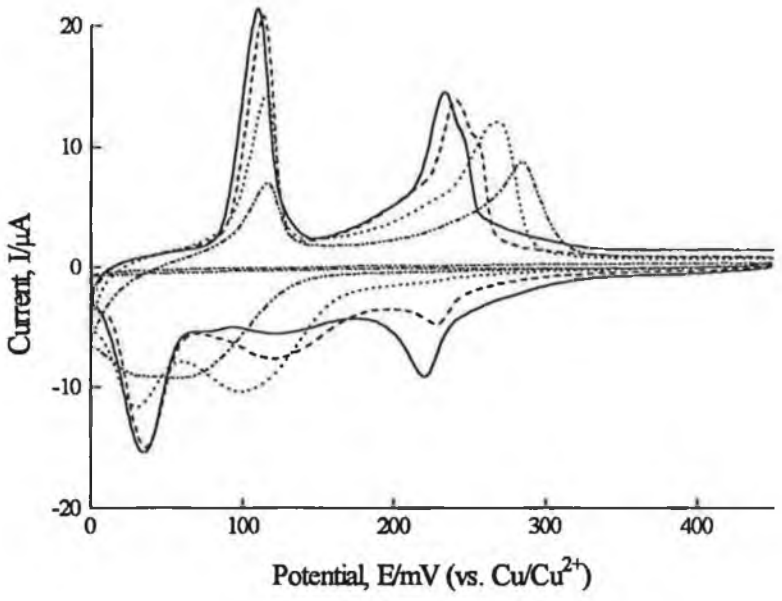

Figure 7 Cyclic voltammograms of Cu UPD on 2MBT modified Au(111) in 0.1 M H_2SO_4 + 1 mM Cu^{2+} at a scan rate of 10 mVs^{-1}. Immersion times shown are (a) 10 (——), (b) 40 (– – –), (c) 90 (·····), (d) 180 (—·—·) and (e) 360 (—·—) s in 1 × 10^{-6} M thiol solution.

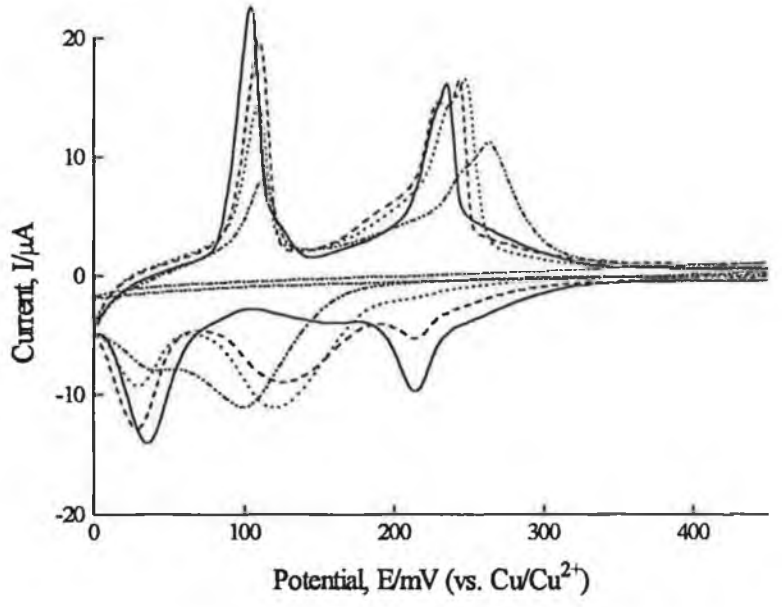

Figure 8 Cyclic voltammograms of Cu UPD on 2MBI modified Au(111) in 0.1 M H_2SO_4 + 1 mM Cu^{2+} at a scan rate of 10 mVs^{-1}. Immersion times shown are (a) 10 (——), (b) 60 (– – –), (c) 110 (·····), (d) 210 (—·—·) and (e) 420 (—·—) s in 1 × 10^{-6} M thiol solution.

desorption occurring at 235 mV after 10 s immersion. For low immersion times, the $(\sqrt{3}\times\sqrt{3})R30°$, (1×1) and new features coexist as shown in Fig. 8b. As with 2MBT, the initial stages of self-assembly result in an attenuation of the $(\sqrt{3}\times\sqrt{3})R30°$ peak, which is completely removed following 110 s of self-assembly, relative to that corresponding to the (1×1) phase. The new peak gradually shifts to more negative potentials and remains at a maximum intensity between 110 and 210 s immersion as observed in Fig. 8c. The corresponding stripping peak is seen at 240 mV, and gradually shifts towards more positive potentials. Again, the broadness of this new feature indicates that a range of different adsorption sites have become available to the metal adatom. In Fig. 8d, it becomes clear that as the immersion time progresses, the presence of 2MBI leads to a profound alteration in the bonding mode of Cu to the substrate. It becomes increasingly difficult to resolve deposition peaks into energetically distinct domains while the desorption peaks are more readily identified. Deposition and dissolution features become less intense, broaden and shift in potential leading to complete passivation of the substrate to UPD, shown in Fig. 8e, after 420 s of self-assembly.

In Fig. 9a, the integrated area versus immersion time plot for 2MBT is characterised by a rapid decrease for 10 s immersion followed by a plateau region (20-150 s), eventually leading to blocking following 360 s immersion. Similarly, the integrated response plot for 2MBI shown in Fig. 9b consists of an initial rapid drop in response area following 10 s immersion before entering a plateau region (20-210 s). The response area then decreases rapidly, approaching full thiol coverage following 420 s immersion. The curves suggest a multistep self-assembly process involving the rapid blocking of substrate sites followed by a much slower occupancy of remaining vacant sites, during which time the overlayer approaches its final structure to form a full 'physical monolayer'.

Background experiments performed for both 2MBT and 2MBI sub-monolayer and 'physical monolayer' films in 0.1 M sulphuric acid indicates that neither molecule is electroactive in the Cu UPD potential region. This data was not applied to correct integrated areas for capacitive current effects due to the inherent difficulties in accounting for the influence of coadsorbed anions during UPD, particularly in the presence of preadsorbed thiols.

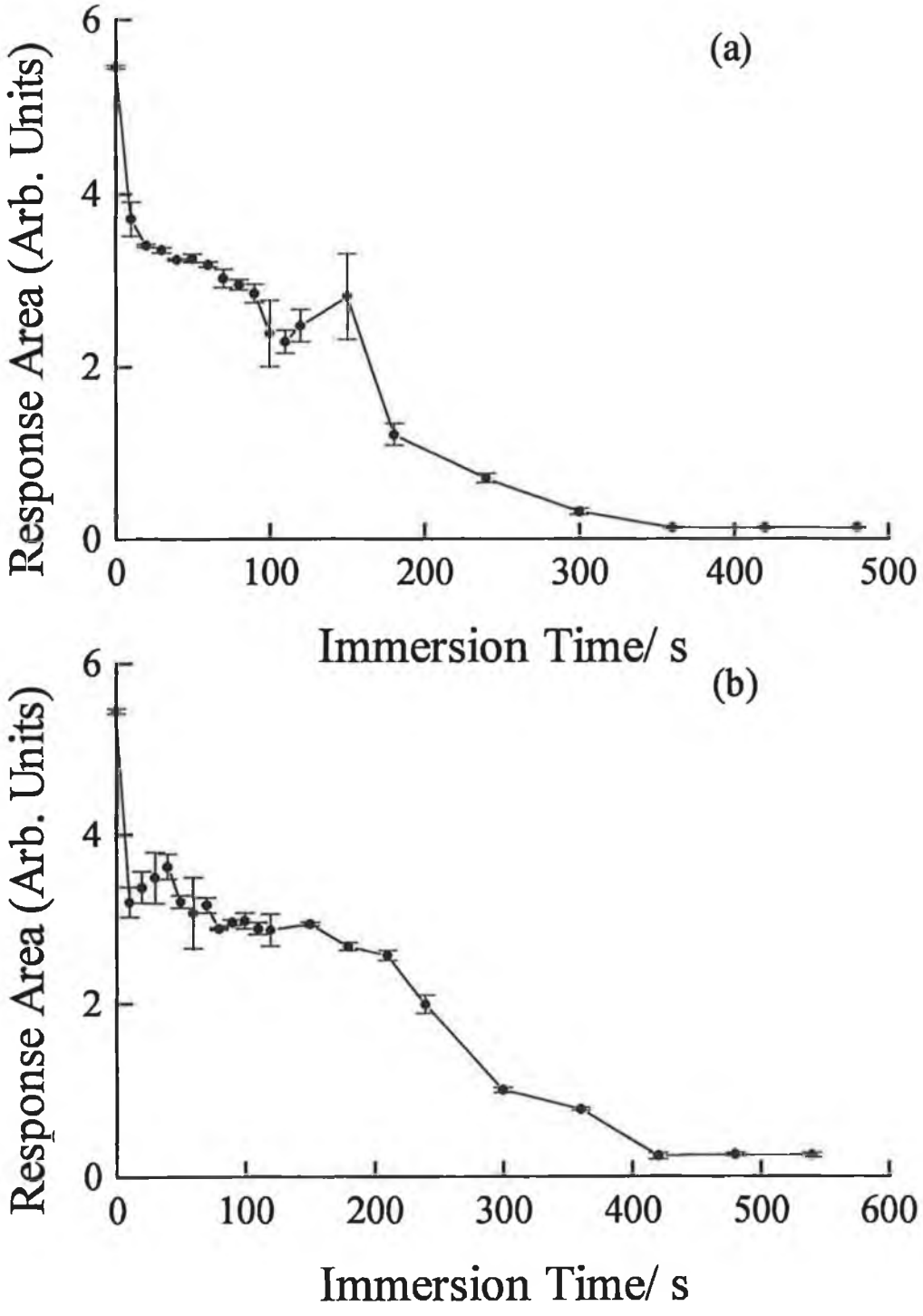

Figure 9 Integrated electrochemical response from Cu UPD cyclic voltammograms as a function of immersion time in 10^{-6} M (a) 2MBT and (b) 2MBI solutions. The error bars represent the standard deviation from the mean value of duplicate samples.

3.4 A proposed growth mechanism For heterocyclic thiols on Au(111)

When atoms or molecules adsorb on single crystalline surfaces, they often form ordered structures over a wide range of coverages. The driving force for this process originates in mutual lateral attractive or repulsive interactions. An important distinction exists between adsorbate-adsorbate and adsorbate-substrate interactions. For thiol chemisorption on Au(111), it is likely that the thiol adsorption site will be determined by optimum thiolate-Au(111) bonding configurations while thiolate-thiolate interactions will dictate the long-range ordering of the overlayer.

Examination of Cu UPD and specific anion adsorption on thiol modified Au(111) can be used to infer conclusions regarding the self-assembly process applicable to heterocyclic thiols which may differ significantly from the molecular ordering found in simple *n*-alkanethiol systems on Au. Bain *et al.* [58] and Hahner *et al.* [59] have proposed a mechanism for *n*-alkanethiol adsorption comprising an initial step in which a large percentage of a monolayer adsorbs rapidly, with the remaining vacant sites requiring significantly longer to fill, which is attributed to consolidation of the film. Buck *et al.* have reported that self-assembly from solution follows Langmuir kinetics, i.e., the sticking coefficient is proportional to the uncovered portion of the surface [60]. A conflict of views exists over the structure of partially formed thiol monolayers self-assembled from the liquid phase. At sub-monolayer coverage, thiols have been reported to island by Cohen *et al.* [61], while Wasserman *et al.* [62] have described the incomplete monolayer in terms of a uniform dispersed phase. Hence, it is unclear whether a 'universal' self-assembly process exists or indeed whether, as is likely, the growth mechanism is system dependent. The two main thiol self-assembly mechanisms that must be considered involve dispersed growth and two-dimensional island growth illustrated in Fig. 10a and b respectively

(1) Two-dimensional dispersed phase growth with random (disordered) or uniform (ordered) distribution of thiol molecules due to repulsive adsorbate-adsorbate lateral interactions producing a high number of metal adatom bonding sites adjacent to the organic adsorbate. This mechanism forces Cu adatoms to adsorb in a local environment which is significantly different to that of unmodified Au(111) substrate. Even at very low thiol coverage, this would result in significant alterations in Cu UPD

features, as the organic adsorbate dispersion should hinder the formation of the open $(\sqrt{3}\times\sqrt{3})R30°$ structure, and drive the Cu growth through completely different structural phases.

(2) Growth of large two-dimensional islands, formed by mutually attractive short-range thiolate interactions, leaving large areas of unadorned substrate available for Cu UPD at low immersion times. Under these circumstances, the $(\sqrt{3}\times\sqrt{3})R30°$ Cu phase should continue to exist up to high thiol coverages. As the adsorbate islands increase in area with increasing immersion times, a new UPD feature would be expected to appear due to Cu interactions with modified Au(111) at thiol island boundaries. Overall, a slow damping of UPD features characteristic to unmodified Au(111) may be expected to occur, accompanied by a minor contribution from Cu-thiol island edge interactions at high thiol coverages.

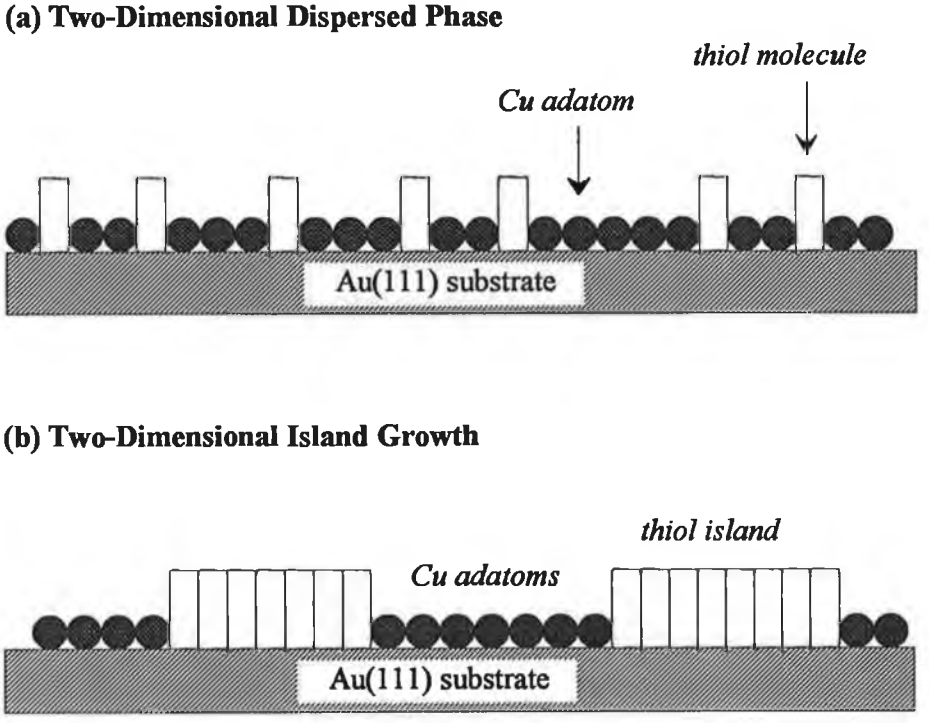

Figure 10 A schematic representation of the possible growth mechanisms for liquid phase self-assembly of 2MBT and 2MBI on Au(111): (a) two-dimensional dispersed phase and (b) two-dimensional island growth.

An intermediate case exists, involving growth of small dispersed two-dimensional islands leaving considerable areas of unmodified substrate for Cu UPD at low thiol coverages. The $(\sqrt{3}\times\sqrt{3})R30°$ Cu phase would be significantly attenuated, and simultaneously, metal adatom-thiol interactions should produce a distinct current-potential response at low thiol coverages. In this situation, Cu not only deposits on unperturbed Au(111), but may also bond to substrate sites in the immediate vicinity of thiol island edges, resulting in the Cu adatom experiencing a different bond energy compared to metal ions bonding on pure Au. If a number of small islands are formed initially, the effect of Cu-thiol interactions will be much greater than in the previous model involving the growth of large two-dimensional islands (at the same thiol coverage). Hence, island boundary-Cu interactions would be small at low immersion times, increasing with self-assembly as more Cu adatoms are forced to bond in the region of thiol molecules, reaching a maximum at intermediate thiol coverages before decreasing gradually as the islands coalesce and completely block Cu deposition.

The resemblance in UPD transformations for both 2MBT and 2MBI implies that their effect on Cu UPD is similar, suggesting a similar lateral distribution. Based on modifications to the electrochemical features for Cu UPD, it is reasonable to conclude that both thiols interact strongly with Au(111) at sub-monolayer coverages and subsequently inhibit Cu deposition at 'physical monolayer' coverages. This strength of adsorption is reinforced by XPS data presented in section 3.1, indicating thiolate formation with Au(111) [32]. White and Abruna have investigated the influence of various nitrogen- and sulphur-containing additives (ionic and molecular) on the UPD of Cu on Pt(111) [63]. In contrast to our work, the additives were adsorbed on Pt(111) from the electrolyte as opposed to pretreating the electrode prior to immersion in the electrochemical cell. They concluded that sulphur ligands cause the most dramatic effects, evidenced as a reduction in the UPD shift and, in the case of propanedithiol, complete inhibition of Cu deposition.

At low immersion times, the thiol (2MBT and 2MBI) presence perturbs but does not eliminate the $(\sqrt{3}\times\sqrt{3})R30°$ Cu adlayer, and a new UPD feature, tentatively assigned to Cu-thiol island edge bonding, appears located between the $(\sqrt{3}\times\sqrt{3})R30°$ and (1×1) peaks. The broad nature of this is attributed to the existence of several different adsorption sites created by thiol chemisorption. This supports the premise of a

situation in which the formation of small dispersed two-dimensional islands of thiol is the most likely growth mechanism in operation; thus, inhibiting but not quenching the open $(\sqrt{3}\times\sqrt{3})R30°$ Cu adlayer phase at low immersion times. The fact that island growth occurs as opposed to random dispersion of individual molecules implies that either a certain degree of cooperative attraction exists between the heterocyclic structures, or that a high local coverage of thiol is required to lift the reconstruction to a (1×1) phase on which adsorption is energetically preferred. As these dispersed islands grow, the $(\sqrt{3}\times\sqrt{3})R30°$ phase is gradually quenched, and the Cu-thiol interaction dominates as more Cu adatoms are forced to interact with the organic adsorbate.

For longer immersion times, as self-assembly proceeds towards blocking coverages, the deposition features are substantially depressed with respect to the dissolution sweep, which may indicate the formation of an incommensurate and/or disordered structure upon deposition. Alternatively, the formation of the Cu adlayer is substantially faster than its removal. This points to a mechanism whereby the organic adsorbate provides less inhibition for adatom bond formation with available substrate sites in comparison to Cu desorption from those sites. Nichols *et al.* have observed the opposite effect when depositing Cu on Au(111) in the presence of a benzothiazonium derivative (present in the electrolyte) [47]. They attributed the suppression of stripping features, relative to deposition features, to penetration of Cu under the adsorbate layer, or partial displacement of the adsorbate layer by the metal adatom. It is feasible to consider a scenario in which metal ion penetration through the 2MBT or 2MBI assembly occurs on the forward sweep, followed by interactions between the thiolate and Cu species, thus hindering the departure of metal adatoms on the reverse sweep. The stability of the resultant thiolate-Cu-substrate complex is indicated by the difficulty in its removal relative to its formation as evidenced by the presence of stripping peaks close to blocking coverages.

Probing the growth mode of thiols by UPD must be interpreted with care, as metal electrodeposition may actually modify the lateral distribution of the organic layer, and thus not reflect the true self-assembly mechanism from solution, provided sufficient mobility is present in the adlayer. An *in situ* SPM study of sub-monolayer thiol adsorption both with and without Cu UPD would confirm whether Cu deposition

leads to thiol redistribution. However, the electrochemical response induced by the organic overlayer structure is stable and reversible over the range of coverages studied in the potential range of interest, as evidenced by the retention of the voltammetric pattern on subsequent cycles.

Complete blocking is achieved for longer immersion times indicating that heteroaromatic thiols form compact molecular assemblies without a substantial density of 'pin-holes' at saturation coverage. This suggests that an equilibrium structure is reached, as strong pinning of thiolate species at non-equilibrium sites is likely to preclude a completely efficient assembly of the film to the densities and structure required to prevent Cu adatoms from 'leaking' through to the Au substrate.

The current-response versus immersion time curves (Fig. 9) should be interpreted with caution due to the well recognised discrepancy between charge-derived coverage and that obtained from structural studies using spectroscopic techniques. This discrepancy is attributed to specific anion adsorption during Cu UPD [56]. Anion coadsorption effects may account for the rapid decrease in current-response after 10 s immersion in thiol solution and the discontinuities in the curves at 150 and 40 s for 2MBT and 2MBI, respectively. It is possible that these features may be intrinsically linked to structural transitions, enhanced/retarded anion mobility, or the removal of anions from the surface due to the presence of chemisorbed thiols. A future electrochemistry/XPS study will address the influence of adsorbing anions and the validity of these curves to quantitatively analyse thiol uptake from solution as a function of immersion time. Nevertheless, the selection of a two-dimensional island growth mechanism (small islands) would appear to be reinforced by adsorption isotherm data (Fig. 9).

3.5 Thiol inhibition of Cu underpotential and bulk deposition on Au(111)

The complete blocking of Cu deposition in the underpotential region and the inhibition of bulk processes have been investigated upon modification of the Au(111) surface with a full 'physical monolayer' of chemisorbed thiol. For comparison, the electrodeposition of Cu on Au(111) at sub-monolayer (UPD) and multilayer (bulk deposition) levels is shown in Fig. 11a. The UPD of Cu, discussed extensively in section 3.3, occurs in two distinct steps, forming the $(\sqrt{3}\times\sqrt{3})R30°$ and (1×1) metal adlayer structures, while the bulk deposition processes occur over a wide potential region with a peak maxima at approximately -225 mV. The deposition onset for bulk processes occurs at -49 mV, and is related to the transition from monolayer to multilayer growth as the energetic influence of the Au(111) surface structure disappears. On the reverse sweep, the removal of bulk Cu is observed as a single sharp peak at 82 mV, which is concurrent with the dissolution of the (1×1) phase, followed by the $(\sqrt{3}\times\sqrt{3})R30°$ stripping peak.

Nichols *et al.* have been studied and classified the electrochemical growth of Cu bulk deposits [47,64]. Following the formation of the underpotentially deposited Cu monolayer, the application of increasingly negative potentials results in the growth of three-dimensional flat-topped Cu islands on top of the pseudomorphic monolayer. The growth morphology, characterised by ***in situ*** STM, is described by the Stranski-Krastanov mode attributed to a relatively strong Cu-Au interaction compared with Cu-Cu interactions. Appreciable strain exists in the UPD monolayer prior to bulk deposition due to the mismatch between the lattice spacings of bulk Cu (0.256 nm) and bulk Au (0.288 nm). The importance of this misfit, after excursions negative of the Nernst potential, is evidenced by the subsequent growth of three-dimensional Cu crystallites, on top of the predeposited two-dimensional monolayer, as opposed to highly strained layer-by-layer growth.

When Au(111) is pretreated with 2MBI to the extent that all underpotential deposition processes are completely suppressed, the resulting modification on bulk Cu processes is shown in Fig. 11b. In the presence of chemisorbed thiol, the initiation of bulk deposition is shifted negatively to -190 mV accompanied by an abrupt rise to a peak maximum at -250 mV. In contrast, bulk removal is shifted positively and

comprises a single broad peak at 132 mV. Underpotential stripping features are not observed. Upon continuous cycling under normal electrochemical conditions of scan rate and applied potential, the adsorption and desorption of bulk Cu changes dramatically. In Fig. 12a, the onset of bulk deposition and the stripping peak potentials approach that found on unmodified Au(111), while the blocked underpotential region becomes obscured in a broad capacitance region extending from 200 to 450 mV. Limiting the potential range to the UPD region reveals that UPD is not restored with successive cycles.

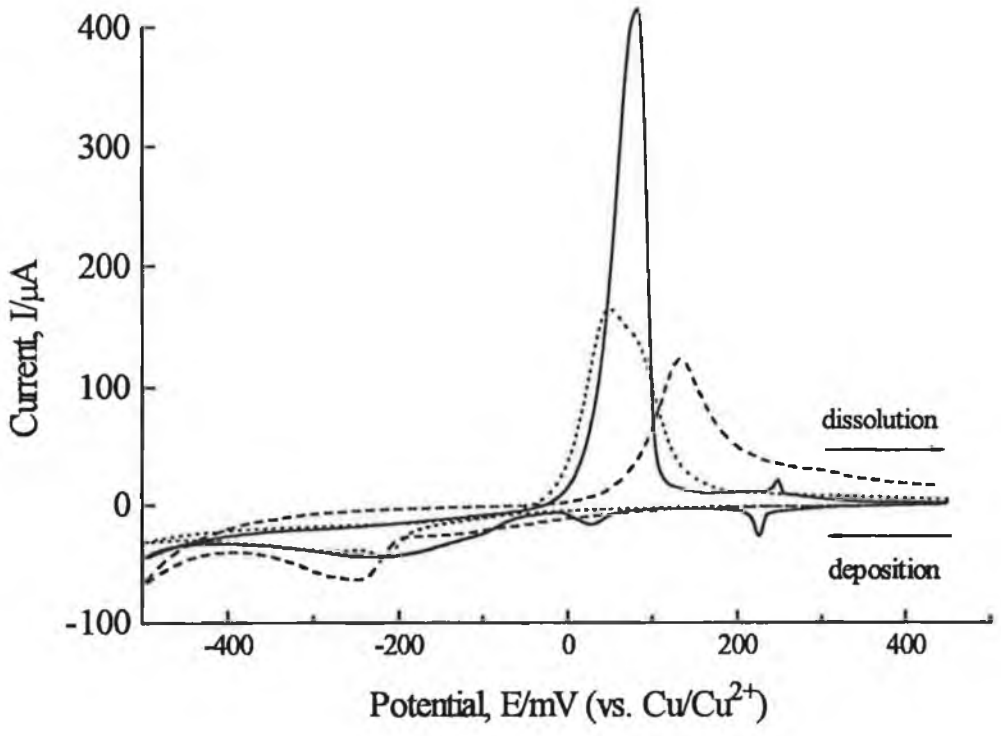

Figure 11 Cyclic voltammograms of Cu UPD and bulk deposition on (a) unmodified (——), (b) 2MBI modified (– – –) and (c) 2MBT modified (·····) Au(111) in 0.1 M H_2SO_4 + 1 mM Cu^{2+} at a scan rate of 10 mVs^{-1}.

Electrodeposition of bulk Cu on Au(111) in the presence of 2MBT is similar to 2MBI, in that all underpotential processes are completely inhibited. The initial cycle encompassing the UPD and bulk regions is shown in Fig. 11c. At -175 mV, the onset for the growth of bulk deposition is observed sharply rising to a peak maximum at -217

mV representing a negative potential shift for bulk onset and positive shift for peak maximum relative to unmodified Au(111). Bulk stripping shifts negative and occurs as a broad peak with a maximum at 49 mV accompanied by a shoulder at approximately 80 mV. Again, after repeated cycles, striking modifications to the voltammetric response are found to occur. This is evidenced as the stripping feature resolving into two overlapping peaks accompanied by a shift towards bulk deposition on unmodified Au(111) as shown in Fig. 12b.

Self-assembly of 2MBI and 2MBT results in the complete passivation of the electrode surface towards UPD such that the only observable process involves bulk deposition and stripping. The initiation of bulk Cu growth is shifted negative in the presence of 2MBI and 2MBT, representing a significant overpotential of 125-140 mV to bulk processes. This signifies a strong interaction between the substrate and the adsorbate, which must be overcome to facilitate Cu deposition. The deposition onset is followed in each case by a rapid rise to a peak maximum, which suggests kinetic inhibition to electron transfer events between the Cu ions at the electrified interface and the electrode surface. Additionally, the organic adsorbate, which blocks the $(\sqrt{3}\times\sqrt{3})R30°$ and (1×1) Cu adlayer phases, can be envisaged as providing a significant complication to nucleation and growth processes necessary to allow Cu growth in the form of three-dimensional islands. Not only is Cu forced to deposit in the presence of a 'physical monolayer' of chemisorbed thiol but, in addition, the pseudomorphic 'precursor' Cu monolayer has been prevented from forming at underpotentials, thus eliminating the gradual potential induced transition from UPD to bulk deposition. Hence, the nature of the bulk Cu deposit that is highly dependent on the Cu-Au lattice mismatch, Cu-Cu interactions and substrate structure can be predicted to undergo major modifications. For both thiol systems studied, upon reversing the scan direction, the bulk stripping peak is significantly attenuated, in comparison to unmodified Au(111). In addition, variation in peak potential and shape were observed due to the vastly different environment from which the Cu is stripped in comparison with unmodified substrate. The absence of any UPD features preceding bulk dissolution indicates that the thiol is retained on the surface, and interacts more strongly with the substrate than Cu.

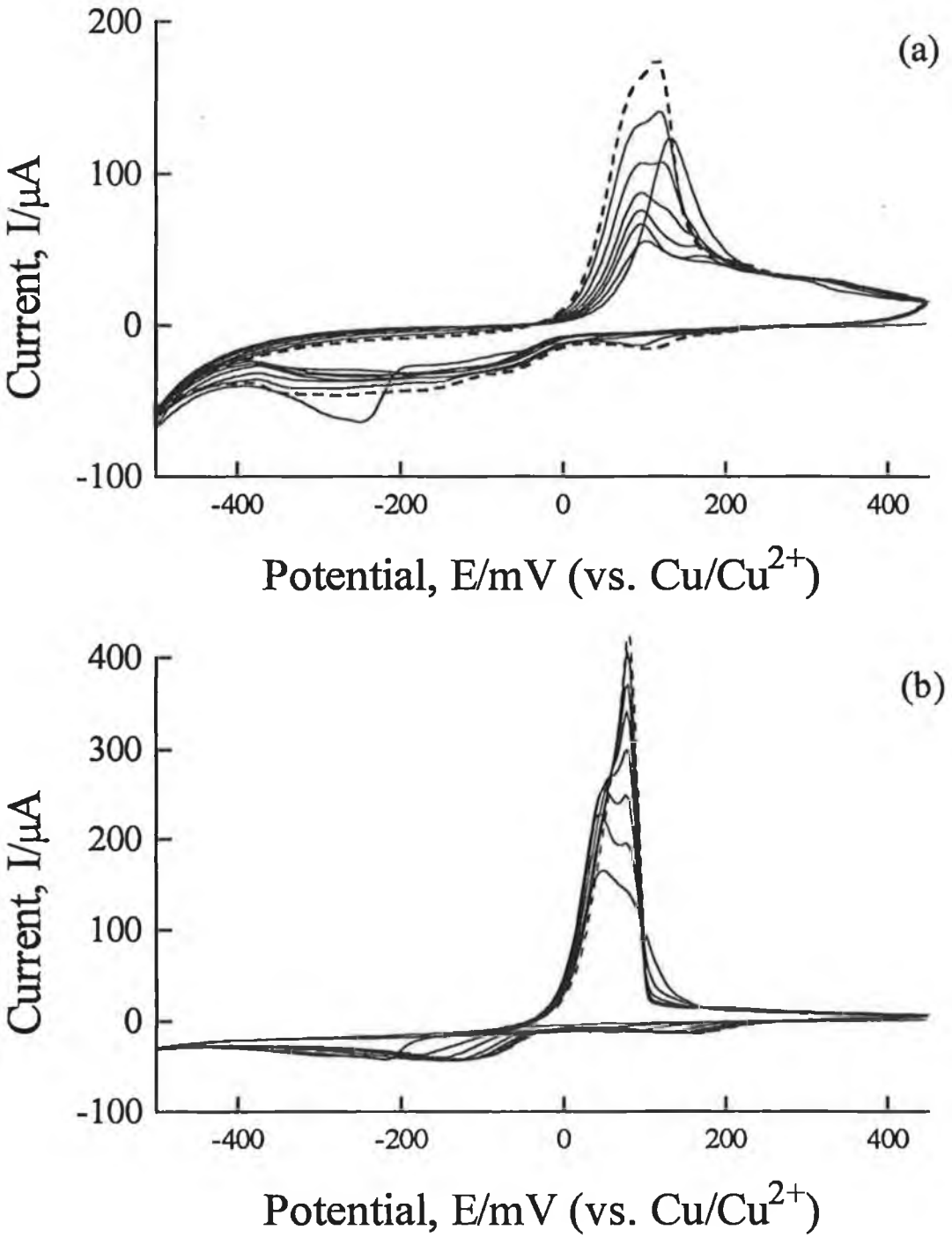

Figure 12 Cyclic voltammograms of Cu UPD and bulk deposition on thiol modified Au(111) in 0.1 M H_2SO_4 + 1 mM Cu^{2+} at a scan rate of 10 mVs^{-1}. (a) 2MBI and (b) 2MBI modified Au(111) showing the first 7 consecutive scans (——) and the final scan (– – –), corresponding to cycle 10 and 8 for 2MBI and 2MBT, respectively, beyond which no change in the electrochemical response occurred.

Harford *et al.* describe a doublet Ag stripping peak on Pt modified with 2-mercaptopyridine which shifts to more positive potentials, accompanied by an increase in integrated charge, due to the oxidation of bulk Ag upon varying the Pt oxide layer coverage prior to adsorption of the organic film [65]. In this work, the observed changes in peak shape and potential with continued cycling are interesting. The implication of this is that the organic adlayer is substantially perturbed by bulk deposition and/or stripping, resulting in gross reductions in the adsorbate blocking properties towards bulk Cu processes. Voltammetric features shift towards bulk phase growth on unmodified Au(111) with a concomitant increase in peak-integrated charge, while passivation of the surface towards UPD is maintained. A detailed explanation for this phenomenon is not available presently and further investigation is in progress.

The effects of heterocyclic adsorbates at full 'physical monolayer' coverage have been detailed for various systems. Harford *et al.* report the influence of pyridine and mercaptan derivatives on the electrodeposition of Ag on polycrystalline Pt [65]. Heterocycles bonding through a nitrogen atom significantly hinder UPD and bulk deposition with the proposed mechanism consisting of the adsorbate remaining bonded to the topmost Ag adlayer as bulk Ag is stripped. In contrast, mercaptopyridine completely inhibits Ag UPD, and the onset of bulk deposition is shifted negative by 130-150 mV. There is no evidence of UPD stripping peaks, prompting the authors to suggest that the molecules remain bonded to the Pt substrate at all times and immediately displace the metal monolayer following bulk stripping (shifted positive by 15-25 mV) in agreement with our results. Taylor and Abruna have investigated the effects of organic adsorbates on the UPD of Ag on Pt(111) and find that the modifications to metal deposition are highly dependent on the nature and structure of the adsorbate species [66]. Nitrogen-containing heterocycles inhibit the second but not the first layer of Ag growth with evidence of kinetic limitations in the formation of the adlayer structure, and the existence of disorder and/or deposition on energetically distinct sites. The authors claim that this is suggestive of the formation of a substrate-Ag-adsorbate structure in which Ag binds to the substrate underneath the organic molecule. Again, all UPD processes were quenched in the presence of sulphur-containing heterocyclic adsorbates, and bulk deposition was observed but suffered a significant overpotential (70 mV), indicative of a strong sulphur-Pt bond. They state

that the absence of UPD stripping features implies that the adsorbate displaces the Ag monolayer following bulk removal, indicating that the sulphur-Pt bond strength exceeds that between Ag and Pt. Nichols *et al.* have studied bulk Cu deposition on Au(111) in the presence of benzothiazonium derivative and, based upon STM characterisation, assign a Frank-van der Merwe growth mode [47]. The organic additive appears to inhibit three-dimensional crystallite growth in favour of the formation of thin Cu films (4-7 monolayers thickness) grown at constant height laterally across the surface. Nichols *et al.* have also investigated the effects of crystal violet on Cu electrodeposition on Au(111) [64]. Again, three-dimensional Cu growth was inhibited by the organic adsorbate which forces Cu to grow parallel to the substrate.

3.6 Oxidative instability of thiols on Au(111)

Bharathi *et al.* have reported the blocking of Cu UPD following modification of polycrystalline Au with 2MBT self-assembled from a 1 mM thiol solution in acetone [26]. In addition, the authors report that upon cycling, the 2MBT modified electrode in the higher potential region (HPR), between 0 and 1300 mV (vs. MSE) at 100 mVs^{-1} for 15 min in 1.0 M sulphuric acid, reversal of Cu UPD blocking occurs. Subsequent HPR cycling for 20 min results in the return of the blocking effect. A second experiment (combined treatment) was described by Bharathi *et al.* involving HPR cycling for 15 min, which apparently 'opens' the monolayer, followed by cycling in the lower potential region (LPR) between 400 and -400 mV (vs. MSE) at 100 mVs^{-1} for 20 min in 1.0 M sulphuric acid. The double layer capacitance associated with the LPR gradually decreased, explained by the authors as a structural rearrangement resulting in the 'closing' of the monolayer. This was explained as being due to a molecular reorientation of 2MBT molecules. They suggest that 2MBT adsorption is irreversible, stable against oxidation, and propose a potential-dependent ring 'opening' and 'closing' property for 2MBT illustrated in Fig. 13.

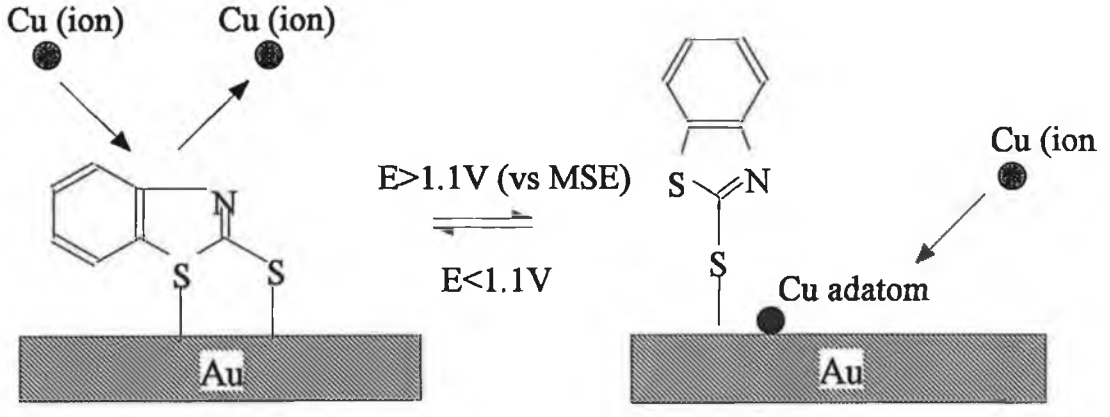

Figure 13 A schematic representation of a structural mechanism proposed by Bharathi *et al.* involving potential-dependent 'opening' and 'closing' of a 2MBT monolayer self-assembled on polycrystalline Au [26].

We have investigated the possibility of a structural reorientation of 2MBT, and the structurally related 2MBI, held responsible for the cycling-induced restoration of Cu UPD, its subsequent blocking, and the reduced charging current in the LPR. In addition, the experiments have been extended to include not only examination of the combined treatments on the LPR double layer capacitance, but also its effect on Cu UPD, which should be blocked if the reorientation model proposed by Bharathi *et al.* is correct.

Initial experiments were performed on unmodified Au(111). In agreement with reported enhancement of surface roughness on Au due to oxide formation and reduction, we find that subjecting the electrode to the HPR results in a 40% increase in the Cu UPD integrated current-response [67,68]. In contrast, cycling in the LPR results in a 44% decrease in integrated charge in the LPR which, upon transfer to Cu containing electrolyte, does not modify Cu UPD. Thus, combining the treatments (sequentially) has no effect on Cu UPD coverage. Hence, while oxide formation and removal increases the surface roughness, the LPR cycling counteracts this effect and results in a Cu UPD which is essentially unmodified with respect to integrated area on the untreated substrate. However, minor changes in peak shape in the form of broadening and potentials shifts (5-10 mV) are apparent as shown in Fig. 14a.

Rapid and continuous cycling of the Au(111) surface modified with a full 'physical monolayer' of chemisorbed 2MBT or 2MBI self-assembled from 1×10^{-6} M thiol solutions in the HPR for 15 min results in the return of features characteristic to Cu UPD. Subsequent cycling in the HPR for 20 min did not restore blocking. LPR treatment for 20 min reduces the capacitance of the double layer, but does not effect thiol blocking of UPD. Fiaud *et al.* have reported a decrease in the double layer capacitance (-0.05 to -0.5 V vs. SCE) of a Cu electrode in acidic media upon addition of 2MBT, and explained this decrease on the basis of the presence of a compact thiol film [69]. In fact, we find that upon cycling in the HPR, transfer to the LPR shows a marked increase in the double layer capacitance signalling that the adsorbed layer has become more porous, perhaps due to irreversible desorption of the organic phase in the HPR. The combined treatment of thiol modified Au(111) produces a dramatic reversal of the Cu UPD blocking effect, as shown in Fig. 14b and c, with a peak structure and integrated response which is almost identical to the treated unmodified

substrate. Hence, HPR cycling does eliminate the blocking effect of the thiol monolayers, but in conflict with the findings of Bharathi *et al.*, continued HPR or LPR cycling does not restore blocking. Identical results were obtained from films formed by self-assembly from 1 mM thiol solutions.

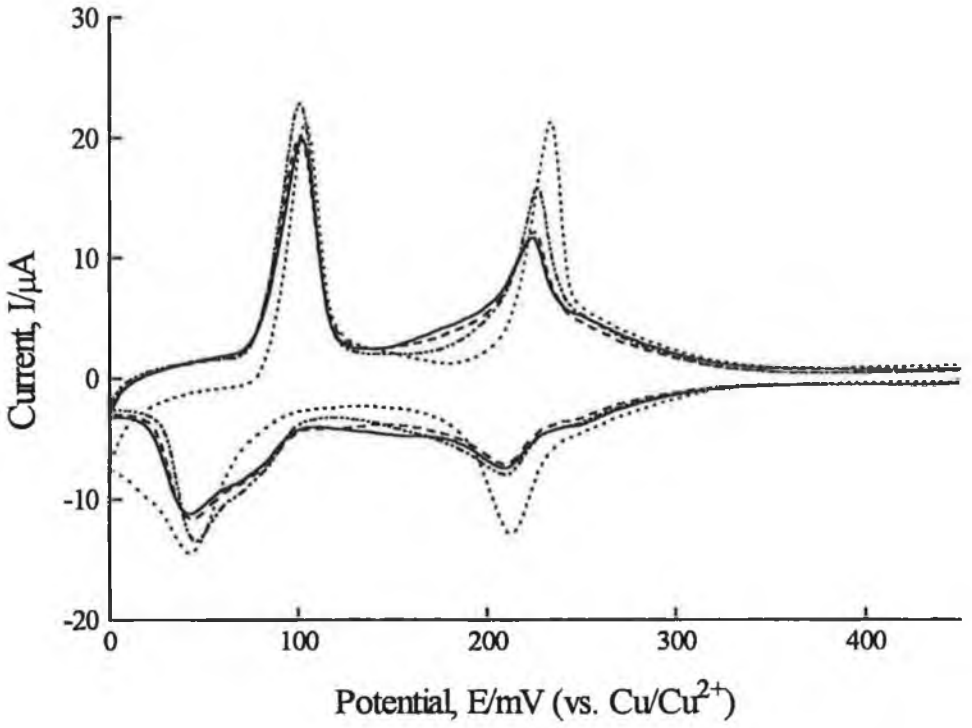

Figure 14 Cyclic voltammograms of Cu UPD, at a scan rate of 10 mVs^{-1} in 0.1 M H_2SO_4 + 1 mM Cu^{2+}, on (a) unmodified (–···–···), (b) 2MBI modified (——) and (c) 2MBT modified (– – –) Au(111) subjected to HPR and LPR cycling treatments. Cu UPD on the untreated and unmodified (·····) Au(111) is shown for comparison.

Interestingly, it has been found that rapid cycling in the HPR for prolonged periods of time is not necessary for the restoration of Cu UPD. Upon subjecting a 'physical monolayer' of 2MBT on Au(111) to a single cycle in this region at 10 mVs^{-1} underpotential Cu growth returns with attenuation of the $(\sqrt{3}\times\sqrt{3})R30°$ phase. Based upon UPD modification studies presented in section 3.3, the adsorption peak at 123 mV can be attributed to the presence of a sub-monolayer coverage of thiol species on the electrode surface. Similarly, UPD processes are evidenced upon subjecting 2MBI

modified Au(111) to a single cycle in the HPR with major modifications in the $(\sqrt{3}\times\sqrt{3})R30°$ adsorption and desorption regions. The 150 mV peak is again related to the existence of chemisorbed thiol remaining on the treated surface. Subjecting both thiol modified electrodes to a second and third cycle in the HPR restores Cu UPD completely, indicating that all of the residual chemisorbed species is removed as shown in Fig. 15a and b. Subsequent HPR or LPR treatment does not restore the blocking properties observed in the presence of untreated adsorbed thiol monolayers.

We relate the restoration of UPD to the oxidative instability of these particular thiols in the HPR. In the first cycle in the HPR, oxidation of Au at 1270 mV, which has been pretreated with either 2MBI or 2MBT, is decreased with the absence of the characteristic prewave shoulder in comparison with oxidation of unmodified Au(111). Successive cycles show an increase in oxide formation (1280 mV) and its reduction (870 mV), with the emergence of the prewave shoulder at 1130 mV in the third cycle, which is comparable to unmodified Au(111) under identical conditions. This transformation is in direct agreement with the restoration of Cu UPD on the third cycle. Such behaviour shown in Fig. 15a and b, may be attributed to a slight attenuation of substrate oxidation in the presence of the protective thiol adlayer which is desorbed during or after oxide formation; thus, exposing the electrode surface for further oxidation and metal UPD. It has been postulated that a metal-oxygen place-exchange mechanism [45,70,71] is operative during oxide formation and its removal, which is known to cause several changes in the Au surface morphology, including the formation of pits, monolayer clusters (islands) and related disordering and roughening processes [67,68]. If considerable surface disruption takes place during oxide formation, increasing the surface area and defect density, thiolate species may remain bound at defect sites which have a higher heat of adsorption than the atomically flat close-packed surface. This may explain the partial desorption of the organic films during a single cycle in the HPR.

In agreement with the results of Bharathi *et al.* we found that passivation of Au(111) to Cu UPD is reversed upon exposure of the substrate to cycles of oxide formation and reduction, but this occurs much sooner in our studies. Observations of the continued presence of UPD features (although slightly modified) upon subsequent treatment of the electrode in the HPR or LPR, disputes their proposal of a potential-

dependent reorientation of the molecule. 2MBT has three atoms available for bonding with the substrate, i.e., the nitrogen and sulphur heteroatoms and the sulphur atom in the thiol functional group. The sulphur heteroatom of the thiazole ring is expected to have weak coordination ability due to the participation of its lone electron pairs in the aromatic delocalised bonding of the molecule, resulting in reduced electron density on the sulphur atom; hence, a decrease in its electron donating tendency, making formation of two highly strained sulphur-Au linkages unfavourable. In addition, loss of the ability to block Cu UPD upon HPR cycling is also found for 2MBI, which is much less inclined to undergo a potential-dependent ring 'opening' and 'closing' which would involve binding to Au through its thiolate sulphur and one of its nitrogen heteroatoms. More importantly, the changes in peak shape and potential are almost identical to those observed on treating unmodified substrate to the same cycling conditions; hence, may not be attributed to the monolayer.

An explanation for the conflict between the results presented here and those of Bharathi *et al.* is difficult to rationalise. It is worth mentioning that our preliminary reorientation experiments were performed exactly as described by Bharathi *et al.*, i.e., self-assembly of 2MBT on polycrystalline Au from a 1 mM solution in acetone with cycling treatment carried out in 1.0 M sulphuric acid with and without Cu^{2+} ions. However, during a study of background solvent effects, we found that even high purity spectrophotometric grade acetone (99.5+ % assay, Aldrich) causes considerable attenuation of Cu UPD peaks following immersion times as low as 15 s. For this reason we elected to work with methanol-based solutions and the more well-defined surface of a single crystal. In considering the work of Bharathi *et al.*, several possibilities must be discussed. Stripping of 2MBT during oxidation of the surface and its subsequent readsorption prior to or during the LPR treatment was considered. However, in our own work, allowing the electrode to 'sit' under nitrogen flow and in meniscus contact with the electrolyte did not facilitate readsorption of thiol from the liquid phase. Due to the absence of UPD modification to the extent witnessed in the results presented in section 3.3, slow self-assembly of any stripped thiol is negligible. The free molecule would exist in the thioketo form in the acidic environment of the electrolyte and complexation with metal ions in solution (Cu(I)2MBT and $Cu(I)_2$2MBI compounds may be prepared by precipitation from aqueous solutions of Cu ions) via

coordination to the thiol/thioketo sulphur is highly probable, making readsorption even less likely [72]. However, operation under less stringent experimental conditions may have allowed contamination of their substrate. We found that inadequate provision of an inert environment in the cell, insufficient electrolyte degassing, and the use of a 'contaminated' electrochemical cell which has previously been exposed to thiol modified electrodes promotes a gradual build-up of impurity species resulting in significant modification of Cu UPD. This could easily be misinterpreted as thiol blocking through ring 'closing.'

Ohswa and Suetaka have investigated the corrosion inhibition mechanism of Cu by 2MBT using XPS, spectro-electrochemistry, UV-visible and infrared spectroscopy showing the formation of a Cu(I)2MBT film on the surface [72]. Infra-red spectroscopy indicates that the films, some hundreds of molecules thick, are compact and strongly adherent to the metal surface, with the aromatic rings of the Cu(I)2MBT complex oriented nearly parallel to the surface. The authors have identified dibenzothiazolyl-disulphide (DBDS) as a primary electrooxidation product of 2MBT. While electrooxidation of 2MBT did not occur under their potential conditions (-0.8 V vs. SCE), the presence of DBDS was detected. This was attributed to the creation of a basic environment in the vicinity of the electrode surface under cathodic polarisation. They explained that production of DBDS is marked in basic solutions where the parent molecule 2MBT takes an ionised form ($R\text{-}S^{-}H^{+}$) which is readily oxidised by small amounts of dissolved oxygen in the electrolyte to a disulphide. In contrast, in acidic solutions, the 2MBT thioketo tautomer is predominant, and oxidation is less probable except in the presence of free Cu ions which are necessary to promote oxidation, resulting in a mixture of DBDS and Cu(I)2MBT.

We believe that desorption of 2MBI and 2MBT monolayers in our study is not facilitated by reaction with dissolved oxygen present in the electrolyte due to the rigid provision of an inert atmosphere within the cell, and electrolyte degassing. In addition, it would appear that the adsorbate layer is stable to the acidic electrolyte, and polarisation conditions applied. Hence, we must assume that the mechanism for thiol desorption is intrinsically linked to substrate oxidation-reduction involving either a displacement reaction or oxidation of the thiolate species. Many groups have investigated factors such as applied potential, substrate, solvent, water and oxygen

influencing self-assembled monolayer stability under electrochemical conditions [73-76]. It appears that adsorbate loss increases with increasingly positive or negative potentials from 0.0 V (vs. Ag|AgCl) with rates of removal highly dependent on the nature of the solvent/electrolyte and, although a mechanism remains undetermined, it has been suggested that substrate oxidation reactions may be relevant to thiol instability at positive potentials in agreement with our findings.

An XPS and AES study of 2MBI and 2MBT acting as corrosion inhibitors on Cu has shown that the thiol group sulphur within the surface complexes may undergo oxidative-dimerisation leading to film degradation [77]. Upon exposure to atmospheric oxygen, two thiol residues combine via the thiocarbonyl group to form a disulphide (-S-S-) bridge. This dimeric structure can undergo further oxidation in air producing thiosulphonate (-S-SO_2-) species. In addition, based on our own XPS data, 2MBI and 2MBT in the crystalline state have been shown to undergo oxidation to sulphonate species [32]. Garrell *et al.* have investigated the effect of oxidation state on formation and stability of sulphur containing aromatic (Ar) molecules on Au [73]. Relative adsorptivities of Ar-SO_3^- << Ar-SO_2^- << Ar-S were attributed to differences in the adsorbate-surface charge transfer interactions such that, in solution thiol, thiol displaces sulphinite and readily displaces sulphonate. Any attempts to electrochemically prepare monolayers of Ar-SO_3^- or Ar-SO_2 from benzenethiol chemisorbed on Au were unsuccessful due to loss of the thiol layer between 0.8 and 1.0 V (vs. SCE) coinciding with substrate oxidation processes. Hence, if the 2MBT and 2MBI monolayers are oxidised to a sulphur containing species in a higher oxidation state during the HPR treatment, irreversible desorption is highly probable. The mechanism of thiol desorption and whether thiols are oxidised prior to desorption remain unsolved questions.

We conclude that oxidation-reduction of Au(111) results in the progressive loss of the surface-confined thiolate species. This oxidative instability is important in determining conditions for successful use of self-assembled monolayers of heterocyclic thiols in electrochemical applications. In our investigations of a possible potential-induced structural reorientation, the production of an oxide layer during HPR cycling apparently causes desorption of the thiol from the electrode|electrolyte interface perhaps due to oxidation of the organic phase or its displacement by Au oxide.

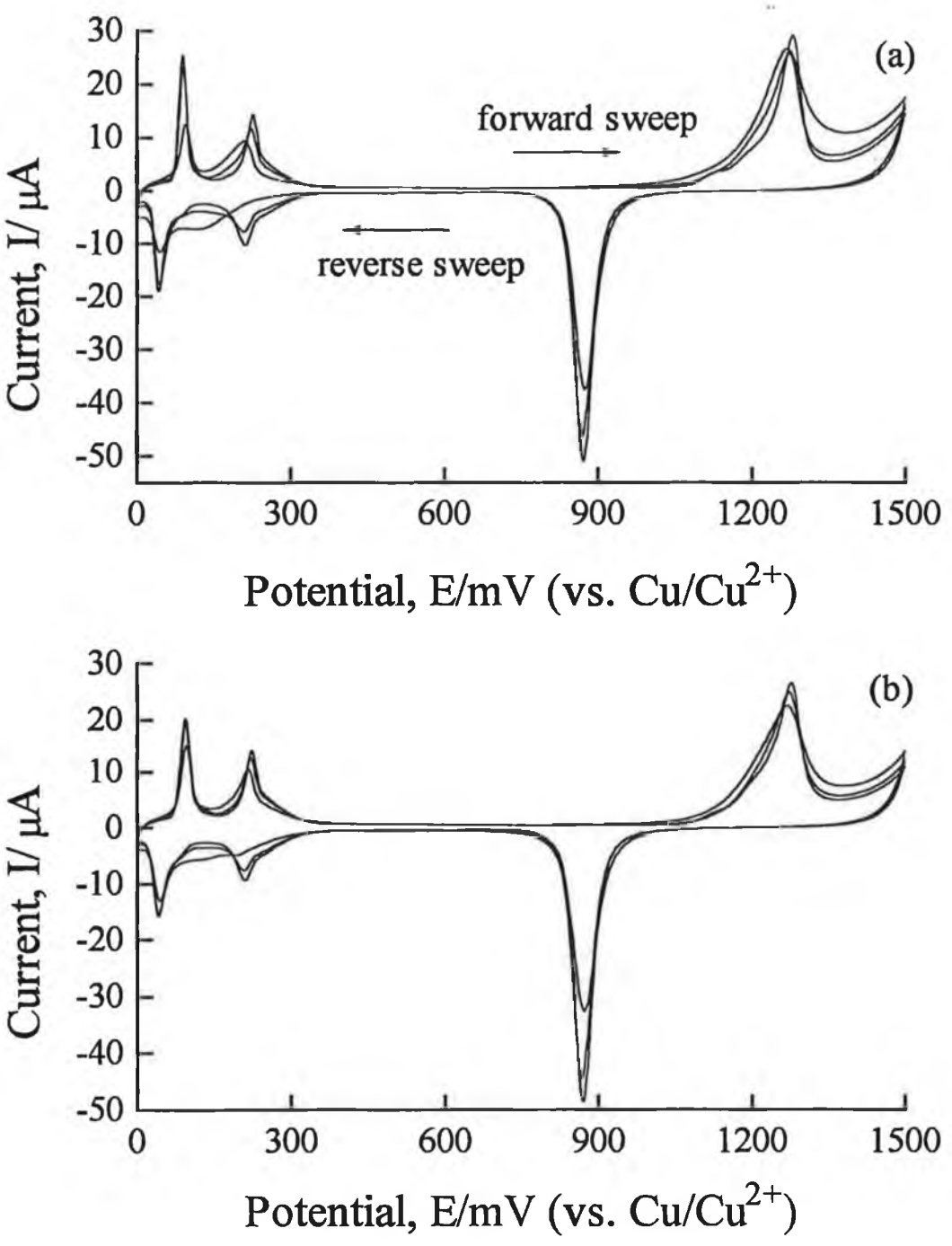

Figure 15 Cyclic voltammograms of Cu UPD and oxidation-reduction showing the first 3 consecutive cycles on (a) 2MBT and (b) 2MBI modified Au(111) in 0.1 M H_2SO_4 + 1 mM Cu^{2+} at a scan rate of 10 mVs^{-1}. Potential scan initiated at 450 mV and swept in the positive direction.

4. Conclusions

XPS analysis of 2MBI and 2MBT films prepared by self-assembly from the liquid phase indicates that the primary adsorbate species is a thiolate. The ability of thiol chemisorption to lift the Au(111)-($\sqrt{3}\times22$) reconstruction to the (1×1) structure has been inferred from the absence of a 'fingerprint' peak for Au(111) in sulphuric acid associated with the reversible removal of the substrate reconstruction. Evidence for adsorbate two-dimensional islanding is suggested from the suppression of anion order-disorder transitions.

We have characterised the influence of these assemblies, at sub-monolayer and monolayer coverages, on the UPD of Cu on Au(111). The creation of new adsorption-desorption features, attributed to metal adatom-thiol interactions, at low immersion times and the survival of the open Cu adlayer structure also supports a mechanism of self-assembly involving small two-dimensional island growth. A multistep adsorption process occurs with initial rapid thiol adsorption followed by a much slower progression to full 'physical monolayer' formation which completely blocks Cu UPD and hinders bulk processes. The significant overpotential for bulk electrodeposition and the retention of UPD blocking, despite substantial changes in the bulk region upon cycling, is indicative of strong thiol-Au interactions with evidence of kinetic inhibition effects.

Subjecting 2MBT and 2MBI layers to substrate oxide formation and reduction results in partial loss of adsorbate from the surface. Successive cycles in this potential region results in irreversible thiol desorption and complete restoration of Cu UPD. Hence, the oxidative instability of these monolayers precludes any possible potential-dependent reorientation, disputing a previously reported structural mechanism of ring 'opening' and 'closing'.

5. References

[1] D.M. Kolb, M. Przasnyski and H. Gerischer, J. Electroanal. Chem., **54** (1974) 25.

[2] D.M. Kolb, in: Advances in Electrochemistry and Electrochemical Engineering, Vol. 11, Eds. H. Gerischer and C.W. Tobias (John Wiley & Sons, New York, 1978).

[3] A. Adzic, in: Advances in Electrochemistry and Electrochemical Engineering, Vol. 13, Eds. H. Gerischer and C.W. Tobias (John Wiley & Sons,Inc., New York, 1984). [4] M.P. Soriaga, Prog. Surf. Sci., **39** (1992) 325.

[4] T. Hachiya, H. Honbo and K. Itaya, J. Electroanal. Chem., **315** (1991) 275.

[5] P. Zelenay, L.M. Rice-Jackson and A. Wieckowski, J. Electroanal. Chem., **283** (1990) 389.

[6] M.S. Zei, G. Qiao, G. Lehmpfuhl and D.M. Kolb, Ber. Bunsenges, Phys. Chem., **91** (1987) 349.

[7] M.P. Soriaga, in: The Structure of Electrified Interfaces, Eds. J. Lipowski and P.N. Ross (VCH, New York, 1992).

[8] A. Ulman, An Introduction to Ultrathin Organic Films: from Langmuir-Blodgett to Self-Assembly (Academic, New York, 1991).

[9] L.H. Dubois and R.G. Nuzzo, Annu. Rev. Phys. Chem., **43** (1992) 437.

[10] S.D. Evans, E. Uranker, A. Ulman and N. Ferris, J. Am. Chem. Soc., **113** (1991) 4121.

[11] C.M. Whelan, M.R. Smyth, C.J. Barnes and N.M.D. Brown, in preparation.

[12] S.-C. Chang, I. Cho and Y.-T. Tao, J. Am. Chem. Soc., **116** (1994) 6792.

[13] H.-Z. Yu, Y.-Q. Wang, J.-Z. Cheng, J-W. Zhao, S.-M. Cai, H. Inokuchi, A. Fujishima and Z.-F. Liu, J. Electroanal. Chem., **395** (1995) 327.

[14] R.J. Willicut and R.L. McCarley, J. Am. Chem. Soc., **116** (1994) 10823.

[15] J.M. Tour, L. Jones II, D.L. Pearson, J.J.S. Lamba, T.P. Burgin, G.M. Whitesides, D.L. Allara, A.N. Parikh and S.V. Atre, J. Am. Chem. Soc., **117** (1995) 9529.

[16] R.N. Goyal, A. Minocha and A.P. Nautiyal, J. Electroanal. Chem., **200** (1986) 119.

[17] J. Clavilier, V. Svetlicic and V. Zutic, J. Electroanal. Chem., **386** (1995) 157.

[18] A.J. Bard, H.D. Abruna, C.E.D. Chidsey, L.R. Faulkner, S.W. Feldberg, K. Itaya, M. Majada, O. Melroy, R.W. Murray, M.D. Porter, M.P. Soriaga and H.S. White, J. Phys. Chem., **97** (1993) 7147.

[19] M.H. Holzle, U. Retter and D.M. Kolb, J. Electroanal. Chem., **371** (1994) 101.

[20] O.M. Magnussen, J. Hotlos, G. Beitel, D.M. Kolb and R.J. Behm, J. Vac. Sci. Technol., B **9** (1991) 969.

[21] L. Blum, H.D. Abruna, J.H. White, M.J. Albarelli, J.G. Gordon, G.L. Borges, M.G. Samant and O.R. Melroy, J. Chem. Phys., **85** (1986) 6732.

[22] O.R. Melroy, M.G. Samant, G.L. Borges, J.G. Gordon, L. Blum, J.H. White, M.J. Albarelli, M.McMillan and H.D. Abruna, Langmuir, **4** (1988) 728.

[23] G. Tourillon, D. Guay and A. Tadjeddine, J. Electroanal. Chem., **289** (1990) 389.

[24] S. Wu, J. Lipkowski, T. Tyliszczak and A.P. Hitchcock, Prog. Surf. Sci., **50** (1995) 227.

[25] S. Bharathi, V. Yegnaraman, G. Prabhakara Rao, Langmuir, **9** (1993) 1614.

[26] J. Clavilier, R. Faure, G. Guinet and R. Durand, J. Electroanal. Chem., **107** (1980) 205.

[27] D.A. Scherson and D.M. Kolb, J. Electroanal. Chem., **176** (1984) 353.

[28] O.M. Magnussen, J. Hagebock, J. Hotlos and R.J. Behm, Faraday Discus., **94** (1992) 329.

[29] G.J. Edens, X. Gao and M.J. Weaver, J. Electroanal. Chem., **375** (1994) 357.

[30] P. Mrozek, M. Han, Y.-E. Sung and A. Wieckowski, Surf. Sci., **319** (1994) 21.

[31] C.M. Whelan, M.R. Smyth, C.J. Barnes and N.M.D. Brown, in preparation.

[32] R.W. Evans and G.A. Attard, J. Electroanal. Chem., **345** (1992) 337.

[33] R.F. Wilson and P. Merchant, Jr., J. Inorg. Nucl. Chem., **29** (1967) 1993.

[34] J. Dehand and J. Jordanov, Inorg. Chim. Acta, **17** (1976) 37.

[35] C.N.R. Rao, R. Venkataraghavan and T.R. Kasturi, Can. J. Chem., **42** (1964) 36.

[36] T. Yoshida, K. Yamasaki and S. Sawada, Bull. Chem. Soc. Jpn., **52** (1979) 2908.

[37] R.G. Nuzzo, B.R. Zegarski and L.H. Dubois, J. Am. Chem. Soc., **109** (1987) 733.

[38] R.G. Nuzzo, L.H. Dubois and D.L. Allara, J. Am. Chem. Soc., **112** (1990) 558.

[39] C.D. Bain, H.A. Biebuyck and G.M. Whitesides, Langmuir, **5** (1985) 723.

[40] P.E. Laibinis, C.D. Bain and G.M. Whitesides, J. Phys. Chem, **95** (1991) 7017.

[41] H. Bethe, Ann. Phys., **5** (1930) 325.

[42] L.H. Dubois, B.R. Zegarski and R.G. Nuzzo, J. Chem. Phys., **98** (1993) 678.

[43] W. Deng, D. Yang, Y. Fang and C. Bai, Sci. China A, 39 (1996) 225.

[44] H. Angerstein-Kozlowska, B.E. Conway, A. Hamelin and L. Stoicoviciu, J. Electroanal. Chem., **228** (1987) 429.

[45] D.M. Kolb, Prog. Surf. Sci., **51** (1996) 109.

[46] R.J. Nichols, E. Bunge, H. Meyerand H. Baumgartel, Surf. Sci., **335** (1995) 110.

[47] L. Blum and D.A. Huckaby, J. Electroanal. Chem., **375** (1994) 69.

[48] D.A. Huckaby and L. Blum, J. Electroanal. Chem., **315** (1991) 255.

[49] L. Blum, M. Legault and P. Turq, J. Electroanal. Chem., **379** (1994) 35.

[50] O.M. Magnussen, J. Hotlos, R.J. Nichols, D.M. Kolb and R.J. Behm, Phys. Rev. Lett., **64** (1990) 2929.

[51] S. Manne, P.K. Hansma, J. Massie, V.B. Elings and A.A. Gerwirth, Science, **251** (1991) 183.

[52] N. Ikemiya, S. Miyaoka and S. Hara, Surf. Sci., **311** (1994) L641.

[53] R.J. Nichols, D.M. Kolb and R.J. Behm, J. Electroanal. Chem., **313** (1991) 109.

[54] A. Tadjeddine, D. Guay, M. Ladouceur and G. Tourillon, Phys. Rev. Lett., **66** (1991) 2335.

[55] D.M. Kolb, D.L. Rath, R. Wille and W.N. Hansen, Ber. Bunsenges, Phys. Chem., **87** (1983) 1108.

[56] Y. Nakai, M.S. Zei, D.M. Kolb and G. Lehmpfuhl, Ber. Bunsenges, Phys. Chem., **88** (1984) 340.

[57] C.D. Bain, E.B. Troughton, Y.T. Tao, J. Evall, G.M. Whitesides and R.G. Nuzzo, J. Am. Chem. Soc., **111** (1989) 321.

[58] G. Hahner, Ch. Woll, M. Buck and M. Grunze, Langmuir, **9** (1993) 1955.

[59] M. Buck, M. Grunze, F. Eisert, J. Fischer and F. Trager, J. Vac. Sci. Technol., A **10** (1992) 926.

[60] S.R. Cohen, R. Naamam and J. Sagiv, J. Phys. Chem., **90** (1986) 3054.

[61] S.R. Wasserman, G.M. Whiteides, I.M. Tidswell, B.M. Ocko, P.S. Pershan and J.D. Axe, J. Am. Chem. Soc., **111** (1989) 5852.

[62] J.H. White and H.D. Abruna, J. Electroanal. Chem., **300** (1991) 521.

[63] R.J. Nichols, W. Beckmann and H. Meyer, J. Electroanal. Chem., **330** (1992) 381.

[64] S.T. Harford, D.L. Taylor and H.D. Abruna, J. Electrochem. Soc., **141** (1994) 3394.

[65] D.L. Taylor and H.D. Abruna, J. Electrochem. Soc., **140** (1993) 3402.

[66] D.J. Trevor, C.E.D. Chidsey and D.N. Loiacono, Phys. Rev. Lett, **62** (1989) 929.

[67] X. Gao and M.J. Weaver, J. Electroanal. Chem., **367** (1994) 259.

[68] C. Fiaud, C. Aucouturier, S. Jannin and J. Talbot, Bull. Soc. Chim. Fr., (1970) 456.

[69] A. D'Agostino and P. Ross, Surf. Sci., **185** (1987) 88.

[70] B.E. Conway, Prog. Surf. Sci., **49** (1995) 331.

[71] M. Ohsawa and W. Suetaka, Corros. Sci., **19** (1978) 709.

[72] C.A. Widrig, C.Chung and M.D. Porter, J Electroanal. Chem., **310** (1991) 335.

[73] W.R. Everett and I. Fritsch-Faules, Anal. Chim. Acta, **307** (1995) 253.

[74] W.R. Everett, T.L. Welch, L. Reed and I. Fritsch-Faules, Anal.Chem., **67** (1995) 292.

[75] R.L. Garrell, J.E. Chadwick, D.L. Severance, N.A. McDonald and D.C. Myles, J. Am. Chem. Soc., **117** (1995) 11563.

[76] D. Chadwick and T. Hashemi, Surf. Sci., **89** (1979) 649.

Chapter 3

A XPS Study of Heterocyclic Thiol Self-Assembly on Au(111)

Abstract

The adsorption of the heterocyclic thiol 2-mercaptobenimidazole (2MBI) self-assembled on Au(111) from the liquid phase has been studied using high resolution X-ray photoelectron spectroscopy (XPS). On the basis of chemical shifts of the nitrogen (1s) and sulphur (2p) electron binding energies for liquid assembled layers, it is concluded that the molecule bonds to Au in the thiol form. A secondary coordination with the surface via the unprotonated nitrogen heteroatom is also possible. Angular dependence of core level intensities and a packing density/layer thickness estimation is consistent with a single monolayer of 2MBI adopting a 'flat-lying' orientation, although slight inclination of the plane of the molecule cannot be ruled out. Liquid phase self-assembly resulted in films which also contained oxygen and excess carbon. Direct *in situ* sublimation of 2MBI onto Au(111) yielded oxygen-free layers, however, partial decomposition of the molecule occurs resulting in the formation of atomic sulphur. In the case of *ex situ* sublimed films, atomic and higher oxidation state sulphur are observed.

1. Introduction

The chemical derivatisation of solid surfaces provides a readily accessible route towards the controlled manipulation of interfacial properties and behaviour in applications such as corrosion inhibition, wettability, and adhesion [1]. Well-defined model organic surfaces act as templates for electronic and optical devices, chemical sensors, lubricants and catalysts, and may be used to generate novel configurations with a view to designing electroactive systems, electron barriers and model biological membranes [2-10].

Alkyl derivatives have become prototype molecules to form self-assembled monolayers (SAMs) that exhibit high organisation and are formed spontaneously as a consequence of exposure of a solid substrate to polar functional groups capable of anchoring the molecule via a strong chemisorption bond [11-14]. While adsorption is the result of the affinity of the polar moiety to the surface, the driving force for self-assembly originates from free energy minimisation involving lateral hydrophobic van der Waals interactions between the saturated alkyl chains which interact only very weakly with the surface [15]. In order to achieve a high packing density, and hence maximise the sulphur-surface and interchain interactions, the molecules orient with saturated chains largely normal to the surface [16-18]. Although a variety of surfaces, e.g., Au, Ag, Cu, Al, Pt, Al_2O_3, Si, and alkyl derivatives have been examined as a means of assembling organised systems, adsorption of *n*-alkanethiols on Au is arguably the best characterised SAM system [19]. Gold is a much utilised substrate in self-assembly studies due to its highly inert nature and slow rate of oxidation and contamination from the ambient environment relative to more reactive metals [20].

In contrast, information regarding the adsorption of aromatic and heteroaromatic thiols is sparse. The introduction of π-systems into the two-dimensional assembly is interesting in terms of its effect on packing and orientation. It has been reported that under certain conditions aromatic groups may be introduced into these assemblies without adversely affecting the packing and order of the monolayer [21,22]. Unsaturated thiols offer advantages with respect to their structure and chemical reactivity which provide the essential properties for derivatisation with multiple chemically specific functional groups and metal complexation. Many studies

have focused on the inclusion of such planar, rigid groups within alkyl chains effectively disrupting the cylindrical symmetry. It has been suggested that optimisation of the position of the aromatic group relative to the monolayer-air interface is essential for the formation of well-ordered surfaces [22]. Clearly heteroaromatic molecules offer considerably more complexity, and to date such self-assembly systems have predominantly featured in surface electrochemical studies in an attempt to understand their bonding on electrode surfaces, molecular orientation, and oxidation/reduction behaviour [23-30].

This study focuses on the self-assembly of the cyclic aromatic thiol 2-mercaptobenzimidazole (2MBI). The 2MBI molecule illustrated in Fig. 1a has a single thiol functional group which may be anticipated to act as the primary chemisorption centre. In addition, one or both of the two nitrogen atoms in the heterocyclic side ring may also act as secondary centres for interaction with the surface. As shown in Fig. 1a, 2MBI may exist in two tautomeric forms. The sulphur atom is protonated in the thiol form leaving two chemically distinct nitrogen heteroatoms one protonated and one unprotonated. In contrast, in the thioketo form both nitrogens are protonated [31-34].

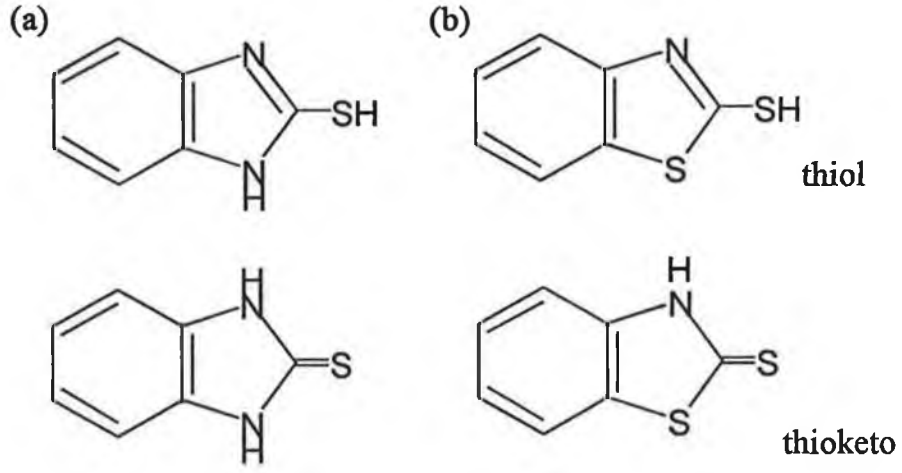

Figure 1 Thiol and thioketo forms for (a) 2-mercaptobenzimidazole (2MBI) and (b) 2-mercaptobenzothiazole (2MBT).

The proposed heterocyclic thiol self-assembly is vastly different from *n*-alkanethiol monolayers due to the structural complexity of the 2MBI molecule. The quadrupolar forces in benzene rings tend to favour an 'edge-to-face' molecular orientation. However, the tendency to arrange the molecules in a mutually opposing configuration may be seriously restricted in the case of chemisorption bond formation between the Au surface and sulphur and/or nitrogen atoms within the 2MBI molecule. In addition, van der Waals forces will still be present and may exert some influence on the packing and orientation of the molecular assembly. A range of basic questions require answering including the form of the adsorbate-substrate interaction, whether adsorption occurs molecularly or partial decomposition occurs upon adsorption, and if molecular, whether the adsorbate is oriented with the plane of the ring system parallel or perpendicular to the surface in 'flat-lying' and 'upright' geometries, respectively.

Such questions are best answered by utilising a model substrate as a template. In this work, we utilise a Au(111) single crystal in combination with monochromated XPS to probe monolayers formed by self-assembly from methanolic solution and by direct sublimation. The former method is that used traditionally for *n*-alkanethiol SAM formation and has the advantage that adsorption can be terminated once the molecular monolayer is complete. This is not necessarily the case for adsorption of dissolved solids such as 2MBI for which liquid phase adsorption may lead to multilayer formation, in the case of a supersaturated solution, and hence, restricting the thiol coverage to a monolayer may require calibration of the 2MBI solution concentration and self-assembly time [35]. Vapour phase film formation eliminates solvent effects on the monolayer and substrate and many technological applications of SAMs may require their formation in the absence of solvent. However, adsorption by vacuum sublimation at 300 K may lead also to multilayer formation making fabrication of a single molecular monolayer more difficult to control.

2. Experimental

Experiments were performed utilising a Scienta ESCA 300 photoelectron spectrometer at the RUSTI unit at the Daresbury CLRC Laboratory, U.K. The spectrometer was equipped with a fast entry load-lock pumped by a turbo-molecular pump to allow rapid insertion of liquid phase self-assembled and *ex situ* sublimed 2MBI films. The sample preparation chamber, allowing 2MBI sublimation in an ultra-high-vacuum (UHV) environment, and the main analyser chamber were both pumped by trapped diffusion pumps and operated at base pressures in the low 10^{-9} Torr range. XPS experiments were carried out using a monochromated Al K_α rotating anode X-ray source operated at 14 KV and 20 mA. Photoelectrons were detected by a hemispherical analyser and a two-dimensional position-sensitive detector (micro-channel plates with CCD camera).

Calibration of the binding energy scale was carried out using the Ag Fermi edge at 0.0 ± 0.07 eV, Ag (3d) photoemission at 368.26 ± 0.08 eV and the Ag MNN Auger line at 1128.78 ± 0.05 eV providing instrumental calibration within $\pm$ 0.1 eV [36]. Charging in insulating samples (2MBI solid phase), which are referenced to the carbon (1s) binding energy reported for benzene-like carbon at 284.7 eV, was minimised by use of an electron flood gun [37].

Different combinations of pass energy and exit slit-aperture width of the analyser allowed variation of the energy resolution. Spectra illustrating peak fitting to experimental data was carried out using mixed Gaussian/Lorentzian (the so-called Voigt function) lineshapes. The energy spread of the monochromator output (0.26 eV) and the analyser resolution (0.55 eV) exceed the natural width of the carbon (1s), nitrogen (1s), oxygen (1s) and sulphur (2p) core levels [36]. Hence, spectrometer induced Gaussian broadening must be included in the peak fitting analysis (Gaussian: Lorentzian mixing ratios are given in the figure captions). The fitting, unconstrained with the exception of the peak shape, consists of a minimum number of peaks consistent with a reasonable fit to the raw data and the molecular structure of 2MBI.

The electrostatic analyser had a large acceptance angle (10°) washing out any photoelectron diffraction and ensuring that signal variation as a function of take-off angle (where the sample manipulator allowed angular resolved studies with an

accuracy of ± 1°) is dominated by inelastic scattering and a 'continuum model' may be used in modelling without recourse to the detailed atomic/molecular structure of the adsorbate-substrate complex.

Measurements on 2MBI self-assembled monolayer and multilayer stability to X-ray flux were obtained with Kratos XSAM800 photoelectron spectrometers (University of Ulster, Coleraine, N.I. and Tampere University of Technology, Finland) with fast entry load-locks and sample preparation chambers pumped by rotary and trapped diffusion pumps, respectively. The spectrometers, operated at a base pressure of 10^{-8} Torr or better, were equipped with unmonochromated Al and Mg K_α dual anode X-ray sources operated at 12 KV and 20 mA, a hemispherical analyser and channeltron multiplier. Spectrometer calibration was achieved with respect to a number of Au core levels. Stability checks of the liquid phase self-assembled mono- and multi-layers to the X-ray beam and secondary electrons produced by photoemission in the underlying Au substrate were performed. The carbon (1s), nitrogen (1s) and sulphur (2p) core levels were collected directly after insertion of the samples into the analysis chamber (analysis time ≈ 10 min). The lineshape and relative intensity of the core levels was then monitored (hourly) as a function of irradiation time over a period of 15 h continuous exposure. The films showed no evidence of degradation.

The Au single crystal (8 mm × 6 mm × 1.5 mm) cut to within 0.5° of the (111) plane (Metal Crystals and Oxides) was firmly attached to a molybdenum backing plate by spot welding two tantalum wires passed through 0.25 mm spark eroded holes drilled through the sides of the sample parallel to the polished front face. The sample could be heated in the preparation chamber up to 700 K, with the temperature being measured using a thermocouple which was not directly in contact with the sample, hence, the annealing temperatures are upper limits due to thermal lag between the heated backing plate and the sample.

A clean Au(111) surface was prepared by repeated cycles of argon ion bombardment (3 KV) and annealing to 600-700 K. The sample was deemed clean when no contaminants could be observed above the XPS noise level in a wide 'survey' scan. Particular attention was paid to the possibility of residual carbon, oxygen, nitrogen and sulphur by multi-scanning areas centred on the major XPS peaks. In all cases the surface was depleted of each element to below the detection limits. As silicon

has been reported as a contaminant of Au surfaces, we also carefully examined the binding energy region of the major Si core levels [38]. Again, no contamination could be observed above the noise level.

Liquid phase SAMs were prepared as follows: a spectroscopically pure Au(111) surface was prepared by argon ion bombardment and thermal annealing. After cooling to room temperature the sample was transferred into the load-lock system, purged with nitrogen gas, followed by rapid transfer into a 1×10^{-6} M methanolic (HPLC grade, 99.9% assay, LAB SCAN, Analytical Sciences) solution of 2MBI (98% purity, used as supplied by Aldrich) at ambient temperature ($20 \pm 1°$) and under continuous mild agitation. Minimum exposure of the substrate to the laboratory atmosphere was achieved to by means of an inert atmosphere glove-box system. The immersion time required to form a monolayer had previously been calibrated electrochemically using Cu underpotential deposition (the experimental details are given elsewhere) [35]. Upon removal from the self-assembly solution, the sample, rinsed with copious amounts of solvent and protected with a droplet of solvent, was inserted into the load-lock which was immediately evacuated and the sample re-transferred into the preparation chamber.

An alternative strategy adopted was deposition by *in situ* and *ex situ* sublimation onto a spectroscopically pure argon bombarded and thermally annealed Au(111) surface. *In situ* sublimation was achieved by gentle heating of 2MBI contained in a quartz tube located in the preparation chamber onto a Au(111) surface at 300 K, while *ex situ* sublimation involved exposure of the substrate under ambient conditions to 2MBI vapour produced upon gentle heating of a Pyrex tube containing 2MBI powder. Multilayer films of 2MBI may readily be formed at 300 K with monolayer films resulting from careful slow dosing or alternatively by thermal desorption of the multilayers.

3. Results and Discussion

3.1 2MBI solid phase

As a starting point high resolution XPS spectra of 2MBI powder were obtained. Figure 2 shows XPS spectra of the carbon (1s), nitrogen (1s), sulphur (2p) and oxygen (1s) core levels. Examination of the structural formula of 2MBI (Fig. 1a) reveals that there are different kinds of carbon within the molecule. While rigorously there are seven inequivalent carbon environments, in practice XPS may not distinguish between the four benzene-like carbon atoms not in direct contact with the heterocyclic side ring. Hence, in the carbon (1s) spectrum it may be expected that at least three or four distinct chemically shifted carbon (1s) core level emissions (thioketo and thiol forms, respectively) will be observed depending on the tautomeric conformation adopted by the molecule. The minor high binding energy peak at 287.7 eV is assigned to the most electron deficient carbon atom in the five-membered side ring connected to the electronegative sulphur and nitrogen atoms. The main peak is clearly made up of at least two components with binding energies of 285.8 and 284.7 eV. The high binding energy shoulder is assigned to the two carbon atoms within the benzene ring attached to single nitrogen heteroatoms with the main carbon peak due to the remaining benzene-like carbon atoms. The solid lines in Fig. 2a illustrates a fit to the experimental data, consisting of three peaks at binding energies 287.7, 285.8 and 284.7 eV, with the expected 1:2:4 intensity ratio.

The nitrogen (1s) spectrum yields information regarding the tautomeric conformation, thiol or thioketo, adopted in the solid phase. Figure 2b illustrates that a single nitrogen (1s) core level emission at 400.9 eV is observed indicating that the chemical environment of the two nitrogen atoms are similar, suggesting that the thioketo form of 2MBI is favoured [31-34]. This was confirmed by transmission FT-IR spectroscopy of 2MBI solid and multilayer films deposited by sublimation onto NaCl plates which clearly demonstrated the absence of the S-H stretching vibration expected at approximately 2600 cm^{-1}, instead, an intense peak at 1100 cm^{-1} may be assigned to the C=S vibration, further confirming the thioketo form dominates.

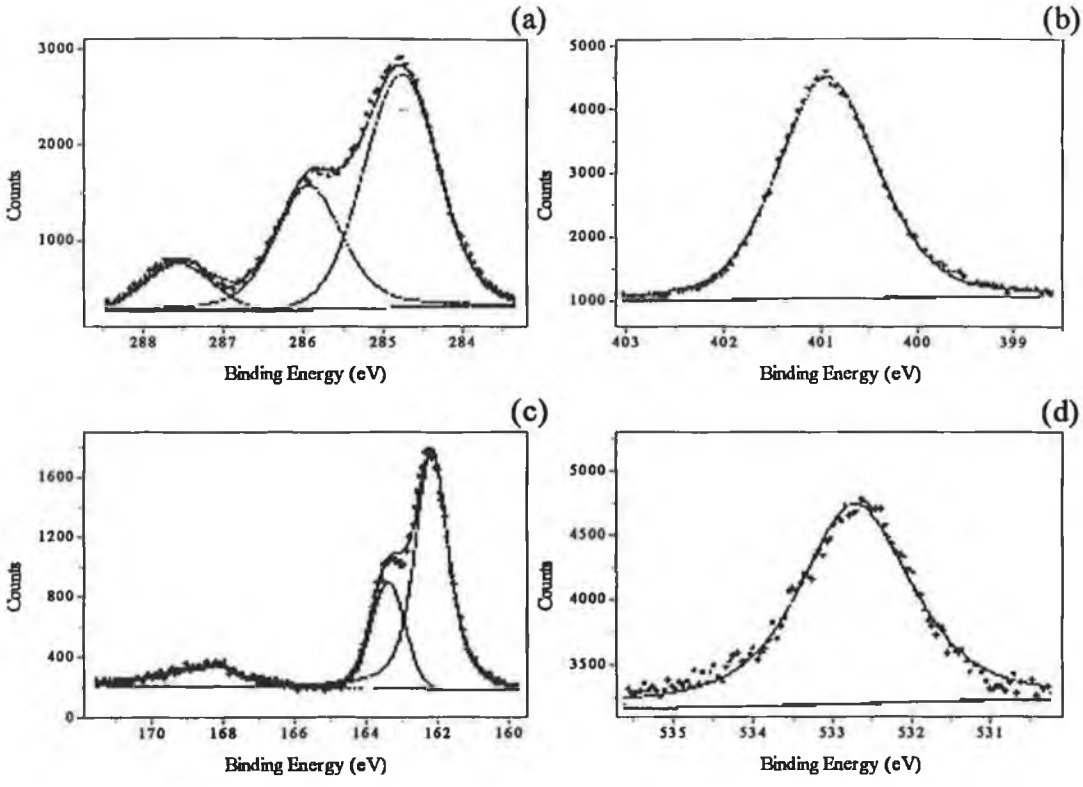

Figure 2 High-resolution XPS spectra of the (a) carbon (1s), (b) nitrogen (1s), (c) sulphur (2p) and (d) oxygen (1s) core levels from solid phase 2MBI. Raw data (+++) and fit to the experimental data using a Voigt lineshape (—). Gaussian:Lorentzian mixing ratio: 20:80.

In Fig. 2c the sulphur (2p) core level is characterised by two $2p_{3/2}/p_{1/2}$ spin-orbit split doublets. The dominant $2p_{3/2}$ emission at 162.2 eV, accompanied by the $2p_{1/2}$ component at 163.4 eV, is typical of thioketo sulphur [34]. Deconvolution of the sulphur emission (solid line Fig. 2c) reveals the characteristic splitting ratio of 2:1 and peak separation of 1.2 eV. A weaker chemically shifted high binding energy peak at approximately 168 eV due to oxidised sulphur, correlates with the presence of a clear oxygen (1s) emission at 532.6 eV (Fig. 2d). This is not surprising as 2MBI and similar conjugated thiols are known to be reactive towards oxidation [39]. The oxygen (1s) peak is fit with a single Voigt lineshape and has a full-width-at-half-maximum (FWHM) of 1.7 eV suggesting that only one type of clearly resolved oxygen

environment exists within the sample. Since the inelastic mean free path of Al K_α-induced sulphur (2p) photoelectrons is around 5 nm, it appears that a thin shell of oxidised 2MBI forms where intimate contact between atmospheric oxygen and surface molecules occurs. However, as the thickness of this oxidised layer is only of the order of 1 nm this should create no problems regarding the solution phase self-assembly of 2MBI.

In order to check the reliability of the elemental quantification using the Scienta spectrometer, the atomic percentage (±0.5%) ratio of carbon, nitrogen and sulphur was calculated by integration of the areas under the carbon (1s), nitrogen (1s) and sulphur (2p) peaks after application of a Shirley background subtraction and correction for atomic sensitivity factors including analyser transmission. The experimental carbon:nitrogen:sulphur ratio measured was 7.0:1.8:1.1 which is in good agreement with the expected 7:2:1 ratio.

It was found that the oxidised sulphur (2p) component constitutes 10% of the detected sulphur species. Upon comparison of the 168 eV peak intensity with the relative amount of oxygen present, assuming all of the oxygen present is bonded to sulphur, is tentatively assigned to a sulphinite moiety (SO_2^-). An XPS and AES study of 2MBI monolayer and multilayer (> 4 nm) films acting as corrosion inhibitors on Cu has shown film degradation due to oxidative-dimerisation of the thiol group sulphur within the surface complexes [40]. Upon exposure to atmospheric oxygen two thiol residues combine via the thiocarbonyl group to form a disulphide (-S-S-) bridge which can undergo further oxidation in air producing thiosulphonate (-S-SO_2-) species. Hence, it is important to determine whether the 2MBI solid phase has, in addition to oxidising, formed the intermediate disulphide (R-S-S-R) structures which may self-assemble on Au. The sulphur (2p) photoemission from R-S-S-R would overlap with the 2p contribution from the thiolate giving rise to inconsistencies in the $2p_{3/2}$ and $2p_{1/2}$ core level intensity ratios [41,42]. The existence of disulphide species cannot be ruled out, however, deconvolution of the sulphur (2p) spectrum shows the correct spin-orbit splitting ratio (2:1) suggesting that large amounts of disulphide species are not present.

Garrell *et al.* have investigated the effect of oxidation state on formation and stability of sulphur containing aromatic molecules on Au [43]. Relative adsorptivities of aromatic-sulphonate << sulphinite << thiolate were attributed to differences in the

adsorbate-surface charge transfer interactions such that in solution thiol displaces sulphinite and readily displaces sulphonate. Hence, if the 2MBI solid is partially oxidised to a sulphur containing species in a higher oxidation state prior to preparation of SAMs, irreversible adsorption of any sulphinite or sulphonate species is less probable than that of the thiol moiety.

3.2 2MBI self-assembled on Au(111) from the liquid phase

Fig. 3 illustrates the carbon (1s), nitrogen (1s), sulphur (2p) and oxygen (1s) core levels for a SAM formed by liquid phase assembly from methanolic solution of 2MBI. The carbon (1s) region shown in Fig. 3a consists of a main peak at 284.8 eV corresponding to benzene ring carbon with broadening on the high binding energy side (286-287 eV) attributed to carbon involved in bonding with the electronegative sulphur and nitrogen atoms.

Most interestingly, a doublet nitrogen (1s) core level with peaks of similar intensity at binding energies 398.4 and 399.6 eV is observed in Fig. 3b strongly suggestive of two chemically distinct nitrogen atoms. It is possible that the orientation of the molecule is such that one of the nitrogen heteroatoms interacts with the surface regardless of tautomeric form. However, it is highly probable that such an interaction would result in nitrogen deprotonation as has been previously reported upon 2MBI compound formation with metal ions [44]. In addition, the observed chemical shift is large (1.2 eV) and is consistent with that expected for a protonated and unprotonated nitrogen suggesting that 2MBI is bonded in its thiol form [34]. Further evidence for the presence of the thiol tautomer is provided upon analysis of a self-assembled 2-mercaptobenzothiazole (2MBT) monolayer film prepared from the liquid phase [35]. This structurally related molecule (Fig. 1b) which may also exist in two conformations, the thiol and thioketo tautomers, contains two sulphur environments (a sulphur heteroatom and a thiol/thioketo sulphur) and a single nitrogen heteroatom. A single nitrogen (1s) peak was observed at 398.6 eV for the 2MBT layer which corresponds closely to the 398.4 eV peak ascribed to the 2MBI unprotonated nitrogen atom.

In Fig. 3c sulphur (2p) emission appears in the form a two component peak, spin-orbit split $2p_{3/2}$ and $2p_{1/2}$ core levels at 162.0 and 163.2 eV, respectively, consistent with the formation of a thiolate intermediate. This indicates that the primary interaction in the monolayer is via a Au-S bond with loss of the sulfhydryl hydrogen [12,13,42,45,46]. It is more difficult to ascertain that a secondary interaction via the lone pair of electrons on the unprotonated nitrogen occurs.

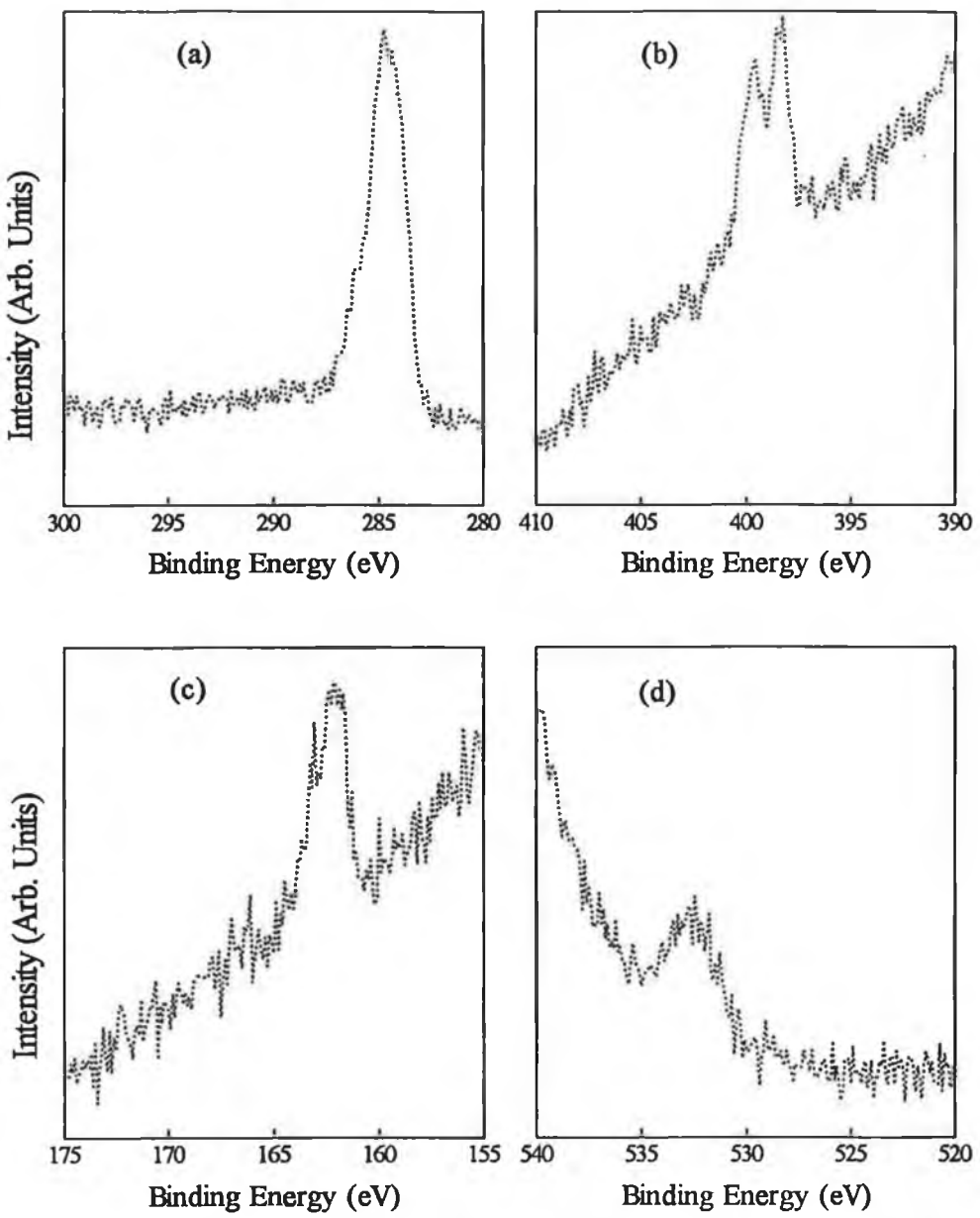

Figure 3 High-resolution XPS spectra of the (a) carbon (1s), (b) nitrogen (1s), (c) sulphur (2p) and (d) oxygen (1s) core levels from a monolayer of 2MBI self-assembled on Au(111) from the liquid phase (10^{-6} M methanolic solution).

Liquid phase 2MBI monolayers are always characterised by the presence of oxygen as a broad asymmetric peak at 532.5 eV as shown in Fig. 3d. In contrast to the

solid phase, examination of the sulphur (2p) core level (166-169 eV) shows no evidence of large amounts of sulphinite/sulphonate formation. Similarly, the nitrogen (1s) core level (403-408 eV) shows no strong indication of oxidation of the nitrogen heteroatoms.

In order to investigate the stoichiometry of the liquid phase SAM the areas of the carbon (1s), nitrogen (1s) and sulphur (2p) levels were integrated and yielded a carbon:nitrogen:sulphur ratio of 7.0:1.5:0.6. Evidently, the films were somewhat carbon rich which distorts the carbon (1s) peak shape, precluding any detailed peak fitting analysis. Quantification of the amount of oxygen within the film indicated a carbon to oxygen ratio of 7.0:0.8 indicating a significant amount of oxygen within the film which is in excess of that expected for simple oxidation of the sulphur group to sulphinite/sulphonate species. The oxygen (1s) peak FWHM of 2.9 eV is considerably larger than in the case of the solid phase (FWHM 1.7 eV) suggesting that more than one type of chemically distinct oxygen is present.

As a relatively inert metal towards chemisorption of oxygen, carbon monoxide, water and hydrocarbons at 300 K, Au does not form a stable oxide under ambient conditions and is reported to be resistant towards atmospheric contamination [20,37,47]. However, we found that exposure of a spectroscopically pure Au(111) surface to the load-lock and atmospheric conditions resulted in emission from carbon (1s) at 284 eV with minor high binding energy components (285-286 eV) and a broad asymmetric oxygen (1s) peak at 532-533 eV. Similar spectra were obtained upon immersion of Au in pure solvent (methanol without thiol). The coverage of carbon was estimated by comparison of the carbon (1s) to Au ($4f_{7/2}$) core level intensity ratio with that of a ($\sqrt{3}\times\sqrt{3}$) ethanethiol monolayer on Au(111) consisting of a known coverage of 0.67 monolayers of carbon (see section 3.3). This calculation yields a value of 1.4-2.1 monolayers of carbon on the Au surface following immersion in methanol for 5 minutes and/or exposure to the load-lock and laboratory atmosphere. Based on the oxygen (1s) to carbon (1s) core level intensity ratio, this implies an oxygen coverage of 0.14-0.18 monolayers (the carbon and oxygen ratio varies somewhat depending on the sample treatment, i.e., load-lock, atmospheric conditions, methanol). In comparison, the oxygen and carbon coverage of the liquid phase assembled 2MBI layer is 0.18 and 2.1 monolayers, respectively. Of this carbon approximately 45% was found to be

contamination based on the measured atomic percentage ratios and knowledge of the molecular stoichiometry of the adsorbate. Identification of the exact source of contamination within the 2MBI layer is difficult due to the overlap of the adventitious carbon (1s) contribution with that of the benzene-like carbon within the 2MBI molecule itself. Similarly, the oxygen (1s) region from the 2MBI layer shows a lineshape and binding energy almost indistinguishable from that observed upon exposure of the Au sample to the load-lock, laboratory ambient and methanol. Hence, under our transfer conditions, the Au surface would appear to be covered with a physisorbed layer of organic material prior to derivatisation with 2MBI.

XPS analysis has allowed us to estimate the extent of substrate contamination prior to self-assembly and the amount of oxygen and excess carbon within the 2MBI layers. Static secondary ion mass spectrometry (SSIMS) constitutes an alternative method of determining the chemical nature of the carbon and oxygen containing species present on the surface and would greatly enhance this study with respect to distinguishing between adventitious and adsorbate contributions to the SAM [48-50].

These observations are similar to those recently reported by Evans *et al.* in which carbon (284-285 eV) and/or oxygen (531-533 eV) were found consistently on evaporated Au films after immersion in a range of spectroscopic grade solvents (ethanol, water, tetrahydrofuran and dichloromethane) [51]. Subsequently, the presence of oxygen in SAMs of octadecanethiol chemisorbed on Au following immersion from such solvents was observed (with the exception of dichloromethane). Bain *et al.* have estimated the thickness of a similar layer of non-volatile carbon- and oxygen-containing contaminants on Au as 0.6 nm using XPS [11]. It seems that, prior to immersion in the self-assembly solution, the Au surface will be covered by physisorbed hydrocarbons. While *n*-alkanethiol SAMs are reported to readily displace such contaminants, the behaviour of heterocyclic thiol in such a displacement mechanism remains unknown (although 2MBI self-assembly appears to displace the majority of adventitious carbon) [19]. The presence of oxygen and excess carbon within the 2MBI SAM may have its origin in a number of sources: from solvent inclusion within the layer, hydrocarbon physisorption via the momentary contact with the atmospheric environment, or residual impurities in the gas or transported from the vessel walls of the load-lock.

3.3 2MBI layer thickness and molecular orientation

Attenuation of the Au($4f_{7/2}$) signal upon self-assembly was used to estimate the thickness of the 2MBI overlayer. The decrease in substrate XPS intensity upon deposition of a film of thickness *d* is given by the relationship:

$$I_d = I_o \exp(-d/\lambda \sin\theta)$$

where (I_o) and (I_d) are the Au($4f_{7/2}$) signal before and after adsorption of 2MBI, λ is the inelastic mean free path (IMFP) and θ is the take-off angle = 90° (the angle between the sample surface and the photoelectrons accepted by the analyser). It has been reported by Laibinis *et al.* that the IMFP in hydrocarbon films is proportional to the kinetic energy (500-1500 eV) [52]:

$$\lambda\,(\text{Å}) = 9.0 + 0.022\,\text{KE (eV)}$$

where KE is the kinetic energy of the Au($4f_{7/2}$) photoelectron (1402.6 eV). This gives an estimate of the IMFP in the 2MBI layer as 40 Å yielding a layer thickness of 4.5 Å. However, as this equation applies only to *n*-alkanethiols, an error may be expected when using it for cyclic systems such as 2MBI as an additional loss mechanism (due to the conjugated π-system) is present and the two-dimensional density of the 2MBI layer will be different. The IMFP for photoelectrons in hydrocarbon layers may also be determined using the Bethe equation which takes the material density into consideration [53]:

$$\lambda \cong (\text{KE}) / [E_p^2 \beta \ln(\gamma \text{KE})]$$

where KE is the kinetic energy of the Au($4f_{7/2}$) photoelectron (1402.6 eV), E_p is the free-electron plasmon energy (19.7 eV), β and γ are empirical parameters. We estimated E_p from

$$E_p = 28.8\,(N_v\,\rho/A)^{1/2}$$

where N_v is the total number of valence electrons per molecule (46), ρ is the density of the material (1.52 gcm^{-3}), and A is the molecular weight (150.20). While γ (0.123 eV^{-1}) can be related to the density of the material by

$$\gamma = 0.151\rho^{-0.49}$$

the value of β (0.034 $eV^{-1}Å^{-1}$) is taken from the work of Laibinis *et al.* [52]. Using these expressions, a value of 21 Å was calculated for the IMFP yielding a thickness of

2.3 Å for the 2MBI layer on Au(111). The calculation of absolute layer thickness by XPS clearly involves precise values of escape depths, a parameter difficult to obtain with a high degree of accuracy for organic systems. It is clear that large errors are involved in the determination of layer thickness by this method dependent on the value of the IMFP adopted. Nevertheless, such a small layer thickness (2.3-4.5 Å) is not inconsistent with a single monolayer adopting a 'flat-lying' geometry, with the plane of the ring parallel or close to parallel with the Au(111) surface, and does not accommodate a layer of 'upright' molecules for which we would expect a layer thickness of approximately 10 Å (based on van der Waals dimensions).

To further probe the surface coverage, the S(2p) to Au($4f_{7/2}$) ratio was measured from the 2MBI film and compared with that measured from a film of known sulphur atomic density [54,55]. Gas phase saturation chemisorption of ethanethiol on Au(111) at 300 K, which forms a $(\sqrt{3}\times\sqrt{3})R30°$ overlayer, yields a coverage of 0.33 monolayers of sulphur. The S(2p) to Au($4f_{7/2}$) ratio for the ethanethiol layer was measured at close to normal emission on a laboratory Mg K_α source [54]. Ignoring the differential attenuation of the sulphur and Au signals by the different nature of the monolayers, which would be small at high outgoing kinetic energies utilised, we have estimated the corresponding coverage for 2MBI to be 0.16 monolayers of sulphur. The number of atoms in an ideal Au(111)-(1×1) surface is 1.39×10^{15} cm^{-2} which implies that 2MBI has a surface density of 2.2×10^{14} molecules cm^{-2}. This must be compared with packing densities (molecules adsorbed per unit area) for 'flat-lying' and 'upright' molecular orientations of 1.7×10^{14} and 2.9×10^{14} cm^{-2}, respectively, on the basis of adsorption without overlap of van der Waals' radii. These calculations suggest the molecule adopts an intermediate tilted geometry favouring a 'flat-lying' or close to 'flat-lying' orientation and are strongly suggestive of a single molecular monolayer being formed. We have only considered the closest packing allowed by the van der Waals dimensions of the adsorbate but alternate possibilities exist in which the molecules are not parallel but arrange in a staggered 'edge-to-face' geometry resulting in lower packing densities.

In an attempt to confirm the molecular orientation, the variation of the carbon (1s) to sulphur (2p) and carbon (1s) to nitrogen (1s) ratios were measured as a function of take-off angle between normal emission and grazing (80° off-normal). In

the case of a 'flat-lying' molecule, no variation in the ratios would be expected as a function of take-off angle while an 'upright' molecule would lead to a rapid rise in the carbon to sulphur/nitrogen ratio at large take-off angles due to attenuation of the sulphur/nitrogen signals by the overlying heteroaromatic carbon framework. Figure 4 illustrates the measured data and the calculated curves (based on IMFP values for the carbon, nitrogen and sulphur photoelectrons estimated using the Bethe equation) for a molecular orientation for 'flat-lying', 'upright' and intermediate orientations of 50° and 70° (with respect to the surface normal) assuming that the molecule is co-planar. The angular dependence appears to support the case for a largely 'flat-lying' surface bound configuration although a slight inclination (±20°) of the plane of the ring cannot be ruled out.

A variety of rigid planar structures, aromatic thiols and structurally related heteroaromatic compounds, adsorbed on Ag(111) and Pt(111) surfaces have been reported to adsorb with the phenyl ring perpendicular to the surface or in a tilted, nearly 'upright' orientation which exhibits long range order in the surface layer [28-30]. An exception is found in those molecules prevented from assuming a vertical orientation by steric constraints such as bulky constituents, in particular, those adjacent to the aromatic heteroatoms which do not coordinate to the metal surface, inducing interactions that prohibit vertical or near vertical bonding configurations [30]. While bulky substituents are not a feature of the 2MBI molecular structure, it is reasonable to tentatively attribute the 'flat-lying' orientation to a bonding arrangement which is favoured by the thiolate sulphur-carbon bond angle and facilitates coordination of both the thiolate sulphur and the unprotonated nitrogen heteroatom to the Au(111) surface.

Thus, we conclude that 2MBI forms a 'flat-lying' monolayer predominantly via thiolate intermediate bonding, with two distinct environments of the nitrogen heteroatoms suggestive of one protonated and one unprotonated heteroatom and perhaps a secondary interaction via the lone pair of electrons on the unprotonated nitrogen. Stoichiometric films are difficult to attain due to the presence of oxygen and excess carbon.

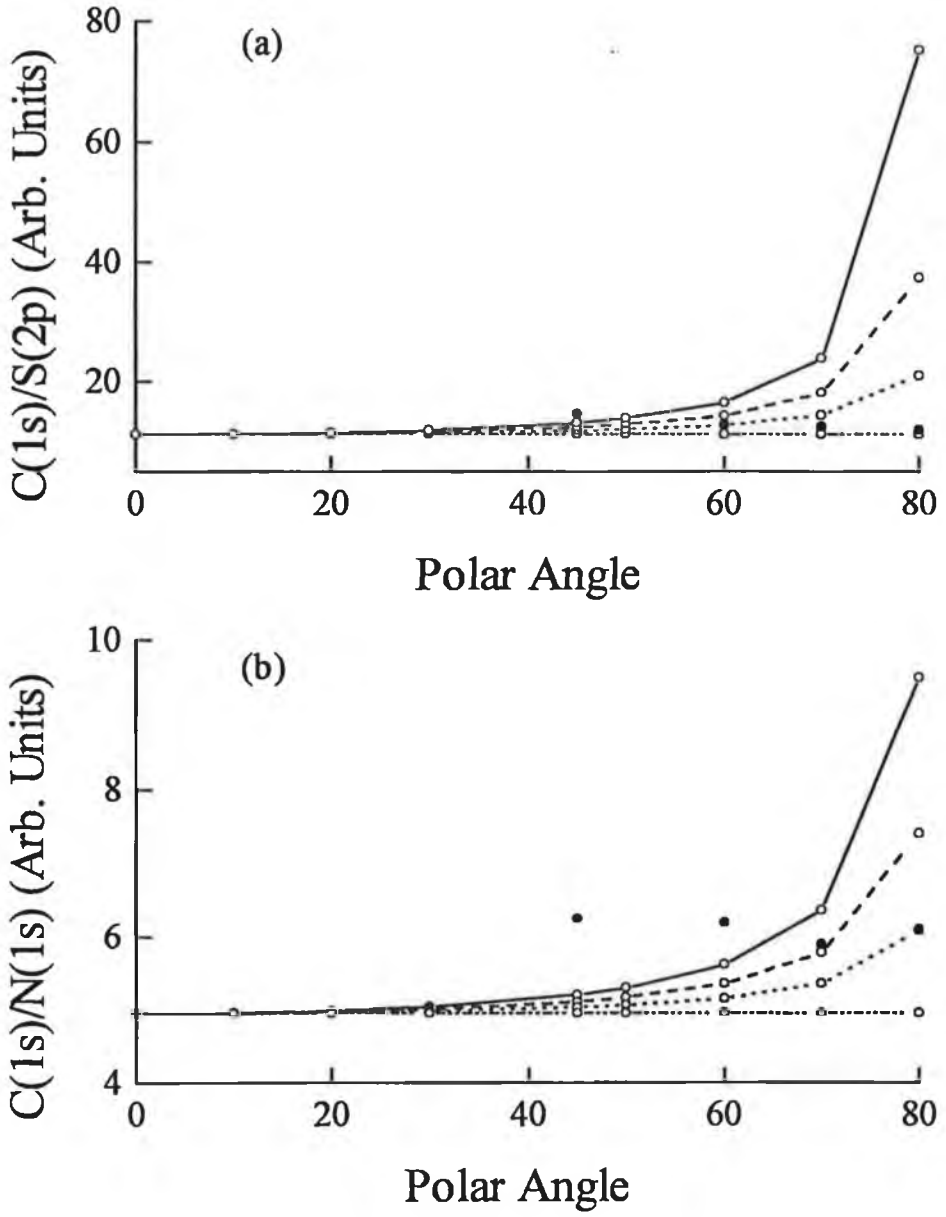

Figure 4 Measured variation of the (a) carbon (1s) to sulphur (2p) and (b) carbon (1s) to nitrogen (1s) core level intensities (•) as a function of take-off angle between normal and grazing (80° off-normal). Calculated curves show the angular dependence of the (a) carbon (1s) to sulphur (2p) and (b) carbon (1s) to nitrogen (1s) core level intensities for 'flat-lying' (—·····—), 'upright' (——) and intermediate orientations of 50 (– – –) and 70° (·····) of the plane of the heterocyclic ring with respect to the Au(111) surface normal (assuming that the 2MBI molecule is co-planar).

3.4 2MBI self-assembled on Au(111) from the vapour phase

In order to examine if oxygen-free 2MBI SAMs could be prepared, adsorption via controlled sublimation in UHV was performed. Few studies have detailed SAMs prepared from the gas phase and those that have compared liquid and gas phase *n*-alkanethiols (high vapour pressure liquids at room temperature) layers have suggested that the properties of both films are similar [55-57]. As 2MBI is a solid at room temperature and pressure, with a melting point of 301-305°C, it may be expected that multilayer films would be stable. A minimum film thickness was estimated from the S(2p) to Au($4f_{7/2}$) ratio assuming layer-by-layer growth, however, it should be noted that this is an underestimate in the case where the multilayers consist of clusters of 2MBI.

Fig. 5 illustrates high resolution carbon (1s), nitrogen (1s) and sulphur (2p) core level spectra from multilayers estimated as a minimum of three layers of 2BMI vacuum deposited on Au(111). In Fig. 5a, the main carbon (1s) emission at 284.7 eV is almost identical to that of bulk 2MBI powder with higher binding energy peaks at 285.9 and 287.7 eV with an intensity ratio of 4:2:0.8. The chemical shifts differ slightly from the solid phase sample possibly due to the influence of the first monolayer chemically bonded to Au and, in agreement with the liquid phase assembled layer, peaks shift to lower binding energy compared with the solid phase. In Fig. 5b, the nitrogen (1s) emission is similar to that found for the solid phase with a single peak at 400.5 eV. However, the sulphur (2p) region is significantly more complicated with at least two sets of spin-orbit split 2p emissions present. While the major peak in Fig. 5c at 162.4 eV, and the 163.6 eV shoulder, may be assigned to first layer molecular 2MBI involved in thiolate bond formation with Au and a thioketo contribution from subsequent layers, a minor feature at 161.1 eV is consistent with the presence of atomic sulphur. The presence of atomic sulphur indicates that partial decomposition of the molecule has occurred during evaporation and/or adsorption. Inspection of the oxygen (1s) region indicated an oxygen-free layer. Integration of the relative atomic carbon:nitrogen:sulphur ratio yields 7.0:2.1:1.5 indicating a film rich in sulphur.

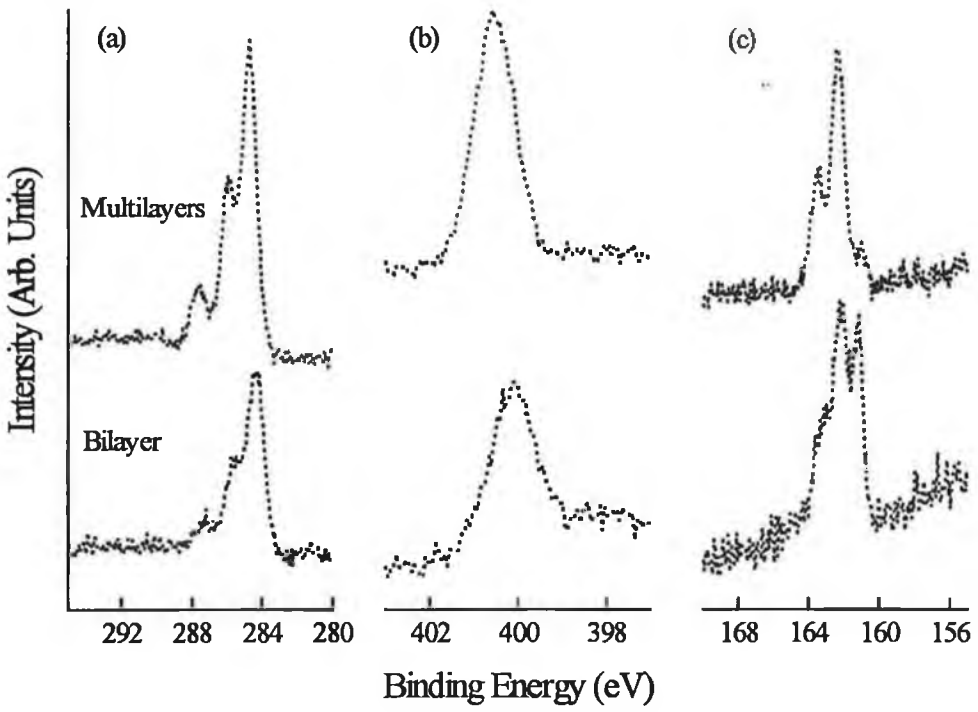

Figure 5 High-resolution XPS spectra of the (a) carbon (1s), (b) nitrogen (1s), and (c) sulphur (2p) core levels from a bilayer and multilayers of 2MBI deposited by direct *in situ* sublimation onto Au(111).

It was observed that upon heating the sample to 600 K, contributions to the sulphur (2p) region from the thiolate and atomic sulphur had equalised in intensity indicating desorption of 2MBI. Further heating to 700 K caused a significant reduction in the amount of nitrogen, sulphur and carbon leaving a monolayer (estimated from the S(2p) to Au($4f_{7/2}$) ratio) of material on the surface consisting mainly of atomic sulphur (161.1 and 162.3 eV spin-orbit split peaks) and carbon (284-285 eV).

Hence, while oxygen-free SAMs may be formed readily by this method, the multilayer film is still of poor quality due to incorporation of significant amounts of atomic sulphur. Thermal desorption of the 2MBI multilayers results in a mixed monolayer containing both thiolate and atomic sulphur.

A two-monolayer (minimum thickness) vacuum deposition also results in an oxygen-free film with a carbon (1s) lineshape similar to that found for the multilayer

film, as shown in Fig. 5a. The nitrogen (1s) core level shown in Fig. 5b consists of a peak at 400.2 eV, an asymmetric feature on the low binding energy side (399-400 eV) of the peak maximum, and possibly a weaker chemically shifted peak at approximately 398 eV assigned to the second layer thioketo and the two first layer thiol nitrogens, respectively. The sample is rich in sulphur with the presence of an atomic peak of greater relative intensity than was the case for the three-monolayer sublimed film. It is interesting to note from Fig. 5c, that the atomic sulphur is enhanced substantially in comparison with the molecular species in the case of the bilayer film, perhaps suggesting that a Au surface-mediated degradation of 2MBI occurs upon adsorption from the vapour phase. Quantification yields a carbon:nitrogen:sulphur intensity ratio of 7.0:1.4:2.0 indicating the presence of excess sulphur relative to nitrogen and insufficient nitrogen relative to carbon. Thus, in addition to the difficulty of controlling exact monolayer formation via the sublimation method, decomposition led to no improvement in the level of integrity of the monolayer. The results from gas phase adsorption in UHV suggest that the composition and chemical nature of the film is somewhat dependent on the evaporation rate, i.e., the exact temperature at which 2MBI is sublimed.

Finally, the propensity of 2MBI towards both oxidation and partial pyrolysis upon sublimation is illustrated in Fig. 6, which shows high resolution carbon (1s), nitrogen (1s), sulphur (2p) and oxygen (1s) core level spectra taken from a multilayer film at least 10 monolayers thick. The film was formed by direct sublimation under ambient conditions in the laboratory environment onto Au(111).

The carbon (1s) lineshape is reminiscent of that of solid 2MBI with the major peak at 284.6 eV, typical of benzene-like carbon and suggestive that the majority of 2MBI retains its integrity without significant pyrolysis as shown in Fig 6a. While adventitious carbon (due to the exposure of the Au(111) surface to ambient conditions prior to *ex situ* dosing) may also be present, its contribution to the main carbon (1s) peak is minimal due to the thickness of the overlying 2MBI multilayer film. The high binding energy shoulder at 285.7 eV and the distinct high binding energy state at 287.0 eV due to the electron deficient carbon atoms in the heterocyclic side ring are clearly visible. The nitrogen (1s) core level shown in Fig. 6b reveals a complex lineshape with

the major peak at 400.9 eV, asymmetric on the low binding energy side (399-400 eV) and a weak emission at 398-399 eV (attributed to the first monolayer).

In Fig. 6c, the sulphur (2p) region is very different from that of the 2MBI liquid and *in situ* prepared films. It now consists of at least three components which are assigned to overlapping emission from the sulphur atoms in unoxidised molecular 2MBI, atomic sulphur resulting from pyrolysis (161-165 eV) and an oxidised sulphur species at higher binding energies. We note the presence of very strong oxidation of the sulphur indicated by the spin-orbit split peak at 168-169 eV which constitutes almost 30% of the total sulphur species detected [40,41]. The oxygen core level shown in Fig. 6d, asymmetric on the high binding energy side, is centred at 531.5 eV and with the ratio of oxidised sulphur to oxygen equal to 1.0:2.7 is consistent with that expected for sulphonate species (assuming all of the oxygen present is bonded to sulphur) [37].

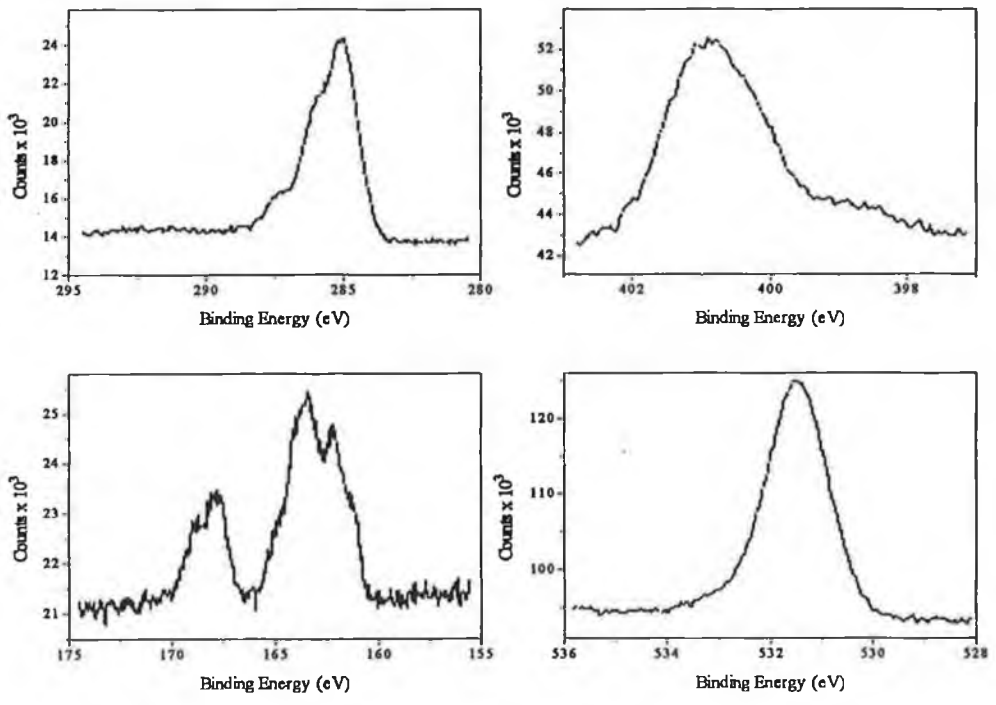

Figure 6 High-resolution XPS spectra of the (a) carbon (1s), (b) nitrogen (1s), (c) sulphur (2p) and (d) oxygen (1s) core levels from multilayers of 2MBI deposited by direct *ex situ* (under ambient conditions) sublimation onto Au(111).

The spectral lineshapes are complicated by the fact that, while the films are multilayered, the emission from the first chemisorbed monolayer will still make some contribution to the data and, in particular, extensive oxidation and partial decomposition of the molecule occurs. Thus, no efforts were made to deconvolute the core level spectra in this case. Integration of the carbon:nitrogen:sulphur core level intensities yields an atomic ratio of 7.0:2.2:1.7 suggestive of excess sulphur produced by pyrolysis.

In conclusion, it appears that direct sublimation leads to formation of multilayer films accompanied by significant oxidation at the sulphur centre to a sulphonate group. Furthermore, partial pyrolysis occurs leading to excess sulphur relative to nitrogen and carbon. Hence, the quality of the films sublimed under ambient conditions in which contamination from ambient may occur and in which oxidation is substantial leads to films of the worst quality of the three methods investigated.

4. Conclusions

Adsorption of 2MBI on Au(111) via self-assembly from methanolic solution leads to formation of a thiolate intermediate. Two nitrogen (1s) core peaks of equal relative intensity consistent with one protonated and one unprotonated nitrogen within the molecule suggests the possibility of a secondary interaction with the Au(111) surface via the lone pair on the unprotonated nitrogen. Quantitative elemental analysis along with study of the angular dependence of the core level intensities suggests that the molecule adopts a 'flat-lying' geometry with the plane of the ring parallel or close to parallel to the Au(111) surface. The 2MBI monolayers formed by liquid phase assembly were always characterised by the presence of oxygen within the layer observed as a broad oxygen (1s) binding energy at 532.5 eV.

Growth of 2MBI layers by direct UHV sublimation yielded oxygen-free films. However, elemental quantification indicated the film to be sulphur rich. High resolution scans of the sulphur (2p) core level indicated the presence of atomic sulphur suggesting partial decomposition of 2MBI upon evaporation and/or adsorption. *Ex situ* prepared layers were further complicated by the presence of oxygen and substantial sulphonate formation.

We conclude that formation of high quality 2MBI films is a non-trivial task due to carbon and oxygen impurities incorporated by liquid phase assembly and in the case of direct adsorption from the vapour phase in UHV and ambient the presence of atomic and oxidised sulphur prevails.

5. References

[1] A.J. Bard, H.D. Abruna, C.E.D. Chidsey, L.R. Faulkner, S.W. Feldberg, K. Itaya, M. Majada, O. Melroy, R.W. Murray, M.D. Porter, M.P. Soriaga and H.S. White, J. Phys. Chem., **97** (1993) 7147.

[2] P.N. Prasad and D.J. Williams, Introduction to Nonlinear Optical Electronics in Organic Molecules and Polymers, Wiley, New York, 1990.

[3] L.J. Kepley and R.M. Crooks, Anal. Chem., **64** (1992) 3191.

[4] I. Rubinstein, S. Steinberg, Y. Tor, A. Shanzer and J. Sagiv, Nature, **332** (1988) 426.

[5] J.J. Hickman, D. Ofer, P.E. Laibinis, G.M. Whitesides and M.S. Wrighton, Science, **252** (1991) 688.

[6] M. Sneydarkova, M. Rehak and M. Otto, Anal. Chem., **65** (1993) 665.

[7] I. Willner, E. Katz, A. Riklin and R. Kasher, J. Am. Chem. Soc., **114** (1992) 10965.

[8] K.L. Prime and G.M. Whitesides, Science, **252** (1991) 1165.

[9] A. Kumar and G.M. Whitesides, Appl. Phys. Lett., **63** (1993) 2002.

[10] P.S. Stayton, J.M. Olinger, M. Jiang, P.W. Bohn and S.G. Sligar, J. Am. Chem. Soc., **114** (1992) 9298.

[11] C.D. Bain, E.B. Troughton, Y.-T. Tao, J. Evall, G.M. Whitesides and R.G. Nuzzo, J. Am. Chem. Soc., **111** (1989) 321.

[12] R.G. Nuzzo, B.R. Zegarski and L.H. Dubois, J. Am. Chem. Soc., **109** (1987) 733.

[13] R.G. Nuzzo, B.R. Zegarski and D.L. Allara, J. Am. Chem. Soc., **112** (1990) 558.

[14] L.H. Dubois, B.R. Zegarski and R.G. Nuzzo, J. Am. Chem. Soc., **112** (1990) 570.

[15] L.H. Dubois and R.G. Nuzzo, Annu. Rev. Phys. Chem., **43** (1992) 437.

[16] A. Ulman, J.E. Eilers and N. Tillman, Langmuir, **5** (1989) 1147.

[17] M.D. Porter, T.B. Bright, D.L. Allara and C.E.D. Chidsey, J. Am. Chem. Soc., **109** (1987) 3559.

[18] J. Hautman and M.L. Klein, J. Chem. Phys., **91** (1989) 4994.

[19] A. Ulman, An Introduction to Ultrathin Organic Films: from Langmuir-Blodgett to Self-Assembly (Academic, New York, 1991).

[20] P.E. Laibinis, G.M. Whitesides, D.L. Allara, Y.-T. Tao, A.N. Parikh and R.G. Nuzzo, J. Am. Chem. Soc., **113** (1991) 7152.

[21] S.-C. Chang, I. Chao and Y.-T. Tao, J. Am. Chem. Soc., **116** (1994) 6792.

[22] S.D. Evans, E. Urankar, A. Ulman and N. Ferris, J. Am. Chem. Soc., **113** (1991) 4121.

[23] S. Bharathi, V. Yegnaraman, G. Prabhakara Rao, Langmuir, **9** (1993) 1614.

[24] S.T. Harford, D.L. Taylor and H.D. Abruna, J. Electrochem. Soc., **141** (1994) 3394.

[25] D.L. Taylor and H.D. Abruna, J. Electrochem. Soc., **140** (1993) 3402.

[26] J. Clavilier, V. Svetlicic and V. Zutic, J. Electroanal. Chem., **386** (1995) 157.

[27] K.R.N. Goyal, A. Minocha and A.P. Nautiyal, J. Electroanal. Chem., **200** (1986) 119.

[28] G.N. Salaita and A.T. Hubbard, Catal. Today, **12** (1992) 465.

[29] J.Y. Gui, F. Lu, D.A. Stern and A.T. Hubbard, J. Electroanal. Chem., **292** (1990) 245.

[30] S.A. Chaffins, J.Y. Gui, B.E. Kahn, C.-H. Lin, F. Lu, G.N. Salaita, D.A. Stern, D.C. Zapien, A.T. Hubbard and C.M. Elliott, Langmuir **6** (1990) 957.

[31] R.F. Wilson and P. Merchant, Jr., J. Inorg. Nucl. Chem., **29** (1967) 1993.

[32] J. Dehand and J. Jordanov, Inorg. Chim. Acta, **17** (1976) 37.

[33] C.N.R. Rao, R. Venkataraghavan and T.R. Kasturi, Can. J. Chem., **42** (1964) 36.

[34] T. Yoshida, K. Yamasaki and S. Sawada, Bull. Chem. Soc. Jpn., **52** (1979) 2908.

[35] C.M. Whelan, M.R. Smyth and C.J. Barnes, J. Electroanal. Chem., **441** (1998) 109.

[36] D. Law and G. Beamson, private communication.

[37] J.F. Moulder, W.F. Stickle, P.E. Sobol and K.D. Bomben, Handbook of Photoelectron Spectroscopy, Perkin-Elmer Corporation, Physical Electronics Division, Eden Prairie, MN 55344, 1992.

[38] N.D.S. Canning, D. Outka and R.J. Madix, Surf. Sci., **141** (1984) 240.

[39] J.M. Tour, L. Jones II, D.L. Pearson, J.J.S. Lamba, T.P. Burgin, G.M. Whitesides, D.L. Allara, A.N. Parikh and S.V. Atre, J. Am. Chem. Soc., **117** (1995) 9529.

[40] D. Chadwick and T. Hashemi, Surf. Sci., **89** (1979) 649.

[41] Z. Mekhali, J. Riga, J.-J. Pireaux and J. Delhalle, submitted to Langmuir

[42] C.D. Bain, H.A. Biebuyck and G.M. Whitesides, Langmuir, **5** (1989) 723.

[43] R.L. Garrell, J.E. Chadwick, D.L. Severance, N.A. McDonald and D.C. Myles, J. Am. Chem. Soc., **117** (1995) 11563.

[44] M. Ohsawa and W. Suetaka, Corros. Sci., **19** (1978) 709.

[45] C.-J. Zhong and M.D. Porter, J. Am. Chem. Soc., **116** (1994) 11616.

[46] D.A. Hutt and G.J. Leggett, Langmuir, **13** (1997) 3055.

[47] M.A. Chesters and G.A. Somorjai, Surf. Sci., **52** (1975) 21.

[48] M.J. Tarlov and J.G. Newman, Langmuir, **8** (1992) 1398.

[49] B. Hagenhoff, A. Benninghoven, J. Spinke, M. Liley and W. Knoll, Langmuir, **9** (1993) 1622.

[50] A. Schnieders, R. Mollers, M. Terhorst, H.G. Cramer, E. Niehuis and A. Benninghoven, J., J. Vac. Sci. Technol., **B14** (1996) 2712.

[51] S.D. Evans, S.D. Cooper and S.R. Johnson, RUSTI Annual Report 1995-1996.

[52] P.E. Laibinis, C.D. Bain and G.M. Whitesides, J. Phys. Chem, **95** (1991) 7017.

[53] H. Bethe, Ann. Phys., **5** (1930) 325.

[54] C.M. Whelan, M.R. Smyth and C.J. Barnes, unpublished data.

[55] L.H. Dubois, B.R. Zegarski and R.G. Nuzzo, J. Chem. Phys., **98** (1993) 678.

[56] O. Chailapakul, L. Sun, C. Xu and R.M. Crooks, J. Am. Chem. Soc., **115** (1993) 12459.

[57] R.C. Thomas, L. Sun, R.M. Crooks and A.J. Ricco, Langmuir 7 (1991) 620.

Chapter 4

A HREELS, XPS and Electrochemical Study of Benzenethiol Adsorption on Au(111)

Abstract

Benzenethiol adsorption from the liquid phase on Au(111) has been studied using high resolution electron energy loss spectroscopy (HREELS), X-ray photoelectron spectroscopy (XPS) and electrochemistry. The absence of a S-H stretching vibration and the presence of benzene-like bands indicates that the sulfhydryl hydrogen is lost during adsorption, consistent with the formation of a thiolate intermediate. Based upon the intensity of the out-of-plane C-H deformation, an adsorption geometry with strong inclination of the plane of the phenyl ring towards an upright orientation on the Au(111) surface is favoured. XPS provides further evidence that the primary adsorbate species is bonded to Au through the sulphur atom. The monolayer film thickness, absolute sulphur surface coverage and molecular packing density confirm a bonding arrangement in which the phenyl ring is aligned largely perpendicular to the substrate surface.

Attenuation of a voltammetric peak, associated with reversible removal of the Au(111)-($\sqrt{3}\times22$) reconstruction, and inhibition of chloride anion adsorption, suggest that benzenethiol chemisorption gradually deconstructs the Au(111) surface to the (1×1) bulk truncated phase and self-assembles through a mechanism involving growth of two-dimensional islands. Specifically adsorbing anions leads to formation of a (1×1) surface structure, causing reorganisation of the organic adlayer, reducing the ability of the Au(111) surface to undergo reversible reconstruction.

The influence of benzenethiol on the underpotential deposition (UPD) of Cu on Au(111) is investigated. At sub-monolayer thiol coverages, a series of broad adsorption features are observed. In contrast, desorption peaks are readily identified from sub-monolayer to high thiol coverages. It appears that saturation coverage of benzenethiol passivates the surface towards Cu adsorption and desorption processes. A benzenethiol coverage dependent study of Cu UPD supported by XPS uptake data, suggests a multistep adsorption mechanism comprising an initial rapid adsorption step with benzenethiol adopting a flat-lying bonding geometry, followed by a slow orientational phase transition to form islands of densely packed upright adsorbate.

1. Introduction

Derivatisation of solid surfaces with coherently organised molecular assemblies has long featured as a means of controlling the structure and behaviour of the electrode|electrolyte interface [1]. An approach comprising electrode modification with functionalised alkanes, resulting in well defined two-dimensional self-assembled monolayers (SAMs), has provided model systems for understanding fundamental physical, chemical and biological interfacial processes [2]. The organic adlayer structure is strongly dependent on the substrate and its morphology, the nature of the substrate-adsorbate bond and intermolecular forces between the adsorbate molecules. To this end chemisorption of *n*-alkanethiols on well defined single crystal Au surfaces have received much attention in recent years [2,3].

The structure of incomplete *n*-alkanethiols layers and, hence, the mechanism of film formation, has been determined using a range of techniques [4]. It has been proposed that self-assembly consists of an initial adsorption process which occurs rapidly, dominated by sulphur-metal chemisorption, described by simple diffusion controlled Langmuir kinetics. This is followed by a slow ordering step in which lateral intermolecular van der Waals interactions between the alkyl chains are maximised [4a,b]. In the case of alkyl chains containing bulky aromatic groups (chromophores), it has been reported that both adsorption steps are coupled and that chain disorder impedes the chemisorption kinetics [5]. In addition, the quality of the monolayer produced has been found to be dependent on both the size of the chromophore, its dipole moment and its position in the alkyl chain, with the packing arrangement adopted by the aromatic groups dominating the monolayer structure [5,6].

In contrast, the intermediate phases formed by aromatic systems, such as benzenethiol adsorbed on Au(111) at sub-monolayer coverages, remains largely unknown. Despite numerous studies of nitrogen and sulphur containing aromatic thiols on metal surfaces such as Au, Pt and Ag, there is little consensus on the structure and behaviour of such SAMs [7-10]. The chemisorbed molecules may distribute over the substrate surface in a dispersed phase or, alternatively, two-dimensional thiol islands with a local structure similar to that of the complete monolayer may form, depending on whether net repulsive or attractive lateral interactions dominate. The two-

dimensional assembly may adopt an upright molecular orientation with respect to the surface, in which the sulphur-metal bond dominates, or a flat-lying bonding geometry with the possibility of interactions between the π-orbitals of the phenyl ring and the substrate. This situation may be further complicated by coverage dependent reorientation. It may be anticipated that, at low adsorbate coverage, a molecule such as benzenethiol will adopt a flat-lying bonding geometry; thus, maximising the interaction of the phenyl ring π-electrons with the surface in addition to forming a strong directional sulphur-metal chemisorption bond. However, as benzene only physisorbs on Au(111), the energy gain due to interaction of a phenylthiolate π-system with the Au surface is predicted to be small [11]. As the surface coverage is increased, an orientational transition may occur to an upright configuration to maximise the number of sulphur-Au bonds formed and hence maximise the two-dimensional packing density of the monolayer.

Underpotential deposition (UPD) describes the formation of monolayer metal deposits on a foreign metal substrate at potentials positive from the reversible Nernst potential for formation of bulk phase [12]. Several groups have shown that coadsorption of organic molecules significantly alters underpotential and bulk deposition mechanisms [8a,13-16]. Similarly, derivatisation of the electrode surface by organic monolayers often provides a means of stabilising a surface reconstruction or deconstructing the surface structure to the (1×1) bulk phase and retarding anion adsorption [17].

This paper forms part of a comprehensive investigation of the simplest aromatic thiol, benzenethiol, adsorbed from the liquid and gas phase on Au(111) and on an atomically stepped Au(322) surface [8c,d]. The focus of the work presented here has been directed towards the surface spectroscopic characterisation of benzenethiol chemisorbed from the liquid phase on Au(111), with a view to elucidating the nature of the adsorption mechanism, adsorbate bonding and molecular orientation. In a previous paper we described a novel approach for probing the growth mechanism of self-assembling heteroaromatic thiols, 2-mercaptobenzothiazole and 2-mercaptobenzimidazole, which involves assessing their influence on the specific adsorption of anions and Cu underpotential deposition (UPD) on Au(111) [8a]. Similarly, we follow the Cu UPD process on Au(111) in the presence of benzenethiol

layers of varying coverages and postulate a growth mechanism for this system. The behaviour of specifically adsorbing chloride anions on benzenethiol modified Au(111) has also been investigated to follow the effect of thiol adsorption on the ($\sqrt{3}\times22$) surface reconstruction.

2. Experimental

A Au(111) single crystal (6 × 8 ×1.5 mm) oriented to within 0.5° of the (111) plane (Metal Crystals and Oxides) was used as a substrate for benzenethiol self-assembly. Grooves and slots spark eroded into the edges and through the bulk of the crystal (positioned close to the unpolished, back face) allowed electrical connection to a potentiostat, attachment of a thermocouple and spot-welding to sample manipulators/mounts for XPS/HREELS analysis.

In electrochemical studies, the Au(111) working electrode was prepared by the flame-annealing technique, cooled in a flow of inert gas (high purity nitrogen), before quenching and formation of a meniscus contact with the electrolyte solution [18]. Cyclic voltammograms for Au(111) in 0.1 M chloride and sulphuric acids were found to be in good agreement with literature reports [19]. A clean Au(111) surface was prepared for high resolution XPS/HREELS experiments by repeated *in situ* cycles of argon ion bombardment (3 KV) and thermal annealing to 600-700 K. The sample was deemed clean when no contaminants could be observed above the XPS/HREELS noise level. Particular attention was paid to the possibility of residual sulphur and hydrocarbon contamination by multi-scanning areas centred on the carbon (1s) and sulphur (2p) core levels and vibrational regions identified with metal-sulphur and aliphatic/aromatic stretching modes [20,21].

For electrochemistry and XPS uptake measurements, liquid phase self-assembly of sub-monolayer and monolayer films was performed by immersion of a clean Au(111) surface (flame-annealed, inert gas-cooled) in 1×10^{-6} M benzenethiol (99+% purity, Aldrich) solution at ambient temperature (20 ± 1 °C) and under continuous mild agitation. HPLC grade methanol was used as solvent (99.9% assay, LAB SCAN, Analytical Sciences). A concentration of 1×10^{-6} M benzenethiol allows films from sub-monolayer to 'physical monolayer' (equivalent to the 300 K saturation coverage of benzenethiolate on Au(111) following chemisorption from the liquid phase) coverages to be formed by controlling the immersion time. 'Physical monolayer' films formed under these conditions were found to block Cu UPD as effectively as films prepared by immersion (> 6 h) in 1×10^{-3} M benzenethiol solution. Following film formation, the sample was rinsed with copious amounts of methanol and quickly transferred to the

electrochemical cell/spectrometer. In the case of HREELS and high resolution XPS measurements, liquid phase SAMs were prepared by immersion (> 6 h) of a clean Au(111) surface (argon ion-bombarded and thermally annealed) in 1×10^{-3} M benzenethiol solution at ambient temperature followed by rinsing with methanol.

Electrochemical experiments were performed in a two-compartment Pyrex glass cell described previously [8a]. The electrochemical cell, its accessories and all glassware required for the preparation of electrolyte and thiol solutions were cleaned by soaking for >12 h in a dilute solution of $KMnO_4$ (99.8% purity, Aldrich) in concentrated sulphuric acid (97-99% GPR, BDH). These items were then rinsed thoroughly and steamed with deionised water (18.2 $M\Omega cm^{-1}$).

Deaerated aqueous 0.1 M sulphuric and hydrochloric acids (doubly distilled, ultrapure grade, Aldrich) were prepared with deionised water and 1 mM Cu^{2+} solution was prepared by dissolution of $CuSO_4.5H_2O$ (99.999% purity, Merck) in base electrolyte. All working solutions were purged and blanketed with research grade nitrogen (99.9995%, B.O.C. Special Gases) purified by an oxygen trap (Supelco Chromatography) which decreases oxygen impurities to less than 0.005 p.p.m.

Electrode potentials in Cu^{2+} containing solution are given with respect to the reversible $Cu|Cu^{2+}$ electrode (Cu wire, 99.999% purity, Goodfellow Cambridge) cleaned by immersion in concentrated nitric acid (69% GPR, BDH) and rinsing with copious amounts of deionised water. Electrode potentials in solutions not containing metal ions are referenced to a standard Ag|AgCl (1 M KCl) half-cell (Bioanalytical Systems). Cyclic voltammetry was performed using a BAS CV-50W potentiostat (Bioanalytical Systems). The working electrode was immersed in the electrolyte under potential control, and care was taken to avoid potentials where oxide formation and bulk deposition of Cu occur. The voltammograms shown are the result of the first potential sweep (unless otherwise indicated in the figure captions).

Background experiments for the immersion of the Au(111)-($\sqrt{3}\times22$) surface in methanol were performed. The reconstruction is lifted to the (1×1) phase following 150 to 170 s exposure to solvent, however, the characteristic response due to an order-disorder transition within the anion adlayer remains at least up to 600 s immersion (longer times not investigated). Exposure of Au(111) to methanol for > 300 s results in slight attenuation in Cu UPD peaks, which may be due to the accumulation

of adsorbed impurity species present in the solvent or to decomposition of methanol at substrate defect sites. To summarise, the contribution of solvent effects to the observed electrochemistry are not substantial for the immersion times of interest.

High resolution XPS measurements were performed utilising a Scienta ESCA 300 photoelectron spectrometer (operated at base pressures in the low 10^{-9} Torr range) at the RUSTI unit, Daresbury CLRC Laboratory, U.K. A monochromated Al K_α rotating anode X-ray source was operated at 14 KV and 20 mA. Photoelectrons were detected by a hemispherical analyser and a two-dimensional position-sensitive detector (micro-channel plates with CCD camera). Calibration of the binding energy scale was carried out using the Ag Fermi edge, Ag (3d) photoemission and the Ag MNN Auger line providing instrumental calibration within ± 0.1 eV [22]. The large acceptance angle of the electrostatic analyser (10°) ensures that any photoelectron diffraction effects are washed out and signal variation as a function of take-off angle which may be defined ± 1° is dominated by inelastic scattering and hence a continuum model may be used in modelling without recourse to the detailed atomic/molecular structure of the adsorbate-substrate complex.

Different combinations of pass energy and slit-aperture width allowed variation of energy resolution. The 0.26 eV width of photon source and the analyser resolution of 0.34 eV exceed the natural width, described by a Lorentzian function, of the carbon (1s) and sulphur (2p) core levels. Hence, spectrometer induced Gaussian broadening must be included in the peak fitting analysis. Peak fitting to experimental data was carried out using a mixed Gaussian-Lorentzian lineshape and a minimum number of peaks consistent with a reasonable fit to the raw data and the molecular structure of the adsorbate. The fits were unconstrained, with the exception of the peak shape.

Benzenethiol uptake measurements were carried out using a Kratos XSAM800 photoelectron spectrometer operated at a base pressure of 10^{-9} Torr or better, equipped with a unmonochromated Al and Mg K_α dual anode X-ray source operated at 13 KV and 18 mA, a hemispherical analyser and multi-detector array. Spectrometer calibration was achieved with respect to a number of Au core levels. Stability checks on the organic films to the X-ray beam and secondary electrons produced by photoemission in the underlying Au substrate were performed by monitoring (analysis time ≈ 20 min) the lineshape and relative intensity of core levels as a function of

irradiation time over a period of 3 h continuous exposure. The films showed no evidence of degradation.

The HREELS spectrometer was equipped with a fast entry load-lock pumped by a turbo-molecular pump to allow rapid sample insertion. The sample preparation and main analyser chambers were both pumped by trapped diffusion pumps and operated at base pressures in the low 10^{-10} Torr range. HREELS spectra were recorded at 6.0 eV primary electron beam energy in specular geometry ($\theta_i = \theta_r = 70°$) using a 180° hemispherical monochromator and analyser described in more detail elsewhere [23]. Typical optimum energy resolution of the elastic electron peak from clean Au(111) was 10 meV (~80 cm^{-1}) and 1×10^5 counts s^{-1}, in terms of full-width-at-half-maximum (FWHM) and count rate, respectively.

3. Results and Discussion

3.1 Electron energy loss spectroscopy

In Fig. 1, the HREELS spectrum from a monolayer derived from benzenethiol liquid phase self-assembly contains the vibrational bands expected from the parent compound with the absence of the S-H stretching mode (2580 cm^{-1}) [21]. Electron energy loss frequencies are summarised in Table 1 and proposed assignments are made by correspondence with accepted gas phase infrared (IR) assignments and several previous HREELS studies of benzenethiol adsorption on metal surfaces [8c,8d,9,24]. Specific vibrational bands in Fig. 1 indicate the molecular structure of the adsorbate species. Although the S-H stretching vibration is not particularly strong in an IR spectrum from the parent compound, its absence in the HREELS spectrum suggests that the sulfhydryl hydrogen is lost during adsorption on Au(111), consistent with the formation of a phenyl thiolate surface intermediate. In the case of a S-H bond oriented parallel to the surface, the S-H stretching vibration is dipole forbidden and, hence, only a weak intensity would be observed due to impact scattering in specular geometry ($\theta_i = \theta_r = 70°$). However, previous HREELS work indicates that a S-H stretch should be clearly seen and, in addition, S-H bond scission is predicted based on several studies of benzenethiol adsorption on Au and other metals surfaces [9,24,25]. Unfortunately, Au-SC_6H_5 stretching (~ 460 cm^{-1}) is difficult to identify due to the weak nature of its energy loss superimposed on the tailing elastic peak and the C-S stretching frequency (~700 cm^{-1}) is obscured by ring modes [9,24]. However, given that benzene does not adsorb on Au at 300 K, the presence of aromatic vibrational bands, in particular the C-H stretching and out-of-plane deformation features (3010 and 742 cm^{-1}, respectively), excludes the occurrence of extensive C-S bond scission, indicating that in the adsorbed state benzenethiol retains its molecular framework [11].

Table 1 Electron energy losses and band assignments for benzenethiol adsorption on Au(111).

Assignment[A]	C_6H_5SH (gas)[B]	C_6H_5S/Au(111)
	cm^{-1} (meV)	
ν(C-H)	3000-3030	3010 (373)
ν(S-H)	2580	
ν(C-C), γ(C-H)	1450-1600	1450-1600 (180-200)
δ(C-H)	1065-1075	1020 (127)
γ(C-H)	740-760	742 (92)

[A]ν = stretch; δ = in-plane bend; γ = out-of-plane bend. [B]Shen *et al.* [24a].

In specular scattering geometry, the relative intensity of the out-of-plane C-H deformation (742 cm^{-1}) to the C-H stretching vibration (3010 cm^{-1}) provides information on the orientation of the phenyl ring relative to the Au(111) surface plane by applying the metal-surface selection rule (only modes with a dipole moment component normal to the surface are active) [26]. In the case of a phenyl ring orientated normal to the Au surface, the out-of-plane C-H deformation which has a dipole moment perpendicular to the ring would have zero intensity (although impact scattering may give rise to a low intensity vibrational band even in specular geometry). In contrast, the energy loss due to in-plane C-H stretching, which has its dipole moment within the plane of the ring, should be strongly excited. Conversely, for a flat-lying molecule with its phenyl ring parallel to the Au surface, the 742 cm^{-1} band should be of maximum intensity with a weak 3010 cm^{-1} band due to impact scattering. As the in-plane C-H stretching band is the dominant feature in Fig. 1, relative to the C-H deformation mode, this indicates that the benzenethiolate intermediate adopts an adsorption geometry with its phenyl ring strongly inclined relative to the Au(111) surface. However, the out-of-plane C-H deformation mode does not disappear completely suggesting a perfectly upright geometry does not occur.

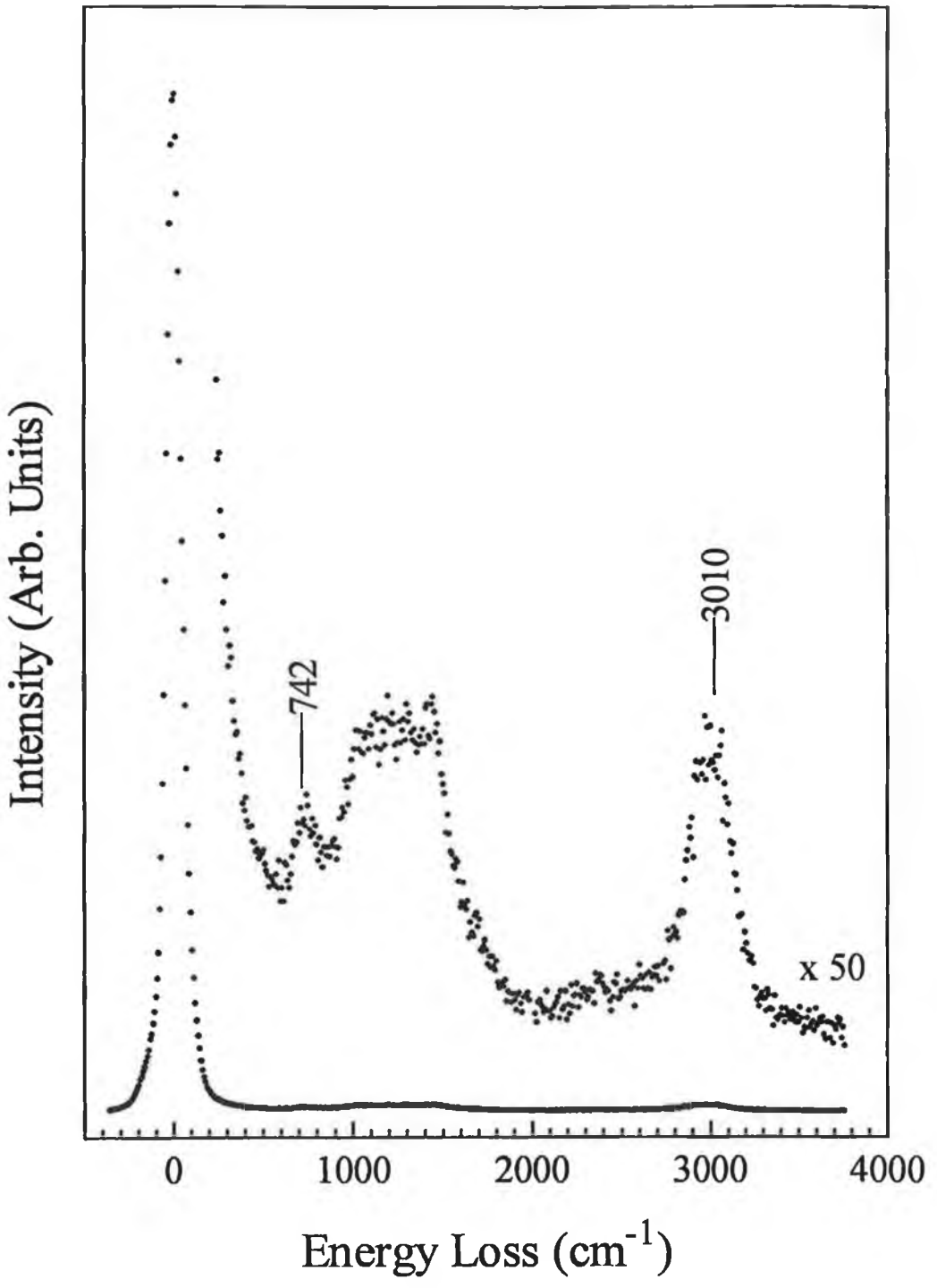

Figure 1 HREELS spectrum of a benzenethiol monolayer adsorbed on Au(111) recorded in specular scattering geometry ($\theta_i = \theta_r = 70°$) at a primary beam energy of 6.0 eV.

3.2 X-ray photoelectron spectroscopy

3.2.1 Identification of surface intermediates

Fig. 2 shows an Al K_α induced XPS spectra of the sulphur (2p) and carbon (1s) core levels collected at grazing emission (70° with respect to the surface normal) at an instrumental resolution of 0.34 eV. In Fig. 2a, the sulphur (2p) core level spectrum from a liquid phase self-assembled benzenethiol monolayer film on Au(111) reveals a two component peak assigned to the $2p_{3/2}$ and $2p_{1/2}$ spin orbit split levels with binding energies of 162.3 and 163.5 eV, respectively. Deconvolution of the sulphur (2p) emission lineshape reveals the characteristic intensity ratio of 2:1 and peak separation of 1.2 eV [20]. The binding energy of this state suggests the presence of a C-S bond, consistent with chemisorbed benzenethiolate, with no evidence of surface atomic sulphur or higher oxidation state species [8c,24b,25a].

There are four inequivalent carbon environments within the molecule, however, XPS may not distinguish between the aromatic carbon atoms not in direct contact with the thiolate functional group. In Fig. 2b, the minor high binding energy component, giving rise to asymmetry in the carbon (1s) lineshape, is assigned to the electron deficient carbon bonded to the electronegative sulphur atom. The main carbon (1s) photoemission is attributed to the indistinguishable phenyl group carbon atoms. Fig. 2b illustrates a fit to the experimental data assuming a surface phenyl thiolate with two distinct chemically shifted carbon (1s) core level emissions occurring at 286.1 and 284.5 eV, with a relative intensity ratio of 1.1:5.0.

Elemental quantification in terms of atomic percentage (±0.5%) ratio of carbon and sulphur was calculated from spectra collected at normal emission by integration of the areas of the carbon (1s) and sulphur (2p) peaks after application of a Shirley background subtraction and correction for atomic sensitivity factors including analyser transmission [22]. The experimental carbon to sulphur ratio of 6.0:1.1 compares favourably with the expected 6:1 ratio.

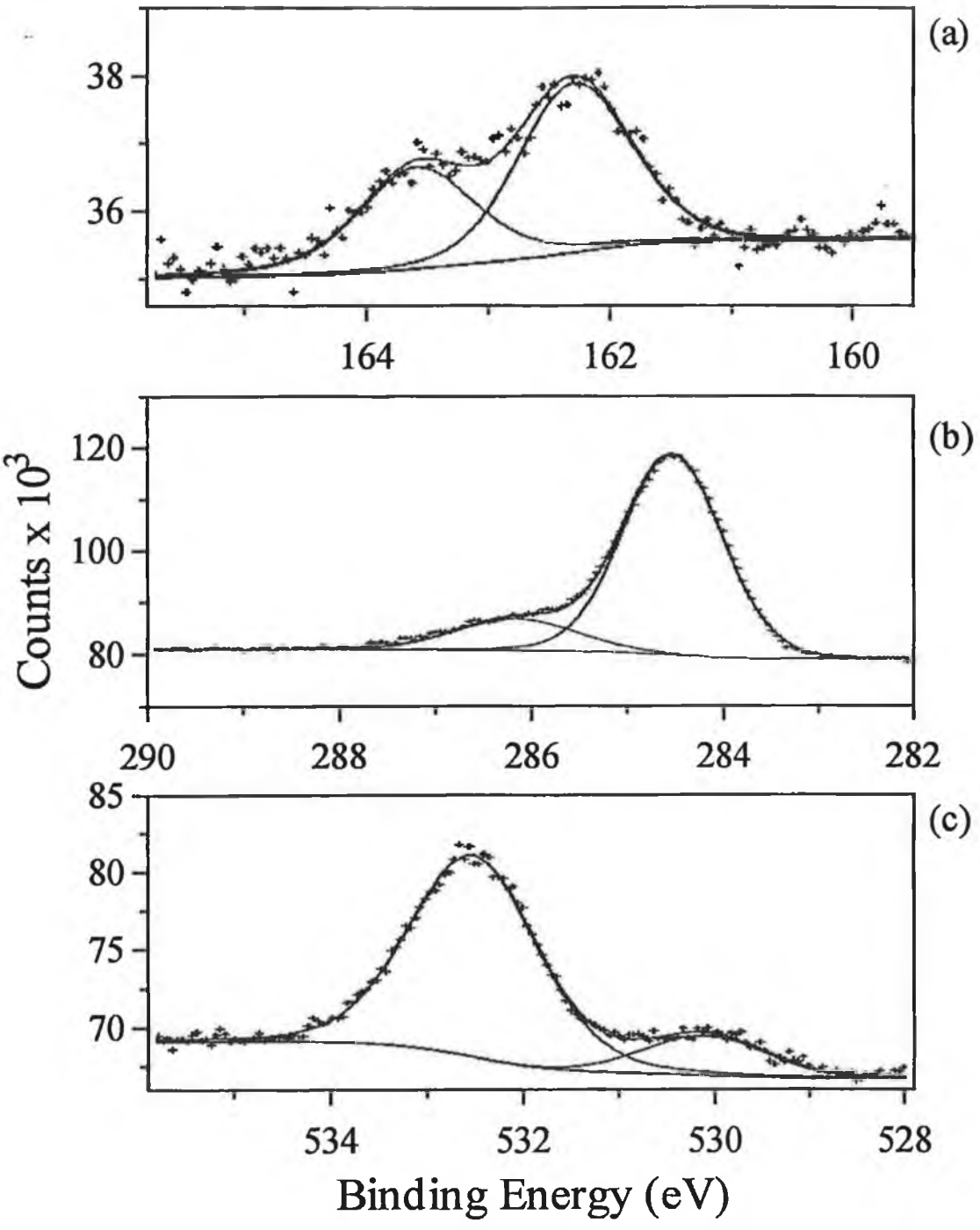

Figure 2 High-resolution XPS spectra of the (a) sulphur (2p), (b) carbon (1s) and (c) oxygen (1s) core levels from a benzenethiol monolayer self-assembled on Au(111). Raw data (+++) and fit to the experimental data using a mixed (80:20) Gaussian:Lorentzian lineshape (—).

Liquid phase monolayers are characterised by the presence of oxygen (1s) photoemission at 532.4 and 530.0 eV (relative intensities of 4.2:1.0) shown in Fig. 2c. These binding energies correspond closely with those expected for carbon bound oxygen (531-533 eV), SiO_2 (532.3 eV) and gold oxide (529-533 eV) [20,27]. As silicon has been reported as a contaminant of Au surfaces, the silicon (2s) core level binding energy region and SiO_2 energy loss regions were carefully examined but no contamination could be observed above the noise level.

Quantification yields a carbon to oxygen ratio of 3.0:1.0 indicating a significant amount of oxygen within the film. The carbon to oxygen ratio decreases to 3.0:0.8 at grazing emission (70° off-normal) suggesting that a portion of the oxygen may be located at the Au-SAM interface as opposed to the SAM-vacuum interface. This is particularly true of the lower binding energy peak (530.0 eV), which suffers a 40% intensity decrease at grazing emission relative to normal, consistent with the presence of gold oxide, while the dominant oxygen (1s) component (532.4 eV) decreases by only 15% upon changing the angle of emission from normal to grazing angles.

Examination of the sulphur (2p) core level (166-169 eV) shows no evidence of large amounts of sulphinite/sulphonate formation within the monolayer (although this does not hold true for incomplete layers as discussed later in section 3.4). Photoemission from oxygen bound carbon would overlap with the contribution from carbon atom bonded to the thiolate group giving rise to inconsistencies in the high binding energy carbon intensity ratio relative to aromatic carbon. This may explain the carbon (1s) intensity ratio of 1.1:5.0 as opposed to the expected ratio of 1:5. Evans *et al.* have also observed the presence of oxygen (531-533 eV) in SAMs of octadecanethiol chemisorbed on evaporated Au following immersion from oxygen containing solvents [28]. Interestingly, Ron and Rubinstein have investigated the formation of oriented thiol monolayers on plasma preoxidised Au using XPS and combined electrochemical-depth profiling and show the existence of a layer of encapsulated oxide under the SAM [27a]. The authors find no evidence of oxidation for monolayers prepared on freshly evaporated Au and, in addition, report that the oxide formed by oxidising pretreatments is reduced by alcohols during the adsorption process. Hence, under the conditions of film preparation used in the case of benzenethiol self-assembly (no substrate preoxidising treatment and immersion in

methanolic solution), the presence of oxygen is unexpected. At present, the nature and source of this contamination (chemisorbed/physisorbed contaminants from the solvent and/or exposure to atmospheric conditions) remains undetermined and further investigation is required [8b].

3.2.2 Layer thickness and molecular orientation

Attenuation of the Au ($4f_{7/2}$) signal upon self-assembly was used to estimate the thickness of the benzenethiolate overlayer using methods discussed in detail in previous studies [8a,b]. The relationship describing the decrease in substrate XPS intensity upon deposition of a film of thickness d is:

$$I_d = I_o \exp(-d/\lambda \sin \theta)$$

where (I_o) and (I_d) are the Au ($4f_{7/2}$) signal before and after adsorption of benzenethiol, λ is the inelastic mean free path (IMFP) of the Au ($4f_{7/2}$) photoelectrons and θ is the take-off angle = 20° (the angle between the sample surface and the photoelectrons accepted by the analyser). The IMFP has been calculated using methods detailed by Laibinis *et al.* for photoelectrons in hydrocarbon layers giving estimates of 39.9 Å and, taking the material density into consideration, 29.2 Å [29,30]. These IMFP values yield layer thicknesses for the benzenethiolate layer on Au(111) of 8.3 and 6.0 Å, respectively. However, as these equations apply only to *n*-alkanethiols, an error may be expected when using it for benzenthiolate due to additional loss mechanisms (e.g. π to π^*) present in the aromatic ring system in addition to the fact that the two-dimensional density will be different. Calculation of layer thickness by XPS involves precise values of escape depths, a parameter difficult to obtain with a high degree of accuracy for organic systems, as illustrated by the variation encountered in the use of the two methods. Nevertheless, such a layer thickness (6.0-8.3 Å) is not inconsistent with a monolayer adopting an upright geometry with the plane of the phenyl ring perpendicular or close to perpendicular with respect to the Au(111) surface.

To estimate the absolute surface elemental coverage, the sulphur (2p) to Au ($4f_{7/2}$) ratio was measured at normal emission from the benzenethiolate film and compared with that (measured on a laboratory Mg K_α source) from a film of known

sulphur atomic density. Gas phase chemisorption of ethanethiol to saturation on Au(111) at 300 K leads to formation of a $(\sqrt{3}\times\sqrt{3})R30°$ overlayer structure with an absolute sulphur coverage of 0.33 monolayers [31]. By measurement of the sulphur (2p) to Au ($4f_{7/2}$) intensity ratio from the ethanethiol $(\sqrt{3}\times\sqrt{3})R30°$ phase and the saturated benzenethiolate film, we have calculated the corresponding surface coverage for benzenethiolate [32]. Ignoring differential attenuation of the sulphur and Au signals by the different nature of the monolayers (which should be small at the high outgoing kinetic energies utilised), this yields a value of 0.45 monolayers of sulphur and hence 2.45 and 0.8 monolayers of carbon and oxygen, respectively. In comparison, a surface coverage of 0.62 monolayers of sulphur at saturation has been reported for benzenethiol gas phase adsorption in an upright configuration on Cu(111) [25a]. Taking the difference in surface atomic densities between Cu(111) and Au(111) into consideration, this corresponds to a coverage of 0.49 monolayers relative to the Au(111)-(1×1) surface atomic density, correlating closely with the value of 0.45 monolayers determined in this study.

As the Au(111)-($\sqrt{3}$ ×22) surface reconstruction is lifted to (1 × 1) bulk truncated phase upon chemisorption of benzenethiol to saturation (as shown in section 3.3.1), the substrate surface atomic density is 1.39×10^{15} atoms cm^{-2}. Hence, a coverage of 0.45 monolayers corresponds to a surface density of 6.3×10^{14} sulphur atoms cm^{-2}. This must be compared with packing densities (molecules adsorbed per unit area) for upright and flat-lying molecular orientations, on the basis of van der Waals' radii, of 6.8×10^{14} and 2.9×10^{14} molecules cm^{-2}, respectively [33]. Clearly, the experimentally derived sulphur surface density is in keeping with a layer of upright or slightly tilted molecules, but rules out a completely flat-lying arrangement.

Previous studies of benzenethiol chemisorption on Au(111) films have been performed, using cyclic voltammetry, reflection-absorption infrared spectroscopy, scanning tunneling microscopy (STM), ellipsometry and contact angle measurements [10a,b,e]. A disordered layer consisting of an upright benzenethiolate intermediate inclined towards the Au surface was reported, following self-assembly from solution [10a,b]. The film was reported to have a layer thickness of 1.3 Å and surface coverage (based on electrochemical determination of thiolate desorption from the electrode surface) corresponding to only 60% of a full $(\sqrt{3}\times\sqrt{3})R30°$ overlayer structure, i.e., 0.2

monolayers of sulphur. Tao *et al.* attribute the underestimate of layer thickness (relative to the dimensions of the molecule) to uncertainty associated with ellipsometry measurements, and possibly due to substrate contamination. The large discrepancy in coverage estimation relative to our results, may be due to the sensitivity of surface spectroscopic relative to electrochemical techniques, the nature of the surface bound species and their stability (discussed in section 3.4) and possible contamination effects. Similarly, Sabatani *et al.* and Abduaini *et al.* report a non-perpendicular orientation of the phenyl ring with respect to the surface plane and poor packing of the molecules within the monolayer [10e,f]. Carron and Hurley have used surface enhanced Raman spectroscopy (SERS) to determine the molecular orientation of benzenethiol adsorbed on evaporated Au films and, in agreement with our results, report a tilt angle of 14±1.5° with respect to the surface normal [10g].

In conclusion, the principle energy losses detected by HREELS, the absence of a S-H stretching mode and the sulphur (2p) photoemission binding energy support the assignment of a benzenethiolate intermediate bonding to Au(111) following liquid phase assembly to saturation coverage. This result is in direct agreement with previous surface bonding characterisation of benzenethiol adsorption on other metal surfaces which indicate the formation of a surface bound thiolate species [8c,8d,9,24,25]. XPS analysis shows that stoichiometric films are difficult to attain due to the presence of gold oxide, carbon bound oxygen and/or SiO_2.

The relative intensity of the out-of-plane C-H deformation to the C-H stretching vibration, estimates of film thickness, sulphur coverage and molecular packing density, support a bonding arrangement with the phenyl ring assuming a largely perpendicular orientation relative to the Au(111) surface. Similarly, the phenyl group has been found to be in an upright configuration after self-assembly from the liquid phase on Ag(111) and Pt(111) electrodes [9]. For monolayers prepared by gas phase adsorption to saturation, a small inclination (~ 20°) of the ring off-normal has been reported on Rh(111), Cu(111), Cu(110), Mo(110), Ni(100), Ni(110) and Ni(111) with the exception of a flat-lying geometry reported on Au(110), Au(111) and Au(322) [24,25,8c,8d].

3.3 Electrochemistry

3.3.1 Specific anion adsorption on thiol modified Au(111)

The behaviour of the Au(111)-($\sqrt{3}\times22$) reconstructed surface structure and specifically adsorbing anions as a function of immersion time in benzenethiol solution has been investigated. The characteristic current-potential curves for a clean, well defined Au(111) surface in aqueous electrolyte consisting of chloride anions, shown in Fig. 3, is in excellent agreement with that previously reported in the literature [19]. A prominent positive current peak (A) exhibited on the forward scan, at 112 mV (vs. Ag/AgCl), is associated with a structural transition involving the reversible removal of the ($\sqrt{3}\times22$) reconstruction to the bulk truncated (1×1) phase. The broad feature seen at 330 mV (B) corresponds to a medium monolayer coverage of the (1×1) electrode surface by mobile anions, while a small order-disorder transition peak observed at 662 mV (C) reflects the formation of a well ordered two-dimensional anion overlayer. Reversing the potential sweep direction, the corresponding dissolution peaks, C', B', and A', are observed at 656, 200-400 and 70 mV, respectively.

It can be seen from Fig. 3a, that immersion of a flame-annealed, reconstructed Au(111) surface in 10^{-6} M benzenethiol for 10 s results in the attenuation of the peak A, accompanied by a 26 mV shift to more positive potentials in the first cycle. Similarly, peaks C/C' decrease in intensity and shift 5 mV to higher potentials.

Subjecting the modified electrode to a second cycle produces marked changes in the voltammogram (Fig. 3b). Peak A is restored to lower potentials (117 mV) but is substantially diminished, and a second peak appears at 155 mV. Repeated cycling produced no further changes in the electrochemical response observed. Increasing the immersion time to 40 s, results in identical peak potentials and cycling induced changes, with progressive attenuation of peaks A/A' and B/B'. In addition, the ordered anion overlayer peaks, C/C', are substantially broadened and continuously to shift to higher potentials.

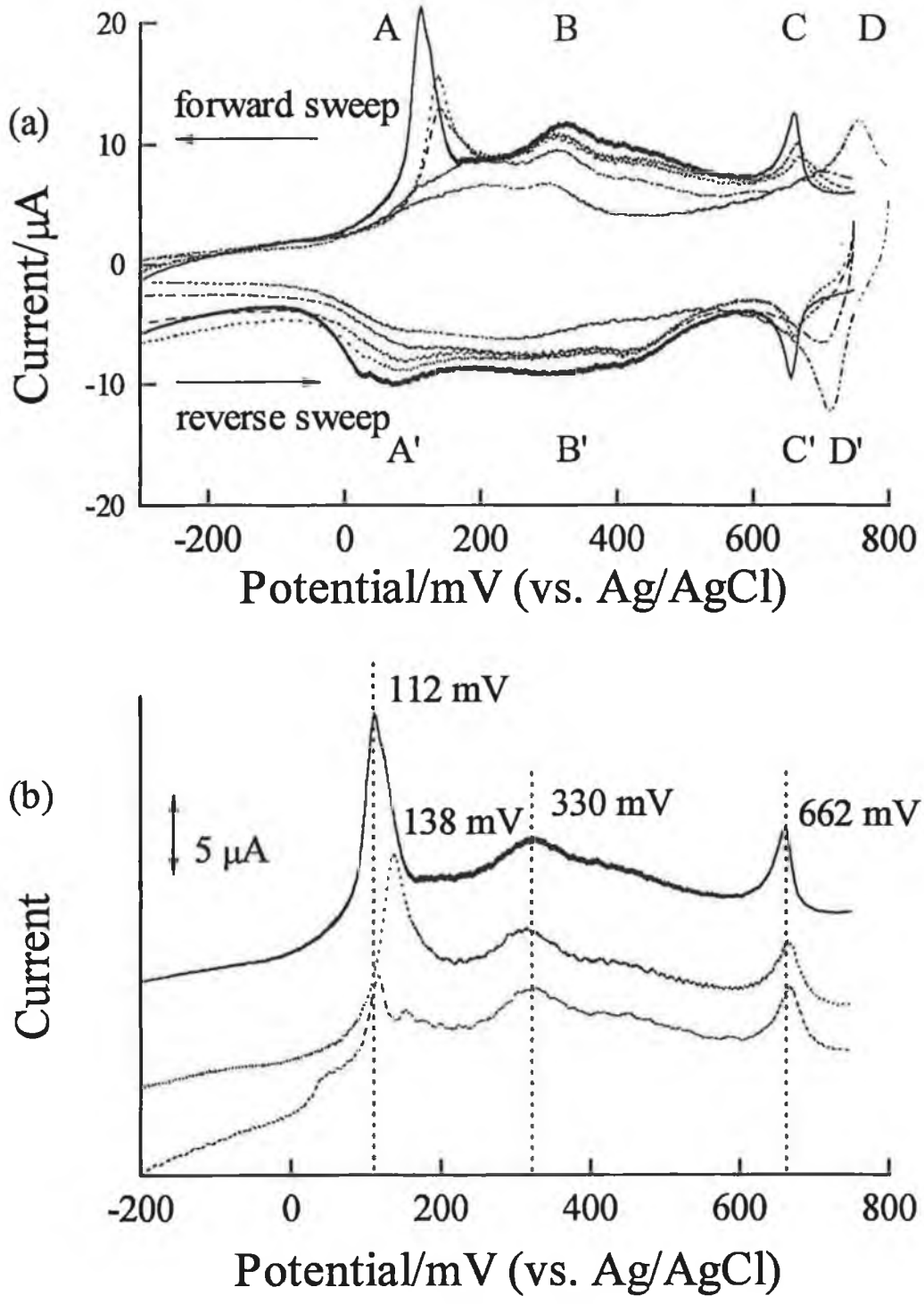

Figure 3 Cyclic voltammograms of Au(111) in 0.1 M HCl at a scan rate of 100 mVs^{-1}. (a) First cycle for unmodified (—) and modified Au(111) following immersion times of 10 (·····), 40 (– –), 70 (–·–·) and 110 (–···–) s in 1 × 10^{-6} M benzenethiol solution. (b) Showing the potential region of interest for unmodified (—) and modified Au(111) following 20 s immersion, on the first (·····) and second (– –) cycles.

Following 70 s immersion, peak A has disappeared, suggesting that the area of unmodified Au is less than that required to support the reconstruction. The remainder of the voltammogram is unchanged in its general appearance, however, C/C' are substantially broadened, with suggestion of a second component in this potential region (690-750 mV). Finally, following 110 s immersion, a single set of peaks are observed (D/D') at 750 and 715 mV accompanied by a broad capacitive double-layer. This indicates that the order-disorder transition, resulting in the formation of well ordered domains of anions, no longer occurs due to the presence of chemisorbed organic species on the Au(111) surface. However, it is not possible to assign a definite immersion time (70-110 s) for the disappearance of C/C' due to the close proximity and overlap of D/D'. Longer immersion times resulted in no further changes, except for a slight decrease in the double-layer capacitance perhaps due to consolidation of the SAM (see section 3.4), suggesting that during an immersion time of 110 s a 'physical monolayer' of benzenethiol has self-assembled. Similar behaviour has been observed in the presence of the more weakly adsorbing sulphate anion.

3.3.2 Interpretation of anion adsorption on thiol modified Au(111)

The gradual decrease in the magnitude of peaks A and C/C' are attributed to removal of the reconstruction and inhibition of two-dimensional chloride overlayer formation. These results suggest that, at sub-monolayer coverages, benzenethiol self-assembles through a mechanism which involves two-dimensional islands. Such a growth mechanism would leave areas of clean reconstructed Au(111) at low/intermediate thiol coverages, upon which two-dimensional anion island growth may still occur. In contrast, if the thiol were to chemisorb in a completely dispersed mode, we would expect quenching of peaks A and C/C' at lower immersion times than those observed. However, broadening and shifting of peaks C/C' to more positive potentials, from very low immersion times, indicate that adsorbing anions experience inhibition effects, perhaps due to interaction with the organic adsorbate island edges. The positive potential shift of peak A to 138 mV, suggests that chemisorption of

chloride anions is retarded in the presence of the organic adsorbate requiring more positive potentials before specific anion adsorption can occur [17].

We tentatively assign the changes in the voltammogram observed in the second cycle (10 to 60 s immersion) to a reorganisation of the benzenethiolate adlayer. Based upon the attenuation of peak A, it is reasonable to conclude that substantial areas of the substrate are no longer capable of reversible reconstruction. The Au(111)-($\sqrt{3}\times22$) to (1×1) transition may be predicted to yield a defect-rich surface with the creation of monatomic Au islands (which act as nucleation sites for restoration of the reconstruction) [17]. The thiolate may preferentially bond at defect sites, which have a higher heat of adsorption than the atomically flat close-packed surface. Following anion lifting of the reconstruction (in areas not previously occupied by the organic adsorbate), the thiols reorganise and bind to defect sites, blocking the nucleation process at these sites and reducing the mobility of Au atoms (required to form the more densely packed surface structure), resulting in the attenuation and negative potential shift observed for peak A.

3.3.3 Thiol induced modification of Cu UPD on Au(111)

Sun and Crooks examined the structure and distribution of individual Cu islands incorporated in defect sites contained in octadecylthiol layers on Au(111) as a function of self-assembly time [4g]. The rate of defect disappearance was followed by STM and allowed the authors to follow the kinetics of self-assembly. Similarly, the effect of benzenethiol chemisorption on Cu UPD features on Au(111), collected as a function of immersion time in 10^{-6} M solution, may suggest a growth mechanism for this class of thiol.

In Fig. 4, a voltammogram for the UPD of Cu on Au(111) in 0.1 M sulphuric acid (vs. $Cu|Cu^{2+}$) is in good agreement with previous studies [34]. At positive potentials, adsorbed sulphate anions are replaced by Cu adatoms which initially form a random phase. This step is accompanied by readsorption of anions, creating a ($\sqrt{3}\times\sqrt{3}$) template, leaving a honeycomb lattice for adsorption of Cu observed at 212 mV (Cu coverage of 2/3 monolayers). As the Cu (1×1) phase is formed, anions are displaced by

Cu from their ($\sqrt{3}\times\sqrt{3}$) positions, filling the remaining 1/3 of available Au adsorption sites, corresponding to the completion of a pseudomorphic monolayer coverage of Cu at 40 mV. The corresponding ($\sqrt{3}\times\sqrt{3}$) and (1×1) dissolution peaks are found at 232 and 99 mV, respectively. A shoulder on the positive side of the (1×1) stripping peak (approximately 130 mV) indicates the presence of defect sites [34c,d]. While this does suggest that the surface is not perfect, the voltammogram compares well with those previously reported.

A selection from a series of voltammograms resulting from immersion of Au(111) in benzenethiol are shown in Fig. 4. The electrochemical response induced by the organic overlayer structure is stable and reversible over the range of coverages studied in the potential range of interest, as evidenced by the retention of the voltammetric pattern on subsequent cycles. It can be seen that following 10 s immersion, deposition of Cu in the form of a ($\sqrt{3}\times\sqrt{3}$) structure at 212 mV is attenuated and its corresponding dissolution occurs at 239 mV. A new broad feature has emerged at approximately 125 mV, prior to completion of a full monolayer coverage of Cu which is shifted to more negative potentials by 15 mV. On the dissolution sweep, stripping of the (1×1) phase is observed at 102 mV, however, there is no evidence of the shoulder on the positive side of this peak, suggesting that defect sites are no longer accessible to Cu adatoms due to their occupancy by benzenethiol.

For low immersion times, the new adsorption features, a broad shoulder (165-185 mV) on the lower potential side of the ($\sqrt{3}\times\sqrt{3}$)R30° peak and the 125 mV peak, become increasingly prominent and shift towards bulk potentials. In contrast, the ($\sqrt{3}\times\sqrt{3}$)R30° and (1×1) adsorption peaks at 112 and 22 mV, respectively, decrease in magnitude following 30 s immersion and dissolution features are seen to shift slightly (< 5 mV) to more positive potentials. Quenching of the ($\sqrt{3}\times\sqrt{3}$)R30° phase follows 60 s immersion, replaced by a complex series of broad adsorption features, suggesting that the presence of thiolate species may induce a disordered Cu growth phase adsorbing on a number of energetically distinct sites. In contrast, the (1×1) adsorption phase (18 mV) and both stripping peaks (107 and 252 mV) are slowly attenuated and remain well defined. Typically, the deposition peaks become almost indistinguishable as the monolayer presence dominates as shown by the 90 s immersion. The appearance of stripping features indicates that, although deposition is

ill-defined, the formation of a Cu adlayer does occur. Following 120 s immersion, a single broad UPD peak is observed at 260 mV on the desorption cycle. Finally, Cu UPD is completely inhibited following 140 s of benzenethiol self-assembly suggesting complete passivation of the substrate to UPD.

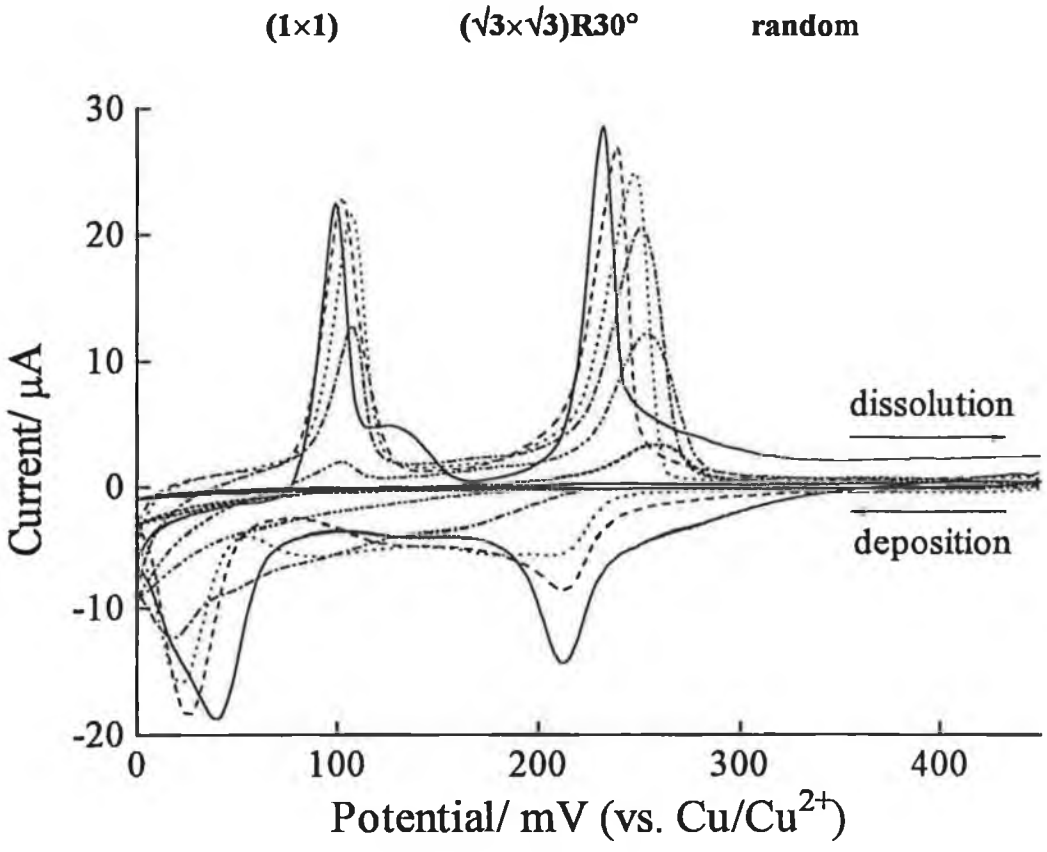

Figure 4 Cyclic voltammograms of Cu UPD on benzenethiol modified Au(111) in 0.1 M H_2SO_4 + 1 mM Cu^{2+} at a scan rate of 10 mVs^{-1}. Immersion times shown are 10 (— —), 30 (·····), 60 (–·–·), 90 (–··–··), 120 (– – –) and 140 (—) s in 1 × 10^{-6} M thiol solution. A cyclic voltammogram of Cu UPD on unmodified Au(111) showing the random, (√3×√3)R30° and (1×1) Cu adatom growth phases is shown for comparison (—).

3.4 A proposed growth mechanism for benzenethiol on Au(111)

Net repulsive adsorbate-adsorbate lateral interactions favours a two-dimensional dispersed phase growth mode (Fig. 5a). The resulting high density of metal adatom bonding sites adjacent to the organic adsorbate, from very low immersion times, should cause significant alterations in Cu UPD features and, in particular, hinder the formation of the open $(\sqrt{3}\times\sqrt{3})R30°$ structure. In contrast, mutually attractive long range thiolate interactions, promotes the formation of two-dimensional islands (Fig. 5b). This leaves large areas of unmodified substrate available for Cu UPD in the form of the $(\sqrt{3}\times\sqrt{3})R30°$ phase, at low immersion times, and a slow attenuation of UPD features characteristic to unmodified Au(111) may be expected. However, as the adsorbate islands expand with longer immersion times, contributions from Cu-thiol island edge interactions should become increasing apparent.

At low immersion times (10 to 60 s), a series of new, ill-defined adsorption features, attributed to the existence of different adsorption sites created by thiol chemisorption, are observed at potentials between the $(\sqrt{3}\times\sqrt{3})R30°$ and (1×1) peaks. The fact that the organic adsorbate inhibits, but does not eliminate, the open $(\sqrt{3}\times\sqrt{3})R30°$ Cu adlayer phase, supports the formation of two-dimensional islands, implying that a certain degree of cooperative attraction exists between the aromatic molecules.

As immersion times increase (60-90 s), Cu adsorption is substantially depressed in comparison with Cu stripping features, which may indicate the formation of an incommensurate and/or disordered structure upon deposition. Alternatively, the organic adsorbate provides less inhibition for adatom bond formation with available substrate sites in comparison to Cu desorption. Nichols *et al.* attributed the suppression of Cu stripping features on Au(111) relative to deposition features to penetration of metal adatoms under a layer of benzothiazonium derivative or partial displacement of the adsorbate layer by Cu [15b]. The Cu ions may penetration through the organic assembly on the forward sweep, resulting in interactions between the thiolate and Cu species; thus, hindering the departure of metal adatoms on the reverse sweep. The stability of the resultant thiolate-Cu-substrate complex is indicated

by the difficulty in its removal relative to its formation as evidenced by the presence of stripping peaks close to blocking coverages.

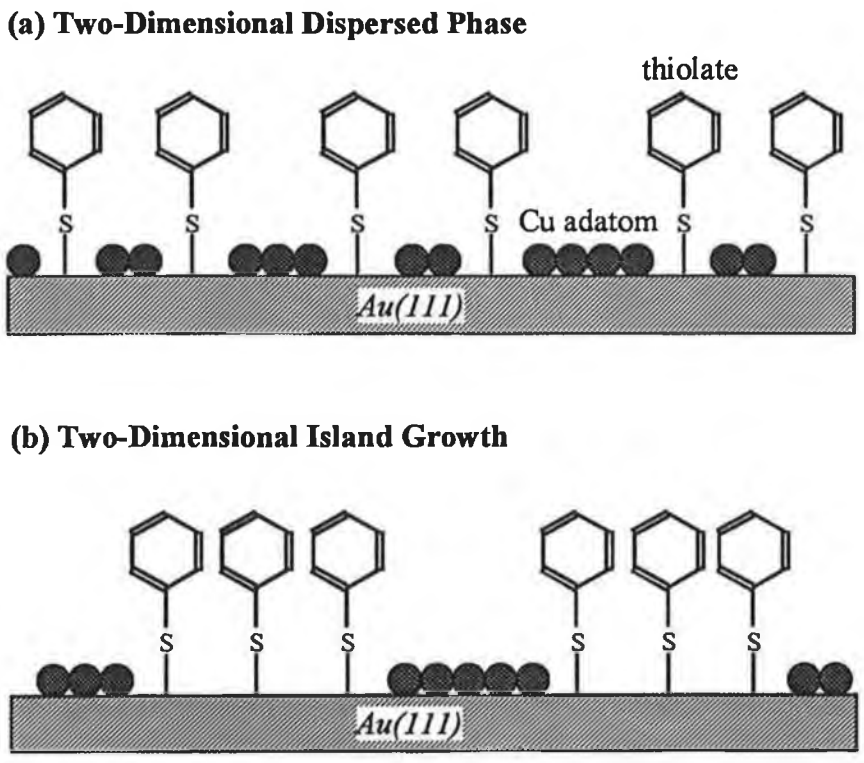

Figure 5 A schematic representation of the possible growth mechanisms for liquid phase self-assembly of benzenethiol on Au(111): (a) two-dimensional dispersed phase and (b) two-dimensional island growth.

There is no evidence of Cu deposition/stripping following 140 s of benzenethiol self-assembly, suggesting complete passivation of the substrate to UPD. Similar blocking behaviour toward Cu UPD has been reported for *n*-alkanethiol modified Au(111) [13]. While a dynamic current cannot be detected in the voltammogram, *in situ* STM reveals a homogeneous distribution of Cu nanoparticles in the UPD region on top of the organic layer, requiring 20 min (at 150 mV vs. SCE) to form 2/3 of a monolayer of Cu on a decanethiol SAM. It is possible that a similar process would occur in the case of Cu UPD on benzenethiol derived layers, where the deposition kinetics are too slow, due to electron tunneling barrier afforded by the thiol,

to permit observable UPD currents to flow. However, it is highly unlikely that substantial Cu electrocrystallisation has occurred on the aromatic SAM at a scan rate of 10 mVs^{-1} utilised in our study.

In Fig. 6a, the Cu UPD integration versus immersion time in benzenethiol is presented. This data was corrected for capacitive current effects, however, it is accepted that difficulties exist in accounting for the influence of coadsorbed anions during UPD particularly in the presence of preadsorbed thiols [34e]. Fig. 6a is characterised by a rapid decrease for 10 s immersion, followed by a plateau region (10-40 s), and a gradual decrease in response area eventually leading to blocking (140 s). This suggests a multistep self-assembly process initially involving the rapid blocking of substrate sites, followed by a much slower occupancy of remaining vacant sites, during which time the overlayer approaches its final structure to form a 'physical monolayer'.

The validity of using Cu UPD to follow thiol uptake from solution as a function of immersion time was established by *ex situ* XPS measurement of the ratio of the integrated intensity of the sulphur (2p) to Au ($4f_{7/2}$) core level emissions shown in Fig. 6b. In agreement with the Cu UPD integrated response, the trend in the variation of sulphur (2p) to Au ($4f_{7/2}$) emission intensities suggest a multistep growth mechanism, comprising an initial rapid assembly followed by a slow reordering/consolidation process. XPS measurements reveal that immersion times for which the initial rapid uptake of adsorbate, the disappearance of the Cu adsorption peak assigned to the $(\sqrt{3}\times\sqrt{3})R30°$ phase and complete 'physical monolayer' are observed, correspond to 0.14, 0.23 and 0.38 monolayers of sulphur, respectively, equivalent to 30, 50 and 85 % relative to full monolayer coverage. In contrast, the corresponding values based upon Cu UPD data are 15, 35 and 100 %, indicating an underestimate of the adsorbate surface coverage at low immersion times and the blocking of UPD processes in advance of completion of the adsorbate layer. Nevertheless, the shape of the curve presented in Fig. 6b and the fact that a sulphur coverage corresponding to approximately 50% of the final sulphur coverage is required to quench the open $(\sqrt{3}\times\sqrt{3})R30°$ Cu phase, lift the substrate reconstruction completely and inhibit the formation of ordered anion overlayers, support a self-assembly mechanism involving growth of two-dimensional islands, in accordance with specific anion adsorption and Cu UPD results.

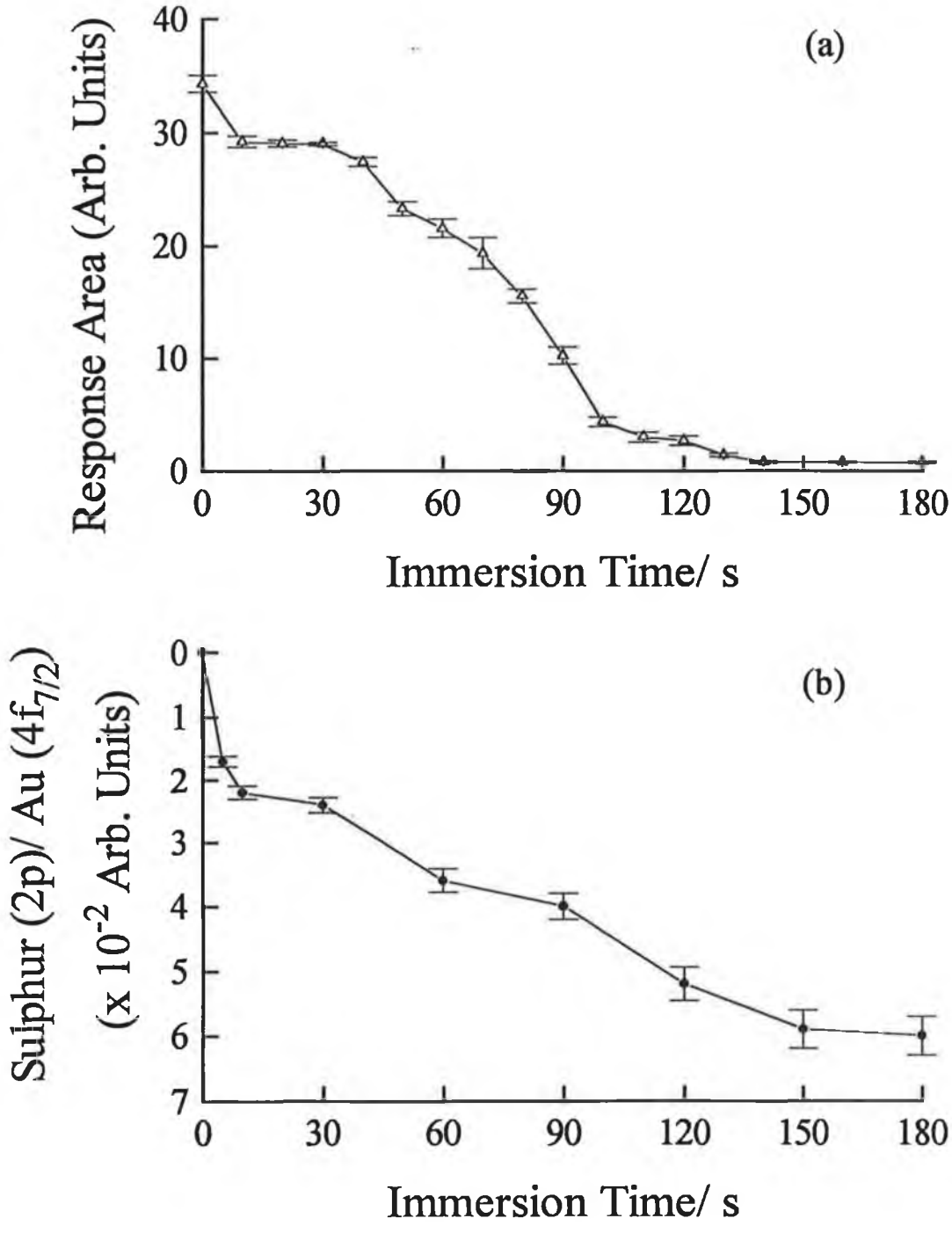

Figure 6 (a) Integrated electrochemical response from Cu UPD cyclic voltammograms (error bars represent the standard deviation from the mean value of duplicate samples) and (b) variation of sulphur (2p) to Au ($4f_{7/2}$) intensities (±5%) from benzenethiol modified Au(111) as a function of immersion time in 1×10^{-6} M benzenethiol solution.

A multistep, two-dimensional island growth mechanism, accompanied by lifting of the Au(111)-($\sqrt{3}\times22$) reconstruction, has been reported for gas phase self-assembly of *n*-alkanethiols on Au(111) [35]. At low exposures, island growth along the Au(111)-($\sqrt{3}\times22$) surface structure has been observed by STM with alignment of the molecular axis with the surface plane. The surface then undergoes a phase transition with the development of thiolate islands in which the molecular axis is aligned along the surface normal. These islands grow laterally, at the expense of the surface-aligned phase, and finally coalesce to form a compact monolayer. Similarly, benzenethiol liquid phase self-assembly may be further complicated by coverage dependent reorientation. Adsorption from the gas phase at 300 K leads to a largely flat-lying benzenethiolate intermediate, at both sub-monolayer and 'physical monolayer' coverages [8c,d]. Low energy electron diffraction (LEED) observations reveal an increase in the diffuse background without long range ordering with respect to the substrate and persistence of the ($\sqrt{3}\times22$) surface reconstruction even upon prolonged dosing (>100 L). Hence, it appears that the considerably higher thiol fluxes achieved in solution, may be required to lift the reconstruction and form an upright bonding configuration. It is quite probable that adsorption from the liquid phase gives rise to a flat-lying intermediate at low coverage and a mixture of orientations at intermediate coverages (>10 s immersion), eventually leading to a compact layer of upright molecules. A slow reorientation mechanism would explain the gradual progression towards the final monolayer structure shown in Fig. 6. *In situ* STM characterisation of sub-monolayer self-assembly of benzenethiol both with and without Cu UPD and specifically adsorbing anions would be of particular value in this case in order to clarify the adsorption behaviour and confirm whether a coverage dependent reorientation of the adsorbate occurs.

The discrepancy in absolute adsorbate coverages obtained by XPS versus Cu UPD may be explained upon examination of the nature of the surface intermediates which, at sub-monolayer coverages, comprise considerable amount of higher oxidation state sulphur. This is evidenced by the presence of a broad sulphur (2p) peak at 168-170 eV and oxygen (1s) emission at 532.5 eV. The oxidation of aromatic thiols adsorbed on Au has been detected following exposure to atmospheric conditions [36]. The effect of oxidation state on formation and stability of benzenethiol monolayers on

polycrystalline Au has been investigated by Garrell *et al.* [10d]. SERS has shown that sulphinite and sulphonate species can coexist on the Au surface and a dynamic equilibrium exists between solution and adsorbed species, such that sulphonate is displaced by sulphinite, which is itself readily displaced by benzenethiolate.

It appears that immersion of Au(111) in benzenethiol solution results in sub-monolayer films of mixed thiolate, sulphinite and sulphonate species, however, for simplification we continue to refer to the adsorbate layer as benzenethiol. According to XPS, prior to electrochemical experiments the aryl-sulphinite and -sulphonate species correspond to between 15 and 40% of the total sulphur bound on the surface, depending on the immersion time. Based on XPS and electrochemical measurements, Eliadis *et al.* report that Cu deposition and stripping on *n*-alkanethiol layers on Au(111) occurs in a completely reversible manner, without adversely affecting the thiolate-Au bond [14]. However, the same authors suggest that if sulphonate moieties are formed during film preparation, such species are unlikely to be retained on the surface due to their high solubility. It is thus possible that the sulphinite/sulphonate adsorbates irreversibly desorb from the electrode, due to Cu electrodeposition and/or enhanced solubility promoted by ionic interaction in the presence of electrolyte, resulting in the lower surface coverage determined by Cu UPD integration (compared with XPS).

In contrast, only benzenethiolate is observed by XPS following 'physical monolayer' formation, as sufficient immersion time is allowed for thiol displacement of any adsorbed sulphinite/sulphonate species. This suggests that benzenethiol forms a compact molecular assembly close to saturation coverage preventing Cu adatoms from penetrating through to the Au substrate. The progression to complete coverage may require longer immersion times due to expulsion of contaminants/solvent molecules.

The presence of oxygen within the benzenethiolate 'physical monolayer' (discussed in section 3.2.1) and the detection of higher oxidation state species within the sub-monolayer films is a subject of considerable interest as highlighted by the work of Ron and Rubinstein [27a]. Adsorption of benzenethiol (sub-monolayer and saturation coverages) from the gas phase on preoxidised Au(111) eliminates the possibility of adventitious contamination from the laboratory ambient and solvent

effects and may provide insight into the influence of oxygen in the chemical mechanism of self-assembly and the existence of sulphinite/sulphonate species within the SAM.

4. Conclusions

HREELS and XPS characterisation of benzenethiol monolayers on Au(111) prepared by self-assembly from the liquid phase indicates that the primary adsorbate species is a thiolate. The intensity of the out-of-plane C-H deformation, monolayer film thickness, sulphur coverage and molecular packing density, support an adsorption geometry in which the phenyl ring is aligned largely perpendicular to the substrate surface. However, XPS analysis of sub-monolayer films shows that a mixture of thiol and higher oxidation state sulphur species are present on the Au(111) surface. Oxygen contamination of both sub-monolayer and monolayer films is consistently observed.

The ability of benzenethiol chemisorption to lift the Au(111)-($\sqrt{3}\times22$) reconstruction to the (1×1) structure has been inferred from the attenuation of a substrate reconstruction peak for Au(111) in the presence of chloride anions. Evidence for formation of two-dimensional adsorbate islands is suggested from the suppression of anion order-disorder transitions and the gradual lifting of the surface reconstruction. Sub-monolayer and monolayer thiol coverages have a profound effect on the UPD of Cu on Au(111). New adsorption-desorption features at low immersion times, attributed to metal adatom-thiol interactions, and the survival of the open ($\sqrt{3}\times\sqrt{3}$)R30° Cu adlayer structure, support a mechanism involving two-dimensional thiol island growth. At 'physical monolayer' coverages, there is no evidence of Cu growth on Au(111). Qualitatively, Cu UPD integration and XPS uptake data are in good agreement, and indicate a multistep adsorption process involving initial rapid self-assembly, possibly corresponding to a flat-lying adsorbate covered surface, followed by a much slower progression to full 'physical monolayer' formation in which the thiolate intermediate may reorientate to form islands of densely packed upright molecules.

5. References

[1] Bard, A.J.; Abruna, H.D.; Chidsey, C.E.D.; Faulkner, L.R.; Feldberg, S.W.; Itaya, K.; Majada, M.; Melroy, O.; Murray, R.W.; Porter, M.D.; Soriaga, M.P.; White, H.S. *J. Phys. Chem.*, **1993**, 97, 7147.

[2] Ulman A. *An Introduction to Ultrathin Organic Films: from Langmuir-Blodgett to Self-Assembly*, Academic: New York, 1991.

[3] (a) Dubois, L.H.; Nuzzo, R.G. *Annu. Rev. Phys. Chem.* **1992**, 43, 437. (b) Ulman, A. *Chem. Rev.* **1996**, 96, 1533.

[4] (a) Bain, C.D.; Troughton, E.B.; Tao, Y.T.; Evall, J.; Whitesides, G.M.; Nuzzo, R.G. *J. Am. Chem. Soc.* **1989**, 111, 321. (b) Hahner, G.; Woll, Ch.; Buck, M.; Grunze, M. *Langmuir* **1993**, 9, 1955. (c) Buck, M.; Grunze, M.; Eisert, F.; Fischer, J.; Trager, F. *J. Vac. Sci. Technol. A* **1992**, 10, 926. (d) Cohen, S.R.; Naamam, R.; Sagiv, J. *J. Phys. Chem.* **1986**, 90, 3054. (e) Wasserman, S.R.; Whiteides, G.M.; Tidswell, I.M.; Ocko, B.M.; Pershan, P.S.; Axe, J.D. *J. Am. Chem. Soc.* **1989**, 111, 5852. (f) Thomas, R.C.; Sun, L.; Crooks, R.M. *Langmuir* **1991**, 7, 620. (g) Sun, L.; Crooks, R.M. *J. Electrochem. Soc.* **1991**, 138, L23.

[5] Evans, S.D.; Uranker, E.; Ulman, A.; Ferris, N. *J. Am. Chem. Soc.* **1991**, 113, 4121.

[6] (a) Chang, S.-C.; Chao, I.; Tao, Y.-T. *J. Am. Chem. Soc.* **1994**, 116, 6792. (b) Tao, Y.-T.; Chang, S.-C.; Ma, L.-F. *J. Chin. Chem. Soc.* **1995**, 42, 659.

[7] Soriaga, M.P. In *The Structure of Electrified Interfaces*; Lipowski, J., Ross, P.N., Eds.; VCH: New York, 1992.

[8] (a) Whelan, C.M.; Smyth, M.R.; Barnes, C.J. *J. Electroanal. Chem.* **1998**, 441, 109. (b) Whelan, C.M.; Smyth, M.R.; Barnes, C.J.; Brown, N.M.D.; Anderson, C.A. *Appl. Surf. Sci.*, in press. (c) Whelan, C.M.; Smyth, M.R.; Barnes, C.J.; Brown, N.M.D.; Walker, C.G.H., submitted. (d) Whelan, C.M.; Smyth, M.R.; Barnes, C.J.; Brown, N.M.D.; Walker, C.G.H., in preparation.

[9] (a) Gui, J.Y.; Lu, F.; Stern, D.A.; Hubbard, A.T. *J. Electroanal. Chem.* **1990**, 292, 245. (b) Stern, D.A.; Wellner, E.; Salaita, G.N.; Laguren-Davidson, L.; Lu, F.; Batina, N.; Frank, D.G.; Zapien, D.C.; Walton, N.; Hubbard, A.T. *J. Am. Chem. Soc.* **1988**, 110, 4885.

[10] (a) Tao, Y.-T.; Wu, C.-C.; Eu, J.-Y.; Lin, W.-L.; Wu, K.-C.; Chen, C.-h. *Langmuir* **1997**, 13, 4018. (b) Dhirani, A.-A.; Zehner, R.W.; Hsung, R.P.; Guyot-Sionnest, P.; Sita, L.R. *J. Am. Chem. Soc.* **1996**, 118, 3319. (c) Zehner, R.W.; Sita, L.R. *Langmuir* **1997**, 13, 2973. (d) Garrell, R.L.; Chadwick, J.E.; Severance, D.L.; McDonald, N.A.; Myles, D.C. *J. Am. Chem. Soc.* **1995**, 117, 11563. (e) Sabatani, E.; Cohen-Boulakia, J.; Bruening, M.; Rubinstein, I. *Langmuir* **1993**, 9, 2974. (f) Abduaini, A.; Kera, S., Aoki, M.; Okudaira, K.K.; Ueno, N.; Harada, Y. *J. Electron Spectrosc. Relat. Phenom.* **1998**, 88-91, 849. (g) Carron K.T.; Hurley, L.G. *J. Phys. Chem.* **1991**, 95, 9979.

[11] (a) Netzer, F.P. Langmuir **1991**, 7, 2544. (b) Weiss, K.; Gebert, S.; Wuhn, M.; Wadephol, H.; Woll, Ch. *J. Vac. Sci. Technol. A* **1998**, 16, 1017.

[12] Budevski, B.; Staikov, G.; Lorenz, W.J. *Electrochemical Phase Formation and Growth*, VCH: Weinheim, 1996.

[13] (a) Gilbert, E.S.; Cavalleri, O.; Kern, K. *Phy. Chem.* **1996**, 100, 12123. (a) Cavalleri, O.; Gilbert, S.E.; Kern, K. *Surf. Sci.* **1997**, 377-379, 931. (c) Cavalleri, O.; Gilbert, S.E.; Kern, K. *Chem. Phys. Lett.* **1997**, 269, 479.

[14] Eliadis, E.D.; Nuzzo, R.G.; Gewirth, A.A.; Alkire, R.C. *J. Electrochem. Soc.* **1997**, 144, 96.

[15] (a) Nichols, R.J.; Beckmann, W.; Meyer, H. *J. Electroanal. Chem.* **1992**, 330, 381. (b) Nichols, R.J.; Bunge, E.; Meyerand, H.; Baumgartel, H. *Surf. Sci.* **1995**, 335, 110. (c) Nichols, R.J.; Bach, C.E.; Meyer, H. *Ber. Bunsenges. Phys. Chem.* **1993**, 97, 1012. (d) Batina, N.; Will, T.; Kolb, D.M. *Faraday Discuss.* **1992**, 94, 93.

[16] Sondag-Huethorst, J.A.M.; Fokkink, L.G.J. *Langmuir* **1995**, 11, 4823.

[17] Kolb, D.M. *Prog. Surf. Sci.* **1996**, 51, 109 and references therein.

[18] Clavilier, J.; Faure, R.; Guinet, G.; Durand, R. *J. Electroanal. Chem.* **1980**, 107, 205.

[19] (a) Magnussen, O.M.; Hagebock, J.; Hotlos, J.; Behm, R.J. *Faraday Discus.* **1992**, 94, 329. (b) Mrozek, P.; Han, M.; Sung, Y.-E.; Wieckowski, A. *Surf. Sci.* **1994**, 319, 21. (c) Edens, G.J.; Gao, X.; Weaver, M.J. *J. Electroanal. Chem.* **1994**, 375, 357.(d) Shi, Z.; Lipkowski, J. *J. Electroanal. Chem.* **1996**, 403, 225.

[20] Moulder, J.F., Stickle, W.F., Sobol, P.E., Bomben, K.D. *Handbook of Photoelectron Spectroscopy*; Perkin-Elmer Corporation, Physical Electronics Division: Eden Prairie, MN 55344, 1992.

[21] (a) Socrates, G. *Infrared Characteristic Group Frequencies*; John Wiley & Sons: Great Britian, 1980. (b) Pauchert, C.J. *The Aldrich Library of FTIR Spectra*; Aldrich Chemical Co. Inc.: Milwaukee, Wisconsin, W.I., 1985.

[22] Law, D.; Beamson, G., private communication.

[23] Thiry, P.A., Ph.D. thesis, FUNDP, Namur, 1984.

[24] (a) Shen, W.; Nyberg, G.L. *Surf. Sci.* **1993**, 298, 143. (b) Roberts, J.T.; Friend, C.M. *J. Chem. Phys.* **1988**, 88, 7172. (c) Chen, D.A.; Friend, C.M.; Xu, H. *Surf. Sci. Lett.* **1998**, 395, L221. (d) Weldon, M.K.; Napier, M.E.; Wiegand, B.C.; Friend, C.M.; Uvdal, P. *J. Am. Chem. Soc.* **1994**, 116, 8328. (e) Rufel, T.S.; Huntley, D.R.; Mullins, D.R.; Gland, J.L. *J. Phys. Chem.* **1994**, 98, 13022. (f) Kane, S.M.; Rufael, T.S.; Gland, J.L.; Huntley, D.R.; Fischer, D.A. *J. Phys. Chem. B* **1997**, 101, 8486. (g) Huntley, D.R. *J. Phys. Chem.* **1992**, 96, 4550. (h) Bol, C.W.J.; Friend, C.M.; Xu, X. *Langmuir* **1996**, 12, 6083.

[25] (a) Argon, P.A.; Carlson, T.A. *J. Vac. Sci. Technol.* **1982**, 20, 815. (b) Agron, P.A.; Carlson, T.A.; Dress, W.B.; Nyberg, G.L. *J. Electron Spectrosc. Relat. Phenom.* **1987**, 42, 313. (c) Takata, Y.; Yokoyama, T.; Yagi, S.; Happo, N.; Sato, H.; Seki, K.; Ohta, T.; Kitajima, Y.; Kuroda, H. *Surf. Sci.* **1991**, 259, 266. (d) Jaffey, D.M.; Madix, R.J. *J. Am. Chem. Soc.* **1994**, 116, 3020.

[26] Ibach, H., Mills, D.L. *Electron Energy Loss Spectroscopy and Surface Vibrations*; Academic: London, 1982.

[27] (a) Ron, H.; Rubinstein, I. *Langmuir* **1994**, 10, 4566. (b) Canning, N.D.S.; Outka, D.; Madix, R.J. *Surf. Sci.* **1984**, 141, 240. (c) Pireaux, J.J.; Liehr, M.; Thiry, P.A.; Delrue, J.P.; Caudano, R. *Surf. Sci.* **1984**, 141, 221.

[28] Evans, S.D.; Cooper, S.D.; Johnson, S.R. RUSTI Annual Report; Daresbury CLRC Laboratory: U.K, 1995-1996.

[29] Laibinis, P.E.; Bain, C.D.; Whitesides, G.M. *J. Phys. Chem* **1991**, 95, 7017.

[30] Bethe, H. *Ann. Phys.* **1930**, 5, 325.

[31] Dubois, L.H.; Zegarski, B.R.; Nuzzo, R.G. *J. Chem. Phys.* **1993**, 98, 678.

[32] Whelan, C.M.; Smyth, M.R.; Barnes, C.J., unpublished data.

[33] Pauling, L.C. *The nature of the Chemical Bond*, 3rd ed.; Cornell University Press; New York, 1960.

[34] (a) Hachiya, T.; Honbo, H.; Itaya, K. *J. Electroanal. Chem.* **1991**, 315, 275. (b) Zelenay, P.; Rice-Jackson, L.M.; Wieckowski, A. *J. Electroanal. Chem.* **1990**, 283, 389. (c) Holzle, M.H.; Retter, U.; Kolb, D.M. *J. Electroanal. Chem.* **1994**, 371, 101. (d) Holzle, M.H.; Zwing, V.; Kolb, D.M. *Electrochim. Acta.* **1995**, 40, 1237. (e) Wu, S.; Lipkowski, J.; Tyliszczak, T.; Hitchcock, A.P. *Prog. Surf. Sci.* **1995**, 50, 227.

[35] Poirier, G.E.; Pylant, E.D. *Science* **1996**, 272, 1145.

[36] (a) Tour, J.M.; Jones II, L.; Pearson, D.L.; Lamba, J.J.S.; Burgin, T.P.; Whitesides, G.M.; Allara, D.L.; Parikh, A.N.; Atre, S.V. *J. Am. Chem. Soc.* **1995**, 117, 9529. (b) Tarlov, M.J.; Newman, J.G. *Langmuir* **1992**, 8, 1398. (a) Lee, Y.J.; Jeon, I.C.; Paik, W.-k.; Kim, K. *Langmuir* **1996**, 12, 5830.

Chapter 5

Benzenethiol Adsorption on Au(111) Studied by Synchrotron ARUPS, HREELS and XPS

Abstract

Benzenethiol adsorption on Au(111) has been studied using synchrotron angle resolved ultraviolet photoelectron spectroscopy (ARUPS), high resolution electron energy loss spectroscopy (HREELS) and high resolution X-ray photoelectron spectroscopy (XPS).

At sub-monolayer and saturation coverages, the absence of a S-H stretching vibration indicates that the sulfhydryl hydrogen is lost during adsorption. The C-S bond remains intact, consistent with the formation of a thiolate intermediate, as evidenced by the presence of aromatic vibrations, carbon (1s) and sulphur (2p) XPS lineshapes and binding energies and UPS assignment of benzene-like molecular orbitals.

Based upon the intensity of the out-of-plane C-H deformation relative to the in-plane C-H stretch, an adsorption geometry with the plane of the aromatic ring parallel to the Au(111) surface plane is favoured. The polarisation/angular dependence of the molecular orbital intensities in ARUPS confirms that the phenyl ring is aligned largely parallel to the surface and that the orientation is coverage independent. Polar angle dependence of the variation of the carbon (1s) to sulphur (2p) photoemission intensities indicates a flat-lying bonding arrangement with a tilt angle of the phenyl ring of $10\pm10°$ with respect to the surface plane.

The uptake of benzenethiol monitored by work function changes ($\Delta\phi$), low energy electron diffraction (LEED) and attenuation of the Au(111) Shockley surface state, suggests a precursor-mediated adsorption mechanism involving two-dimensional islanding without long range ordering to a 300 K saturation coverage of 3.3×10^{14} sulphur atoms cm^{-2}.

1. Introduction

The adsorption of organic sulphur-containing molecules on single crystal metal surfaces has received much attention in recent years due to their importance in processes such as lubrication, corrosion inhibition and catalytic desulphurisation reactions [1-4]. In the case of *n*-alkanethiol adsorption, several studies have shown that sulphur preferentially interacts with surface metal atoms resulting in deprotonation of the S-H bond to produce a thiolate intermediate with the polymethylene chain tilted (20-40°) with respect to the surface normal [1,5-10].

Aromatic thiols are particularly interesting since substrate-adsorbate bonding will, in principle, involve primarily the sulphur atom, as is the case in *n*-alkanethiol adsorption, and a secondary interaction via the π-orbitals of the phenyl ring, similar to benzene adsorption on transition metal surfaces [11-13]. Hence, the surface bound species if adopting a flat-lying molecular orientation, in addition to sulphur-metal bonding, may gain an increased chemisorption energy due to interaction of the delocalised π-system with the metal surface. Alternatively, a largely upright bonding geometry may be preferred in which the number of metal-sulphur bonds is maximised. Coverage dependent adsorbate-adsorbate packing arrangements and reorientation are also possible for adsorbates such as benzenethiol [14,15]. The interplay and final balance of these system dependent forces, which control the equilibrium structure of an adsorbate-substrate complex, is very difficult to predict.

In previous investigations of benzenethiol adsorption to saturation coverage on Cu(110), Cu(111), Cu(410), Au(110), Ni(100), Ni(110), Ni(111), Mo(110) and Rh(111) crystal surfaces and Ag(111) and Pt(111) electrodes, it has been found that the adsorption is dissociative, with S-H bond cleavage, and thiolate formation dominates [14-30]. ARUPS studies of benzenethiol adsorbed on Cu(110) and Cu(111) indicate that a largely perpendicular molecular orientation is adopted on both surfaces with a c(2×2) surface structure at saturation coverage and alignment of the phenyl rings in the [111] azimuthal direction on Cu(110) [14,16,17]. The adsorption site, molecular orientation and bond distances for the benzenethiol/Ni(100) system have been elucidated using surface extended X-ray absorption fine structure (SEXAFS) and near edge X-ray absorption fine structure (NEXAFS) [20]. The thiolate adsorbs in an

upright configuration at the 4-fold hollow site with S-Ni and S-C distances of 2.25 and 1.84 Å, respectively. NEXAFS data has also been used to assign a 23° tilt (from the surface normal) for the plane of the benzenethiolate ring on Mo(110) [25-27]. In contrast, on the Au(110) surface arguments based on surface coverage estimation by temperature programmed desorption spectroscopy imply a flat-lying bonding geometry is preferred [19].

At low coverages, benzenethiol adsorption on Ni(110) results in atomic sulphur as the primary surface sulphur species, resulting in passivation of the surface against further desulphurisation and stabilisation of a largely upright thiolate species at higher exposures [21]. Coadsorption of benzenethiolate, with a largely flat-lying orientation, and atomic sulphur has also been reported on Cu(110) at low exposures while decomposition resulting in surface atomic sulphur occurs prior to molecular adsorption on Cu(410) [14,18]. Similar to the behaviour of benzenethiol adsorbed on Cu(110), on Rh(111) a benzenethiolate intermediate with the phenyl ring parallel to the surface has been observed at low coverage with a reorientation to a more upright geometry at high coverage [15].

This paper forms part of a comprehensive investigation of benzenethiol adsorption from the liquid and gas phase on Au(111) and on an atomically stepped Au(322) surface [31-33]. The purpose of this study is to characterise the adsorption of benzenethiol from the gas phase on Au(111) at 300 K, using high resolution electron energy loss spectroscopy (HREELS), synchrotron angular resolved ultraviolet photoelectron spectroscopy (ARUPS) and high resolution X-ray photoelectron spectroscopy (XPS). The surface intermediates formed and their molecular orientation as a function of coverage are discussed. Low energy electron diffraction (LEED), work function changes ($\Delta\phi$) and photoemission from surface localised electronic states in the substrate are also used to gain insight to the adlayer bonding and the adsorption mechanism.

2. Experimental

A Au(111) single-crystal (6 × 8 × 1.5 mm) oriented to within 0.5° of the (111) plane (Metal Crystals and Oxides) was firmly attached to a molybdenum backing plate by spot welding two tantalum wires passed through spark eroded holes, drilled through the sides of the sample, parallel to the polished front face. The Au(111) surface was cleaned by repeated cycles of argon ion bombardment (3 KV) and annealing to 600-800 K. The temperature was monitored using a thermocouple attached to the molybdenum backing plate. Hence, as the thermocouple was not directly in contact with the sample, the annealing temperatures are considered upper limits due to possible thermal lag between the backing plate and the sample. LEED revealed a sharp, low background pattern typical of a reconstructed Au(111)-($\sqrt{3}\times22$) surface [34]. The surface cleanliness was quantitatively determined via XPS/HREELS. Particular attention was paid to the possibility of residual sulphur and hydrocarbon contamination by multi-scanning areas centred on the carbon (1s) and sulphur (2p) XPS core levels and vibrational regions identified with metal-sulphur and aliphatic/aromatic stretching modes [35,32,36]. As silicon has been reported as a contaminant of Au surfaces, the silicon (2s) core level binding energy region (140 - 170 eV) and SiO_2 energy loss regions (O-Si-O deformation mode and asymmetric stretching vibration at 484 and 1137 cm^{-1}, respectively) were carefully examined [35,37].

Benzenethiol (>99.9% purity, Aldrich) was purified prior to dosing by repeated freeze-pump-thaw cycles. As desulphurisation of some thiols may occur within the dosing manifold via reaction with the stainless steel walls, gas lines were passivated by repeated exposure to benzenethiol prior to dosing [14]. The purity of the resulting dosing stream was verified mass spectroscopically. Benzenethiol was dosed using a high precision leak valve and uncalibrated Bayard-Alpert ionisation gauge.

The HREELS spectrometer was equipped with sample preparation and main analyser chambers operated at base pressures in the low 10^{-10} Torr range. The analysis chamber consisted of a 180° hemispherical monochromator and analyser described in more detail elsewhere and an Omicron 4-grid reverse view LEED optics [38]. Specular scattering geometry was obtained by locating the (0,0) LEED beam and maximising the elastically scattered peak intensity. HREELS spectra were recorded at 5.0 eV

primary electron beam energy in specular geometry ($\theta_i = \theta_r = 70°$). Typical energy resolution of the elastic electron peak from clean Au(111) was 10 meV (~80 cm^{-1}) in terms of full-width half maximum (FWHM).

The ARUPS measurements were performed on beamline 6.2 at the synchrotron radiation source (SRS) at Daresbury CLRC Laboratory, UK. This beamline has a VUV toroidal grating monochromator and delivers photons in the energy range 15-110 eV, with the highest intensity and monochromator resolution between 15 and 45 eV. The mu-metal UHV chamber operated at a base pressure in the low 10^{-10} Torr region and consisted of an angle resolved electron energy analyser (ADES 400) mounted with two planes of rotation and a single channel electron multiplier. In all studies reported here, the analyser was maintained in the 'in-plane' orientation. ARUPS spectra were recorded at emission angles (θ_e) of between 0 and 45° and the angle of incidence of the light (Ψ_i) was varied between 20 and 70°, where θ_e and Ψ_i are defined with respect to the surface normal (±1°).

High resolution XPS measurements were performed utilising a Scienta ESCA 300 photoelectron spectrometer (operated at base pressures in the low 10^{-9} Torr range) at the RUSTI unit, Daresbury CLRC Laboratory, U.K. XPS experiments were carried out using a monochromated Al K_α rotating anode X-ray source operated at 14 KV and 20 mA. Photoelectrons were detected by a hemispherical analyser and a two-dimensional position-sensitive detector (micro-channel plates with CCD camera). Calibration of the binding energy scale was carried out using the Ag Fermi edge at 0.0 ± 0.07 eV, Ag (3d) photoemission at 368.26 ± 0.08 eV and the Ag MNN Auger line at 1128.78 ± 0.05 eV providing instrumental calibration within ± 0.1 eV [39]. Different combinations of pass energy and exit slit-aperture width of the analyser allowed variation of the energy resolution.

3. Results

3.1 High resolution electron energy loss spectroscopy

In Fig. 1, the HREELS spectra from a benzenethiol monolayer and sub-monolayer coverage are shown. Coverages are quoted as a fraction of monolayer coverage by integration of the intensity of the C-H stretching band at 3047 cm^{-1} and comparison to saturation coverage normalised to the elastic peak [32]. The sub-monolayer coverage was estimated to be 0.25 pML (physical monolayer = pML) where 1.0 pML is equivalent to saturation coverage at 300 K. In specular scattering geometry, the spectra contain the vibrational bands expected from the parent compound with the exception of the S-H stretching mode (2580 cm^{-1}) [36]. The absence of this band, at both high and low surface coverage, suggests that the sulfhydryl hydrogen is lost during adsorption on Au(111), consistent with the formation of a phenyl thiolate intermediate. Of course in specular scattering geometry, the metal-surface selection rule (MSSR) applies, such that only vibrations with a component of the dipole moment change normal to the surface may be observed [40]. Hence, a stretching vibration due to a S-H bond oriented parallel to the surface is only impact allowed. A more detailed HREELS study of benzenethiol adsorption on Au(111), including off-specular data, has verified the occurrence S-H bond cleavage [32].

Electron energy loss frequencies are summarised in Table 1 and proposed assignments are made by correspondence with accepted gas phase infrared (IR) assignments and several previous HREELS studies of benzenethiol adsorption on Cu(110), Rh(111), Ni(111), Mo(110), Ag(111) and Pt(111) [14,15,22,23,26-30]. The weak energy loss superimposed on the tailing elastic peak at 460 cm^{-1} may be assigned to Au-SC_6H_5 stretching. Due to the possibility of low frequency ring modes in this region, this band may not be a pure metal-sulphur stretch and for this reason does not provide unequivocal proof of C-S bond integrity [14]. However, at 300 K benzene does not adsorb on Au and, hence, the presence of aromatic vibrational bands, in particular the C-H in-plane stretching ($\nu_{C\text{-}H}$) and out-of-plane bending ($\gamma_{C\text{-}H}$) at 3047

and 730 cm^{-1}, respectively, indicates that extensive C-S bond scission does not occur and benzenethiol retains its molecular framework following adsorption [41,42].

In specular geometry, application of the MSSR provides information on the orientation of the phenyl ring relative to the Au(111) surface plane [40]. The ν_{C-H} band, which has its dipole moment change upon vibration within the plane of the ring, should be dipole active and hence strongly excited in the case of a phenyl ring orientated normal to the Au surface. The opposite is true for the γ_{C-H} vibration which has a dipole moment perpendicular to the ring. In contrast, for a flat-lying molecule with its phenyl ring parallel to the Au surface, the γ_{C-H} band should be of maximum intensity with a weak ν_{C-H} contribution due to 'impact scattering'. For both sub-monolayer and monolayer spectra, the energy loss at 730 cm^{-1} due to γ_{C-H} is the dominant vibration relative to ν_{C-H} band at 3047 cm^{-1} suggesting that surface intermediate adopts an adsorption geometry which is coverage independent with its phenyl ring largely parallel to the Au(111) surface.

Table 1 The major HREELS band assignments for benzenethiol adsorption on Au(111) at monolayer coverage.

Assignment[A]	**C_6H_5SH (gas)**[B]	**C_6H_5S/Au(111)**
	cm^{-1} (meV)	
ν(C-H)	3000-3030	3047 (378)
ν(S-H)	2580	
ν(C-C)	1450-1600	1556 (193)
		1443 (179)
γ(C-H)		1136 (141)
δ(C-H)/ ν(C-CH)	1065-1075	1016 (126)
γ(C-H)	740-760	730 (91)
ν(Au-SC_6H_5)/ ν(C-S)/ γ(C-C)		460 (57)

[A]ν = stretch; δ = in-plane bend; γ = out-of-plane bend. [B]Shen *et al.* [14].

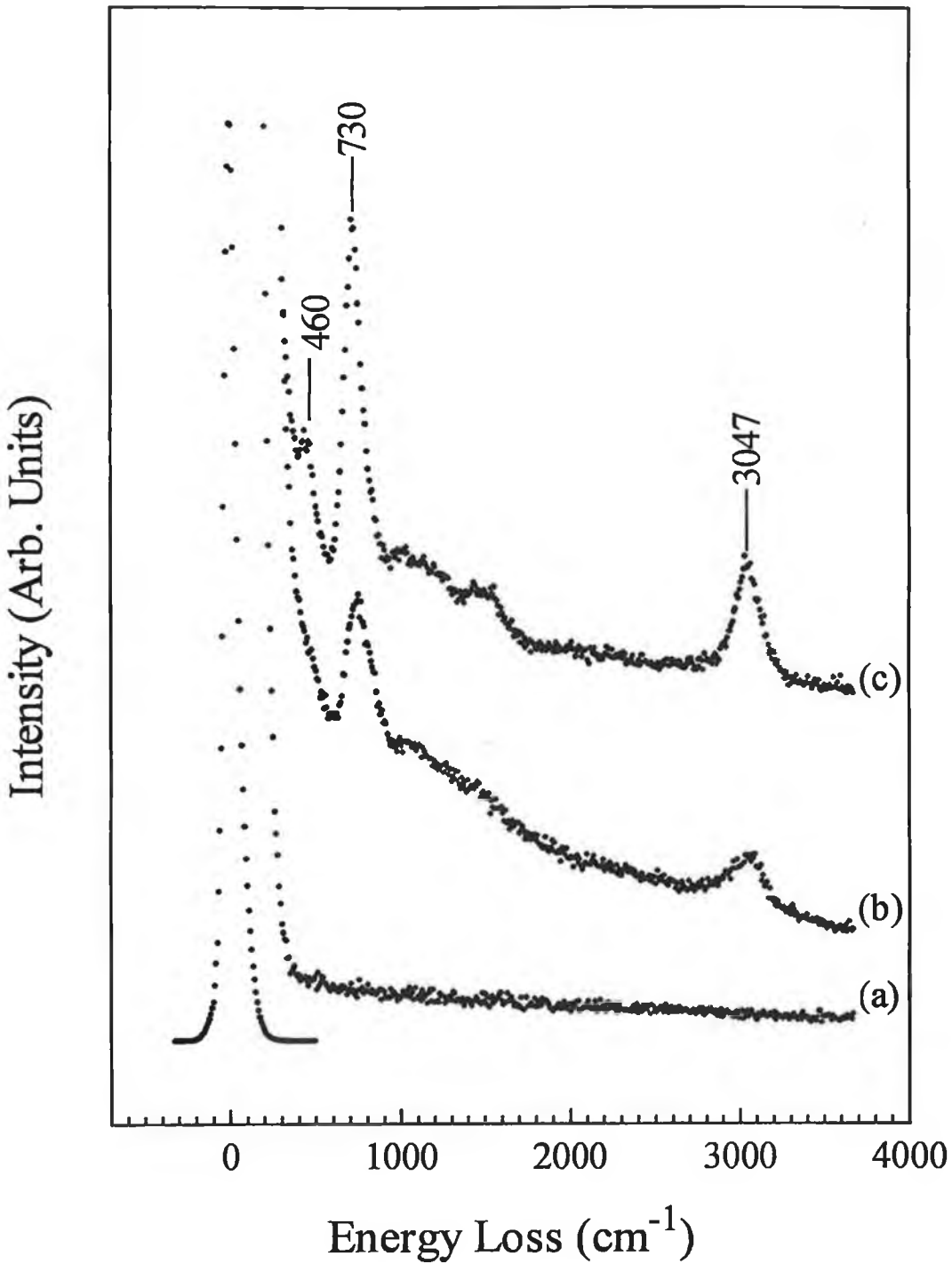

Figure 1 HREELS spectra from (a) clean Au(111) and benzenethiol adsorbed at 300 K on Au(111) at (b) 0.25 pML and (c) 1.0 pML coverage collected in specular scattering geometry ($\theta_i = \theta_r = 70°$) at a primary beam energy of 5.0 eV.

3.2 Angle resolved ultraviolet photoelectron spectroscopy

ARUPS was used to monitor the evolution of the benzenethiol electronic structure from physisorbed multilayers adsorbed on Au(111) at 150 K to chemisorbed sub-monolayers and monolayers formed at 300 K. The change in substrate work function ($\Delta\phi$) following benzenethiol chemisorption (described in section 3.4) was used to estimate surface coverage in the case of ARUPS measurements. A bias voltage of -9.0 V was applied to the sample in order to remove the contribution from slow secondary electrons produced in the energy analyser. Based upon previous studies of benzene adsorption on transition metal surfaces, the benzene-like $3a_{1g}$ orbital does not participate in chemisorption to the substrate and, hence, does not exhibit a bonding shift typical of chemisorbed species relative to gas phase benzene [43]. For this reason the physisorbed multilayer and gas phase spectra of benzenethiol are aligned with the chemisorbed layers (Fig. 2) using the highest binding energy peak (D) which corresponds to emission from the benzene-like $3a_{1g}$ orbital [14,44].

In Fig. 2, correlation between multilayer (50 L dosage) and gas phase spectra is used to identify molecular π- and σ-orbitals of benzenethiol. The multilayer spectrum is in excellent agreement with that reported by Shen *et al.* for condensed benzenethiol multilayers on Cu(110) [14]. The band assignments of gas phase benzenethiol photoemission have been discussed by Carnovale *et al.* [44]. In the low binding energy region, < 5 eV below the substrate Fermi level (E_F), the sulphur 3p orbital perpendicular to the benzene ring interacts with one of the benzene-like $1e_{1g}$ orbital components resulting in a pair of mixed sulphur π orbitals split almost symmetrically about the remaining $1e_{1g}$ orbital energy with purely aromatic π-ring character, giving rise to bands X_1, X_2 and X_3 at 2.2, 3.2 and 4.1 eV, respectively. Three overlapping bands (A), between 5 and 7 eV, are assigned to the $3e_{2g}$ orbitals, the first of which contains a significant amount of sulphur mixing due to S-C σ-bonding, a $1a_{2u}$ π-orbital and S-H σ-bonding orbitals. The highest binding energy emissions (> 7 eV) arise from the split benzene $3e_{1u}$ degenerate orbital and the virtually unaffected $1b_{2u}$ and $2b_{1u}$ orbitals of the phenyl ring. These features are assigned as peaks B and C observed at 7.7 and 8.7 eV, respectively. Finally, peak D at 10.3 eV corresponds to the benzene-like $3a_{1g}$ orbital. Hence, a single band corresponding to the S-H bond and three bands

originating from the aromatic ring containing the major sulphur character while the remaining bands in the spectrum closely resemble those reported for unsubstituted benzene [43,44].

The clean Au(111) spectrum is in good agreement with previous reports [45-47]. Benzenethiol adsorption to saturation ($\Delta\phi = 0.6 \pm 0.02$ eV) reached by an exposure of 10 L is shown in Fig. 2a. The spectrum reveals attenuation of Au-*d* band transitions due to inelastic scattering by the overlayer, quenching of the Shockley surface state (SS) and the emergence of additional bands attributed to the molecular orbitals of the adsorbate. Enhancement of the secondary electron background at low kinetic energies was also observed, consistent with the formation of an overlayer. Phenyl ring induced features are recognised in the region between 7 and 11 eV below E_F. The observed photoemission from bands B, C and D are observed at binding energies close to the gas phase/multilayer assignments (within 0.2 eV). The orbitals with substantial sulphur character (bands X_1, X_2, X_3 and A) are obscured by substrate emission.

In previous studies of *n*-alkanethiol and *n*-dialkyl disulphide adsorption on Cu(410) and benzenethiol adsorption on Cu(110), low intensity bands have been observed between 2 and 5 eV below the Fermi level [6,16]. These bands have been attributed primarily to interactions between the non-bonding π-orbital on the sulphur atom and the substrate $d_{xz,yz}$ orbitals resulting in the formation of π bonding and π^* antibonding levels. Similarly, a low intensity feature is observed at approximately 1.5 eV below E_F and prior to the Au d-band onset following benzenethiol adsorption on Au(111) (clearly discernible in Fig. 4). This adsorbate-induced band can thus be taken as evidence of Au-sulphur bonding.

A reduction of the interference by substrate d-band emission would require use of an incident photon energy (hν) close to the Cooper minimum of Au such that the ionisation cross-section of the 5d levels is minimised, i.e. 200 eV [48]. Even in such circumstances, in-depth study of the low binding energy features of a small organic molecule such as benzenethiol would require careful subtraction techniques. Different incident photon energies within the energy range of 20 to 50 eV were examined, however, substrate *d*-band emission continued to dominate the spectra as expected. Hence, under our experimental conditions, the loss of the sulfhydryl hydrogen during

adsorption cannot be observed directly without use of subtraction techniques. However, as cleavage of the S-H bond has been unambiguously determined by HREELS, use of subtraction techniques was not deemed necessary.

As benzene desorbs from Au at temperatures < 300 K, emission from benzene-like molecular orbitals indicate that the ring structure and, hence, the C-S bond remains intact, consistent with the formation of a benzenethiolate intermediate [41,42]. Adsorbate photoemission from sub-monolayer surface coverages (Fig. 2b and c) shows similar relative band intensities and binding energies for bands B, C and D, indicating that the surface intermediate and its orientation is similar to that formed at saturation exposures.

ARUPS from benzenethiol chemisorbed on Au(111) to saturation coverage at 300 K obtained as a function of angle of emission is shown in Fig. 3. The angular distribution of bands B, C and D from saturation and sub-monolayer coverage overlayers exhibit pronounced intensity variations as a function of emission angle, from 0 to 45° off-normal. An ARUPS study (using an unpolarised HeI resonance radiation source) of benzene on Rh(111) with a flat-lying adsorption geometry shows identical behaviour in terms of angular dependence of band D associated with the totally symmetric $3a_{1g}$ orbital of benzene [12]. Angular-dependence of the UPS band intensities thus suggests that benzenethiolate assumes a largely flat-lying bonding configuration on Au(111).

ARUPS spectra of monolayer and sub-monolayer coverages of benzenethiol exhibit polarisation dependence suggestive of formation of an oriented film. In Fig. 4, normal emission spectra are displayed for various photon angles of incidence (20 to 70° with respect to the surface normal) for saturation coverage of benzenethiol on Au(111). Similar to photoemission behaviour of benzene adsorbed on Rh(111), emission from band D, and to some extent band B, increase with increasing angle of incidence [12]. At lower adsorbate coverages we find qualitatively similar ARUPS behaviour of the adsorbate induced features as a function of angle of emission/photon incidence indicating that the bonding configuration is coverage independent. In contrast, there is little polarisation dependence observed in the case of the physisorbed multilayers, implying random ordering within the benzenethiol condensed phase.

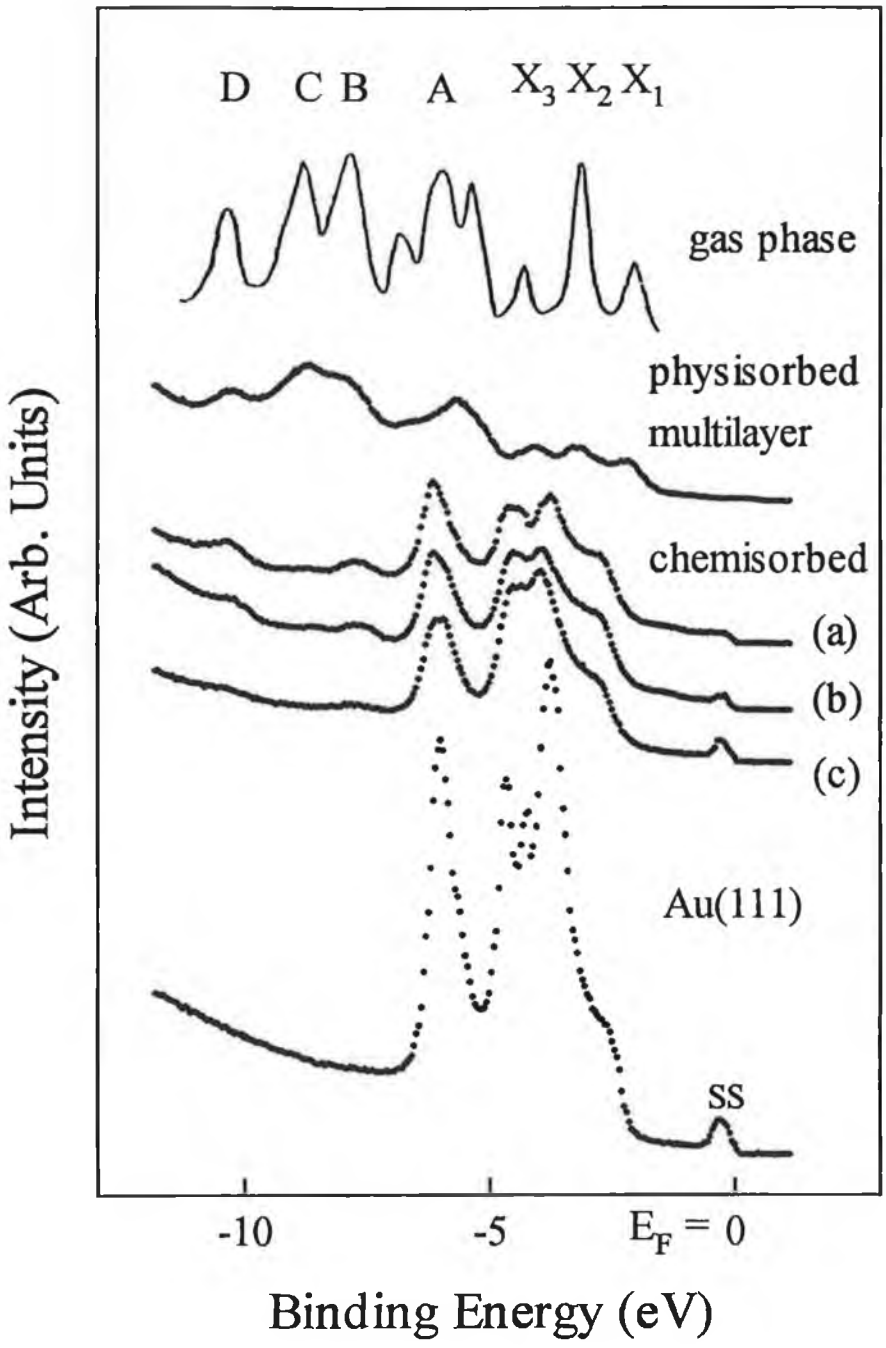

Figure 2 Normal emission UPS spectra of clean Au(111), (a) 1.0, (b) 0.6 and (c) 0.15 pML benzenethiol on Au(111) ($\psi_i = 45°$, $h\nu = 21.2$ eV). Benzenethiol multilayers adsorbed on Au(111) at 150 K and gas phase spectra are included for band assignment. The gas phase spectrum, obtained with HeI (21.2 eV), is adapted from the work of Shen *et al.* [14].

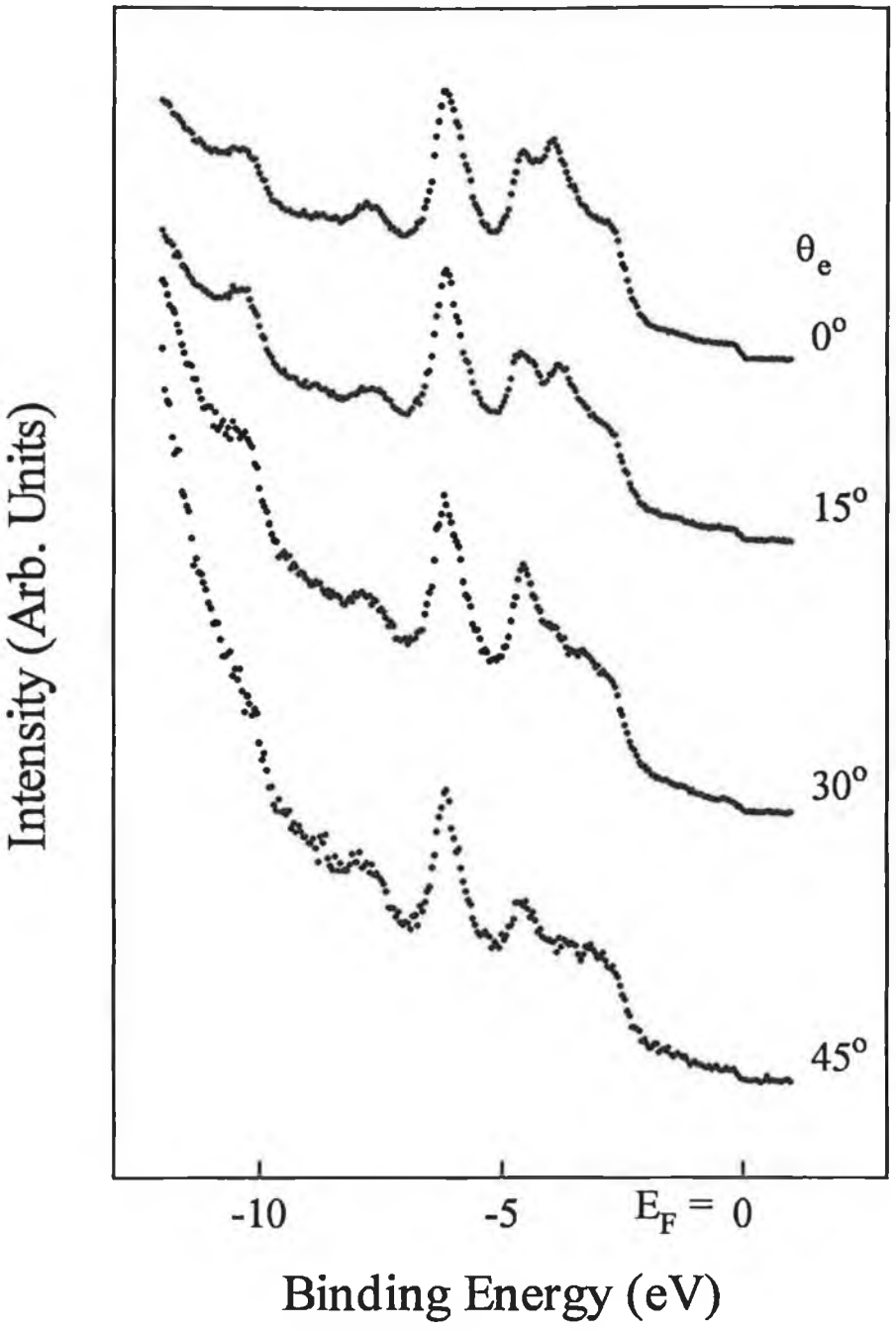

Figure 3 ARUPS spectra of a benzenethiol monolayer on Au(111) as a function of emission angle (θ_e = 0-45°, ψ_i = 60°, hν = 21.2 eV).

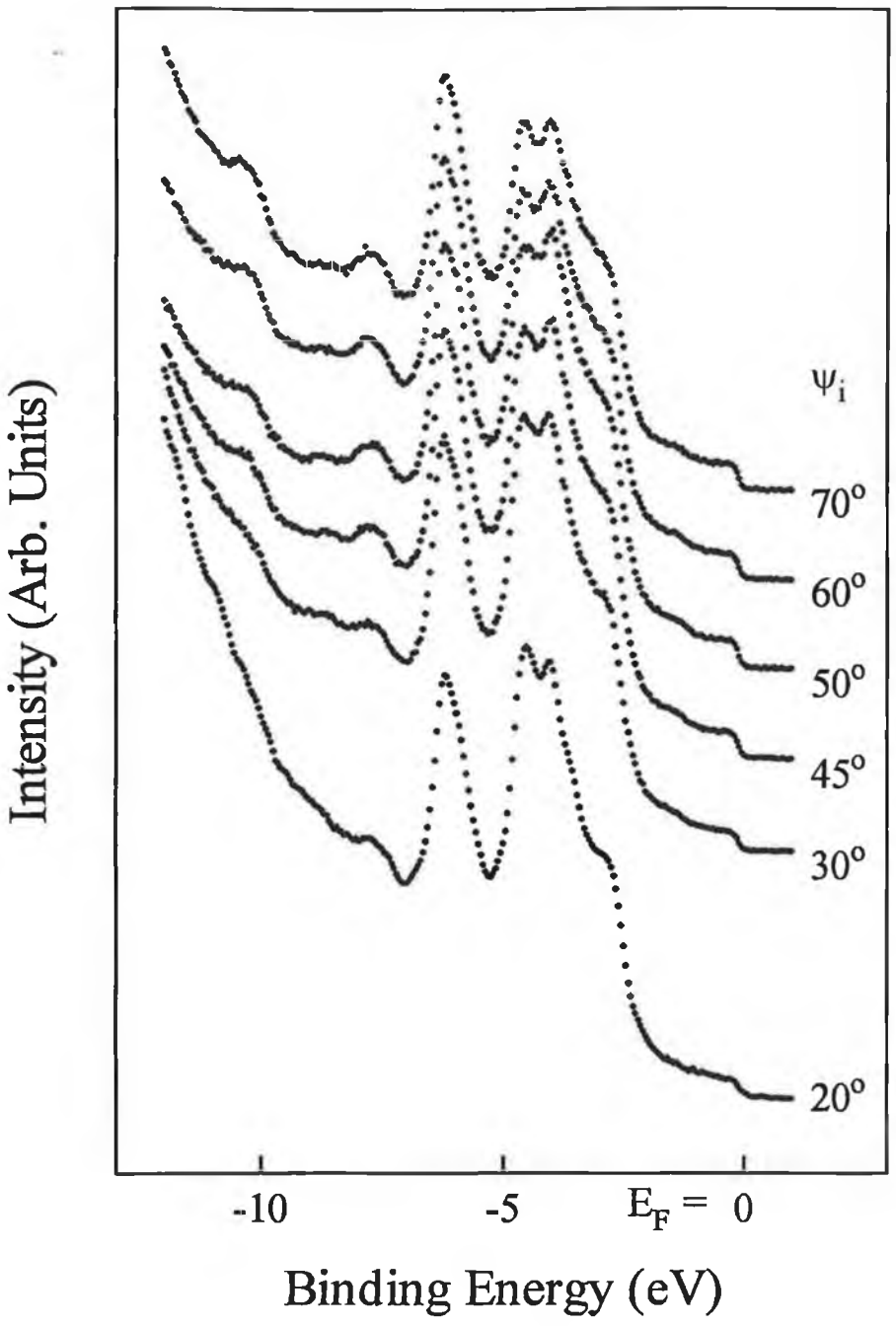

Figure 4 Normal emission UPS spectra of a benzenethiol monolayer on Au(111) as a function of photon angle of incidence (ψ_i = 20-70°, $h\nu$ = 21.2 eV).

The polarisation dependence of the adsorbate molecular orbital intensities shown in Fig. 4 may be discussed quantitatively using the oriented free molecule approach and application of polarisation dependent selection rules.

As benzene is only weakly adsorbed on Au(111), we would not expect any symmetry lowering of the phenyl ring due to surface-molecule interactions and the symmetry of the thiolate intermediate will thus be largely controlled by the molecular orientation. As mentioned earlier, the observed molecular emissions (B, C and D) correspond to photoemission from orbitals having their origin primarily in the phenyl ring with only a minor contribution from sulphur orbitals (see Table 2) [44]. A flat-lying thiolate with the plane of the phenyl ring parallel to the Au(111) surface (with the sulphur atom lying within this plane and ignoring underlying substrate atoms) would have a local C_{2v} symmetry. A similar symmetry applies for a perfectly upright thiolate intermediate. For a tilted intermediate the symmetry will be lowered to C_s. It should be kept in mind that, while it is the presence of the sulphur substituted for a hydrogen atom which reduces the symmetry of the phenyl ring from C_{6v} (typical of flat-lying, undistorted benzene adsorbed on a transition metal surface) to C_{2v}, the symmetry lowering may not be expected to be particularly strong for the orbitals observed above 7 eV as they have little mixing with sulphur orbitals (see Table 2) [44].

A strongly tilted (C_s) thiolate intermediate may be immediately ruled out by the strong polarisation of band D associated with the σ-framework bonding $2a_{1g}$ orbital in benzene. This orbital is clearly preferentially excited by the A_z component of the incident light as predicted for a flat-lying (or upright) C_{2v} symmetry. Figure 5 illustrates the variation in the relative intensity of this band with angle of incidence of the photon beam for benzenethiol on Au(111) along with the measured variation for the $2a_{1g}$ orbital of benzene adopting a perfectly flat-lying geometry on a Rh(111) [12]. The changes in relative intensity are in good agreement suggesting a very similar orientation of the thiolate phenyl ring on Au(111) to that of benzene on Rh(111), i.e., flat-lying. Also shown in Fig. 5 are calculations of the variation in intensity of band D for orientations of the phenyl ring tilted at 0 and 10° with respect to the Au(111) surface plane. Clearly, the experimental data fits best with a flat-lying intermediate and allows quantification of the tilt of the ring as flat-lying with a maximum deviation of +10° with respect to the Au(111) surface plane.

Table 2 Correlation table for some of the molecular orbitals of benzenethiol; theoretically allowed bands at normal emission for respective photon polarisation components are indicated.

D_{6h}	C_{6v}			C_{2v}			Band	%sulphur[A]
		x,y	*z*		*x,y*	*z*		
$2e_{1u}(\sigma)$	e_1	+	–	b_2	+	–	B	8
				a_1	–	+		15
$1b_{2u}(\sigma)$	b_2	–	–	b_2	+	–	C	4
$1b_{1u}(\sigma)$	b_1	–	–	a_1	–	+		14
$2a_{1g}(\sigma)$	a_1	–	+	a_1	–	+	D	9

A % sulphur based on the work of Carnovale *et al.* [42].

The polarisation dependence of bands B, C and D (Fig. 4) are almost identical to those observed for flat-lying benzene on transition metal surfaces. Band C which is very weak at all photon incident angles corresponds to emission from benzene-like $1b_{1u}$ and $1b_{2u}$ σ-orbitals from which excitation is not allowed for a flat-lying molecule within the C_{6v} point group. Clearly emission is observed, although it is very weak compared to that for gas phase benzenethiol (Fig. 2). In contrast, the benzenethiol orbitals are classified as b_2 and a_1, respectively, in the C_{2v} point group, the former being excited by A_{xy} and the latter by A_z such that only a weak polarisation dependence would be expected in line with experimental observations. The weak nature of band C is suggestive that while the thiolate symmetry is C_{2v}, the lowering from C_{6v} (which would predict zero emission) is not strong. Finally, band B while strongly excited does not exhibit strong polarisation dependence. This band is largely due to a benzene-like e_{1u} orbital which in a flat-lying C_{2v} geometry in the case of the thiolate intermediate splits into b_2 and a_1 symmetries which are excited by A_{xy} and A_z components of the incoming light, respectively. Hence, in agreement with experimental observations, in C_{2v} geometry we would not expect a strong polarisation dependence. In the case of C_{6v}

flat-lying benzene, the e_1 orbital will be excited by A_{xy} and decrease substantially in intensity for synchrotron light at grazing incidence when A_z is maximised, indicating a clear effect of symmetry lowering.

To summarise, the polarisation dependence of the observed molecular orbitals allows us to conclude that the phenyl ring adopts a flat-lying geometry with the thiolate having a C_{2v} point group, although the symmetry lowering of the phenyl orbitals from C_{6v} due to substitution of hydrogen by sulphur is rather weak as illustrated by the lack of emission from band C.

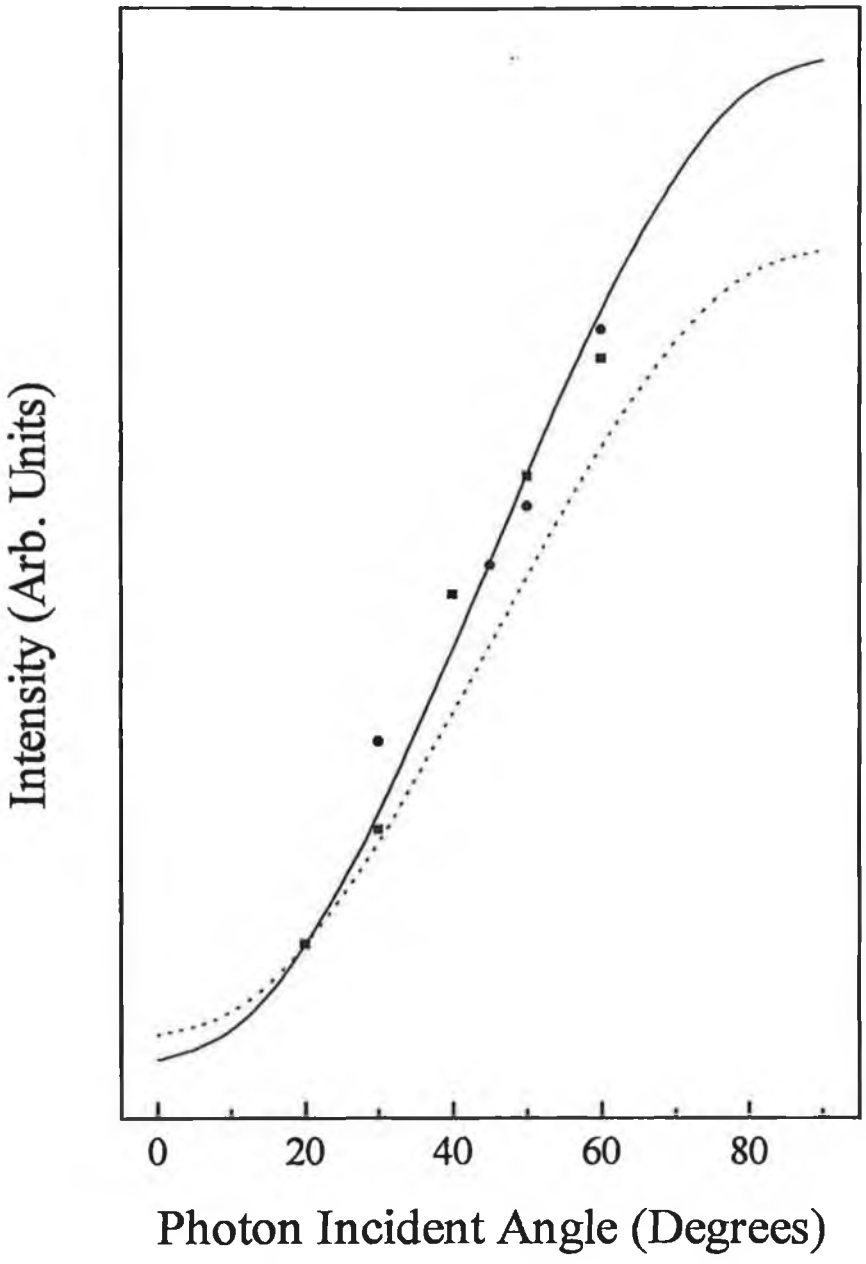

Figure 5 Variation (•) of the intensity of the benzene-like $2a_{1g}$ orbital (band D) as a function of photon angle of incidence (ψ_i = 20-70°, hν = 21.2 eV) for benzenethiol adsorbed to saturation on Au(111) at 300 K. Also shown (■) is the variation from the corresponding band observed for flat-lying benzene on Rh(111) [12]. Calculated curves show the theoretical variation in intensity expected for orientations of phenyl ring tilted 0° (—) and 10° (·····) with respect to the surface plane.

3.3 X-ray photoelectron spectroscopy

Figure 6 shows XPS spectra of the sulphur (2p) and carbon (1s) core levels from a benzenethiol monolayer on Au(111) at 300 K collected at grazing emission (80° with respect to the surface normal) at an instrumental resolution of 0.29 eV. Elemental quantification, in terms of atomic percentage (±0.5%) ratio of carbon and sulphur, was calculated from spectra collected at normal emission by integration of the areas of the carbon (1s) and sulphur (2p) peaks after application of a Shirley background subtraction and correction for atomic sensitivity factors including analyser transmission. Peak fitting to experimental data was carried out using mixed Gaussian/Lorentzian (the so-called Voigt function) lineshapes. The fitting, unconstrained with the exception of the peak shape (Gaussian:Lorentzian mixing ratios are given in the figure captions), consists of a minimum number of peaks consistent with a reasonable fit to the raw data and the molecular structure of the adsorbate.

In Fig. 6a, deconvolution of the sulphur (2p) core level spectrum reveals a two component peak with an intensity ratio of 1.9:1 and peak separation of 1.2 eV. These peaks are assigned to the $2p_{3/2}$ and $2p_{1/2}$ spin orbit split levels with binding energies of 162.1 and 163.3 eV, respectively. The theoretical 2:1 intensity ratio of the sulphur (2p) doublet is not obtained exactly. Magnee *et al.* suggest that deviation from an exact 2:1 intensity ratio may be indicative of disulphide species on the surface [49]. In contrast, Weldon *et al.* and Bol *et al.* attribute 1.7:1 and 1.8:1 intensity ratios for benzenethiol adsorbed to saturation on Rh(111) and Mo(110), respectively, to a contribution by final state effects in the sulphur $2p_{3/2}$ peak [15,27]. While we cannot rule out the possibility of small amount of phenyl disulphide within the monolayer on Au(111), the primary adsorbate species is a thiolate and there is no evidence of surface atomic sulphur or higher oxidation state species. Comparison of the sulphur (2p) binding energies with previous reports of benzenethiol adsorption on Rh(111), Ni(111) and Mo(110) indicates the presence of a C-S bond, consistent with chemisorbed benzenethiolate [15,22,26,27].

In Fig. 6b, the main carbon (1s) photoemission is attributed to the benzene-like carbon atoms while the minor high binding energy component, giving rise to asymmetry in the carbon (1s) lineshape, is assigned to the electron deficient carbon

bonded to the electronegative sulphur atom. Fig. 6b illustrates a fit to the experimental data assuming a surface phenyl thiolate with two distinct chemically shifted carbon (1s) core level emissions occurring at 285.8 and 284.3 eV, with a relative intensity ratio of 1.0:5.1 (close to the 1:5 ratio expected from a flat-lying benzenethiolate intermediate). Quantification yields a carbon to sulphur ratio of 6.0:0.9 which compares favourably with the expected 6:1 ratio.

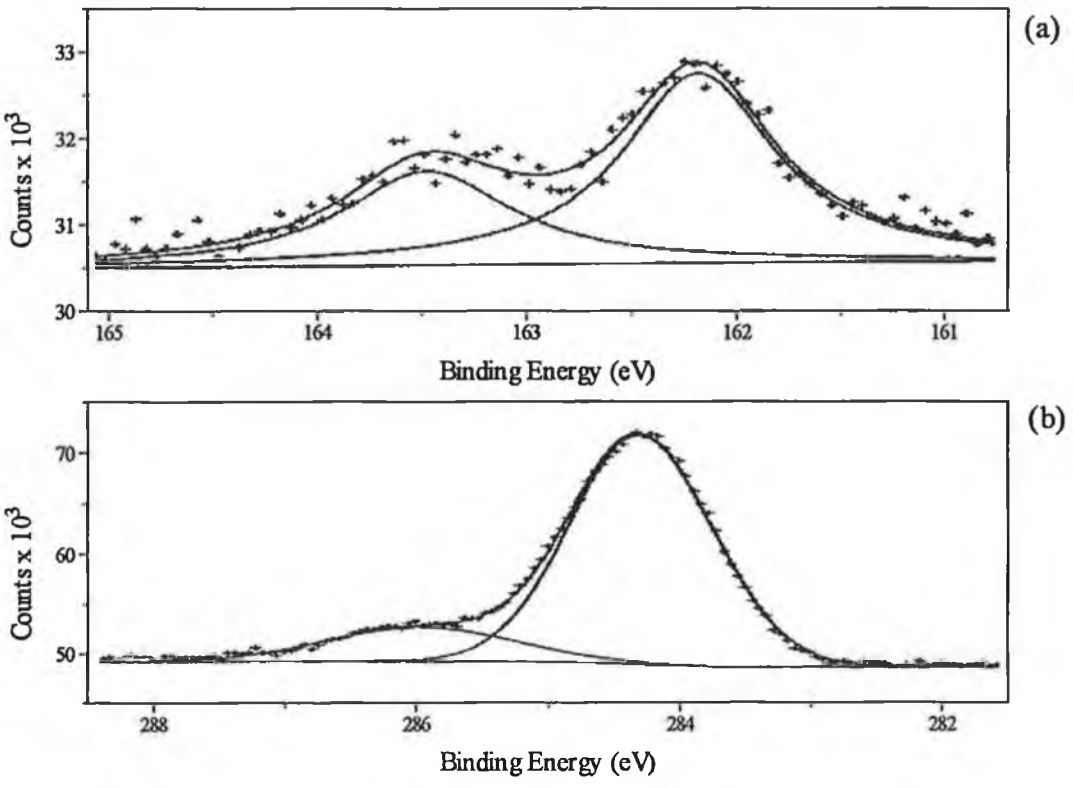

Figure 6 XPS spectra of the (a) sulphur (2p) and (b) carbon (1s) core levels from a benzenethiol monolayer adsorbed on Au(111). Raw data (++++) and fit to the experimental data using a Voigt line shape (——) with a Gaussian:Lorentzian mixing ratio of 20:80.

The absolute sulphur surface coverage for the benzenethiolate film was determined by comparing the sulphur (2p) to Au ($4f_{7/2}$) ratio with that measured (at normal emission on a laboratory Mg K_α source) from a film of known sulphur atomic

density. Gas phase chemisorption of ethanethiol to saturation coverage on Au(111) results in a $(\sqrt{3}\times\sqrt{3})R30°$ overlayer structure corresponding to a coverage of 0.33 monolayers of sulphur [5,50]. Ignoring differential attenuation of the sulphur and Au signals by the different nature of the monolayers, which should be small at the high outgoing kinetic energies utilised, the corresponding sulphur coverage for benzenethiolate is 0.23 monolayers (3.3×10^{14} sulphur atoms cm^{-2}) with respect to the density of the Au(111)-$(\sqrt{3}\times22)$ surface (1.45×10^{15} cm^{-2}). Maximum coverages for upright and flat-lying molecular orientations of benzenethiolate calculated on the basis of adsorption without overlap of van der Waals' radii are approximately 0.2 and 0.4 monolayers, respectively [51]. Hence, the absolute sulphur surface coverage of 0.23 monolayers further supports a layer of flat-lying molecules.

Quantitative adsorbate molecular orientation determination is also possible by measurement of the variation of adsorbate core level intensity ratios as a function of photoelectron take-off angle. This data was collected in the form of polar angle dependence of the variation of the carbon (1s) to sulphur (2p) emission intensities measured between normal and grazing (80° with respect to the surface normal) take-off angles in 10° steps. The electrostatic analyser had a large acceptance angle (10°) washing out photoelectron diffraction and ensuring that signal variation as a function of take-off angle is dominated by inelastic scattering. Hence, a 'continuum model' was used in modelling without recourse to the detailed atomic/molecular structure of the adsorbate-substrate complex. In the case of an upright molecule, substantial inelastic damping of the sulphur photoelectrons by the overlying carbon atoms will occur leading to a substantial rise in the carbon to sulphur ratio at grazing take-off angles. In contrast, no variation in the ratios would be expected as a function of take-off angle in the case of a flat-lying surface intermediate.

A selection of theoretical curves shown in Fig. 7 were calculated for variation of the carbon (1s) to sulphur (2p) emission intensities for flat-lying, upright and intermediate molecular orientations. The calculated curves are based on inelastic mean free paths for the carbon (1s) and sulphur (2p) photoelectrons estimated at 31.5 and 30.0 Å, respectively, based on the method described by Laibinis *et al.* [52]. Inspection of the variation of the experimentally derived carbon (1s) to sulphur (2p) ratio as a function of increasing take-off angle illustrated in Fig. 7 leads us to conclude that the

benzenethiolate monolayer adopts a flat-lying configuration, with the plane of the phenyl ring tilted 10±10° away from the surface plane.

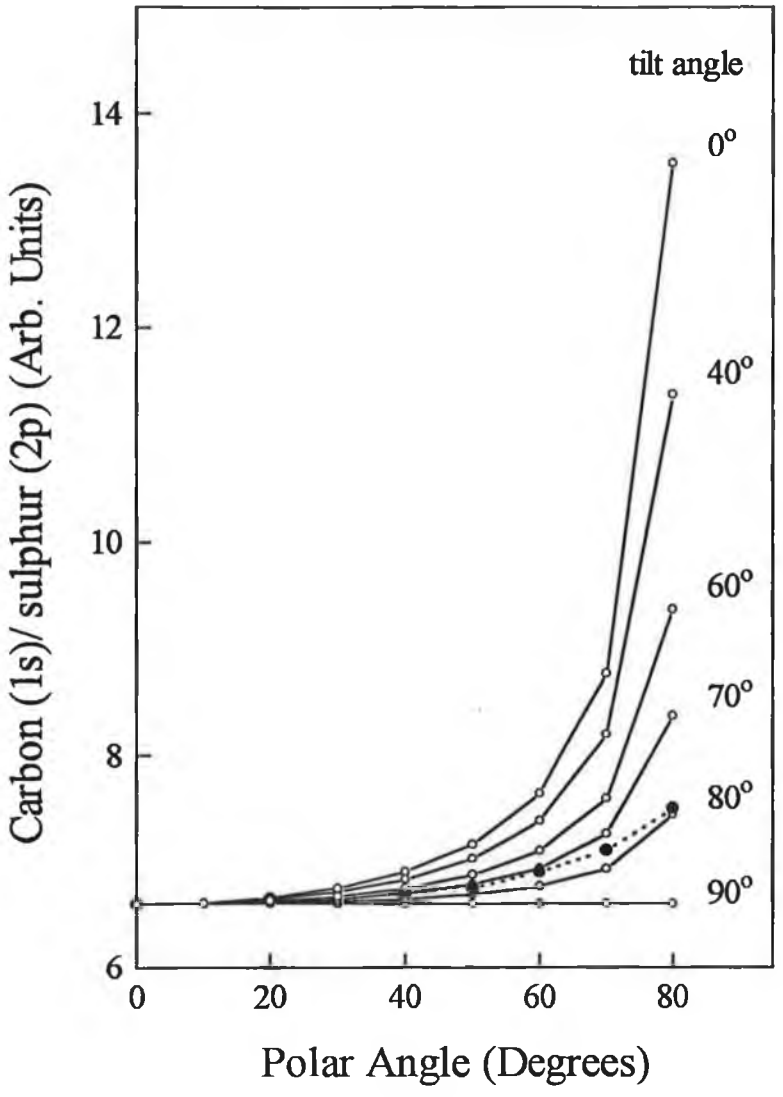

Figure 7 Measured variation of the carbon (1s) to sulphur (2p) core level intensities (•---•---•) as a function of take-off angle between normal and grazing (80° with respect to the surface normal). Calculated curves (o—o—o) show the angular dependence of the carbon (1s) to sulphur (2p) core level intensities for flat-lying (90°), upright (0°) and intermediate orientations 40, 60, 70 and 80° of the plane of the phenyl ring with respect to the Au(111) surface normal.

3.4 Benzenethiol adsorption mechanism on Au(111)

Information regarding substrate structure following adsorption of benzenethiol may be obtained upon examination of the Au *d*-band region and the Shockley surface state. Bands labelled 1 to 3 in Fig. 8a are due to direct bulk transitions while emission at E_1 and a shoulder at E_2 result from states which are spatially localised within the topmost layer of the reconstructed Au(111)-($\sqrt{3}\times22$) surface [47]. The existence of a low intensity band (FWHM = 0.35 eV) observed immediately below E_F, superimposed on the Au sp band emission, is identified as originating in transitions from occupied surface states (SS) located in the uppermost Au atomic layers [45]. Paniago *et al.* have shown that emissions from E_1 and E_2 are highly sensitive to temperature and to the local environment of the surface relative to the bulk atoms [47]. In particular, E_1 is attenuated upon formation of the bulk truncated Au(111)-(1×1) surface structure as shown in Fig. 8b. However, following benzenethiol adsorption to sub-monolayer coverage (0.25 pML) on Au(111)-($\sqrt{3}\times22$), the retention of this emission feature provides indirect evidence that the substrate reconstruction is not lifted at low adsorbate exposures (Fig. 8c). Unfortunately, saturation coverage results in significant attenuation of the Au *d*-band region such that E_1 is no longer discernible, however, low-energy electron diffraction (LEED) has been used to further investigate the adsorption process.

LEED observations reveal benzenethiol adsorption at 300 K led to an increase in the diffuse background without long range ordering with respect to the substrate [33]. In support of this, a decrease in the HREELS elastic peak intensity, which is strongly dependent on surface order, was observed at saturation coverage suggesting that benzenethiolate forms a disordered monolayer on Au(111) [14]. In addition, LEED indicates that adsorption does not lift the ($\sqrt{3}\times22$) surface reconstruction even upon prolonged dosing (>100 L).

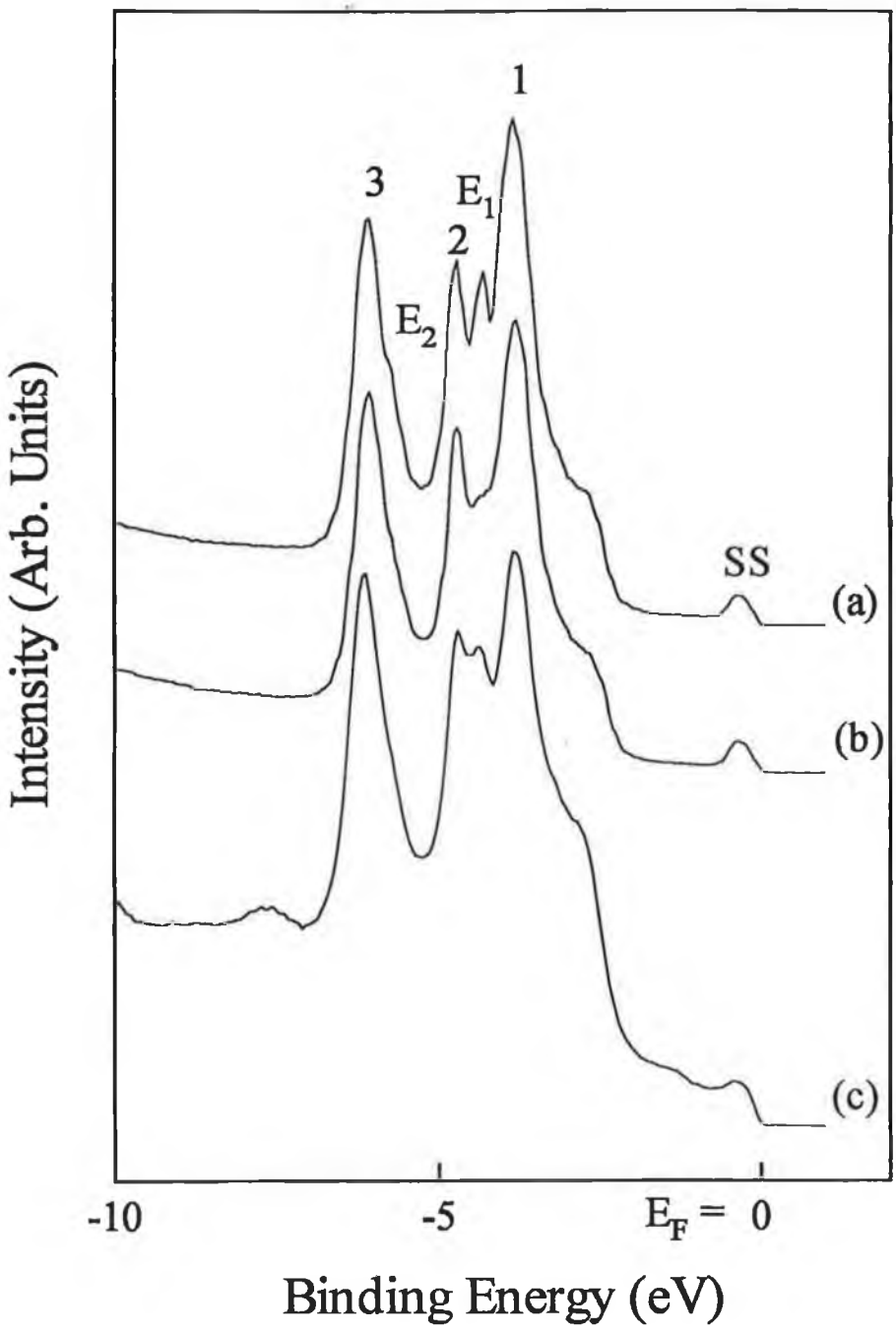

Figure 8 Normal emission UPS spectra of (a) Au(111)-(√3×22), (b) Au(111)-(1×1) and (c) 0.25 pML benzenethiol adsorbed on Au(111)-(√3×22) (ψ_i = 45°, hν = 21.2 eV).

Measurement of work function change ($\Delta\phi$) provides valuable information, as it is critically dependent on the local surface geometry and electronic structure. The full width of the UPS spectra was measured to give a direct estimate of $\Delta\phi$ as a function of benzenethiol exposure. Fig. 9 illustrates the decrease in work function observed with increasing benzenethiol exposure. At 1.0 pML, benzenethiolate induces a $\Delta\phi$ of 0.60 $\pm$ 0.02 eV, similar to the reported values of 0.74 and 0.60 eV following benzenethiol and 1,2-benzenedithiol, respectively, adsorption on Cu(110) [14]. Measurement of $\Delta\phi$ is an accurate method of determining surface coverages and has been used to define benzenethiolate coverages for ARUPS results presented in this article.

The amount of charge transfer induced by Au-benzenethiolate bond formation can be estimated using the Helmholz equation which relates $\Delta\phi$ to the dipole moment of an adsorbate and its image charge [53]:

$$\Delta V = \Delta\phi/e = n\mu/\varepsilon_o$$

where ΔV is the change in surface potential (0.6 V), n is the adsorbate surface density (3.3×10^{18} sulphur atoms m^{-2}, saturation coverage at 300 K determined by XPS), ε_o is the permittivity of free space (8.854×10^{-12} CV^{-1} m^{-1}), e is the charge on an electron (1.6×10^{-19} C) and μ is the dipole moment per adsorbate. Calculation yields a value of 1.6×10^{-30} C m. Comparison of the $\Delta\phi$ and dipole moment for benzenethiol adsorption on Au(111) with similar systems may provide insight into the bonding geometry determined in this study.

In considering benzenethiol adsorption in a flat-lying geometry on a metal surface, it must be emphasised that the sulphur atom and the π-orbitals of the phenyl ring may compete for bonding with the substrate such that both interactions contribute to the observed $\Delta\phi$. The general trend in the $\Delta\phi$ curve for benzenethiol adsorption on Au(111) is reminiscent of benzene adsorption on transition metal surfaces in which a large decrease in work function is observed which is generally linear as a function of exposure [54]. In contrast, adsorption of atomic sulphur tends to increase the work function of metal surfaces [55]. It is interesting to note that benzene only physisorbs on Au(111), precluding direct charge transfer between the thiolate phenyl ring and the metal surface. Hence, a $\Delta\phi$ for the phenyl ring alone must be due to polarisation effects due to the surface electrostatic field on the benzene-like π-cloud along with other changes in electrostatic potential experienced by photoemitted electrons in passing

through the phenylthiolate monolayer. It is likely that benzene adsorption (even in the case of physisorption) will perturb the electrostatic 'double layer' at the Au(111) surface. This is confirmed by a large work function decrease ($\Delta\phi$ = -0.7 eV) reported for weakly bound benzene on Ag(111) [54]. Unfortunately, no measurement of the $\Delta\phi$ for benzene physisorption on Au single crystal surfaces is available. Thus, it is very difficult to disentangle the effect on $\Delta\phi$ due to charge transfer between the chemisorbed sulphur atom at the Au(111) surface and the effect of the flat-lying phenyl ring. However, it would appear that the phenyl ring has the dominant effect due to the similarity in the form of the $\Delta\phi$-exposure curve (Fig. 9) and magnitude of the reduction in ϕ to that of benzene adsorption on metal surfaces. The fact that sulphur does not dominate may be gleaned from the apparent direction of the net charge transfer predicted based on a simple double layer model, i.e., the ϕ decrease indicates charge transfer (or polarisation) from the adsorbate to the metal.

The linear decrease in $\Delta\phi$ which implies a constant sticking probability reveals two important aspects of the adsorption mechanism of benzenethiol on Au(111). Firstly, the absence of a discontinuity in the $\Delta\phi$-exposure curve, which should occur in the case of a molecular reorientation from a flat-lying to upright adsorbate geometry, confirms that no coverage dependent reorientation occurs in this system, in agreement with HREELS and ARUPS results. That flat-lying and upright adsorbates have differing effects on the surface potential may be illustrated by comparison of $\Delta\phi$ data for benzenethiol adsorbed on Au(111) (where a saturation coverage of 0.23 monolayers leads to a $\Delta\phi$ of 0.6 eV) with benzenethiol adsorbed on Cu(111), where the thiolate intermediate assumes an upright orientation [17]. A much higher thiolate saturation coverage of 0.63 monolayers (at 300 K) on Cu(111) leads to a $\Delta\phi$ of only 1.0 eV, i.e., a much smaller change in the surface potential per molecule. Hence, the net charge reorganisation in terms of dipole moment per adsorbate is 7.9×10^{-31} C m for benzenethiol on Cu(111), indicating that the charge transfer between the molecule and the surface is indeed different than in the case of Au(111).

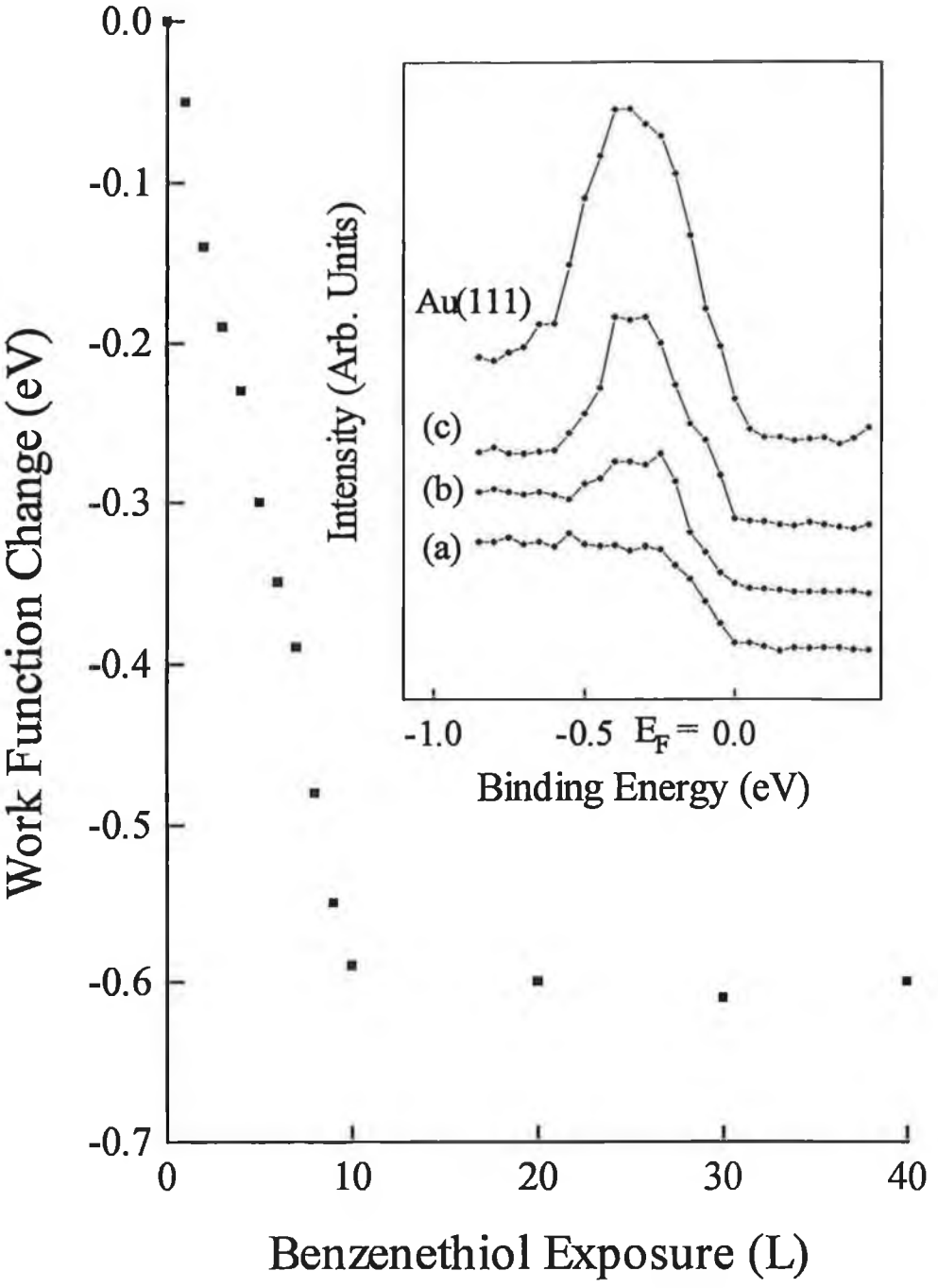

Figure 9 The work function change upon exposure to benzenethiol measured from the full width of a normal emission ARUPS spectrum. Inset, the Au(111) Shockley surface state and its attenuation following adsorption of 0.15, 0.6 and 1.0 pML of benzenethiol.

Secondly, the absence of a change in the slope of the $\Delta\phi$ curve with increasing exposure may be attributed to island formation of benzenethiol on Au(111) which is predicted to lead to a simple linear dependence of $\Delta\phi$ on coverage [56,57]. This can be described in terms of a molecule impinging on a two-dimsensional benzenethiolate island where it is trapped (physisorbed) in a precursor state from which it may diffuse to an empty substrate site on which it chemisorbs. Precursor-mediated adsorption and island formation at low coverage has previously been reported for *n*-alkanethiol adsorption from the gas phase on Au(111) [5]. We postulate that benzenethiol adsorption on Au(111) also proceeds via islanding, indicative of net attractive lateral adsorbate-adsorbate interactions.

In support of $\Delta\phi$ data, the gradual decrease in the Shockley SS observed as a function of benzenethiol exposure favours the formation of two-dimensional islands at low coverage. The inset in Fig. 9 shows the attenuation of SS upon adsorption of 0.15, 0.6 and 1.0 pML of benzenethiol. Even at a relatively high coverage of 0.6 pML, a remnant of the SS is observed. A two-dimensional dispersed phase, with adsorbates distributed homogeneously over the surface (due to repulsive adsorbate-adsorbate lateral interactions) would be expected to lead to a much more rapid attenuation of the Shockley SS. In contrast, attractive adsorbate-adsorbate interactions promote two-dimensional islanding (due to the stabilising nature of short range attractive forces with a high local coverage) allowing the survival of the SS in adsorbate free surface regions.

Finally, the thermal stability of chemisorbed benzenethiol was investigated by examining normal emission ARUPS spectra collected from monolayer and sub-monolayer coverages. It can be seen in Fig. 10 that as a sub-monolayer film is heated from 300 to 700 K, the adsorbate bands are gradually attenuated coincident with the reemergence of the Au *d*-band structure characteristic of clean Au(111) and the Shockley surface state. Similar behaviour was observed in the case of a monolayer saturation coverage. This suggests that, in contrast to behaviour on more reactive metals, the benzenethiolate intermediate desorbs intact without significant decomposition [15,21-23,26]. A more in-depth description of benzenethiol desorption on Au(111) will be presented elsewhere [33].

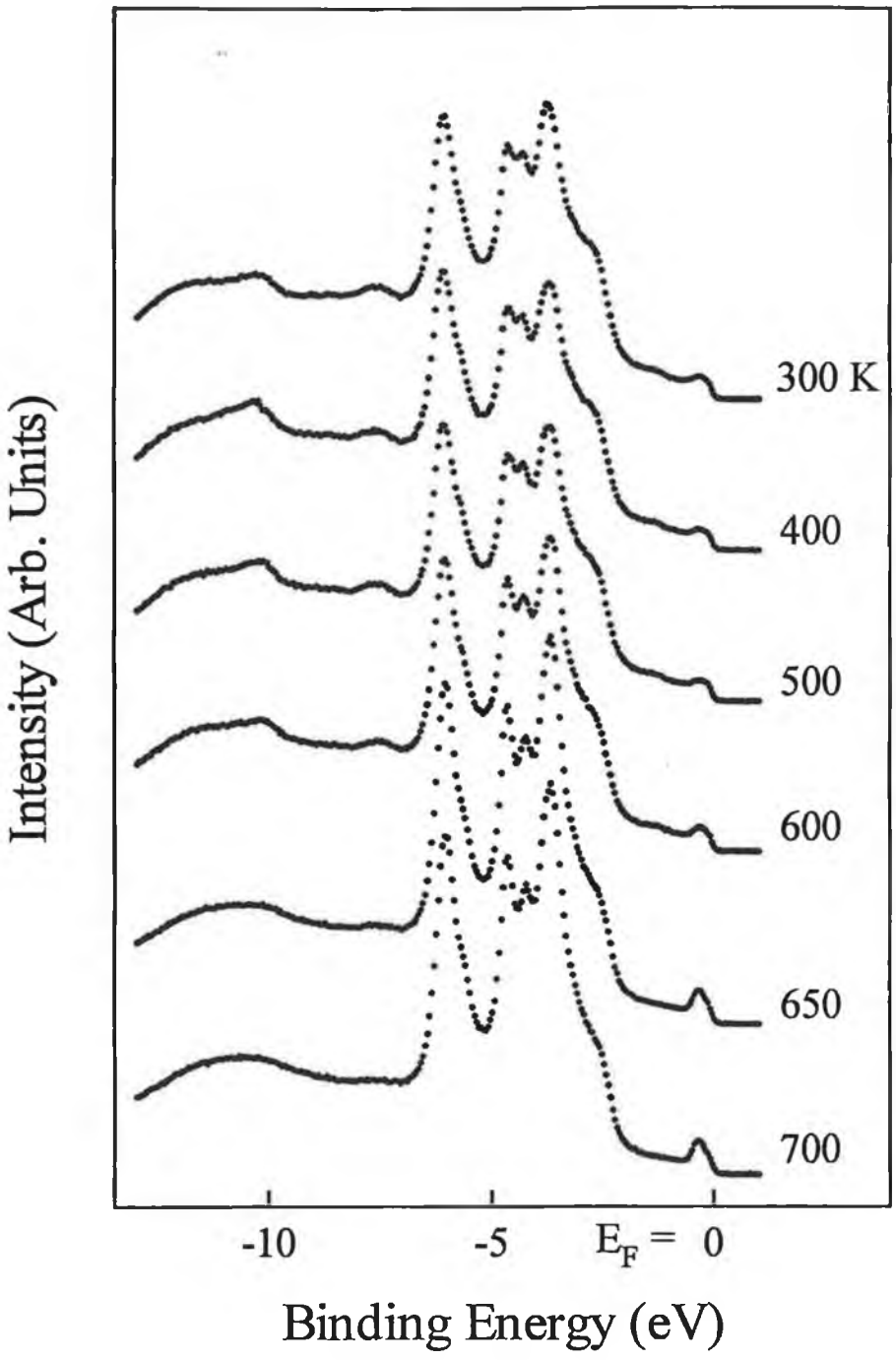

Figure 10 Normal emission UPS spectra as a function of annealing temperature of sub-monolayer benzenethiol adsorbed on Au(111) at 300 K ($\psi_i = 45°$, $h\nu = 21.2$ eV).

4. Discussion

Adsorption to saturation on all metal surfaces studied to date, with the exception of Au, results in a benzenethiolate intermediate assuming a largely upright geometry with a small inclination (~ 20°) of the ring away from the surface normal [14-33]. A flat-lying geometry has been observed for benzenethiol adsorption on Cu(110) and Rh(111) at low exposures [14,15]. Hence, the flat-lying geometry of the phenyl ring relative to the Au(111) surface at saturation coverage and the absence of a reorientation transition to a more upright densely packed monolayer is the most surprising finding within this study.

In general, benzene adsorbs on the late transition metal surfaces with the plane of the ring parallel to the surface, bonding to the substrate predominantly through the π-orbitals [41,43]. Hence, it is understandable that, at low benzenethiolate coverages, a flat-lying geometry occurs as it facilitates bonding between the phenyl ring π-system and the metal surface (although the energy gain due to interaction of the π-system with Au(111) is small). A phase transition to an upright geometry may be expected at higher coverage in order to maximise sulphur-metal interactions [14,15]. It appears that a lower heat of adsorption of benzenethiolate on Au(111) compared with other metal surfaces may result in a preference for a flat-lying monolayer. It is possible that a flat to upright phase transition with increasing surface coverage, resulting in the loss of the interaction of the aromatic ring with the metal combined with surface crowding effects in terms of ring-ring interactions and/or repulsion between neighbouring sulphur atoms, is unfavourable at 300 K. Nevertheless, liquid phase adsorption of benzenethiol on Au(111) does lead to formation of an upright thiolate monolayer which is stable at 300 K in UHV, apparently ruling out destabilisation of an upright thiolate to an extent that rapid thermal desorption occurs at 300 K [31]. It appears more likely that it is the larger flux at the Au(111) surface for liquid phase film assembly that drives the flat-lying to upright transition.

In agreement with the previous adsorption behaviour of *n*-alkanethiols on Au(111), an adsorption mechanism involving a weakly bound molecular precursor state and island formation at low coverage have been found for benzenethiol uptake on Au(111). This is perhaps not surprising as benzenethiol is a liquid at room temperature

implying relatively strong thiol-thiol molecular interactions, suggesting that the molecules arriving above two-dimensional thiolate islands may be trapped into a physisorbed state with a lifetime which is relatively long at 300 K compared to the surface diffusional jump period. Thus, trapped precursor molecules have sufficient time to diffuse to vacant Au sites, leading to a coverage independent sticking probability.

In contrast with *n*-alkanethiols, the inability of benzenethiol adsorption to lift ($\sqrt{3}\times22$) surface reconstruction even upon prolonged exposure (>100 L) is unusual given that chemisorption of atomic or molecular species is generally thermodynamically more favourable on a (1×1) bulk truncated phase than on the more densely packed reconstructed surface. Interestingly, benzenethiol adsorption from the liquid phase on Au(111) to a saturation coverage of 6.3×10^{14} sulphur atoms cm^{-2} leads to lifting of the surface reconstruction [31]. It appears that the considerably higher thiol fluxes achieved in solution, giving rise to more densely packed monolayers, may be required to lift the reconstruction and form an upright bonding configuration. The flat-lying orientation adopted by benzenethiol on Au(111) following gas phase adsorption, and hence the low saturation sulphur coverage of 3.3×10^{14} sulphur atoms cm^{-2}, fails to substitute for the missing neighbours at the surface leaving the Au atoms coordinately unsaturated. Hence, the differences in the heats of adsorption of benzenethiol between reconstructed and unreconstructed surfaces may not be large enough to compensate for the loss in surface energy due to lifting the reconstruction.

5. Conclusions

The absence of a S-H stretching vibration in HREELS from benzenethiol adsorbed to sub-monolayer and saturation coverages on Au(111), identification of vibrations associated with aromatic ring, XPS lineshapes and binding energies from carbon (1s) and sulphur (2p) core levels and the presence of benzene-like UPS bands confirm the formation of a benzenethiolate intermediate.

The intensity of the out-of-plane C-H deformation relative to the in-plane C-H stretch in HREELS spectra and comparison of UPS band intensities as a function of emission and photon incident angle with previous studies of benzenethiol and benzene adsorption on metal surfaces suggest that the phenyl ring is aligned parallel to the surface and the orientation is coverage independent. A 10±10° tilt angle of the phenyl ring relative to the Au(111) surface plane has been estimated from polar angle dependence of the variation of the carbon (1s) to sulphur (2p) XPS intensities.

A precursor-mediated adsorption mechanism involving the formation of two-dimensional benzenethiolate islands is proposed based on the linear decrease in the work function and the gradual attenuation of the Shockley surface state with increasing benzenethiol exposure to a saturation coverage of 3.3×10^{14} sulphur atoms cm^{-2} at 300 K.

6. References

[1] A. Ulman, An Introduction to Ultrathin Organic Films: from Langmuir-Blodgett to Self-Assembly, Academic, New York, 1991 and references therein.

[2] D.R. Jung, D.E. King and A.W. Czanderna, Appl. Surf. Sci., **70/71** (1993) 127.

[3] P.E. Laibinis and G.M. Whitesides, J. Am. Chem. Soc., **114** (1992) 9022.

[4] B.C. Weigand and C.M. Friend, Chem. Rev., **92** (1992) 491.

[5] L.H. Dubois, B.R. Zegarski and R.G. Nuzzo, J. Chem. Phys., **98** (1993) 678.

[6] S.E. Anderson and G.L. Nyberg, J. Electron Spectrosc. Rel. Phen., **52** (1990) 735.

[7] H. Rieley, N.J. Price, R.G. White, R.I.R. Blyth and A.W. Robinson, Surf. Sci., **331-333** (1995) 189.

[8] A. Fernandez, J.P. Espinos, A.R. Gonzalez-Elipe, M. Kerkar, P.B.J. Thompson, J. Ludecke, G. Scragg, A.V. de Carvalho, D.P. Woodruff, M. Fernandez-Garcia and J.C. Conesa, J. Phys.: Condens. Matter, **7** (1995) 7781.

[9] M. Bruckner, B. Heinz and H. Morgner, Surf. Sci., **319** (1994) 370.

[10] B. Heinz and H. Morgner, Surf. Sci., **372** (1997) 100.

[11] S. Lehwald, H. Ibach and J.E. Demuth, Surf. Sci., **78** (1978) 577.

[12] M. Neumann, J.U. Mack, E. Bertel and F.P. Netzer, Surf. Sci., **155** (1985) 629.

[13] S. Haq and D.A. King, J. Phys. Chem., **100** (1996) 16957.

[14] W. Shen, G.L. Nyberg and J. Liesegang, Surf. Sci., **298** (1993) 143.

[15] C.W.J. Bol, C.M. Friend and X. Xu, Langmuir, **12** (1996) 6083.

[16] P.A. Agron, T.A. Carlson, W.B. Dress and G.L. Nyberg, J. Electron Spectrosc. Relat. Phenom., **42** (1987) 313.

[17] P.A. Argon and T.A. Carlson, J. Vac. Sci. Technol., **20** (1982) 815.

[18] S.E. Anderson and G.L. Nyberg, Appl. Surf. Sci., **22/23** (1985) 325.

[19] D.M. Jaffey and R.J. Madix, J. Am. Chem. Soc., **116** (1994) 3020.

[20] Y. Takata, T. Yokoyama, S. Yagi, N. Happo, H. Sato, K. Seki, T. Ohta, Y. Kitajima and H. Kuroda, Surf. Sci., **259** (1991) 266.

[21] D.R. Huntley, J. Phys. Chem., **96** (1992) 4550.

[22] T.S. Rufael, D.R. Huntley, D.R. Mullins and J.L. Gland, J. Phys. Chem., **98** (1994) 13022.

[23] S.M. Kane, T.S. Rufael, J.L. Gland, D.R. Huntley and D.A. Fischer, J. Phys. Chem. B, **101** (1997) 8486.

[24] S.M. Kane, D.R. Huntley and J.L. Gland, J. Am. Chem. Soc., **118** (1996) 3781.

[25] J. Stohr and D.A. Outka, Phys. Rev. B, **36** (1987) 7891.

[26] J.T. Roberts and C.M. Friend, J. Chem. Phys., **88** (1988) 7172.

[27] M.K. Weldon, M.E. Napier, B.C. Wiegand, C.M. Friend and P. Uvdal, J. Am. Chem. Soc., **116** (1994) 8328.

[28] D.A. Chen, C.M. Friend and H. Xu, Surf. Sci., **395** (1998) L221.

[29] J.Y. Gui, D.A. Stern, D.G. Frank, F. Lu, D.C. Zapien and A.T. Hubbard, Langmuir, 7 (1991) 955.

[30] D.A. Stern, E. Wellner, G.N. Salaita, L. Laguren-Davidson, F. Lu, N. Batina, D.G. Frank, D.C. Zapien, N. Walton and A.T. Hubbard, J. Am. Chem. Soc., **110** (1988) 4885.

[31] C.M. Whelan, M.R. Smyth and C.J. Barnes, Langmuir, accepted.

[32] C.J. Barnes, C.M. Whelan, M.R. Smyth, C. Gregoir and J.J. Pireaux, in preparation.

[33] C.M. Whelan and C.J. Barnes, in preparation.

[34] M.A. Van Hove, R.J. Koestner, P.C. Stair, J.P. Biberian, L.L. Kesmodel, I. Bartos and G.A. Somorjai, Surf. Sci., **103** (1981) 189.

[35] J.F. Moulder, W.F. Stickle, P.E. Sobol and K.D. Bomben, Handbook of Photoelectron Spectroscopy, Perkin-Elmer Corporation, Physical Electronics Division, Eden Prairie, MN 55344, 1992.

[36] G. Socrates, Infrared Characteristic Group Frequencies, John Wiley & Sons, Great Britian, 1980.

[37] J.J. Pireaux, M. Liehr, P.A. Thiry, J.P. Delrue and R. Caudano, Surf. Sci., **141** (1984) 221.

[38] P.A. Thiry, Ph.D. thesis, FUNDP, Namur, 1984.

[39] D. Law and G. Beamson, private communication.

[40] H. Ibach and D.L. Mills, Electron Energy Loss Spectroscopy and Surface Vibrations, Academic, London, 1982.

[41] F.P. Netzer, Langmuir, 7 (1991) 2544.

[42] K. Weiss, S. Gebert, M. Wuhn, H. Wadephol and Ch. Woll, J. Vac. Sci. Technol. A, **16** (1998) 1017.

[43] H.-P. Steinruck, J. Phys.: Condens. Matter 8 (1996) 6465.

[44] F. Carnovale, M.H. Kibel, G.L. Nyberg and J.B. Peel, J. Electron Spectrosc. Relat. Phenom., **25** (1982) 171.

[45] P. Heimann, H. Neddermeyer and H.F. Roloff, J. Phys. C: Solid State Phys., **10** (1977) L17.

[46] R. Paniago, R. Matzdorf, G. Meister, A. Goldmann, J. Braun and G. Borstel, Surf. Sci., **347** (1996) 46.

[47] A. Goldmann and R. Matzdorf in: Surface Science, Principles and Current Applications, Ed. R.J. MacDonald, E.C. Taglauer and K.R. Wandelt, Springer, New York, 1996.

[48] J.J. Yeh and I. Lindau, Atomic Data Nucl. Data Tables, **32** (1985) 1.

[49] R. Magnee, Z. Mekhalif, C. Doneux, A.-S. Duwez, C. Gregoire, J. Riga, J. Delhalle and J.J. Pireaux, J. Electron Spectrosc. Relat. Phenom., **88-91** (1998) 855.

[50] C.M. Whelan, M.R. Smyth and C.J. Barnes, unpublished data.

[51] L.C. Pauling, The nature of the Chemical Bond, 3rd ed., Cornell University Press, Ithaca, New York, 1960.

[52] P.E. Laibinis, C.D. Bain and G.M. Whitesides, J. Phys. Chem., **95** (1991) 7017.

[53] G. Attard and C. Barnes, Surfaces, Oxford University Press, New York, 1998.

[54] X.-Z. Zhou, M.E. Castro and J.M. White, Surf. Sci., **238** (1990) 215.

[55] R.J. Madix in: The Chemical Physics of Solid Surfaces and Heterogeneous Catslysis, Vol. 4, Eds. D.A. King and D.P. Woodruff, Elsevier, New York, 1982.

[56] H.J. Borg, J.F.C.-J. Reijerse, R.A. Van Santen and J.W. Niemantsverdriet, J. Chem. Phys., **101** (1994) 10052.

[57] J.N. Russell, Jr., S.M. Gates and J.T. Yates, Jr., J. Chem. Phys., **85** (1986) 6792.

Chapter 6

A HREELS Study of Benzenethiol Adsorption on Au(111) and Au(322)

Abstract

Adsorption of benzenethiol (C_6H_5SH) on a Au(111)-($\sqrt{3}\times22$) reconstructed surface at 300 K leads to formation of molecular long range disordered overlayers without lifting of the surface reconstruction. Absence of the S-H stretching vibration, both in and out of specular scattering geometry, along with identification of modes typical of aromatic benzene-like systems indicates formation of a thiolate intermediate at both saturation and sub-monolayer coverage. Comparison of HREELS band intensities as a function of coverage in the specular direction, where dipole selection rules dominate, indicate that no major coverage dependent reorientation occurs on Au(111). Consideration of relative band intensities, use of dipole selection rules and comparison with previous studies of benzene and benzenethiol adsorption on transition metal surfaces indicates a flat-lying bonding geometry at both monolayer and sub-monolayer coverages.

In contrast, adsorption on Au(322), a surface consisting of mono-atomic (100) steps separating (111) micro-terraces five unit cells wide, leads to formation of an ordered monolayer. The adsorbed intermediate on Au(322) is benzenethiolate at both low and high coverage. An orientational transition occurs as a function of coverage. At low coverages the molecule is strongly inclined with respect to the (111) micro-terraces while at higher coverages adsorbates adopt a more flat-lying geometry. This unusual behaviour appears to be due to coverage dependent occupation of step and terrace sites with a strongly inclined species formed at step sites, preferentially occupied at low coverage, and a second flat-lying state becoming occupied within the monolayer. This study shows clear evidence for step-induced ordering of the thiolate intermediate and the ability of steps to promote a molecular reorientation.

1. Introduction

Self-assembled monolayers (SAMs) are technologically important in a number of fields including corrosion passivation, modification of electrode surfaces and surface wettability [1-3]. In order to gain a fundamental understanding of the role played by SAMs at a molecular level, a range of surface sensitive spectroscopies have been applied to model systems consisting of single crystal surfaces in which the structure of the substrate is well defined. A system which has received much attention is the adsorption of *n*-alkanethiols on Au surfaces. In general, densely packed self-organised molecular layers are formed with the molecule adsorbing via a strong sulphur-Au chemisorption bond involving S-H bond cleavage forming a thiolate intermediate with the polymethylene chain tilted (~30°) with respect to the surface normal [4,5]. A detailed picture of a number of substrate-absorbate systems has emerged and differences between SAMs formed by gas phase adsorption onto ultra-high-vacuum (UHV) prepared single crystal surfaces and by liquid phase assembly onto UHV or flame-annealed substrates have been investigated [5-7].

In contrast, little is known about a separate class of assembled organic monolayers, namely aromatic systems. The simplest aromatic thiol, benzenethiol, potentially offers a SAM system with differing properties to *n*-alkanethiols and is of interest with respect to basic aspects of the surface bonding. With few exceptions, benzene chemisorbs intact at 300 K or below on late transition metal surfaces with the molecular plane parallel to the close packed (111) surfaces [8,9]. Similar to organometallic complexes, bonding to the surface occurs predominantly through the delocalised π-electrons of the aromatic ring system. In the case of benzenethiol adsorption, the sulphur atom and the π-orbitals of the phenyl ring must both be considered as potential participants in bonding to the substrate. Competitive bonding between the sulphur and the phenyl ring π-electrons, may result in an adsorption geometry in which the molecule is tilted or even perpendicular as opposed to flat-lying with respect to the surface plane. In particular, at high adsorbate coverages surface when crowding effects become more important, the conformation adopted may be influenced by steric interactions between the aromatic rings [10,11]. Such interactions are generally minimised by tilted bonding geometries, which would leave the phenyl

ring essentially unperturbed by sulphur atom chemisorption to the substrate and make the C-S and C-H bonds less accessible for activation by the surface.

This paper forms part of a comparative study of the molecular nature of layers formed by liquid and gas phase dosing techniques for this simple cyclic aromatic molecule [12,13]. The technique of high resolution electron energy loss spectroscopy (HREELS) has been used to examine the coverage dependence of the interaction of benzenethiol, adsorbed by standard UHV dosing, on Au(111) and on an atomically stepped Au(322) surface. This study serves to address the effect of atomic steps on SAM formation. The Au(322) surface consists of a periodic array of atomic steps of local (100) geometry separated by micro-terraces of (111) orientation and five unit cells wide. As step and terrace sites will have different heats of adsorption, the adsorbate may exhibit a preference for a particular adsorption site with the possibility of a mixture of molecular orientations being present at higher coverages. Atomic steps may serve as centers to induce or disrupt ordering and to control molecular orientation within the monolayer. An understanding of the role played by controlled defect density would thus be of considerable value in the formation of molecular monolayers.

2. Experimental

The experiments were carried out in an UHV chamber with a base pressure in the low 10^{-10} Torr region. The chamber consisted of a spectrometer vessel containing a HREELS 180° hemispherical monochromator and analyser ensemble described in detail elsewhere [14]. The spectrometer vessel also contained an Omicron 4-grid reverse view low energy electron diffraction (LEED) optics to allow the clean surface crystallography and ordering of the adsorbate to be monitored. The LEED facility also allowed the azimuthal alignment of the sample with respect to the HREELS beam. The spectrometer vessel was linked to a preparation chamber equipped with argon ion sputtering and annealing facilities for sample cleaning. All benzenethiol dosing was performed in the preparation chamber to prevent the spectrometer vessel from contamination by gas phase benzenethiol.

The HREELS spectra were recorded at 5.0 and 1.5 eV both in and out of specular scattering geometry with the specular direction being defined by locating the maximum in the elastic peak. This process is straightforward for the atomically flat (111) surface but presents problems for the stepped surface in which LEED beams may be split by the step periodicity (see results and discussion section). The resolution was defined by the full-width-at-half-maximum (FWHM) of the elastic peak and varied between 5 and 10 meV for the studies reported here.

The Au(111) and Au(322) single crystals (6 × 8 × 1.5 mm) oriented to within 0.5° of the quoted planes (Metal Crystals and Oxides) were attached to a molybdenum backing plate by spot welding tantalum wires passed through 0.25 mm spark eroded holes, drilled through the sides of the sample, parallel to the polished front face. The samples were cleaned *in situ* by cycles of argon ion bombardment (3 kV) and annealing to 600-800 K. As the samples had previously been depleted of bulk contaminants, *in situ* cleaning was facile, requiring only a few bombard/anneal cycles. After cleaning, the (111) surface exhibited the sharp low background ($\sqrt{3}\times22$) reconstruction typical of Au(111) [15]. LEED from the (322) sample revealed a sharp low background pattern with energy dependent spot splitting characteristic the step-terrace structure predicted for bulk truncation with mono-atomic steps separating (111) terraces of five unit cells width [16]. HREELS is extremely sensitive to low levels of hydrocarbon

contamination and is also an excellent probe of the existence of silicon oxides in the surface region [17]. No contaminants above the HREELS detection limits were observed directly after bombard/anneal cycles.

Benzenethiol (99.9% + purity, Aldrich Chemicals) was purified by a series of freeze-pump-thaw cycles. All metal gas dosing lines were purged with benzenethiol prior to dosing experiments to prevent wall-catalysed decomposition. Benzenethiol was adsorbed by exposure at 300 K using a high precision leak valve and an uncalibrated Bayard-Alpert ionisation gauge to quote dose levels. Monolayer coverages were obtained by overdosing samples with several hundred Langmuirs. Previous thermal desorption spectroscopy (TDS) studies have indicated that benzenethiol has a high sticking probability [16]. We will refer to such coverages as room temperature physical monolayer (1 pML) coverage for convenience [18]. Low coverages were formed by careful sub-Langmuir dosing.

Sub-monolayer coverages were quoted as a fraction of a physical monolayer (where 1 pML refers to the maximum coverage obtained at 300 K) coverage by integration of the intensity of the in-plane C-H stretching band (>3000 cm^{-1}) and comparison to the monolayer equivalent after normalising to the elastic peak. In the case of the (111) surface, this procedure should be reasonably accurate as orientational changes as a function of coverage are minimal and the layer remains disordered throughout the coverage regime. On the Au(322) surface, adsorbate orientational and ordering changes with coverage makes an accurate coverage determination difficult. The effect of orientational changes may be minimised by use of off-specular spectra where impact scattering is dominant. However, we accept that the relative coverage of benzenethiol sub-monolayers may be subject to uncertainty.

3. Results

Adsorption of benzenethiol on the reconstructed Au (111)-($\sqrt{3}\times22$) surface led to an increase in the diffuse background with increasing surface coverage indicative of formation of an adlayer with the absence of long range order. The ($\sqrt{3}\times22$) reconstruction persisted even upon prolonged dosing (>100 Langmuirs) at 300 K.

HREELS spectra taken at a primary beam energy of 5.0 eV from a benzenethiol monolayer and sub-monolayer coverage in both specular ($\theta_i = \theta_r = 70°$) and off-specular ($\theta_i = 70°$, $\theta_r = 50°$) scattering geometries are shown in Figs. 1 and 2. The sub-monolayer coverage was estimated to be 0.25 pML. These coverages correspond to 0.06 and 0.23 monolayers of sulphur, respectively [13]. Figs. 1 and 2 contain the vibrational bands expected from molecular benzenethiol with the exception of the S-H stretching mode (2580 cm^{-1}) [19]. The absence of this band, both in specular where dipole scattering dominates and the metal surface selection rule operates (only vibrations with a component of the dipole moment change normal to the surface may be observed) and off-specular where short range impact scattering occurs is clear evidence of the loss of the sulfhydryl hydrogen at both high and low surface coverage [20]. Spectra acquired at a primary beam energy of 1.5 eV further verified the occurrence of S-H bond scission, consistent with the formation of a phenylthiolate surface intermediate.

The main vibrational bands present are summarised in Table 1 and may be assigned with reference to several previous HREELS studies of benzenethiol adsorption on Cu(110), Rh(111), Ni(111), Ni(110), Mo(110), Co-Mo(110) phases, Ag(111) and Pt(111) [19,21-29]. The presence of a phenyl group is indicated by the presence of the intense feature at 730 cm^{-1}, which is unambiguously assigned to out-of-plane C-H deformations (γ_{C-H}) of a benzene ring. A weak energy loss observed at 460 cm^{-1} superimposed on the tailing elastic peak may be attributed to Au-SC_6H_5 stretching. Due to the possibility of aromatic ring modes in this region, and given that the C-S stretching (~700 cm^{-1}) is obscured by C-H out-of-plane bending, the 460 cm^{-1} band is not an unambiguous indicator of C-S bond integrity [19]. However, as benzene desorbs from Au(111) above 200 K, the presence of aromatic vibrational bands

indicates that extensive C-S bond cleavage does not occur following chemisorption of benzenethiol on Au(111) [9,30].

Table 1 The major HREELS band assignments for benzenethiol adsorption on Au(111) and Au(322) at saturation coverage.

Assignment[A]	C_6H_5SH (gas)[B]	C_6H_5S/Au(111)	C_6H_5S/Au(322)
		cm^{-1} (meV)	
ν(C-H)	3000-3030	3047 (378)	3064 (380)
ν(S-H)	2580		
ν(C-C)	1450-1600	1556 (193)	1540 (191)
		1443 (179)	1459 (181)
δ(C-H)/γ(C-H)		1136 (141)	1121 (139)
δ(C-H)/ ν(C-CH)	1065-1075	1016 (126)	984 (122)
γ(C-H)	740-760	730 (91)	726 (90)
γ(C-C)/ ν(Au-SC_6H_5)		460 (57)	468 (58)

[A]ν = stretch; δ = in-plane bend; γ = out-of-plane bend. [B]Shen *et al.* [19].

Two bands are of particular importance in the assignment of the molecular orientation of the thiolate on Au(111). Firstly, the highest energy loss at 3047 cm^{-1} due to the in-plane C-H stretching mode (ν_{C-H}) which has its dipole moment change upon vibration in the plane of the ring. Thus, for specular HREELS, this band will be excited for an upright or slightly tilted molecule but should have zero intensity in dipole scattering for a molecule with the plane of the ring parallel to the surface. However, even for a perfectly flat-lying molecule, the ν_{C-H} band intensity will not totally disappear even in specular geometry as the band remains impact scattering allowed. As impact scattering is more isotropic, the cross-section for this short range scattering mechanism is considerably smaller than for dipole excitation which is strongly peaked

in a cone of width less than 10° FWHM for spectra collected in the specular direction from atomically flat surfaces [31]. The majority of the impact scattering contribution in Fig. 1a may be removed by subtraction of the off-specular spectrum (Fig. 1b). In Fig. 1c, the resultant 'dipole excited spectrum' obtained by such a subtraction with no contribution from the $\nu_{C\text{-}H}$ stretch implies a flat-lying adsorption geometry with the plane of the ring parallel or close to parallel to the Au(111) surface. It should be noted that Yu *et al.* have shown that the impact scattering intensity varies with scattering angle [31]. Hence, subtraction of the impact scattering component from the specular HREELS spectrum to produce a purely dipole excited spectrum suffers from the disadvantage that the impact scattered intensity measured at an off-specular geometry will never be exactly equal to that in specular. While not exact, this procedure does serve to reduce the impact scattering contribution and thus gives a 'cleaner' specular HREELS spectrum dominated by dipole scattering. It should also be noted at this stage, that even for a flat-lying molecule some intensity in a 'dipole forbidden' mode may still be observed even after correction for the impact scattering contribution due to low frequency/high amplitude rocking modes of the aromatic ring which occur on a time scale slower than that of the HREELS excitation [32]. Thus, unless the surface is cooled to freeze these modes into their low amplitude vibrational ground state, it is difficult to make truly quantitative statements about the molecular orientation. Nevertheless, it is fair to conclude that the molecule adopts a largely flat-lying geometry on Au(111) at saturation coverage. This adsorption geometry is analogous to that found in previous studies of benzene on transition metal surfaces [8,9,33,34].

In contrast, the sharp band at 730 cm^{-1} is due to an out-of-plane C-H deformation ($\gamma_{C\text{-}H}$) with a dipole moment perpendicular to the plane of the phenyl ring. Hence, in the specular direction this band should be of maximum intensity for a flat-lying molecule and have zero intensity (excluding molecular vibration effects) when the plane of the ring is perpendicular to the Au(111) surface. Clearly, in the specular spectrum shown Fig. 1a, the $\gamma_{C\text{-}H}$ mode is the dominant band and, once impact scattering is accounted for (Fig. 1c), totally dominates the HREELS spectrum in full agreement with a largely flat-lying adsorbate.

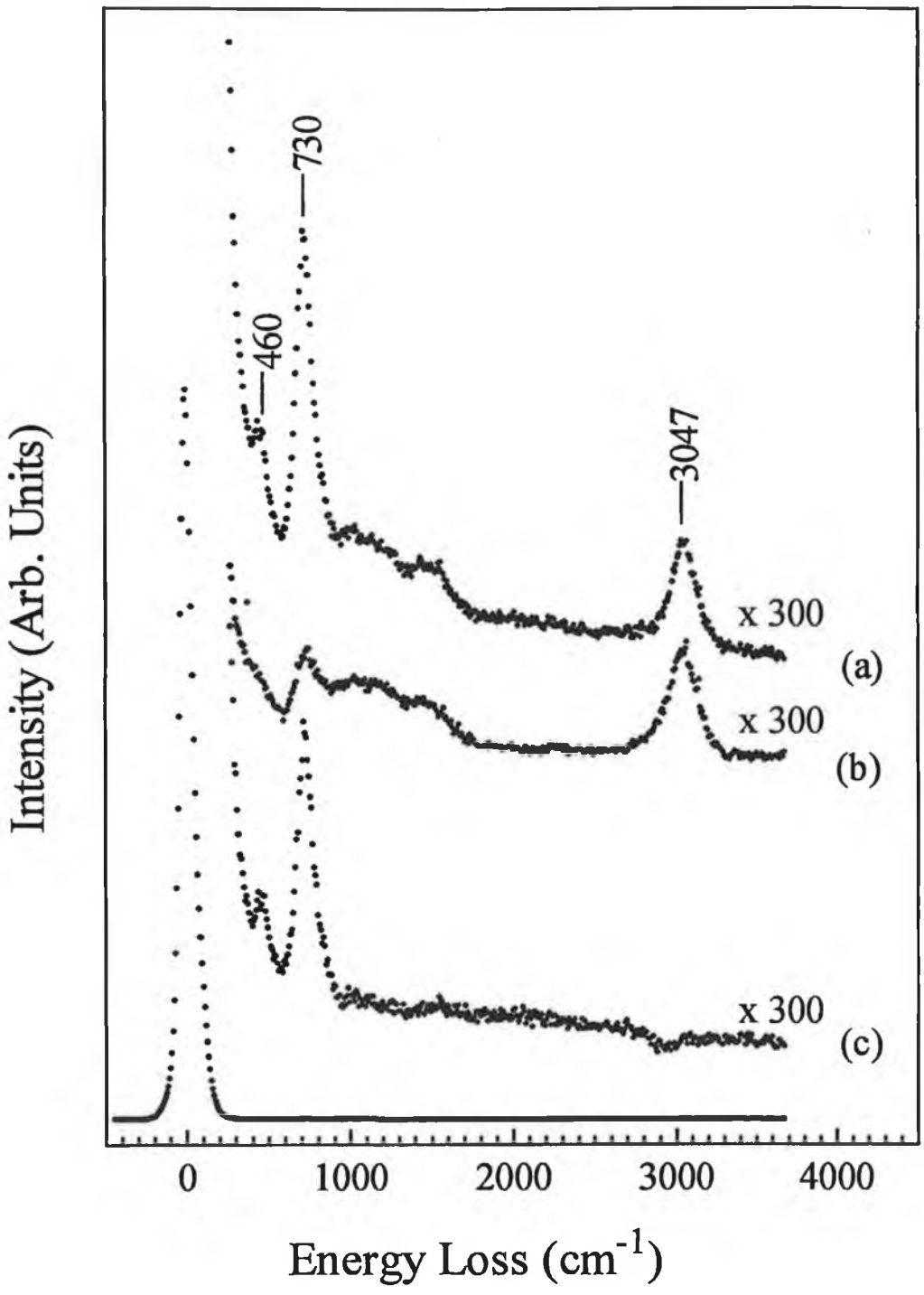

Figure 1 HREELS spectra collected at a primary beam energy of 5.0 eV from benzenethiol adsorbed on Au(111) to saturation coverage at 300 K. Spectra shown are (a) specular ($\theta_i = \theta_r = 70°$), (b) off-specular ($\theta_i = 70°$, $\theta_r = 50°$) and (c) a difference spectrum obtained by subtraction of (b) from (a).

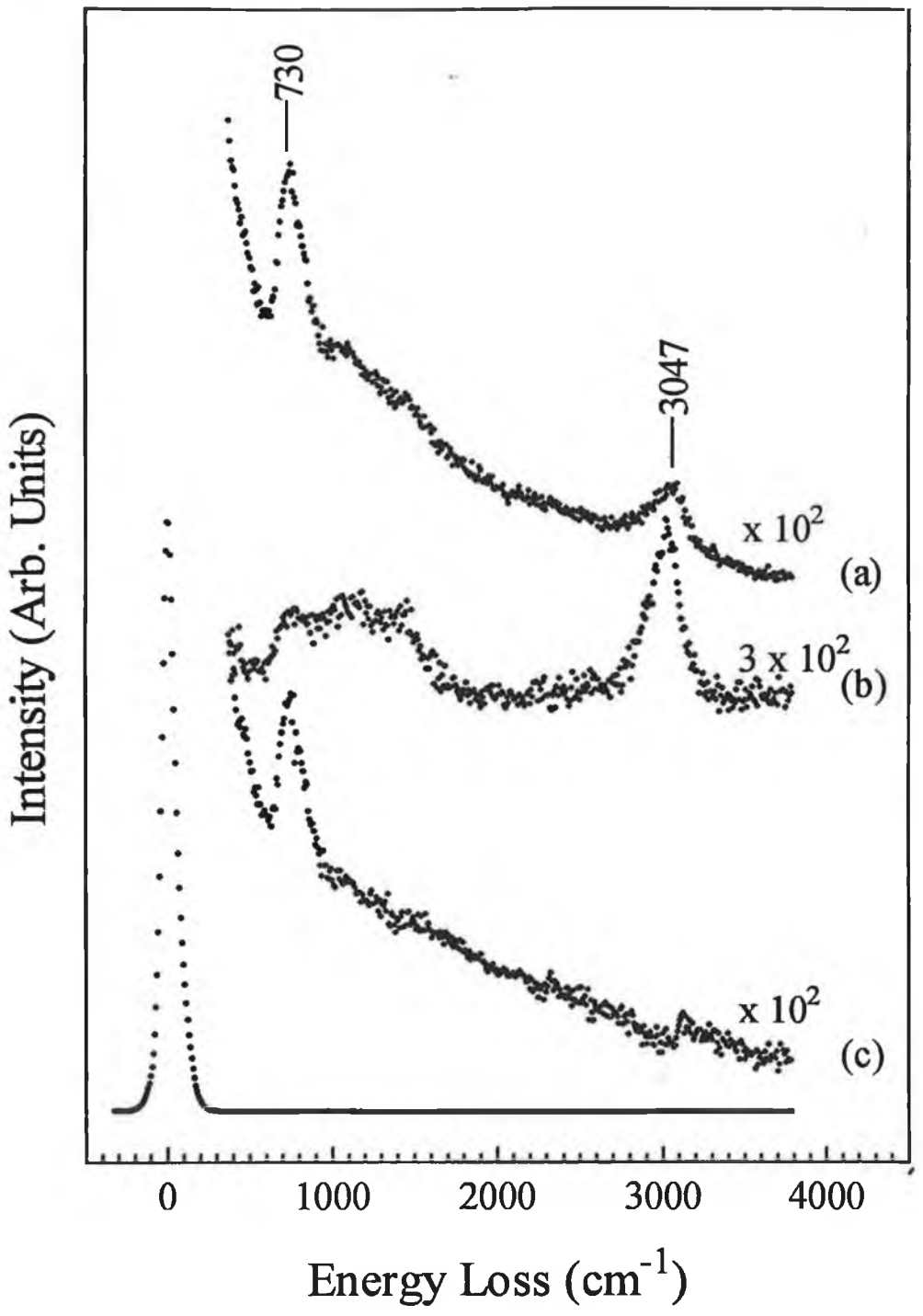

Figure 2 HREELS spectra collected at a primary beam energy of 5.0 eV from benzenethiol adsorbed on Au(111) to sub-monolayer coverage at 300 K. Spectra shown are (a) specular ($\theta_i = \theta_r = 70°$), (b) off-specular ($\theta_i = 70°$, $\theta_r = 50°$) and (c) a difference spectrum obtained by subtraction of (b) from (a).

Integration of the relative intensities of the $\gamma_{C\text{-}H}$ to $\nu_{C\text{-}H}$ bands for a low coverage of benzenethiol shown in Fig. 2 and comparison with values for the monolayer (Fig. 1) are in good agreement which may be taken as evidence that that no major coverage dependent reorientation occurs on Au(111) at 300 K. This behaviour is in direct contrast to previous coverage dependent studies of benzenethiol adsorption on Cu(110) and Rh(111) for which a coverage dependent bonding geometry has been reported with the phenyl ring parallel to the surface at low coverage and a reorientation to a more upright geometry at high coverage [19,21].

We consider the relative intensities of the $\gamma_{C\text{-}H}$ to $\nu_{C\text{-}H}$ bands in the specular scattering geometry, once the impact scattering component has been removed, to be a sensitive monitor of surface orientation. Provided data may be compared with similar values of incident energy and angle of the primary beam and the impact corrected ratio is monitored, the $\gamma_{C\text{-}H}$ to $\nu_{C\text{-}H}$ ratio should be a fingerprint of the molecular orientation. However, the strongly peaked nature of the dipole scattering requires care in sample orientation to maximise the elastic scattering and thus ensure that measurements are taken exactly in the specular direction. Small misalignments of the sample and analyser may cause large errors in quantification of the bonding geometry.

As the $\gamma_{C\text{-}H}$ to $\nu_{C\text{-}H}$ modes are vibrations of the benzene ring which should not be severely perturbed by substitution of sulphur for an aromatic hydrogen, the ratios may also be compared to previous studies of benzene on transition metal surfaces where a range of other surface sensitive techniques, such as near-edge X-ray-absorption fine-structure (NEXAFS), LEED and angle-resolved valence band electronic structure studies, provide quantitative back-up of the adsorption geometry. We have tried where-ever possible to cross-check our data with that of previous determinations, however, in many cases relevant off-specular impact excited spectra are not recorded to allow for a subtraction of the smoothly varying impact scattered contribution [25,26,33,34]. Our comparisons indicate that the $\gamma_{C\text{-}H}$ to $\nu_{C\text{-}H}$ ratio measured for benzenethiol on Au(111), at both high and low coverages, is consistent with a largely parallel orientation of the phenyl ring.

In contrast, previous studies of benzenethiol adsorption on Cu(110), Cu(111), Ni(100), Ni(110), Ni(111), Mo(110), Co-Mo(110) phases, Rh(111), Ag(111) and Pt(111) surfaces, all favour a benzenethiolate intermediate assuming an upright

geometry with a small inclination (~20°) of the ring away from the surface normal at monolayer saturation [19,21-29,35-38]. Both the lack of a coverage dependent orientational transition and the adoption of a largely flat-lying benzenethiolate monolayer on Au(111) are surprising on the basis of past work and will be discussed later.

Adsorption of benzenethiol on the Au(322) surface was very different from its atomically flat counterpart. Bulk truncation of an f.c.c. (322) surface results in a surface consisting of periodic mono-atomic steps of (100) local orientation separated by (111) micro-terraces, five unit cells in width. Spot profile analysis has shown that the LEED pattern obtained is quite consistent with the expected bulk truncation and furthermore the reconstruction of the atomically flat surface is quenched by the presence of periodic defects [16]. Adsorption of benzenethiol leads to no changes in the periodicity of the step/terrace arrangement and at low coverages simply increases the diffuse background intensity in LEED, while higher coverages led to formation of an ordered phase with diffuse extra diffraction features whose origin is fully analysed in a separate article [16]. Observation of additional diffraction features is conclusive evidence of step-induced ordering of the molecular monolayer, a clear sign that defects can induce structural ordering in the benzenethiolate SAM.

Figs. 3 and 4 show equivalent sets of HREELS data from the monolayer and sub-monolayer structures at 5.0 eV primary beam energy collected both in specular ($\theta_i = \theta_r = 70°$) and off-specular ($\theta_i = 70°$, $\theta_r = 50°$) scattering geometries. While defining specular and off-specular geometries is facile for atomically flat surfaces, a difficulty arises when addressing stepped structures as two surfaces exist, namely the macroscopic and the atomically flat micro-terraces (microscopic). A considerable difference exists in this case between these two definitions for a surface (shown schematically in Fig. 5a) with such high step density with the angle subtended by the macroscopic surface being 16.3°.

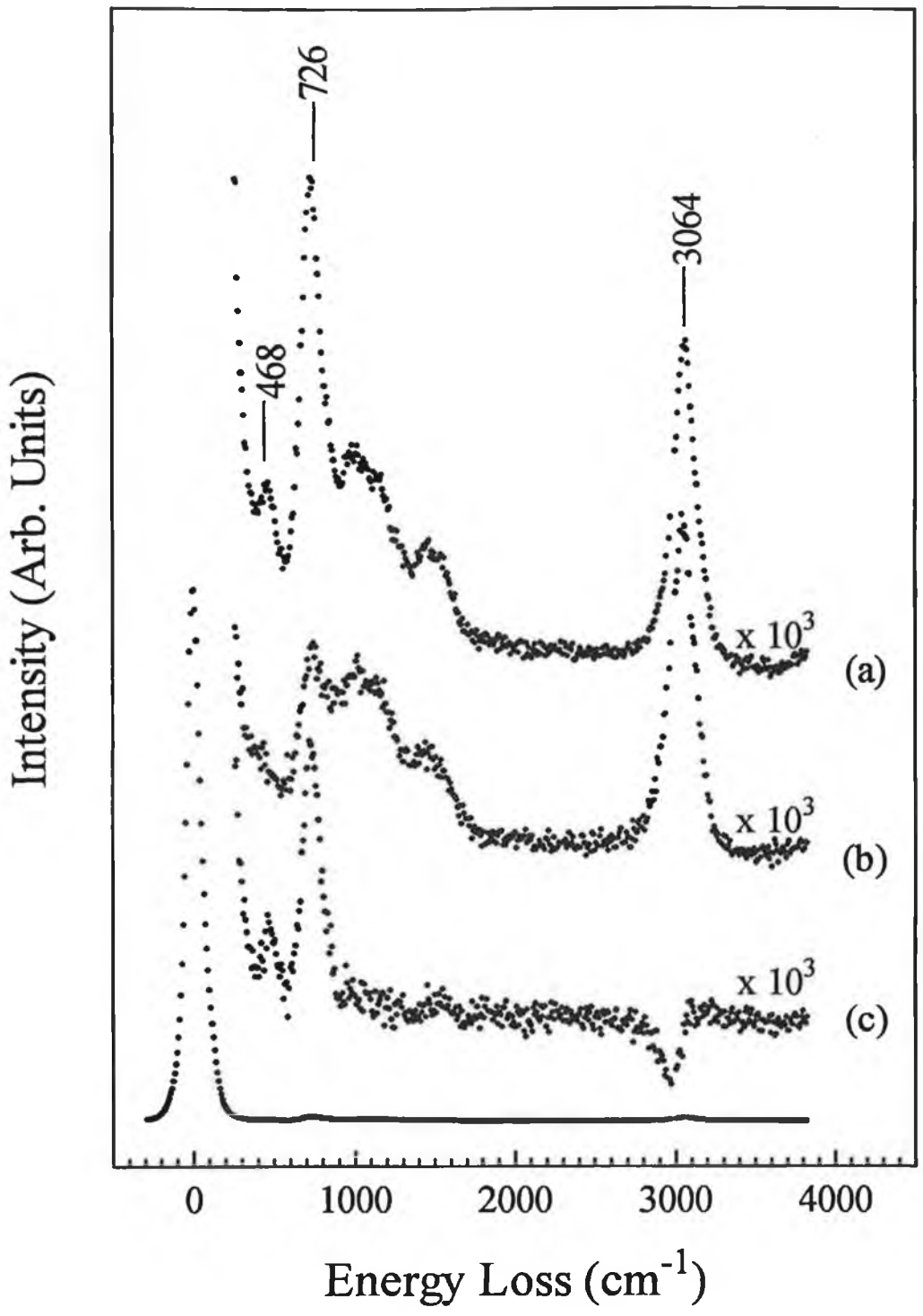

Figure 3 HREELS spectra collected at a primary beam energy of 5.0 eV from benzenethiol adsorbed on Au(322) to saturation coverage at 300 K. Spectra shown are (a) specular ($\theta_i = \theta_r = 70°$), (b) off-specular ($\theta_i = 70°$, $\theta_r = 50°$) and (c) a difference spectrum obtained by subtraction of (b) from (a).

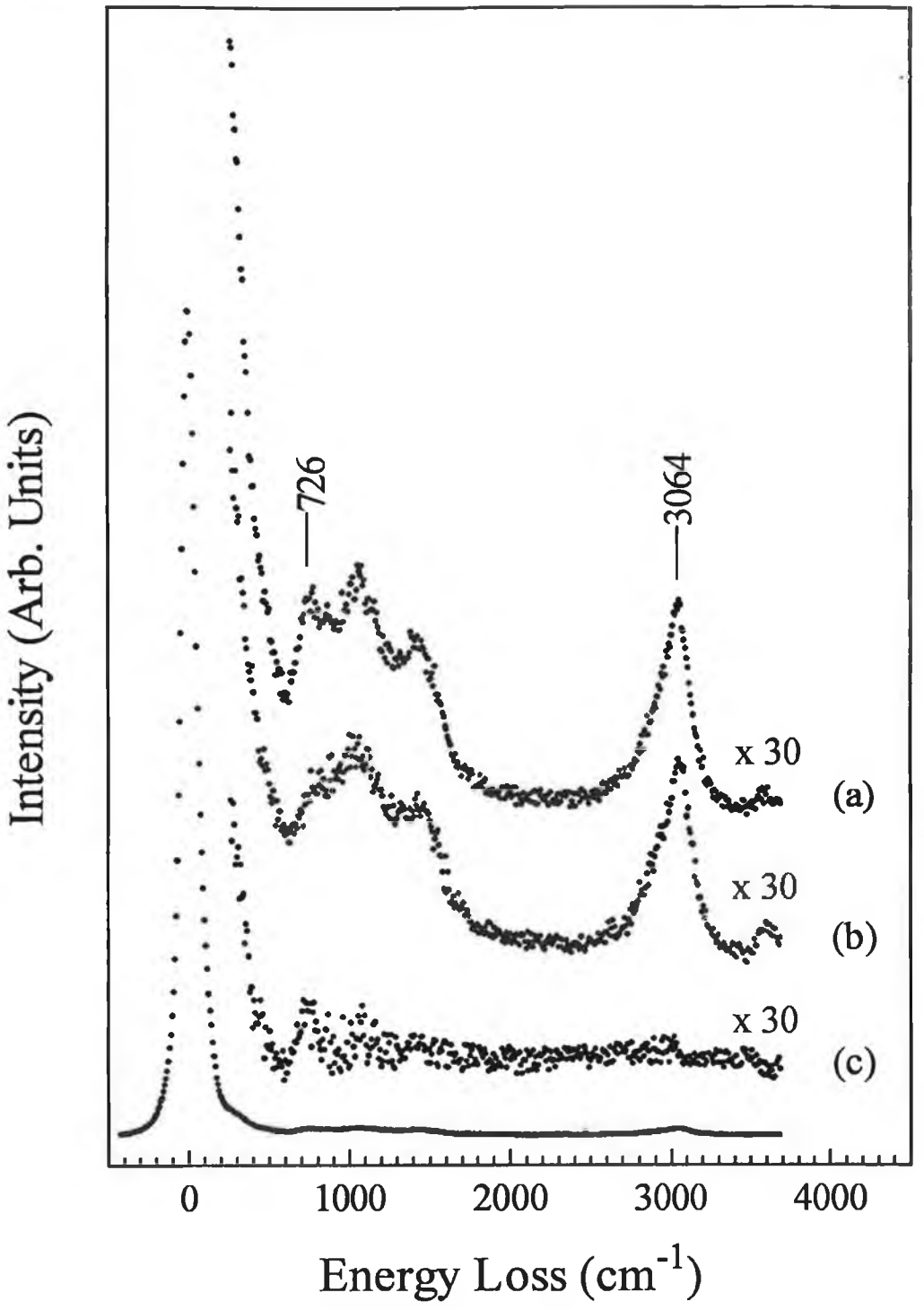

Figure 4 HREELS spectra collected at a primary beam energy of 5.0 eV from benzenethiol adsorbed on Au(322) to sub-monolayer coverage at 300 K. Spectra shown are (a) specular ($\theta_i = \theta_r = 70°$), (b) off-specular ($\theta_i = 70°$, $\theta_r = 50°$) and (c) a difference spectrum obtained by subtraction of (b) from (a).

The introduction of steps creates additional complexities into a HREELS analysis relative to the more generally studied atomically flat surfaces. In the case of dipole scattering for both atomically flat and stepped surfaces, all the scattered intensity is centered on a small angular region surrounding elastically scattered LEED beams. To obtain a dipole scattering dominated spectrum from a stepped surface, one must locate and center the analyser on one of the components of the specular LEED beam which is split by the step-terrace periodicity at certain beam energies. The procedure adopted in this work involved setting the angle of incidence, relative to the macroscopic (322) surface, to the desired value and the analyser was carefully swept to locate the nearest maximum in scattered intensity which represents one of the components of the specular LEED beam. While it is relatively easy to locate a scattering direction into which the dipole scattering channel dominates, care must also be taken when moving the analyser off-specular when recording impact scattered data, to ensure that the detector is not swept over another diffraction feature induced by the step-terrace periodicity. This may be achieved by simply monitoring the elastically scattered intensity as a function of scattering angle and ensuring off-specular data is recorded in a region of smoothly varying low intensity impact scattering.

Use of a stepped surface also has consequences in application of the dipole selection rule. For molecules adsorbed solely on the micro-terraces, since screening should be a local effect in the vicinity of the molecule and the Au atoms to which it is intimately connected, we expect the dipole selection rule to be fulfilled on the micro-(111) terraces themselves. For molecules adsorbed at surface step sites the selection rule is less clear. The broken local symmetry in the vicinity of a step make the application of the dipole selection rule ineffective as the details of the image charge screening in such a site is poorly understood [39]. No definitive studies exist regarding the selection rules in the region of atomic steps for relatively complex molecules such as benzenethiol. Indeed, little is known even about simpler atomic and diatomic adsorbates [40-42]. It is clear that addressing this problem is a topic of considerable interest in its own right, requiring an in depth study for a range of incident energies, angles and azimuthal alignments (parallel and perpendicular to the step site).

Despite this drawback, a number of significant conclusions may still be made. Firstly, as was the case for Au(111), lack of the S-H stretch at all coverages both in

specular and off-specular indicates that the surface intermediate present is a thiolate. Table 1 contains a summary of band frequencies and assignments for the benzenethiolate monolayer on Au(322), indicating a similar series of vibrational bands to those observed on Au(111). It is interesting to note that there is a slight asymmetry in the C-H stretch for low benzenethiol coverage on Au(322) in Fig. 4, indicative of a second unresolved state at low wavenumber. Rufael *et al.* reported two peaks at 2915 and 3011 cm^{-1} for low coverage benzenethiol adsorption on Ni(111) while at saturation coverage a single symmetric band at 3063 cm^{-1} was observed [23]. Given that aliphatic C-H stretching on Ni(111) occurs at 2900 cm^{-1}, the authors speculate that the phenyl ring may rehybridise upon chemisorption (which can cause ring expansion, ring 'puckering' and hydrogen-bond bending) giving rise to the 2915 cm^{-1} vibration [43]. Similarly, the C-H stretching frequency for sp^3 hybidised aliphatic C-H lies at 2960 cm^{-1} on Au(111) [3,7]. Hence, initially the asymmetry in the C-H stretch at 3064 cm^{-1} was suspected to be evidence of partial rehybridisation of the carbon atoms from sp^2 to sp^3 at low coverage benzenethiolate on Au(322) due to the strong interaction of the benzenethiolate intermediate at step sites. However, the occurrence of rehybridisation was subsequent ruled out as further measurements revealed that the asymmetry in the C-H stretch is in fact due to slow beam induced damage of the benzenethiolate layer. Spectra collected at reduced acquisition time resulting in less exposure to the incident beam, clearly showed that the C-H stretching band at 3064 cm^{-1} is symmetric.

The clear variation in intensity between the $\gamma_{C\text{-}H}$ and $\nu_{C\text{-}H}$ modes from low to high coverage unambiguously signals an orientational phase transformation. This is perhaps not surprising as two distinct adsorption sites are present: the (100) step sites and the (111) micro-terraces. If thermodynamic equilibrium is achieved at 300 K, which should be the case given that only local movement is needed to switch between a step and terrace site, it may be expected that adsorption in one of these two distinct sites is favoured and will be preferentially occupied at low coverage. At higher coverages, molecules will be forced to populate the second type of adsorption site. Alternatively, if two-dimensional island growth is preferred, both sites will occupy simultaneously. Nevertheless, it is still likely that nucleation of the islands will occur preferentially at one of the two available sites. Given the structure of the surface, shown schematically in Fig. 5a, we might expect the molecular orientation of the step

and terrace bound thiolate species to differ. In fact, given the terrace width and the van der Waals radius of the intermediate, a 1:1 mix of tilted step-bound thiolate to flat-lying thiolate on the (111) micro-terraces is not unreasonable [44]. A schematic diagram of the possible nature of the benzenethiol monolayer based on the van der Waals radius of a thiolate species is shown in Fig. 5b.

Unfortunately, the majority of the modes observed in HREELS are related to the benzene ring. The only mode reflecting the nature of the Au-sulphur bond is the weak energy loss superimposed on the elastic peak at 468 cm^{-1} which may be assigned to the Au-S stretch, although this mode may not be a pure metal-sulphur stretch as it may couple to low frequency benzene ring modes (ring deformation at 404 cm^{-1}). Thus, we conclude that with the resolution employed HREELS does not allow an unambiguous assignment of whether step or terrace sites are preferentially occupied at low coverage.

(a)

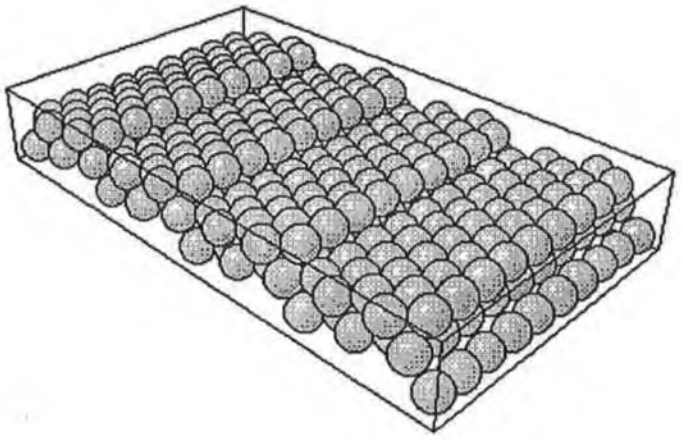

(b)

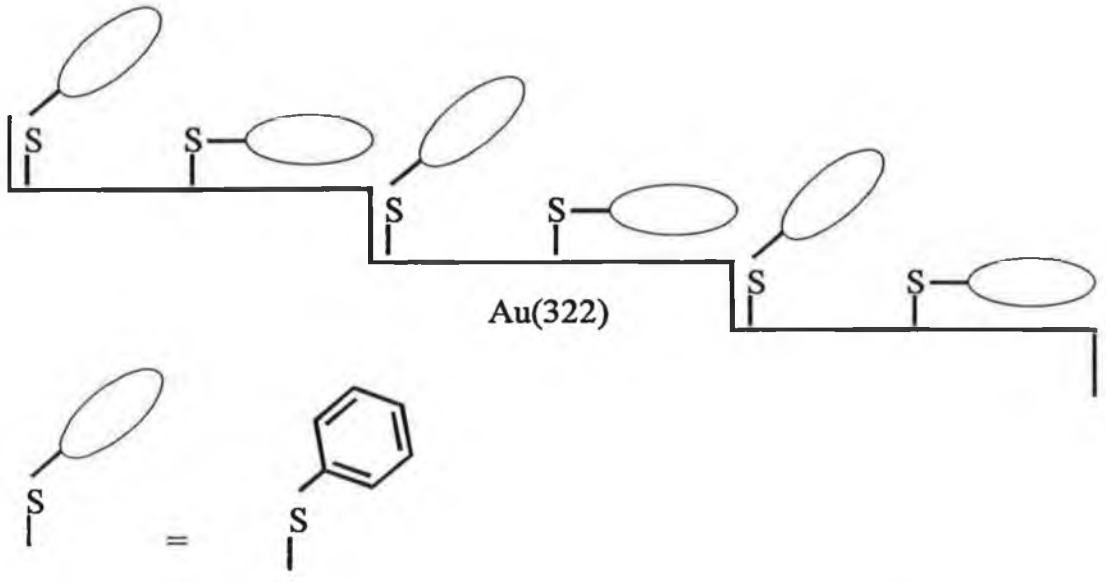

thiolate intermediate

Figure 5 (a) A schematic diagram of the clean Au(322) surface illustrating its composition of (100) steps and (111) terraces of five unit cells width termed 5(111)×(100) surface. (b) A schematic model of the possible structure for a benzenethiolate monolayer on Au(322) indicating two chemically distinct species: an intermediate with the aromatic ring strongly inclined to the (111) micro-facets and a second flat-lying species occupying the (111) terraces in a population ratio of 1:1.

4. Discussion

The first observation worthy of discussion is the absence of lifting of the Au(111)-($\sqrt{3}\times22$) surface reconstruction. Reconstruction generally occurs due to 'surface stress' created by the loss of nearest neighbours of surface atoms which respond to the unbalanced forces by rearranging to create a geometry in which the electron density lost due to their missing neighbours is partially recovered by changes in the bond length of first and second layer atoms. In the case of Au(111), this is achieved by a 4% compression along [110] directions thus forming an outermost layer incommensurate with the hexagonal layer below [15]. Strongly chemisorbed atomic and molecular overlayers are generally found to lift surface reconstructions and return the outermost layer geometry to bulk truncated symmetry [45]. Of course, this is not universally true and certain cases already exist contrary to this general expectation, a notable example being alkali metal adsorption on Au(110) which actually stabilises the (1×2) missing row reconstruction [46].

The benzenethiol molecule is bulky, having a 300 K saturation coverage 0.23 monolayers on Au(111) [13]. As the flat-lying phenyl ring interacts via physisorption or very weak chemisorption on Au(111) this has the effect of leaving many of the Au surface atoms coordinatively unsaturated [9,30]. Thus, even adsorption to monolayer coverage appears to be insufficient to remove the 'surface stress' by polar covalent S-Au bond formation in contrast to n-alkanethiolates on Au(111) [7].

Formation of a thiolate on Au(111) with cleavage of the S-H bond is in direct agreement with previous surface bonding characterisation of benzenethiol adsorption on other metal surfaces [19,21-29,35-38]. Chemisorption of hydrogen is weak on Au(111), hence the resulting atomic hydrogen formed due to S-H bond cleavage will desorb from the surface at 300 K [47]. This is confirmed by the absence of significant mass 2 desorption in TDS [16]. We thus postulate that atomic hydrogen created upon adsorption, desorbs immediately as molecular hydrogen by recombination.

The only previous study of benzenethiol adsorption from the gas phase on gold single crystal surfaces is that of Jaffey and Madix, reporting a TDS study on Au(110) [47]. The authors assert that thiolate formation occurs via S-H bond cleavage and suggest that Au(111) may be even less active for S-H bond dissociation than Au(110).

In contrast to more reactive transition metals, C-S bond cleavage on Au surfaces occurs only at elevated temperatures compared to open d-band metals where it frequently occurs below 300 K. Thus, the thiolate intermediate is stable to much higher temperature on Au(110) and leads to desorption of recombination products derived from the thiolate intermediate including benzenethiol, biphenyl, diphenyl sulphide and dibenzothiophene. Interestingly, from their quantitative TDS work, it is estimated that adsorption at low temperature (100 K) leads to a coverage of 0.25 ML of molecular benzenethiol. However, upon temperature programming to 300 K approximately half of the benzenethiol desorbs molecularly leaving a thiolate coverage between 0.16 and 0.12 ML.

The HREELS data for benzenethiol adsorption on Au(111) are clearly indicative of a flat-lying molecule on the Au(111) surface. This flat-lying geometry serves to maximise the weak interaction of the benzene ring with the Au(111) surface. Studies of benzene chemisorption on (111) transition metal surfaces reveal a flat-lying geometry which serves to maximise the interaction of the benzene π-system with the surface [8,9,30,33,34]. For cyclic molecules which interact primarily by strong chemisorption via a heteroatom either within the ring system or, as in the case of benzenethiol, where the heteroatom is external to the ring system, a trend in which a flat-lying geometry is adopted at low coverages with an orientational phase transition occurring as the coverage is increased is often observed [19,21]. At low coverages when the adsorbate two-dimensional density is low, a flat-lying geometry allows additional chemisorption energy to be liberated via the interaction of the delocalised π-system with the metal. A phase transition to an upright geometry at higher coverage occurs to allow an increased packing density, hence, maximising the number of sulphur-metal bonds formed.

Of significant interest is the result of this study indicating a coverage independent flat-lying geometry which contrasts strongly with past studies reporting that the benzenethiol monolayer adopts an upright or close to upright geometry at monolayer saturation [19,21-29,35-38]. A close to upright geometry at saturation coverage of benzenethiolate on Mo(110) and Ni (100) is supported by complementary NEXAFS studies indicating that the thiolate is inclined about 20° relative to the surface normal [25,26,37,38]. Evidence that the thiolate intermediate is not perfectly upright

when adsorbed from the gas phase on Cu(110), Rh(111), Ni(110), Ni(111) and Mo(110) is provided by HREELS studies of benzenethiol monolayers prepared by liquid phase self-assembly on Ag(111) and Pt(111) electrodes [28,29]. In this case, the C-H stretching vibration dominates the HREELS spectrum and the out-of-plane C-H stretch has an extremely low intensity with the $\nu_{C\text{-}H}$ to $\gamma_{C\text{-}H}$ intensity ratio significantly higher than reported gas phase studies. The similarity of the HREELS spectra from Ag(111) and Pt(111) testify to an almost identical adsorption geometry, and the authors postulate a perfectly upright 'pendant' geometry for the phenylthiolate intermediate.

Maintaining a largely flat-lying geometry on Au(111) implies that the adsorption on Au(111) differs relative to other transition metal surfaces studied to date. It may be speculated that the lack of a transition to a more upright densely packed monolayer on Au(111) may be related to the lower heat of adsorption of the thiolate on Au(111) compared to other substrates. Thermal desorption studies of benzenethiol on Au(111) indicate a thiolate heat of adsorption of ~100 kJ mol^{-1} assuming first order desorption kinetics [16]. The heat of adsorption at higher coverages, in which a flat-lying to upright phase transition is complete, may drop to an extent that it renders the thiolate unstable to thermal desorption at 300 K. It hence remains a possibility that adsorption at low temperature may lead to a flat to upright phase transition along with the possibility of adsorbate ordering. A second possibility involves a kinetic rather than thermodynamic limitation in which the flat-lying monolayer may sterically hinder incoming benzenethiol molecules from making intimate contact with the Au surface necessary for cleavage of the S-H bond. The latter alternative is indeed suggested by studies of liquid phase benzenethiol adsorption on Au(111) for which HREELS and X-ray photoelectron spectroscopy (XPS) indicates a largely upright geometry is favoured with the phenyl ring tilted 20° away from the surface normal [12]. This densely packed phase is stable in UHV at room temperature mitigating against the explanation that the monolayer is unstable to thermal desorption [13]. It seems more likely that the higher effective bombardment rate in the liquid phase is sufficient to increase the room temperature thiolate coverage via a flat-lying to upright transition. The observation that thiol adsorption from solution leads to high surface monolayer coverages has previously been observed and commented on by

Nuzzo and Allara, and it seems that the phenomenon carries over to cyclic aromatic systems such as benzenethiol [48]. A flat-lying to upright transition may also occur in UHV, but may require unfeasible, high dose levels to drive it to completion.

To our knowledge, no studies presently exist on the effect of controlled defect densities on SAMs. The introduction of defects leads to a marked change both in the surface ordering of the thiolate and in molecular orientation. The surface structure of the clean Au(322) surface is shown in Fig. 5a. LEED clearly indicates ordering within the monolayer and a separate LEED study allows suggestions regarding the adlayer periodicity, which may be utilised along with the HREELS data to suggest the possible monolayer structure (Fig. 5b) [16].

Interestingly, on Au(322) an orientational transition is observed which is indicative of a change from a highly inclined to a flat-lying geometry. We suggest that as the benzenethiol coverage is increased, the ratio of step bound to terrace bound adsorbate changes. TDS indicates simultaneous occupation of two desorption states, which may be assigned to step bound and terrace bound species, with increasing coverage, although the relative proportion of molecules in each state indeed changes with surface coverage. Given the results for the atomically flat Au(111) surface, it would seem likely that the adsorbate on the micro-terraces would prefer a flat-lying geometry while molecules bound at (100) step sites would adopt a tilted geometry relative to the micro-terraces. Such a qualitative picture is borne out by the HREELS data which additionally suggests that the step sites are preferentially occupied at low benzenethiol exposures by a tilted thiolate intermediate.

A simple method of qualitatively checking that our postulation of occupation of terrace sites by thiolate intermediates adopting a flat-lying geometry at higher exposures once step sites are saturated is correct, is via subtraction of the dipole dominated HREELS spectra of the sub-monolayer film (Fig. 4a) from that of the monolayer (Fig. 3a). If step sites are occupied at low coverages, this subtraction will represent a HREELS spectrum from terrace bound thiolate species alone. Fig. 6 illustrates such a subtraction, which when compared with a similar spectrum from a flat-lying thiolate monolayer on Au(111) (Fig. 1a) confirms that at higher coverages the (111) micro-terraces are being exclusively populated by flat-lying benzenethiolate and supporting the case for adsorption at the defect sites at low coverages.

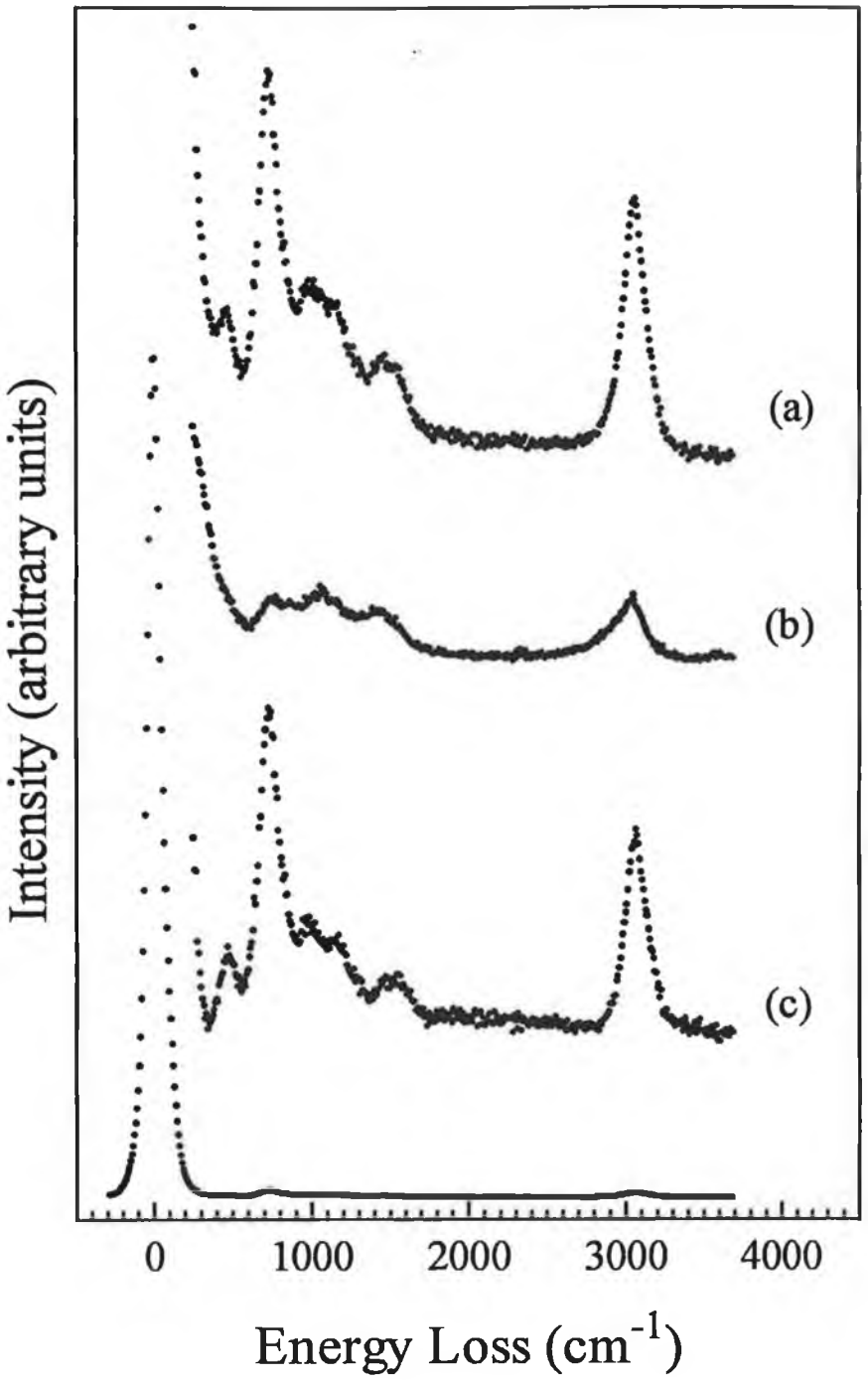

Figure 6 HREELS spectra ($\theta_i = \theta_r = 70°$) collected at a primary beam energy of 5.0 eV from benzenethiol adsorbed on Au(322) at 300 K. Spectra shown are (a) saturation coverage, (b) sub-monolayer coverage and (c) a difference spectrum obtained by subtraction of (b) from (a).

5. Conclusions

We have demonstrated using HREELS as the primary probe, that adsorption of benzenethiol on both Au(111) and (322) leads to formation of a thiolate intermediate at both high and low coverages. On Au(111), the phenylthiolate adopts a flat-lying geometry. At 300 K this bonding geometry is coverage independent in contrast to previous studies of benzenethiol adsorption on transition metals.

In addition, we have demonstrated that the introduction of surface defects in the form of a periodic array of atomic steps separating micro-terraces of (111) orientation leads to changes both in the adsorbate lateral ordering and orientation. A coverage dependent reorientation is observed on Au(322) which we assign to occupation of step and terrace sites, with thiolate species at steps and terraces adopting a different orientation. A model of the adlayer geometry at high coverage on Au(322) has been suggested.

The manipulation of the adlayer structure of aromatic SAMs, for which benzenethiol acts as a prototype system, by controlled addition of surface defects has been shown to be possible. Control of molecular orientation and two-dimensional packing density may prove to be useful in the synthesis of SAMs for a range of applications.

6. References

[1] D.R. Jung, D.E. King and A.W. Czanderna, Appl. Surf. Sci., **70/71** (1993) 127.

[2] A.J. Bard, H.D. Abruna, C.E.D. Chidsey, L.R. Faulkner, S.W. Feldberg, K. Itaya, M. Majada, O. Melroy, R.W. Murray, M.D. Porter, M.P. Soriaga and H.S. White, J. Phys. Chem., **97** (1993) 7147.

[3] A. Ulman, An Introduction to Ultrathin Organic Films: from Langmuir-Blodgett to Self-Assembly, Academic, New York, 1991.

[4] L.H. Dubois and R.G. Nuzzo, Annu. Rev. Phys. Chem., **43** (1992) 437.

[5] A. Ulman, Chem. Rev., **96** (1996) 1533.

[6] G.E. Poirier, Chem. Rev., **97** (1997) 1117.

[7] L.H. Dubois, B.R. Zegarski and R.G. Nuzzo, J. Chem. Phys., **98** (1993) 678.

[8] J.C. Bertolini and J. Massardier in: The Chemical Physics of Solid Surfaces and Heterogeneous Catalysis, Vol. 4, Eds. D.A. King and D.P. Woodruff, Elsevier, New York, 1982.

[9] F.P. Netzer, Langmuir, **7** (1991) 2544.

[10] F.P. Netzer, G. Rangelov, G. Rosina, H.B. Saalfeld, M. Neumann and D.R. Lloyd, Phys. Rev. B, **37** (1988) 10399.

[11] H. Hoffmann, F. Zaera, R.M. Ormerod, R.M. Lambert, L.P. Wang and W.T. Tysoe, Surf. Sci., **232** (1990) 259.

[12] C.M. Whelan, M.R. Smyth and C.J. Barnes, Langmuir, accepted.

[13] C.M. Whelan, C.J. Barnes, C.G.H. Walker and N.M.D. Brown, submitted.

[14] P.A. Thiry, Ph.D. thesis, FUNDP, Namur, 1984.

[15] M.A. Van Hove, R.J. Koestner, P.C. Stair, J.P. Biberian, L.L. Kesmodel, I. Bartos and G.A. Somorjai, Surf. Sci., **103** (1981) 189.

[16] C.M. Whelan, C.J. Barnes, C.G.H. Walker and N.M.D. Brown, in preparation.

[17] J.J. Pireaux, M. Liehr, P.A. Thiry, J.P. Delrue and R. Caudano, Surf. Sci., **141** (1984) 221.

[18] It is likely that true monolayer coverage results in an upright thiolate species, however we suspect that formation of this phase is kinetically inhibited, requiring unreasonably long dosing times leading to significant contamination of the UHV chamber.

[19] W. Shen, G.L. Nyberg and J. Liesgang, Surf. Sci., **298** (1993) 143

[20] H. Ibach and D.L. Mills, Electron Energy Loss Spectroscopy and Surface Vibrations, Academic, London, 1982.

[21] C.W.J. Bol, C.M. Friend and X. Xu, Langmuir, **12** (1996) 6083.

[22] S.M. Kane, T.S. Rufael, J.L. Gland, D.R. Huntley and D.A. Fischer, J. Phys. Chem. B, **101** (1997) 8486.

[23] T.S. Rufael, D.R. Huntley, D.R. Mullins and J.L. Gland, J. Phys. Chem., **98** (1994) 13022.

[24] D.R. Huntley, J. Phys. Chem., **96** (1992) 4550.

[25] J.T. Roberts and C.M. Friend, J. Chem. Phys., **88** (1988) 7172.

[26] M.K. Weldon, M.E. Napier, B.C. Wiegand, C.M. Friend and P. Uvdal, J. Am. Chem. Soc., **116** (1994) 8328.

[27] D.A. Chen, C.M. Friend and H. Xu, Surf. Sci., **395** (1998) L221.

[28] J.Y. Gui, D.A. Stern, D.G. Frank, F. Lu, D.C. Zapien and A.T. Hubbard, Langmuir, **7** (1991) 955.

[29] D.A. Stern, E. Wellner, G.N. Salaita, L. Laguren-Davidson, F. Lu, N. Batina, D.G. Frank, D.C. Zapien, N. Walton and A.T. Hubbard, J. Am. Chem. Soc., **110** (1988) 4885.

[30] K. Weiss, S. Gebert, M. Wuhn, H. Wadephol and Ch. Woll, J. Vac. Sci. Technol. A, **16** (1998) 1017.

[31] L-M. Yu, K. Hevesi, B-Y. Han, J.J. Pireaux, P.A. Thirty, R. Caudano and P.H. Lambin, Surf. Rev. Lett., **2** (1995) 705.

[32] M. Perez Jigato, W.K. Walter and D.A. King, Surf. Sci., **301** (1994) 273.

[33] S. Lehwald, H. Ibach and J.E. Demuth, Surf. Sci., **78** (1978) 577.

[34] J.C. Bertolini, G. Dalami-Imelik and J. Rousseau, Surf. Sci., **67** (1977) 478.

[35] P.A. Agron, T.A. Carlson, W.B. Dress and G.L. Nyberg, J. Electron Spectrosc. Relat. Phenom., **42** (1987) 313.

[36] P.A. Argon and T.A. Carlson, J. Vac. Sci. Technol., **20** (1982) 815.

[37] Y. Takata, T. Yokoyama, S. Yagi, N. Happo, H. Sato, K. Seki, T. Ohta, Y. Kitajima and H. Kuroda, Surf. Sci., **259** (1991) 266.

[38] J. Stohr and D.A. Outka, Phys. Rev. B, **36** (1987) 7891.

[39] M. Surman, private communication.

[40] K. Svensson, I. Richardsson, C. Nyberg and S.A. Anderssons, Surf. Sci., **366** (1996) 140.

[41] Q. Gao, R.D. Ramsier, H.N. Waltenburg and J.T. Yates, J. Am. Chem. Soc., **116** (1994) 3901.

[42] J.D. Batteas, D.E. Gardin, M.A. Van Hove and G.A. Somorjai, Surf. Sci., **297** (1993) 11.

[43] J.E. Demuth and D.E. Eastman, Phys. Rev. B, **13** (1976) 1523.

[44] L.C. Pauling, The nature of the Chemical Bond, 3rd ed., Cornell University Press, Ithaca, New York, 1960.

[45] G.A. Somorjai and M.A. Van Hove, Prog. Surf. Sci., **30** (1991) 201.

[46] D.K. Flynn-Sanders, K.D. Jamison, J.V. Barth, T. Winterlin, P.A. Thiel, G. Ertl and R.J. Behm, Surf. Sci., **253** (1991) 270.

[47] D.M. Jaffey and R.J. Madix, Surf. Sci., **258** (1991) 359.

[48] R.G. Nuzzo and D.A. Allara, J. Am. Chem. Soc., **105** (1983) 4481.

Chapter 7

Conclusions

Interest in the properties of thin-film organic materials, especially coherently organised monolayer assemblies, has grown enormously in recent years. A comprehensive range of data has been accumulated and interpreted for self-assembly of *n*-alkanethiols on various substrates while information regarding the adsorption of conjugated thiols, which clearly offer considerably more complexity, is sparse. This thesis has detailed the study of aromatic and heteroaromatic thiol self-assembly on Au single crystal surfaces using a range of surface spectroscopic and electrochemical techniques. The formation of such SAMs has been investigated in terms of the types of surface intermediates formed, adsorbate orientation and the mechanism of adsorption from the liquid phase and the gas phase which eliminates solvent and substrate contamination effects.

Adsorption of complex conjugated thiols, 2-mercaptobenzothiazole (2MBT) and 2-mercaptobenzimidazole (2MBI), is of interest with respect to the nature of bonding to the substrate which, in principle, may involve the thiol functional group, the sulphur and nitrogen heteroatoms and the conjugated π-system. Based on XPS analysis of these molecules self-assembled on Au(111) from the liquid phase, it is concluded that the primary adsorbate species is consistent with a thiolate. In the case of 2MBI, which was studied more extensively, a secondary coordination with the surface via the unprotonated nitrogen heteroatom is also possible, given that the molecule adopts an orientation in which the ring is parallel or close to parallel to the Au(111) surface. Substrate contamination upon exposure to ambient conditions prior to self-assembly has been consistently observed following thiol adsorption from the liquid phase, such that films contained oxygen and excess carbon. While direct *in situ* sublimation of 2MBI yielded oxygen-free layers, partial decomposition of the molecule occurs resulting in the formation of atomic sulphur. *Ex situ* prepared layers were further complicated by the presence of oxygen and substantial sulphonate formation. Hence, this study highlights the problems associated with sample preparation and it is fair to conclude that formation of high quality heteroaromatic SAMs is non-trivial.

The influence of these assemblies, at sub-monolayer and monolayer coverages, on the UPD of Cu on Au(111) has been used to probe the mechanism of self-assembly. A multistep adsorption process occurs with initial rapid thiol adsorption followed by a much slower progression to full 'physical monolayer' formation which completely

blocks Cu UPD and hinders bulk processes. The ability of 2MBI and 2MBT chemisorption to lift the Au(111)-($\sqrt{3}\times22$) reconstruction to the (1×1) structure has been inferred from the absence of a fingerprint specific anion adsorption peak on Au(111), associated with the reversible removal of the substrate reconstruction.

The structural and behavioural complexities of the heteroaromatic thiols provided the motivation to study the simplest aromatic thiol, benzenethiol. The remainder of the thesis details a comprehensive investigation of benzenethiol adsorption on Au(111) and on an atomically stepped Au(322) surface.

HREELS and XPS characterisation of benzenethiol monolayers on Au(111) prepared by self-assembly from the liquid phase indicates that the primary adsorbate species is a thiolate; however, sub-monolayer films comprise a mixture of thiol and higher oxidation state sulphur species. In addition, oxygen contamination of both sub-monolayer and monolayer films was consistently observed. This is in contrast with the adsorption behaviour of *n*-alkanethiols which reportedly displace adventitious material from the substrate surface during the self-assembly process such that stoichiometric films are readily obtained.

The intensity of the out-of-plane C-H deformation, film thickness, absolute sulphur coverage, molecular packing density and variation of the carbon (1s) to sulphur (2p) emission intensities as a function of take-off angle, support a benzenethiolate adsorption geometry in which the phenyl ring is aligned largely perpendicular to the Au(111) surface.

Again, Cu UPD and specific anion adsorption were used to probe the growth mechanism and in this case are supported by XPS uptake data. A multistep adsorption process is proposed, involving initial rapid self-assembly, possibly corresponding to a flat-lying adsorbate covered surface, followed by a much slower progression to full 'physical monolayer' formation in which the thiolate intermediate may reorientate to form islands of densely packed upright molecules.

Synchrotron ARUPS, HREELS and XPS have been used to study the adsorption of benzenethiol from the gas phase on Au(111) at 300 K. At sub-monolayer and saturation coverages, a thiolate intermediate with the plane of the phenyl ring largely parallel to the Au(111) surface plane is favoured. This coverage independent bonding geometry is in contrast to previous studies of benzenethiol adsorption on

transition metals. The uptake of benzenethiol, monitored by work function changes, LEED and attenuation of the Shockley surface state, suggests a precursor-mediated adsorption mechanism involving two-dimsensional islanding without long range ordering and without lifting of the Au(111)-($\sqrt{3}\times22$) reconstruction.

These results highlight two major differences between adlayers prepared by gas phase and liquid phase adsorption. First, in terms of aromatic SAM composition, stoichiometric films can only be formed by adsorption from the gas phase. Second, the higher effective thiol flux in the liquid phase is necessary to increase the 300 K adsorbate coverage via a flat-lying to upright transition and lift the surface reconstruction to the bulk truncated (1×1) phase. Hence, at saturation coverage, benzenethiolate adopts an upright and flat-lying bonding configuration following self-assembly from the liquid and gas phase, respectively.

The introduction of surface defects in the form of a periodic array of atomic steps separating micro-terraces of (111) orientation leads to changes both in the adsorbate ordering and orientation. Gas phase adsorption of benzenethiol on Au(322) at 300 K has been studied using HREELS. This surface, consisting of mono-atomic (100) steps separating (111) micro-terraces five unit cells wide, leads to formation of an ordered monolayer. The adsorbed intermediate is benzenethiolate at both low and high coverage and an orientational transition from a strongly inclined to a more flat-lying geometry occurs as a function of coverage. This unusual behaviour is assigned to occupation of step and terrace sites, with thiolate species at steps and terraces adopting different orientations. This study shows clear evidence for step induced ordering of the thiolate intermediate and the ability of steps to promote a molecular reorientation compared to a similar adsorbate on an atomically flat surface.

In terms of future work, *in situ* STM characterisation of sub-monolayer self-assembly of benzenethiol both with and without specifically adsorbing anions and Cu UPD would be of particular value in the case of liquid phase self-assembly in order to clarify the adsorption behaviour and confirm whether a coverage dependent reorientation of the adsorbate occurs. Similarly, the gas phase studies indicating a coverage independent flat-lying geometry for benzenethiol adsorbed on Au(111) at 300 K requires further investigation. It is possible that the heat of adsorption at higher coverages achieved by a flat to upright phase transformation may drop to the extent

that it renders the thiolate unstable to thermal desorption at 300 K. It remains a possibility that adsorption at temperatures <300 K may lead to a flat to upright phase transition along with the possibility of adsorbate ordering. Finally, the selection rules applicable in the region of atomic steps is unknown even in the case of simple adsorbates. Addressing this problem is a topic of considerable interest, requiring a study at a range of incident energies, angles and azimuthal alignments.

Appendix

Surface Structural Transitions Induced by Repetitive Underpotential Deposition of Ag on Au(111)

The study of Ag UPD on Au(111), while not related to the main work detailed in this thesis, represents the introduction of electrochemistry using single crystals to the laboratory in DCU. During an initial visit to Dr. Attards' laboratory in the University of Wales at Cardiff interesting changes to the cyclic voltammetry characteristic of Ag UPD on Au(111) were observed. Variation of the supporting anion and substrate oxidation effects were investigated in Dublin and, more recently, a second visit to Cardiff allowed further investigation of the UPD system using *in situ* scanning tunneling microscopy.

Abstract

The underpotential deposition (UPD) of Ag on a Au(111) electrode in aqueous sulphuric acid has been studied by electrochemical scanning tunneling microscopy (ECSTM). The Au(111) surface morphology is substantially altered during repeated cycles in the Ag UPD region. Prior to Ag UPD, the surface consists of large, flat terraces (50 to 200 nm in width) with monatomic and diatomic steps. After several cycles of Ag deposition and dissolution, the surface is characterised by the appearance and growth of a high density of monolayer deep 'pits.' As cycling is continued, the pits expand rapidly to leave isolated Au islands accompanied by receding terrace edges. This process is followed by a slow lateral growth of Au islands which apparently fuse with terrace edges or aggregate with each other to form extended, atomically flat terraces. The surface topography is dominated by straight-edged, narrow terraces (15 to 50 nm in width) running parallel to or crossing each other to form a mesh, in which the terrace edges meet at an angle of 120° or 60°, characteristic of a (111) close-packed plane. The slow transformation of a high quality Au(111) surface in comparison to a defect rich surface suggests that the kinetics of the transition process are related to the surface defect density.

The surface morphological changes accompanying Ag UPD cycling are reflected in the cyclic voltammograms *via* dramatic changes, in both peak shape and potential, attributed to a decrease in the average substrate terrace width. Extremely narrow half widths and large peak magnitudes are observed, after several hours of cycling, indicative of significant long-range order.

The effect of variation of the supporting anion on this transition has also been investigated. Repetitive cycling of Ag UPD on the Au(111) electrode in the presence of perchlorate anions results in similar alterations in peak shape and potential. This weakly adsorbing anion appears to enhance the rate of structural transformation of the Au(111) surface.

1. Introduction

Underpotential deposition (UPD) is a complex phenomenon which describes the formation of monolayer metal deposits on a foreign metal substrate at potentials positive of the reversible Nernst potential for the formation of the bulk phase [1,2]. Prior to the development of *in situ* atomic imaging, conventional electrochemical and spectroscopic techniques had to be relied upon to provide a means of probing the energetics of the UPD system. This allowed only indirect characterisation of the processes taking place at the metal/electrolyte interface and the properties of atoms and molecules adsorbed at this interface leaving many questions unanswered [3,4]. The application of scanning probe microscopies (SPM) has provided new insight into the static and dynamic atomic structure of the electrode surface as well as that of adsorbed layers [5].

There have been several previous studies of the Ag UPD system on Au(111) [6-14]. Uchida *et al.* have presented a quantitative study of Ag UPD on Au(111) in sulphuric acid using an electrochemical quartz crystal microbalance (ECQM) [6]. Chen *et al.* have studied Ag UPD on Au(111) in a range of different electrolytes using cyclic voltammetry and *in situ* atomic force microscopy (AFM) [7,8]. They report that the structure of the Ag monolayer is highly dependent on the nature of the supporting anion. *In situ* scanning tunneling microscopy (STM) of Ag on Au(111) in sulphuric acid has been presented by Hachiya and Itaya [9]. A comprehensive study of sulphate anion coadsorption during Ag UPD on Au(111) has been performed by Mrozek *et al.* using *in situ* AFM and *ex situ* low energy electron diffraction (LEED), Auger electron spectroscopy (AES) and core electron energy loss spectroscopy (CEELS) [10]. In spite of numerous studies using a variety of techniques, there is little agreement on the Ag adlayer structure and coverage in sulphuric acid [6-10].

In more recent publications, Itaya and co-workers have reported on Ag adlattice formation in the presence of the weakly adsorbing perchlorate anion and highlight the sensitivity of Ag UPD growth to halide coadsorption effects as a possible explanation for contradictory SPM results on Ag adlayer structures [11,12]. Deposition of Ag on Au(111) without interference by specifically adsorbing anions has also been investigated by Corcoran *et al.* and Mrozek *et al.* using electrochemical STM

and combined ultra-high-vacuum-electrochemistry (UHV-EC) techniques, respectively [13,14].

In this paper, we describe a profound structural transformation of the Au(111) surface induced by repetitive cycling in the Ag UPD region in sulphuric and perchloric acids. In the presence of the weakly adsorbing perchlorate anion, much more rapid alterations in voltammetric peak shape and potential were observed, indicating that anion coadsorption plays an important role in this structural transition. The voltammograms collected from a freshly prepared Au(111) surface is qualitatively similar to that reported previously and yet the initial stages of this transformation occur rapidly on surfaces with a high defect density, evidenced as modification of the electrochemical response within 10 cycles in the UPD region at 10 mVs^{-1} [6-14]. However, substantial changes in substrate morphology are only observed following repetitive cycling (necessitating the use of a high scan rate). We speculate that the kinetics of the Ag UPD-induced Au(111) transition process are related to the surface defect density. To our knowledge this phenomenon has not been previously reported for metal electrodeposition on Au(111).

2. Experimental

The working electrode (also the STM substrate) was a Au(111) single-crystal bead with a surface area of 0.05 cm^2 prepared at the end of Au wire (99.95% purity, Goodfellow Cambridge) by the method of Clavilier *et al.* [15]. A clean Au(111) surface was prepared prior to electrochemical measurements by the flame-annealing technique [16]. The crystal was then cooled in a flow of inert gas (high purity nitrogen) before quenching and formation of a meniscus contact. To confirm that the electrochemical response obtained is characteristic of the Au(111) face, cyclic voltammograms for Au(111) in 0.1 M sulphuric acid were collected and found to be in good agreement with literature reports [17-20].

Electrochemical experiments were performed in a two-compartment Pyrex glass cell described elsewhere [21]. All glassware, including the electrochemical cell and its accessories, were cleaned by soaking for >12 hours in a dilute solution of $KMnO_4$ (99.8% purity, Aldrich) in concentrated sulphuric acid (97-99% GPR, BDH). These items were then rinsed thoroughly and steamed with deionised water (18.2 $M\Omega cm^{-1}$).

De-aerated aqueous 0.1 M sulphuric and perchloric acids (doubly distilled, ultrapure grade, Aldrich) prepared with deionised water were used as the supporting electrolytes. The 1 mM Ag^+ solutions were prepared by dissolution of Ag_2SO_4 and $AgClO_4$ (99.999% purity, Aldrich) in sulphuric and perchloric acid, respectively. All working solutions were purged and blanketed with research grade nitrogen (99.9995%, B.O.C. Special Gases) purified by an oxygen trap (Supelco Chromatography) decreasing oxygen impurities to less than 0.005 p.p.m. Electrode potentials are given with respect to the reversible Ag/Ag^+ electrode (Ag wire, 99.999% purity, Goodfellow Cambridge) cleaned by immersion in concentrated nitric acid (69% GPR, BDH) and rinsing with copious amounts of deionised water. Cyclic voltammetry was performed using a BAS CV-50W potentiostat (Bioanalytical Systems). The working electrode was immersed in the electrolyte under potential control at 650 mV.

STM images were obtained with a Molecular Imaging electrochemical scanning probe microscope isolated from external vibrations and operating in constant height mode. The STM piezoelectric scanner was calibrated using the Au(111) surface

imaged in air. Images of the flame-annealed Au(111) electrode revealed large, flat terraces exhibiting the characteristic features of a 0.29 nm atom-atom spacing in a hexagonal arrangement (spacings were determined on unprocessed images). Prior to each experiment, an STM tip was prepared by etching W wire (0.25 mm diameter, 99.95% purity, Goodfellow Cambridge) in 2 M NaOH (Fisher Scientific) using a three stage electrolysis and isolating with paraffin wax (BDH) to minimise the electroactive area of the tunneling tip and thus minimise Faradaic currents (background currents < 0.5 nA). Tip potential varied from experiment to experiment but was operated within a potential range excluding both bulk deposition of Ag and oxygen adsorption on the tip surface. The potential of both the Au(111) substrate and the tip were independently controlled by a four electrode potentiostat. Usually, the tip potential was held at constant potential corresponding to the minimum Faradaic current through the tip such that when the substrate potential was varied at convenience, the tunneling voltage changes correspondingly. All images presented in the results section were collected at a working electrode potential of 650 mV.

In addition to cyclic voltammetry conducted using the BAS CV-50W potentiostat, electrochemical measurements was also carried out using the electrochemical scanning probe microscope (to allow comparison between *ex situ* electrochemical and *in situ* ECSTM results). A liquid cell made from Pyrex glass contained the electrolyte. After flame-annealing, the crystal was quickly mounted in the STM cell which was immediately filled with electrolyte to minimise possible surface contamination from the laboratory ambient. Prior to filling the STM cell, the solution was degassed by purging with nitrogen. The STM set-up was held under nitrogen atmosphere to minimise oxygen uptake. A Ag wire, in contact with the electrolyte, served as the reference electrode and all voltages are referenced to this wire. The counter electrode was a Pt wire which was flame annealed prior to each use.

3. Results and Discussion

3.1 Ag UPD on Au(111) in sulphuric acid

Cyclic voltammetry for Ag UPD on Au(111) in 0.1 M H_2SO_4 is shown in Fig. 1. The voltammetry shows several sets of adsorption and desorption peaks corresponding to different processes occurring in the UPD region. In the first cycle, adsorption at 516 mV corresponds to the first UPD process (A) with its desorption peak occurring at 527 mV (A′). Both peaks show broadening and are accompanied by a shoulder at potentials positive of the peak maxima. The full-width-at-half-maximum (FWHM) of these adsorption and desorption peaks are 17 and 18 mV, respectively, considerably larger than the FWHM (< 10 mV) reported by Chen *et al.* [7,8]. A series of small peaks (B) occur at 327 and 237 mV during the deposition sweep (second UPD process) with the corresponding stripping peaks (B′) at 415 and 255 mV. The third UPD process (C) is seen at more negative potentials, prior to second layer growth and the onset of bulk deposition, and consists of two peaks at 128 and 85 mV on the deposition sweep while stripping occurs at 131 and 86 mV (C′). This voltammetry is qualitatively similar to that reported previously, however, some inconsistencies exist with respect to peak potential, FWHM and relative peak heights due to variations in the ordering of the Au(111) surface, concentrations of Ag^+ and sulphuric acid, sweep rates and trace impurities [6-10].

Upon cycling the electrode under conditions identical to the initial scan, several distinct changes in peak potential are observed in conflict with a report that the voltammetry for this system is stable and reversible over many cycles (> 4 hours) [7]. In Fig. 1, cycles 1 to 10 show the first UPD peak maxima (A and A′) shifting to increasingly positive potentials. In addition, the peaks attributed to the third UPD region (C and C′) decrease in magnitude, the second Ag layer/bulk desorption becomes more evident (shifting positive) and a new stripping feature (D′) is seen to emerge at 612 mV.

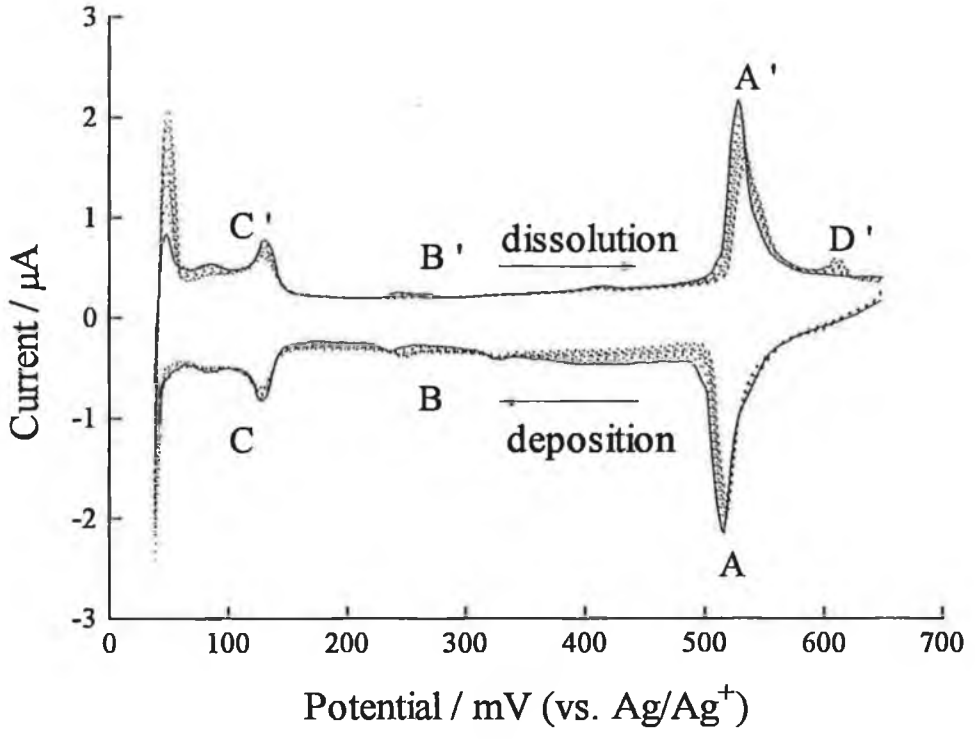

Figure 1 Cyclic voltammograms for Ag UPD (35 to 650 mV vs. Ag/Ag^+) on Au(111) in 1 mM Ag_2SO_4 and 0.1 M H_2SO_4 showing the first cycle (——) and cycles 2 to 10 (– – –) at a scan rate of 10 mVs^{-1}.

The Au(111) electrode was subjected to Ag UPD cycling at 500 mVs^{-1} resulting in dramatic changes in peak potential and magnitude. Slower scan rates gave rise to the same phenomenon but required longer cycling times for completion of the structural transition. A selection of voltammograms taken after different repetitive cycling times are shown in Fig. 2. The new peak (D′) at 612 mV increases in magnitude with its corresponding deposition peak (D) emerging at 598 mV. In contrast, both A and A′ decrease in magnitude and shift to increasingly positive potentials. Peak A′ is seen to split in Fig. 2a (peak maxima at 543 and 533 mV) with the more positive peak becoming the dominant component as seen in Fig. 2c. Cycling results in the loss of the series of small peaks (B/B′) and induces changes in third UPD

region evidenced as an attenuation and broadening of the peaks (C/C'). This trend continues as the original adsorption/desorption features in the first UPD process are gradually replaced by very sharp peaks at 602 and 621 mV (Fig. 2g) with FWHM of 8 and 9 mV, respectively. The peaks in the third UPD region become indistinguishable following 445 minutes cycling (beyond which no further changes were observed). These changes are accompanied by a narrowing of the double layer region, the development of broad peaks at 270 to 290 mV (Fig. 2d) and a positive potential shift for second layer growth and bulk processes. It should be noted that identical results were obtained upon cycling the electrode to 0.0 mV to include a sharp peak attributed to second layer/bulk phase growth by Chen *et al.* or assigned as the third UPD process by Itaya and co-workers [7,9,11].

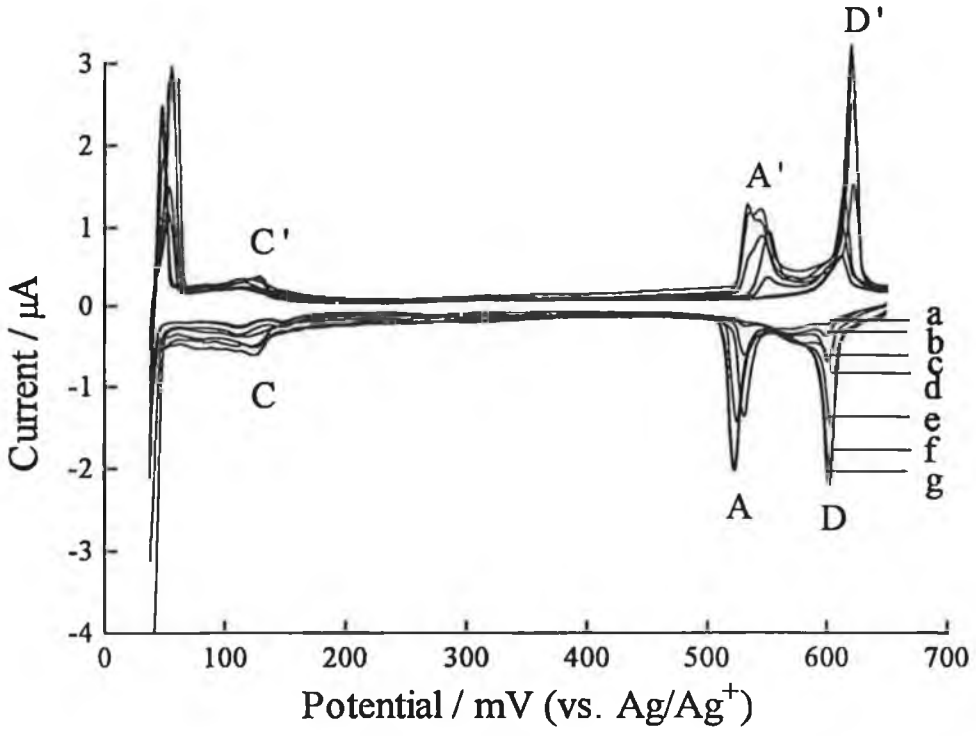

Figure 2 Cyclic voltammograms for Ag UPD (35 to 650 mV vs. Ag/Ag^+) on Au(111) in 1 mM Ag_2SO_4 and 0.1 M H_2SO_4 at a scan rate of 10 mVs^{-1}. Following (a) 45, (b) 75, (c) 105, (d) 140, (e) 260, (f) 405 and (g) 445 minutes of cycling in the Ag UPD region (35 to 650 mV vs. Ag/Ag^+) at a scan rate of 500 mVs^{-1}.

3.2 ECSTM of Ag UPD on Au(111) in sulphuric acid

Prior to Ag UPD, ECSTM images of the Au(111) electrode surface revealed large, atomically flat terrace-step structures in long range scans. Monatomic and diatomic Au steps (0.2 to 0.5 nm in height), separated by terraces 50 to 200 nm in width are shown in Fig. 3. Atomic resolution images on these terraces were obtained and exhibited the hexagonal packing of the Au(111) surface with the expected atom-atom spacing of 0.29 nm. We did not see any reconstructed structure in aqueous solution.

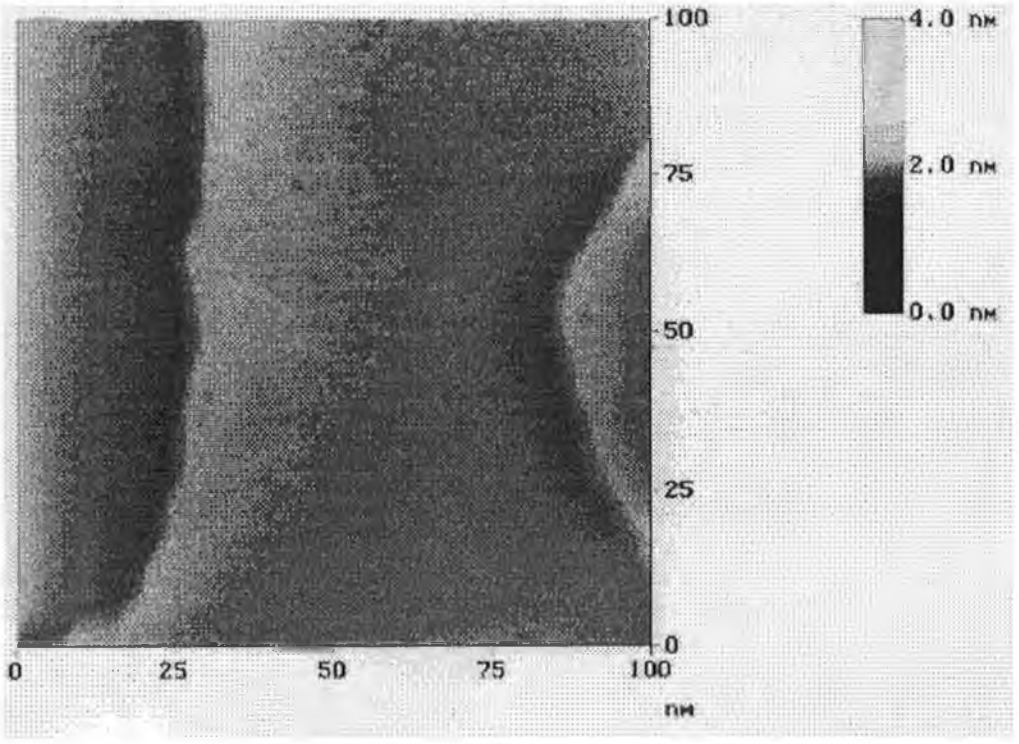

Figure 3 100 nm × 100 nm large scale STM image of Au(111) in 1 mM Ag_2SO_4 and 0.1 M H_2SO_4 prior to Ag UPD (650 mV vs. Ag/Ag^+).

Subsequent to characterisation of the Au(111) substrate morphology, the electrode was subjected to cycles of Ag adsorption and desorption in the UPD region (35 to 650 mV) at a scan rate of 500 mVs^{-1} during which images were collected at different time intervals. The morphological details that developed on the Au(111) surface and corresponding voltammograms following repetitive cycling are shown in Figs. 4 to 7.

After completion of 20 to 45 minutes cycling, images of microscopically rough terraces were consistently observed as shown in Fig. 4a. The surface was characterised by the appearance and growth of a high density of monolayer deep 'pits' (2.5 to 5 nm in diameter). Atomic resolution images could not be obtained due to intrinsic imaging limitations attributed to the surface disorder and instability caused by the creation of a high density of vacancies in the terraces [13]. The corresponding cyclic voltammogram (Fig. 4b) shows the emergence of a new UPD feature at 612 mV (D′) and the splitting of peak A′. In an *in situ* STM investigation of Ag UPD on Au(100) in $HClO_4$, Garcia *et al.* report the occurrence of etch pits at low underpotentials and long-time polarisation (15 minutes) which they relate to surface alloy formation starting at step edges and defects [22]. Localised Ag and Au mixing has been observed during an *in situ* STM investigation of Ag UPD on Au(111) in $HClO_4$ [13]. After holding the potential at 625 mV (vs. Ag/Ag^+) for approximately 3 minutes, Corcoran *et al.* report a degradation in image resolution attributed to mixing of Au and Ag at terrace edges and, in particular, in small localised areas on the terraces.

Alteration in the terrace edge morphology accompanied by substantial surface disruption was observed after 45 to 120 minutes cycling, as shown in Fig. 5a. This corresponds to electrochemical behaviour in which the original and new adsorption/desorption peaks (A/A′ and D/D′, respectively) coexist as shown in Fig. 5b. Ag UPD-induced changes were evident in the form of disordering and roughening as the pits expand rapidly leaving isolated monatomic and diatomic Au islands (of lateral size 5 to 40 nm) accompanied by receding terrace edges. Overall, the cycling process has greatly enhanced the step density. Features characteristic of Au(111) have almost completely disappeared at this stage of the structural transition and no clear atom-resolved corrugation was found.

(a)

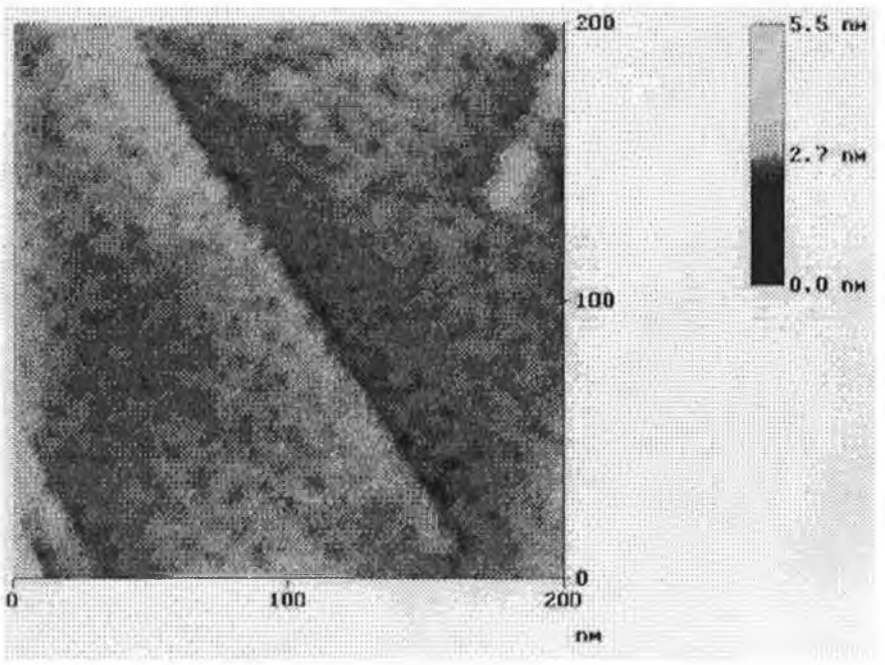

(b)

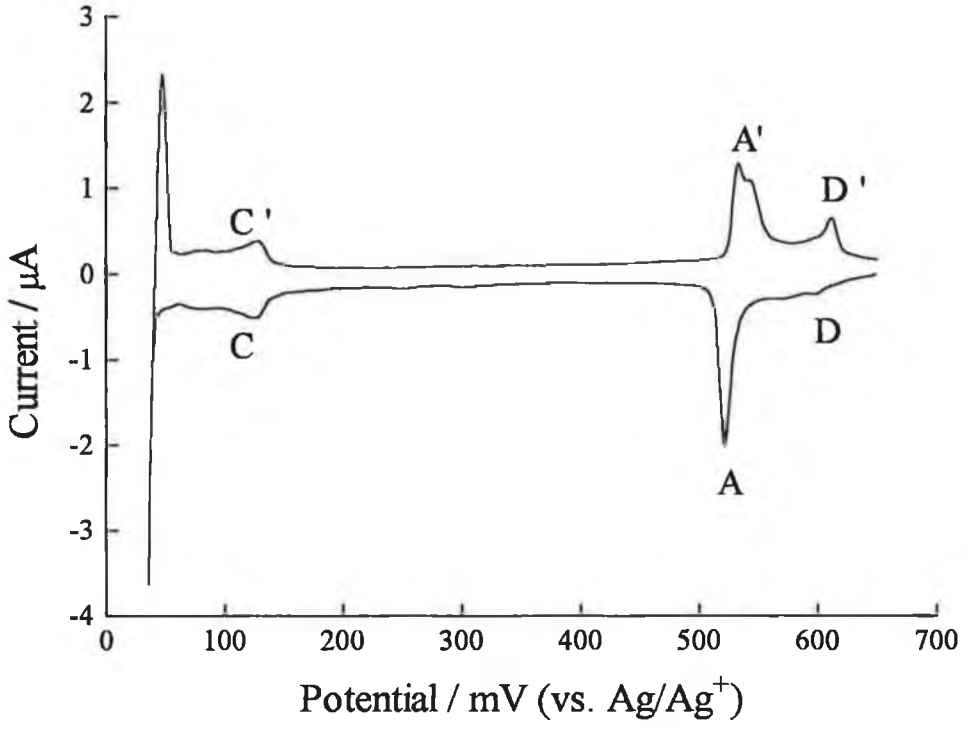

Figure 4 Au(111) in 1 mM Ag_2SO_4 and 0.1 M H_2SO_4 following 45 minutes repetitive cycling in the Ag UPD region (35 to 650 mV vs. Ag/Ag^+) at a scan rate of 500 mVs^{-1}: (a) 200 nm × 200 nm STM image and (b) corresponding cyclic voltammogram at a scan rate of 10 mVs^{-1}.

(a)

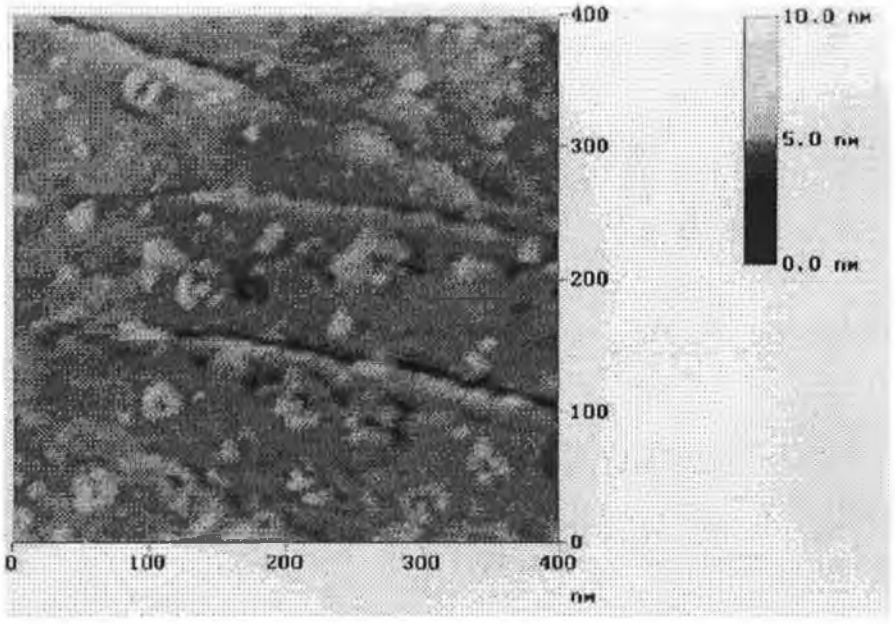

(b)

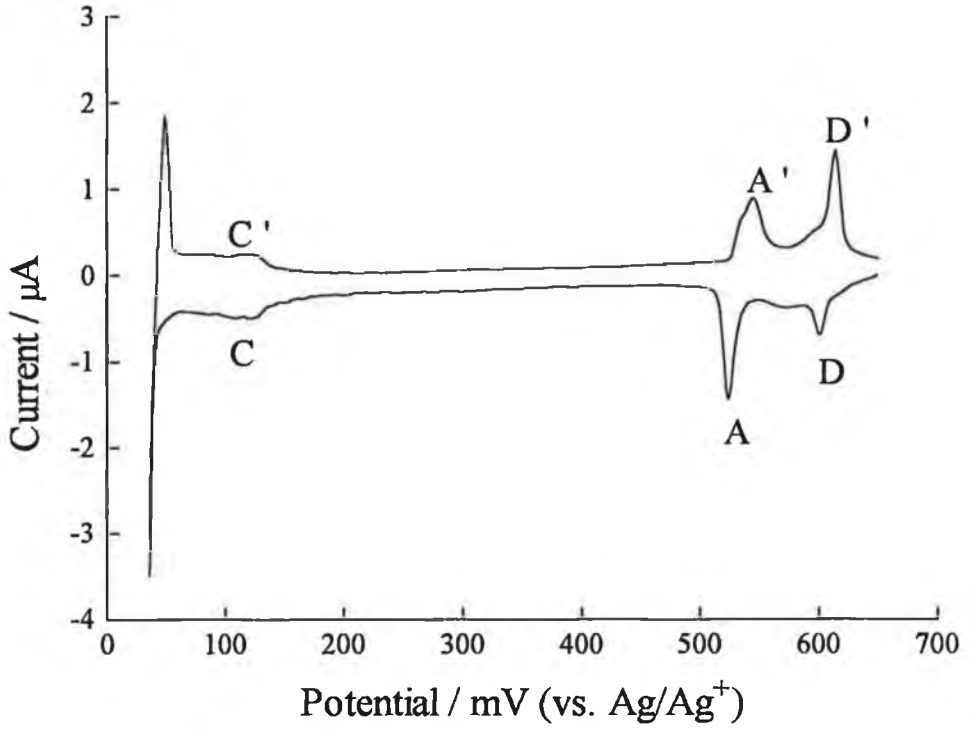

Figure 5 Au(111) in 1 mM Ag_2SO_4 and 0.1 M H_2SO_4 following 105 minutes repetitive cycling in the Ag UPD region (35 to 650 mV vs. Ag/Ag^+) at a scan rate of 500 mVs^{-1}: (a) 400 nm × 400 nm STM image and (b) corresponding cyclic voltammogram at a scan rate of 10 mVs^{-1}.

(a)

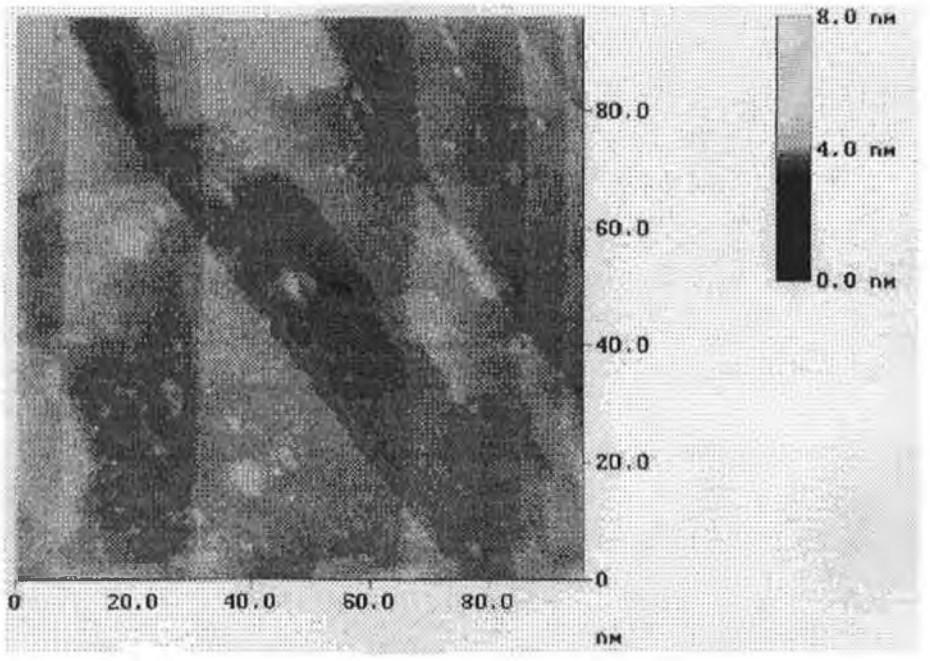

(b)

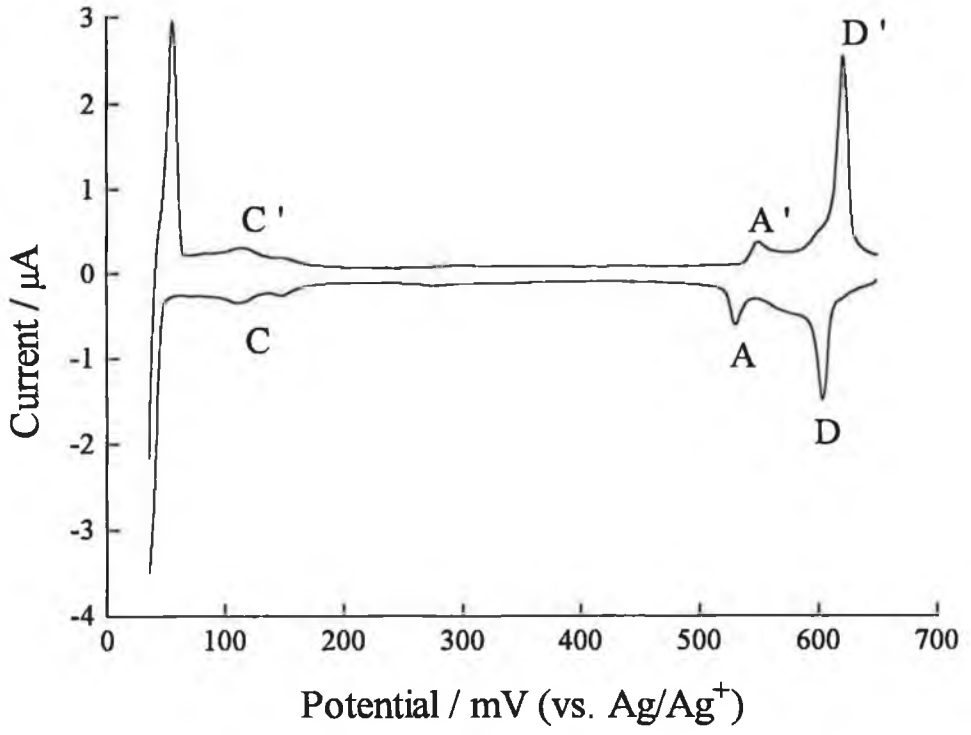

Figure 6 Au(111) in 1 mM Ag_2SO_4 and 0.1 M H_2SO_4 following 260 minutes repetitive cycling in the Ag UPD region (35 to 650 mV vs. Ag/Ag^+) at a scan rate of 500 mVs^{-1}: (a) 95 nm × 95 nm STM image and (b) corresponding cyclic voltammogram at a scan rate of 10 mVs^{-1}.

(a)

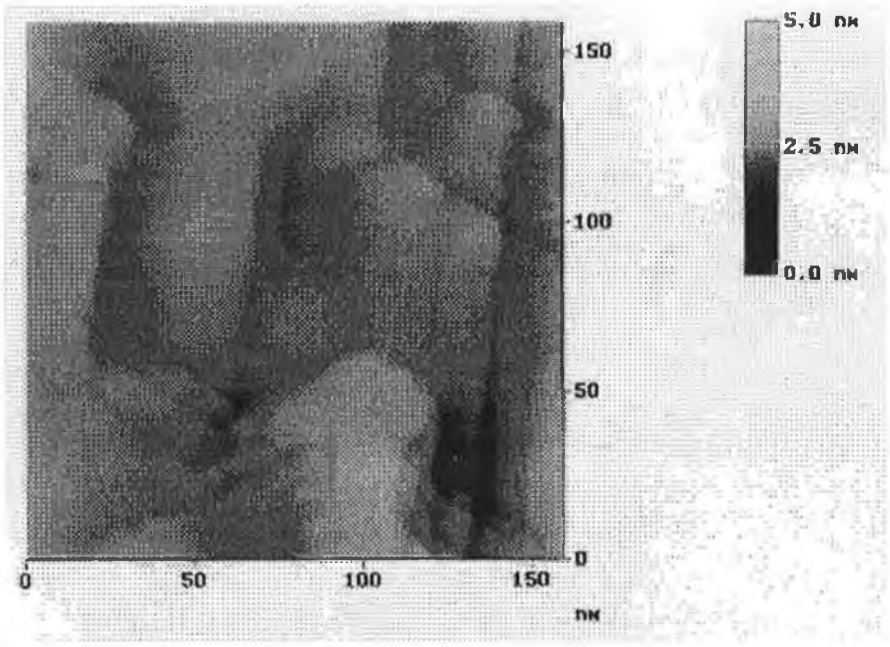

(b)

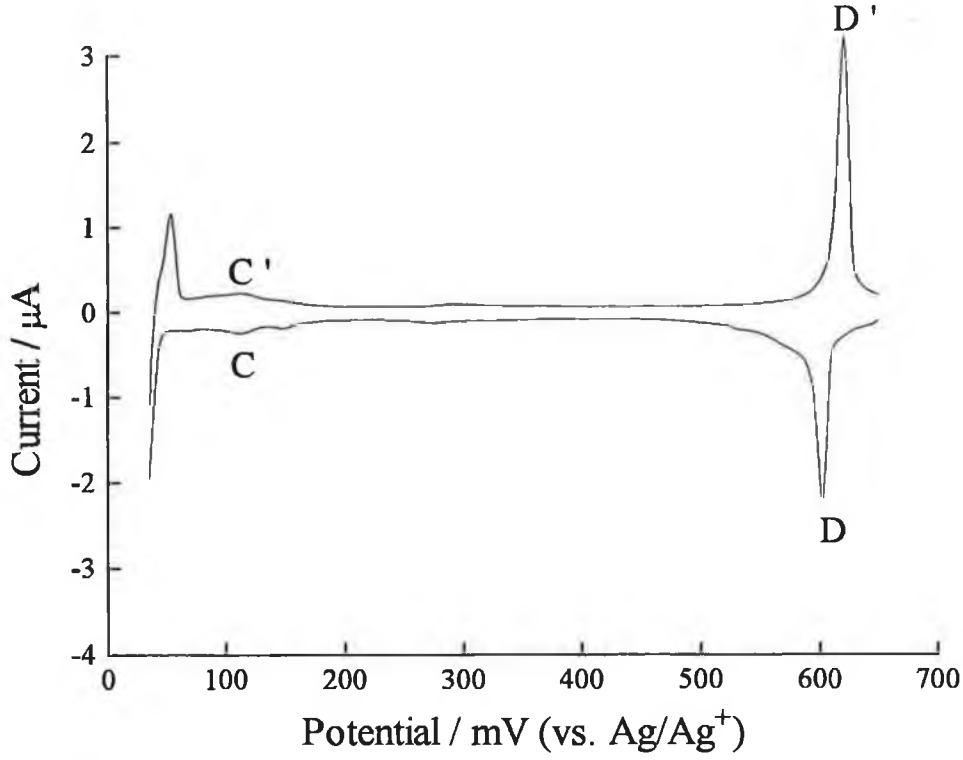

Figure 7 Au(111) in 1 mM Ag_2SO_4 and 0.1 M H_2SO_4 following 445 minutes repetitive cycling in the Ag UPD region (35 to 650 mV vs. Ag/Ag^+) at a scan rate of 500 mVs^{-1}: (a) 160 nm × 160 nm STM image and (b) corresponding cyclic voltammogram at a scan rate of 10 mVs^{-1}.

The degree of surface roughness then began to decline with cycling (>120 minutes) seen as the gradual emergence of ordered structures accompanied by a small amount of disorder restricted to localised regions on the surface. The reordering process involves a slow lateral growth of Au islands which apparently fuse with terrace edges or aggregate with each other to form narrow, imperfect terraces. Subsequent cycling allows Au islands (previously a disordered, random array) to coalesce into larger domains which exhibit some degree of long range order. As suggested by Green *et al.*, these final stages of the structural transformation may be inhibited by the presence of impurity species adsorbed at step edges and defect sites on the electrode surface which must be released before formation of extended terraces [23]. The surface morphology is dominated by a terrace-step structure with terrace edges running parallel or at 60/120° angles with respect to each other following 260 minutes cycling as shown in Fig. 6a. This highly ordered structure is reflected in Fig. 6b in which peaks A and A′ have become minor components of the cyclic voltammogram and peaks D and D′ occur as the dominant Ag UPD process.

Finally, after 445 minutes of Ag UPD cycling, the surface topography is dominated by straight-edged, narrow terraces as shown in Fig. 7a. The terraces, 15 to 50 nm in width, are arranged parallel to or crossing each other to form an extended mesh in which the terrace edges are oriented such that the steps of monatomic height meet at an angle of 60/120° characteristic of a (111) close-packed plane. The expected interatomic spacing on Au(111) could be seen in high resolution images acquired on these atomically flat terraces. The corresponding voltammogram shown in Fig. 7b consists of adsorption/desorption peaks (D/D′) at 602 and 621 mV with extremely narrow half-widths indicative of significant long-range order and a set of minor broad peaks at 270 to 290 mV. We speculate that the adsorption/desorption peak potential shift during the first Ag UPD process, from 516/527 mV to 602/621 mV, is caused by a change in the Au(111) surface terrace width as evidenced by STM images.

Based upon STM and electrochemical observations, a tentative description of the topographical transitions that occur during repetitive cycling of Au(111) in the Ag UPD region in H_2SO_4 can be proposed. These structural changes are indicated schematically in Fig. 8. Cycling in the Ag UPD region results in substantial changes in the Au(111) surface; formation of pits, development of Au islands and receding terrace

edges followed by a re-ordering process which requires several hours of cycling. The end result is a decrease in the average substrate terrace width, signalled by the emergence of the adsorption/desorption peaks (D/D') at 602 and 621 mV, with long range order reflected in voltammetric D/D' peak magnitude and extremely narrow half-widths (<10 mV).

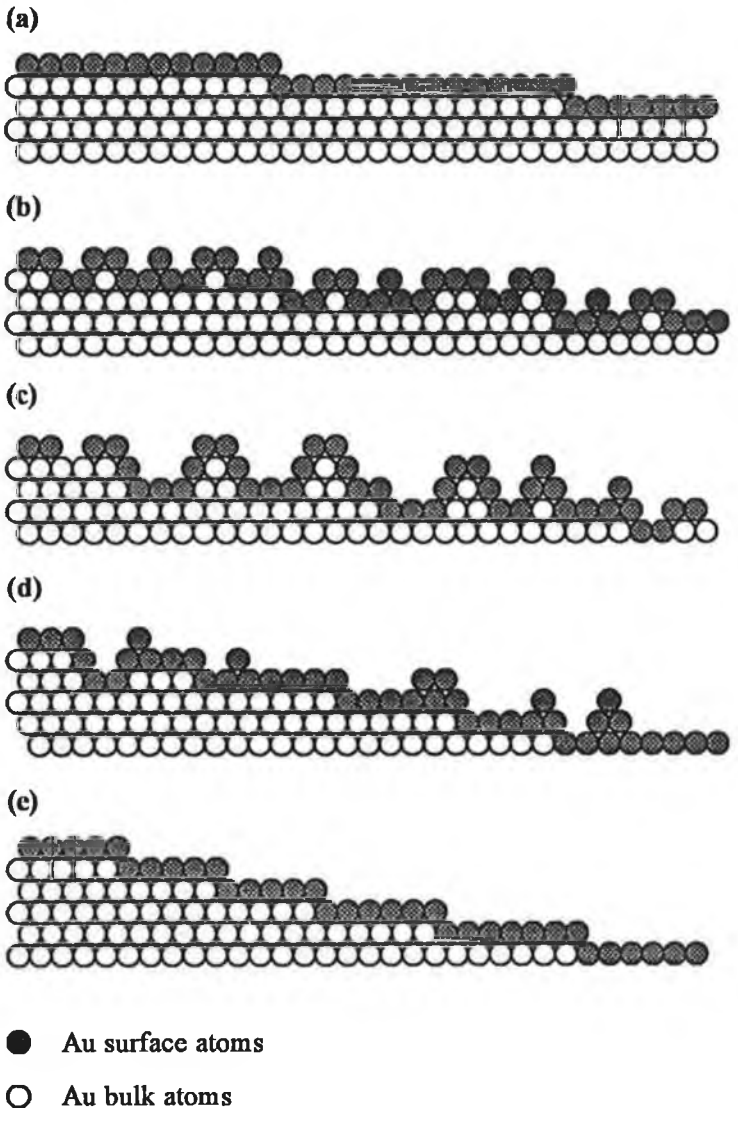

Figure 8 Schematic depiction of the structural transition induced by repetitive Ag UPD on Au(111): (a) substrate surface before cycling, (b) 'pit' formation in the substrate plains, (c) disorder and roughening with receding terrace edges, (d) re-ordering and (e) narrow, atomically flat terraces.

While this behaviour could be reproducibly recovered upon flame-annealing the crystal to restore surface order, following prolonged exposure of the electrode surface to cycling conditions (>12 cycling experiments), the structural transition was found to degrade the quality of the crystal resulting in lower cycling times being required for complete transformation of the surface structure. The morphological changes observed in this study appear to be related to the method of electrode preparation (bulk crystals versus Au films evaporated on mica) giving rise to variations in crystal quality. We speculate that the kinetics of the transition process are related to the initial number of surface defects. A 'perfect' Au(111) surface slowly transforms whereas a 'defective' surface transforms rapidly i.e. the process begins at defects. The dependence of the transition on the surface defect density is evidenced by the observed variation in the rate of transformation between different crystals utilised in our work. Similarly, Holzle *et al.* have described the influence of the step density on the mechanism of adlayer growth and deposition kinetics for Cu UPD and bulk deposition on Au(111) [24].

In an STM study, Green and co-workers observed substantial roughening of a Au(111) surface after a single monolayer of Pb is electrochemically deposited and stripped in perchlorate electrolyte [23,25]. A model for the rearrangement of the first two layers of the Au surface is proposed by the authors, consistent with the STM observations, in terms of surface alloy formation resulting from lateral place-exchange between Pb and Au at substrate steps, and vertical exchange within the terraces. In our study, alloy formation could explain the early surface structural changes, such as pit formation and extensive roughening, and the appearance of the broad peaks at 270 to 290 mV in the cyclic voltammetry. However, because the bond energy relation in UPD is substrate-substrate > substrate-adatom > adatom-adatom bonds, the potential for Ag deposition would be expected to be more negative on the alloyed surface than on pure Au which is not the case for the 602 and 621 mV peaks. However, further measurements using UHV-EC techniques are in progress in order to clarify whether or not alloy formation is occurring during repetitive Ag UPD cycling [26].

3.3 Variation of the supporting anion and substrate oxidation effects

Ag UPD is reported to exhibit substantial electrolyte sensitivity and, in particular, the perchlorate anion is known to only weakly interact with Au and Ag [27-29]. Cyclic voltammograms, similar to that reported previously for Ag UPD in 0.1 M $HClO_4$ electrolyte, are shown in Fig. 9 [7]. In the first cycle, adsorption at 502 mV corresponds to the first UPD process (A) with its desorption peak occurring at 509 mV (A′). Two sets of broad peaks (B) occur at 407 and 290 mV on the deposition cycle with the corresponding stripping peaks (B′) at 410 and 298 mV. The third UPD process (C) consists of two peaks at 133 and 102 mV. On the dissolution sweep, the stripping peaks occur at 138 and 108 mV (C′). As previously reported, these features are substantially broader than the corresponding peaks in H_2SO_4 [7]. In addition, we observe a set of minor peaks at approximately 595 mV (D/D′).

Upon cycling the electrode at 500 mVs^{-1}, several distinct changes in peak shape and potential are observed. In Fig. 9, following 15 minutes cycling the main adsorption/desorption peaks (A and A′) have shifted to more positive potentials. In addition, peaks attributed to the third UPD region (C and C′) decrease in magnitude and undergo a positive potential shift, the second Ag layer desorption/bulk desorption becomes more evident (shifting positive) and the new feature D/ D′ is seen at 600 mV. Subjecting the electrode to 75 minutes cycling results in A and A′ appearing as broad features at approximately 560 and 520 mV with the two main UPD peaks occurring at 597 and 600 mV (adsorption and desorption, respectively) and a broad peak at 470 to 480 mV. Peaks at intermediate potentials in the second UPD region, B and B′, have disappeared while the third UPD process consists of a well-defined peak at 177 mV and a broad peak at 125 mV (corresponding stripping occurs at 185 and 129 mV). Finally, after 210 minutes cycling, the original UPD peaks have been replaced by a set of sharp peaks at 587 and 599 mV (adsorption and desorption, respectively) and a set of small peaks are detected at 254 mV (adsorption) and 274 mV (desorption).

Interestingly, Corcoran *et al.* who observed reproducibility over many cycles for a period of a few hours for Ag UPD on Au(111) in perchloric acid, present a cyclic voltammogram qualitatively similar to that found in this study following 75 minutes of cycling treatment as shown in Fig. 9 [13]. On the adsorption cycle, a UPD peak at 510

mV was reported to increase in height as a 600 mV peak height decreased with increasing surface roughness and Ag-Au mixing. A high density of vacancies in the substrate terraces and altered step edge morphology during Ag stripping was observed with *in situ* STM. The electrochemistry is explained by Corcoran *et al.* in terms of the nucleation of Ag at impurity sites on the Au surface.

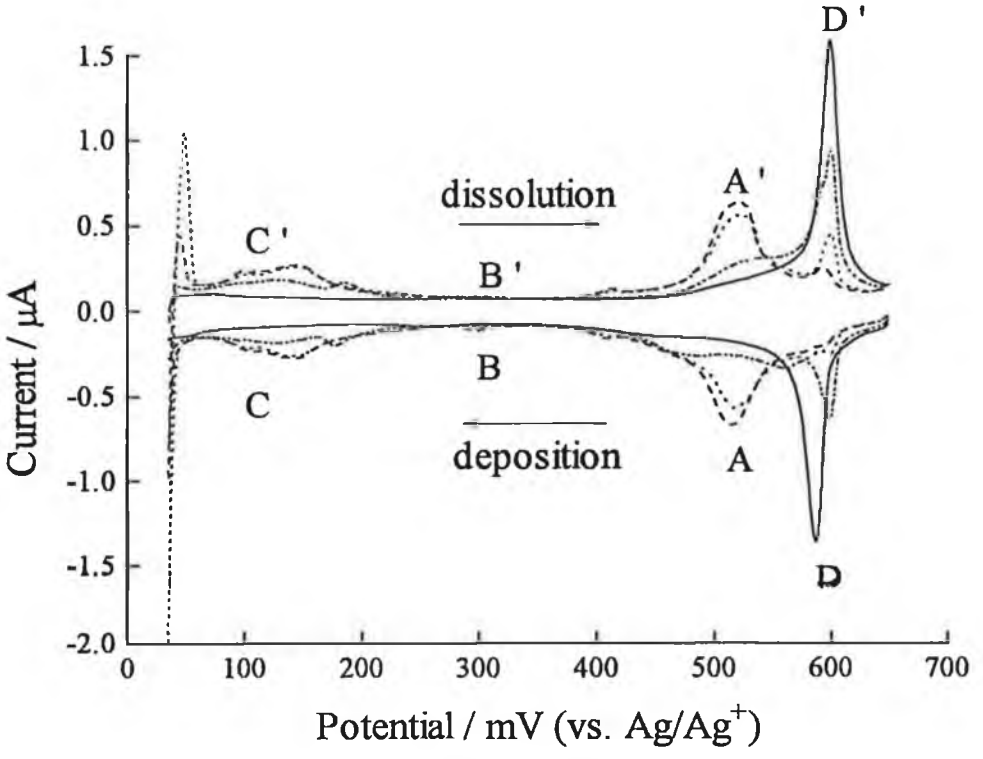

Figure 9 Cyclic voltammograms for Ag UPD (35 to 650 mV vs. Ag/Ag^+) on Au(111) at a scan rate of 10 mVs^{-1} in 1 mM $AgClO_4$ and 0.1 M $HClO_4$ showing the first cycle (---) and following 15 (· · ·), 75 (- · ·- · ·) and 210 (——) minutes cycling in the Ag UPD region at a scan rate of 500 mVs^{-1}.

We find the lower potential peak at 502 mV on a freshly prepared surface and prolonged cycling treatment was required to induce the occurrence of the 587 mV feature. The complex set of peaks observed from 400 to 600 mV following 15 minutes cycling suggest substantial surface disruption caused by repeated Ag UPD. In contrast, the D/D' peaks represent a narrowing of the terrace width with long range order on

the Au(111) surface, assuming these changes in electrochemical behaviour are due to structural transitions similar to those observed in sulphuric acid. However, perchlorate anions appear to enhance the transformation process, as evidenced by the more rapid growth of the new adsorption/desorption features, indicating that anion coadsorption plays an important role in this structural transition.

The morphological changes described in section 3.2 are very similar to those observed during formation and stripping of an oxide monolayer on Au(111) in sulphuric and perchloric acid solutions [30-33]. Hence, the effects of subjecting the Au(111) electrode to cycling conditions in Ag-free electrolyte (0.1 M $HClO_4$ and H_2SO_4) were investigated in order to verify that the observed processes are Ag-induced. Substrate oxidation is of greater concern in the case of perchloric acid as it begins at more negative potentials (approximately 550 mV vs. Ag/Ag^+) and partially overlaps the initial potential applied for Ag UPD.

The Au(111) electrode was cycled at 500 mVs^{-1} for 120 minutes (35 to 650 mV vs. Ag/Ag^+) in 0.1 M $HClO_4$ and then transferred to Ag-containing $HClO_4$ solution for collection of Ag UPD. As shown in Fig. 10, this resulted in the attenuation of all adsorption/desorption peaks, however, there is no evidence of the new UPD peaks at 587 and 599 mV (adsorption and desorption, respectively). This is consistent with *in situ* STM studies on the surface morphological changes accompanying oxidation-reduction cycles on Au(111) in $HClO_4$ which report that potentials at which less than a monolayer of Au oxide is formed, the surface structure is unperturbed [31,32]. Similar peak attenuation with the absence of new higher potential adsorption/desorption features was observed upon cycling in Ag-free H_2SO_4.

Cycling to higher potentials results in substantial surface disruption, by a mechanism of place-exchange, coincident with the formation of a monolayer of Au oxide [30-33]. Although long times are often required for the surface to recover, during oxide reduction the original surface morphology is largely restored as monatomic high Au islands coalesce and monatomic pits fuse with terrace edges. The effects of oxidation-reduction cycles was investigated by inducing the surface structural transition on Au(111) in the Ag UPD region, to the extent that the original adsorption/desorption peaks have disappeared and peaks D/D' dominate, followed by cycling at 10 mVs^{-1} to higher potentials (35 to 1000 mV vs. Ag/Ag^+). A slow scan

rate was used to allow sufficient time for the oxide layer to form as suggested by Vitus and Davenport [31]. The resulting Ag UPD features suggest a progressive transformation of the surface from long range order with narrow terraces to a defect rich state. A typical voltammogram following 120 minutes continuous oxidation-reduction cycling is shown in Fig. 10. Similar changes to Ag UPD adsorption/desorption features were observed upon cycling to higher potentials in Ag-containing H_2SO_4 solution.

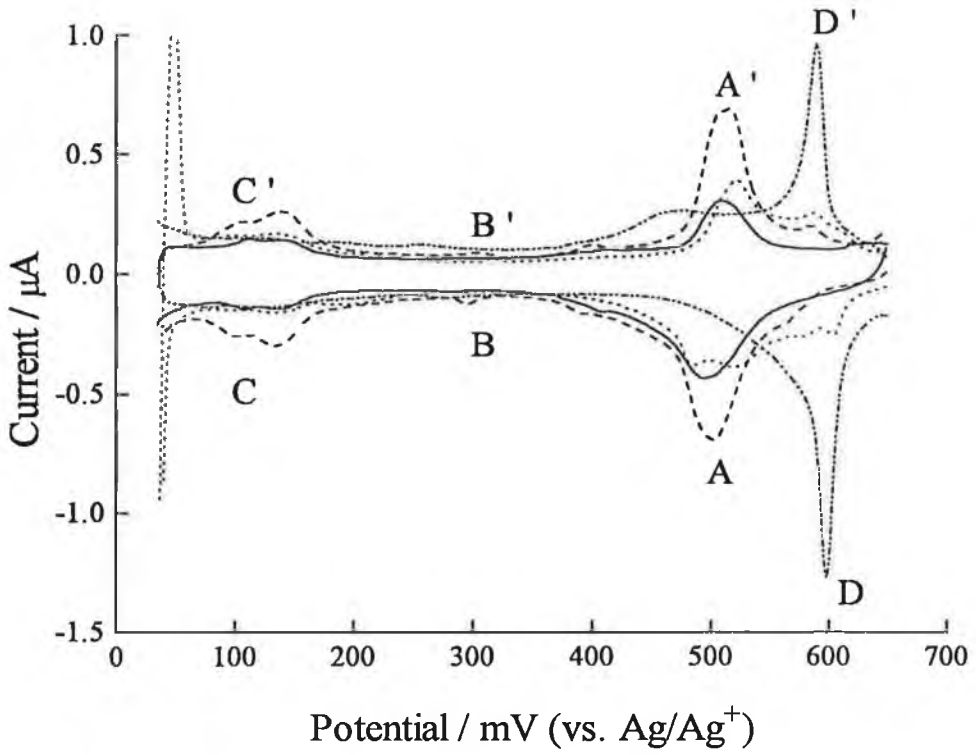

Figure 10 Cyclic voltammograms for Ag UPD (35 to 650 mV vs. Ag/Ag^+) on Au(111) in 1 mM $AgClO_4$ and 0.1 M $HClO_4$ at a scan rate of 10 mVs^{-1} showing the first cycle (– – –) and following 120 minutes cycling in: 0.1 M $HClO_4$ (35 to 650 mV) at a scan rate of 500 mVs^{-1} (——) and 1 mM $AgClO_4$ and 0.1 M $HClO_4$ (35 to 650 mV) at a scan rate of 500 mVs^{-1} (– · ·– · ·) followed by 120 minutes cycling 1 mM $AgClO_4$ and 0.1 M $HClO_4$ (35 to 1000 mV) at a scan rate of 10 mVs^{-1} (· · ·).

To summarise, cycling in Ag-free perchloric and sulphuric acid solutions in the Ag UPD region demonstrates that adsorption of anions alone and/or the onset of substrate oxidation is not responsible for the changes in surface morphology leading to the sharp D/D' features observed upon repeated Ag UPD cycles. In fact cycling to higher potentials (1000 mV vs. Ag/Ag^{+}) at which substantial surface disruption is known to occur, due to the formation of a monolayer of Au oxide, causes the surface to revert to a highly disordered state, intermediate between the initial state characteristic to Ag UPD on Au(111) and the final state induced by repetitive Ag UPD cycling.

4. Conclusions

Repeated cycling in the Ag UPD region in sulphuric acid electrolyte results in substantial changes in the Au(111) surface morphology as evidenced by *in situ* ECSTM. Pit formation, creation of Au islands and receding terrace edges is followed by a slow re-ordering process resulting in a decrease in the average substrate terrace width. In agreement with STM observations, dramatic changes in voltammetric peak potential and magnitude were seen to occur with extremely narrow half-widths (< 10 mV) indicative of significant long range order. Similar changes in peak shape and potential were found to occur upon subjecting Au(111) to identical Ag UPD cycling conditions in perchloric acid with an apparent increase in the rate of surface transformation in the presence of the weakly adsorbing anion. Adsorption of anions in the absence of Ag^+ ions and/or the onset of substrate oxidation does not induce the changes in voltammetric peak potential and magnitude seen to occur in Ag-containing solutions confirming that Ag UPD is primarily responsible for the surface structural transition observed.

5. References

[1] D.M. Kolb, M. Przasnyski and H. Gerischer, J. Electroanal. Chem., **54** (1974) 25.

[2] E. Budevski, G. Staikov and W.J. Lorenz, Electrochemical Phase Formation and Growth.

[3] M.P. Soriaga, in: The Structure of Electrified Interfaces, Eds. J. Lipowski and P.N. Ross (VCH, New York, 1992).

[4] M.P. Soriaga in: Modern Techniques in Electroanalysis, Vol. 139, Eds. P. Vanysek (John Wiley & Sons,Inc., New York, 1996).

[5] M.D. Ward and H.S. White in: Modern Techniques in Electroanalysis, Vol. 139, Eds. P. Vanysek (John Wiley & Sons,Inc., New York, 1996).

[6] H. Uchida, M. Miura and M. Watanabe, J. Electroanal. Chem., **386** (1995) 261.

[7] C. Chen, S.M. Vesecky and A.A. Gewirth, J. Am. Chem. Soc., **114** (1992) 451.

[8] C. Chen and A.A. Gewirth, Ultramicroscopy, **42-44** (1992) 437.

[9] T. Hachinori and K. Itaya, Ultramicroscopy, **42-44** (1992) 445.

[10] P. Mrozek, Y.-E. Sung, M. Han, M. Gamboa-Aldeco, A. Wieckowski, C.-H. Chen and A.A. Gewirth, Electrochimica Acta, **40** (1995) 17.

[11] K. Ogaki and K. Itaya, Electrochim. Acta, **40** (1995) 1249.

[12] S. Sugita, T. Abe and K. Itaya, J. Phys. Chem., **97** (1993) 8780.

[13] S.G. Corcoran, G.S. Chakarova and K. Sieradzki, J. Electroanal. Chem., **377** (1994) 85.

[14] P. Mrozek, Y.-E. Sung and A. Wieckowski, Surf. Sci., **335** (1995) 44.

[15] J. Clavilier, D. Armand, S.C. Sun and M. Petit, J. Electroanal. Chem., **205** (1986) 267.

[16] J. Clavilier, R. Faure, G. Guinet and R. Durand, J. Electroanal. Chem., **107** (1980) 205.

[17] D.A. Scherson and D.M. Kolb, J. Electroanal. Chem., **176** (1984) 353.

[18] O.M. Magnussen, J. Hagebock, J. Hotlos and R.J. Behm, Faraday Discus., **94** (1992) 329.

[19] G.J. Edens, X. Gao and M.J. Weaver, J. Electroanal. Chem., **375** (1994) 357.

[20] P. Mrozek, M. Han, Y.-E. Sung and A. Wieckowski, Surf. Sci., **319** (1994) 21.

[21] C.M. Whelan, M.R. Smyth and C.J. Barnes, J. Electroanal. Chem., **441** (1998) 109.

[22] S.G. Garcia, D. Salinas, C. Mayer, J.R. Vilche, H.-J. Pauling, S. Vinzelberg, G. Staikov and W.J. Lorenz, Surf. Sci., **316** (1994) 143.

[23] M.P. Green, K.J. Hanson, R. Carr and I. Lindau, J. Electrochem. Soc., **137** (1990) 3493.

[24] M.H. Holzle, V. Zwing and D.M. Kolb, Electrochim. Acta., **40** (1995) 1237.

[25] M.P. Green and K.J. Hanson, Surf. Sci. Lett., **259** (1991) L743.

[26] G.A. Attard and X. Fang, unpublished data.

[27] X. Gao, A. Hamelin and M.J. Weaver, J. Chem. Phys., **95** (1991) 6993.

[28] H. Angerstein-Kozlowska, B.E. Conway, A. Hamelin and L. Stoicoviciu, Electrochim. Acta, **31** (1986) 1051.

[29] T. Vitanov, A. Popov and E.S. Sevastyanov, J. Electroanal. Chem., **142** (1982) 289.

[30] Nanoscale Probes of the Solid/Liquid Interface, NATO ASI Series E: Applied Sciences, Vol. 288, Eds. A.A. Gewirth and H. Siegenthaler (Kluwer Academic, Dordrecht, 1995).

[31] C.M. Vitus and A.J. Davenport, J. Electrochem. Soc., **141** (1994) 1291.

[32] D.J. Trevor, C.E.D. Chidsey and D.N. Loiacono, Phys. Rev. Lett., **62** (1989) 929.

[33] X. Gao and M.J.Weaver, J. Electroanal. Chem., **367** (1994) 259.